UNIVERSITÉ DU QUÉBEC À MONTRÉAL

IDENTIFICATION DE L’ESPÈCE D’ARBRES INDIVIDUELS À PARTIR DE DONNÉES D’UN BALAYEUR LIDAR MULTISPECTRAL AÉROPORTÉ

THÈSE

PRÉSENTÉE

COMME EXIGENCE PARTIELLE DU

DOCTORAT EN SCIENCES DE L’ENVIRONNEMENT

PAR

BRINDUSA CRISTINA BUDEI

SEPTEMBRE 2020

REMERCIEMENTS

J’adresse mes remerciements à mes directeurs Richard Fournier et Daniel Kneeshaw pour toute l’aide accordé pour finaliser ma thèse.

Je remercie mon directeur Benoît St-Onge pour tout le travail réalisé ensemble, les conseils, les bourses, les encouragements pendant toute la période de mon doctorat. Je remercie mon co-directeur Chhun-Huor Ung pour tout le support au début de ma thèse.

Je remercie les membres du comité d’encadrement Sylvie Durrieu et Sylvie Daniel pour leurs suggestions pour le projet de thèse et pour l’examen de synthèse.

Je remercie Jean Bégin, Chhun-Huor Ung, Benoît St-Onge et Richard Fournier pour le projet de financement de ma thèse. Je remercie le FQRNT pour les bourses d’études. Je remercie le Centre d’étude de la forêt pour les bourses de déplacements au congrès Silvilaser 2012 et 2017.

Je remercie Kosal Kuhn et Chris Hopkinson pour les données terrain. Je remercie les personnes qui ont travaillé sur la collection des données terrain pour mon premier projet de thèse ou sur le traitement de ces données. Je mentionne Jean-François Milot, Caroline Rivest, Vincent Gadoury et Sylvain Leblanc. Je remercie Jean-François Côté pour les modèles d’arbres.

Je remercie les correcteurs anonymes pour leurs suggestions qui ont contribué à améliorer la qualité des articles publiés. Je remercie aussi les personnes qui ont lu les manuscrits. Parmi ces personnes je mentionne, à part mes directeurs, Chris Hopkinson, Félix-Antoine Audet, Jean-François Prieur, Espartaco Carrera, Parvez Rana, Shalini Oogathoo. Je remercie les personnes qui m'ont donné des suggestions lors des présentations aux conférences, aux colloques ou en laboratoire.

Je remercie Richard Fournier pour les ateliers en lidar terrestre, ainsi que Nicholas Coops et Benoît St-Onge pour les rencontres du programme AWARE qui m'ont permis de connaître un grand nombre de spécialistes en lidar à travers le Canada et la France.

Un grand remerciement s'adresse à mon conjoint, Espartaco Carrera pour tout le soutien tout au long de ces années. Sans sa suggestion je n'aurais jamais commencé le doctorat. J'adresse un grand remerciement à mes parents, à mes sœurs, ainsi qu'à toute ma famille pour toute l'aide et l'encouragement. Je remercie spécialement mes enfants qui ont largement contribué à la prolongation de ma durée d'études doctorales.

Je remercie les membres du laboratoire de cartographie forestière du département de géographie de l'UQAM pour toute aide accordée, pour la belle collaboration pendant toutes les années de mon doctorat et pour les encouragements. Parmi tous les étudiants, je nomme Marie-Claude Jutras Perrault, Mathieu Laforme, Udayalakshmi Vepakomma, Yaser Sadeghi, Yuddy Ramos, Jean-François Prieur, David Hernandez, Judith Noel Gagnon, Simon Grandin, Félix-Antoine Audet, Eugénie Morasse Lapointe, Qian Zeng, Rachel Mathieu, Rachel Perron, Parvez Rana. Je remercie aussi les étudiants du laboratoire de Daniel Kneeshaw au département des sciences biologiques pour les rencontres virtuelles et pour les suggestions lors des présentations de ma recherche.

DÉDICACE

À Espartaco, Rafael, Andrei et Alfredo

À mes parents et à mes sœurs et à toute ma famille

AVANT-PROPOS

Cette thèse est composée de trois articles scientifiques rédigés en anglais, dont deux ont été publié dans des revues scientifiques internationales avec comité de lecture. Les autres sections de la thèse sont rédigées en français selon les exigences de l'Université du Québec à Montréal. J'ai agi à titre de premier auteur pour les trois articles (chapitres) et j'ai été responsable du choix de la problématique, de la revue de littérature, du choix méthodologique, de l'analyse et interprétation des données et de la rédaction.

CHAPITRE II : Brindusa Cristina Budei, Benoît St-Onge, Chris Hopkinson, Félix-Antoine Audet, Identifying the genus or species of individual trees using a three-wavelength airborne lidar system, *Remote Sensing of Environment*, 2018, Volume 204, pages 632-647

CHAPITRE III : Brindusa Cristina Budei, Benoît St-Onge, Variability of multispectral lidar 3D and intensity features with individual tree height and its influence on needleleaf tree species identification, *Canadian Journal of Remote Sensing*, 2018, Volume 44, Issue 4, pages 263-286

CHAPITRE IV : Brindusa Cristina Budei, Benoît St-Onge, Richard Fournier, Daniel Kneeshaw, Effects of viewing geometry on 3D and intensity classification features used for ALS-based tree species identification, À soumettre à *Canadian Journal of Remote Sensing*

Des résultats préliminaires de ces articles ou des méthodologies alternatives testées ont été présentées dans les conférences internationales :

Benoît St-Onge, Brindusa Cristina Budei, Individual tree species identification using the multispectral return intensities of the Optech Titan LiDAR system. *SilviLaser*, 28-30 Septembre 2015, La Grande Motte, France

Brindusa Cristina Budei, Jean-François Prieur, Benoît St-Onge, Richard Fournier, Variability of 3D and intensity features for four tree species within and across sites: a case study on two Canadian sites using Titan multispectral ALS data, *Silvilaser*, 10-12 Octobre 2017, Blacksburg, Virginia, USA

Brindusa Cristina Budei, Benoît St-Onge, Assessing the effects of viewing geometry on 3D and intensity features used for ALS-based tree species identification, *ForestSAT*, 1-5 October 2018, Colledge Park, Maryland, USA

TABLE DES MATIÈRES

REMERCIEMENTS III

DÉDICACE V

AVANT-PROPOS VI

TABLE DES MATIÈRES VIII

LISTE DES FIGURES XII

LISTE DES TABLEAUX XV

LISTE DES ABRÉVIATIONS XVIII

RÉSUMÉ XIX

CHAPITRE 1 INTRODUCTION 1

1.1 Importance de l'identification de l'espèce 1

1.2 Utilisation de l'information spectrale ou structurale obtenue par télédétection pour l'identification de l'espèce par arbre individuel 2

1.3 Lidar multispectral 9

1.4 Étapes méthodologiques utilisées pour l'identification de l'espèce par arbre individuel 0

1.4.1 Étape 1 : Délimitation des couronnes 0
1.4.2 Étape 2 : Calcul des variables 3
1.4.3 Étape 3 : Classification par un algorithme automatique 9

1.5 Objectifs 11

CHAPITRE 2 IDENTIFYING THE GENUS OR SPECIES OF INDIVIDUAL TREES USING A THREE-WAVELENGTH AIRBORNE LIDAR SYSTEM 14

2.1 Introduction 16
2.2 Data and methods 24
2.2.1 Study regions 24
2.2.2 Multispectral lidar data 25
2.2.3 Selection and identification of sample crowns 26
2.2.4 Delineation of sample tree crowns 30
2.2.5 Lidar point cloud statistics of tree crowns 33
2.2.6 Computation of classification features 33
2.2.7 Random forest classification and feature selection 43
2.3 Results 45
2.4 Discussion 54
2.4.1 Feature selection 54
2.4.2 Accuracy improvements in species identification 56
2.4.3 Limitations and generalizability 57
2.5 Conclusion 58
2.6 Acknowledgements 59
CHAPITRE 3 VARIABILITY OF MULTISPECTRAL LIDAR 3D AND INTENSITY FEATURES WITH INDIVIDUAL TREE HEIGHT AND ITS INFLUENCE IN TREE SPECIES IDENTIFICATION 60
3.1 Introduction 62
3.1.1 Changing tree architecture with height / age 64
3.1.2 Variability of crown-wise lidar point cloud quality 65
3.1.3 Lidar penetration depth in tree crown 66
3.1.4 Minimum return height threshold 67
3.1.5 Effects of the normalization of return height by tree height 68
3.1.6 Variation of intensity features with tree age and height 69
3.1.7 Constant species characteristics 71
3.1.8 Strategies for handling ALS feature variations with height in tree species classification 72
3.1.9 Objectives 73
3.2 Data and methods 74
3.2.1 Study site 74
3.2.2 Field and reference data 74
3.2.3 Multispectral ALS data 75
3.2.4 Selection and delineation of sample crowns 75

3.2.5 MSL features used in species identification 77
3.2.6 Effect of the height threshold 81
3.2.7 Relationship between tree height and feature values 83
3.2.8 Species classification strategies 84

3.3 Results 86

3.3.1 Effect of height threshold 86
3.3.2 Relation between tree height and features 89
3.3.3 Classification results 102

3.4 Discussion 113

3.4.1 Variation of 3D features with tree height 113
3.4.2 Variation of intensity features with tree height 114
3.4.3 Classification strategies 115

3.5 Conclusion 118

3.6 Acknowledgements 119

CHAPITRE 4 EFFECTS OF VIEWING GEOMETRY ON MULTISPECTRAL LIDAR-BASED NEEDLE-LEAVED TREE SPECIES IDENTIFICATION 120

4.1 Introduction 122

4.2 Data and methods 126

4.2.1 Reference data on tree species 126
4.2.2 Lidar data and intensity correction for range 127
4.2.3 Net pulse scan angles 129
4.2.4 Multispectral lidar features 133
4.2.5 Tree views selection 134
4.2.6 Feature correlation to mean scan angle 137
4.2.7 RF classification 138

4.3 Results 141

4.3.1 Feature correlation to scan angle 141
4.3.2 Classification accuracy 151

4.4 Discussion 154

4.5 Conclusion 159

4.1 Acknowledgements 159

CHAPITRE 5 CONCLUSION 160

5.1 Défis et limites méthodologique de l'identification des espèces d'arbres par lidar multispectral 161

5.1.1 Facteurs qui influencent l'applicabilité de la méthode ou la possibilité de calcul des variables 162

5.1.2 Facteurs qui influencent le résultat de l'identification par changement des valeurs des variables 164

5.1.3 Paramètres du classificateur *random forest* qui influencent l'exactitude de l'identification 166

5.2 Conclusions à retenir 168

5.3 Perspectives dans l'identification des espèces par arbre individuel 171

APPENDICE A : CONFUSION MATRICES 174

APPENDICE B : CORRELATIONS BETWEEN FEATURES AND MEAN SCAN ANGLE 177

BIBLIOGRAPHIE 192

LISTE DES FIGURES

Figure Page

Figure 1.1 : Configuration des angles des plans de balayage des trois canaux laser du système Titan de Teledyne Optech. 11

Figure 1.2: Configuration du système lidar multispectral, Titan de Teledyne Optech. GPS : Global Positioning System - Système de positionnement par satellites, SNI : système de navigation inertielle. 12

Figure 1.3 : Nuage de points lidar multispectral à partir de tous les canaux (1ère colonne) et à partir de canaux individuels. Les nuages de points sont représentés en vue latérale (en haut) et vue verticale (en bas). 13

Figure 1.4 : Exemple de variation du nuage de points en fonction des espèces de feuillus. La silhouettes des arbres en haut est tirées de Farrar (1995). Dans le nuage de points multispectral en bas, la taille des points est proportionnelle à l'intensité des retours. 14

Figure 1.5 : Exemple de variation du nuage de points en fonction des espèces de conifères. Les silhouettes des arbres en haut sont tirées de Farrar (1995). Dans le nuage de points multispectral en bas, la taille des points est proportionnelle à l'intensité des retours. 15

Figure 1.6 : Différence entre les nuages de points du lidar multispectral en fonction de la hauteur des arbres entre 3 et 30 mètres. L'impact relatif des seuils de délimitation des retours au sol est montré par des lignes bleues – seuil de 40% et lignes rouges – seuil de 2 mètres. 7

Figure 2.1 : Canopy height model (top), color composite (red: C1, green: C2, blue: C3) of the three-channel MSL first-return intensities of the SC site with a sample of manually delineated crowns (a = Pinus, b = Fraxinus, c = Betula, d = Acer, e = Picea; crown f is severely defoliated), and NDVI of type 1 (NDG1, see Table 2.7)............ 31

Figure 2.2: Canopy height model, color composite (red: C1, green: C2, blue: C3) of the three-channel MSL first-return intensities of the YRF site with a sample of manually delineated crowns (crowns : a = Acer saccharum, b = Pinus resinosa, c = Pinus strobus, d = Picea glauca, e = Picea abies), and NDVI of type 1 (NDG1, see Table 2.7)........ 32

Figure 2.3: Variation of selected variables at the genus level (SC) 49

Figure 2.4: Variation of selected variables at the species level (YRF) 50

Figure 3.1: Height distribution of trees per species in the training samples. 77

Figure 3.2: Frequency of r^2 values from regressions between height and features (3D features in the first row, and intensity features in the second row) for trees of all heights (>= 2 m). 90

Figure 3.3: Frequency of r^2 values from regression between height and features (3D features in first line and intensity features in second line), excluding trees less than 7 m high.. 90

Figure 3.4: Relationship between tree height and the ratio of first returns to all returns, all channels merged. 92

Figure 3.5: Relationship between tree height and the sum of the quadratic coefficients of a fitted surface polynomial on the first returns of all channels. 92

Figure 3.6: Relationship between tree height and the NDVI calculated between the green and the middle IR channels. 93

Figure 3.7: Relationship between tree height and the standard deviation of the slope calculated on the first returns. 93

Figure 3.8: Relationship between the skewness of the intensity distribution of the single returns. 94

Figure 3.9: Example of a complex relationship (between tree height and the 75th percentile of the normalized return heights). 94

Figure 3.10: Example of a complex relationship (between tree height and the mean intensity between the 5th and 95th intensity percentile). 95

Figure 3.11: Performance of different classification strategies (STD, SIF, SIF 7 m, HSC 7, HSC 3) and approaches (T = tree removal, V = variable removal, H = hybrid, HR = hybrid with reduced number of variables). 106

Figure 3.12: Performance of different classification strategies (STD, SIF, SIF 7 m, HSC 7, HSC 3) and approaches (T = tree removal, V = variable removal) calculated by 5 m strata. 107

Figure 4.1: Calculation of net scan angle γ (BAD). β represents the inclination of scanning plane for C1 or C2. BC = ED represents the distance between the nadir line and the interception position (C or D), when mirror scan angle = α........................ 130

Figure 4.2: Example of three point clouds (red : C1, blue: C2, green: C3, intensity: point size) of one Pinus resinosa tree, seen by all four flight lines (first column) and its

corresponding four tree views in each of the individual flight line (columns 2 to 5) seen with specified mean scan angle in C2. 132

Figure 4.3: Distributions of mean scan angle of the tree views by channels (C1, C2 and C3) and species. The gray areas represent mean scan angles not achievable in the respective channel due to the Titan system's configuration. 136

Figure 4.4: Difference in mean scan angle between C1 (green points), C3 (blue points) and C2 (red points) for the same tree view. Mean scan angles in C2 were increasingly ordered.. 140

Figure 4.5: Variations of the feature 3D_SL_1st_p75 (75th percentile of the slope of the first returns in each of the three channels) according to scan angle, and per species. 143

Figure 4.6: Variations of the feature I_PE_1st_p95 (95th percentile of the normalized intensity of the first returns in each of the three channels) according to scan angle, and per species. 144

Figure 4.7: Raw and normalized values for the 95th percentile of intensity in the three channels as a function of mean scan angle.. 147

Figure 4.8 : Raw and normalized values from 90th percentiles of first returns for the three normalized vegetation indices as a function of mean scan angle..................... 148

Figure 4.9: RF species identification accuracy by scan angle class. * Channels used in "3D+intensity" are C321 for 3D and C1, C2, C3, C1_C2, C1_C3, C2_C3 for intensity. 153

LISTE DES TABLEAUX

Tableau Page

Table 2.1: Titan system's laser characteristics..22
Table 2.2: Survey characteristics 25
Table 2.3: Number and height (m) statistics of sample crowns 29
Table 2.4: Return density (returns m^{-2}) above 2 m in tree crowns...........................33
Table 2.5: First return intensities above 2 m at different percentiles in tree crowns ..33
Table 2.6: Description of 3D features (prefix = 3D_)...39
Table 2.7: Description of intensity features (prefix = I_) 41
Table 2.8: Number of features retained at each step of selection (SC).......................46
Table 2.9: Number of features retained at each step of selection (YRF)....................46
Table 2.10 : Selected features (SC)..47
Table 2.11: Selected features (YRF)...48
Table 2.12: Identification OOB error rate (SC) 51
Table 2.13: Identification OOB error rate (YRF) 51
Table 2.14: Confusion matrix in % for C321 at the BL/NL level...............................52
Table 2.15: Confusion matrix in % at the genus level (SC).......................................52
Table 2.16: Confusion matrix in % at the genus level (YRF)....................................53
Table 2.17: Confusion matrix in % at the species level (YRF) 54
Table 3.1: Description of 3D features 79
Table 3.2: Description of intensity features 80
Table 3.3: Threshold selection 88

Table 3.4: Correlation between 3D features and tree height (trees less than 7 m high excluded) ... 97

Table 3.5: Correlation between intensity features and tree height (trees less than 7 m high excluded) ... 99

Table 3.6**:** Random forest classification results ... 105

Table 3.7: Feature selection for the STD, SIF and SIF 7 m classification strategies 108

Table 3.8: Feature selection per height stratum for the HSC7 classification strategy, tree removal approach ... 109

Table 3.9: Feature selection per height stratum for the HSC7 classification strategy, feature removal approach ... 110

Table 3.10: Feature selection per height stratum for the HSC3 classification strategy ... 111

Table 4.1: Tree views mean scan angle statistics in each channel and corresponding scan angle class limits used in the balanced RF classification (all units are degrees). ... 141

Table 4.2: Number and percentage of cases having a correlation (*r*) greater than |±0.2| between mean scan angle and features ... 149

Table 4.3: Number and percentage of cases having a correlation (*r*) greater than |±0.2| between mean scan angle and feature values, by species. ... 150

Table 4.4: Percent of features with a correlation (*r*) greater than |±0.2| between mean scan angle and feature values, by return type and by species. ... 151

Table 4.5: Improvement in accuracy between classifications using normalized intensity features compared to classifications using raw intensity features. Results are presented as overall (2nd column) and by mean scan angle class (columns 3 to 5), for classifications with different feature selection (rows). ... 154

Table A.1: Confusion matrix for C321 at the BL/NL level ... 174

Table A.2: Confusion matrix at the genus level (SC) ... 174

Table A.3: Confusion matrix at the genus level (YRF) ... 175

Table A.4: Confusion matrix at the species level (YRF) ... 176

Table B.1: Correlations between 3D features and mean scan angle ... 177

Table B.2: Correlations between raw intensity features and mean scan angle ... 180

Table B.3 : Correlations between normalized intensity features and mean scan angle ... 186

Table B.4 : Comparison of the classification accuracy capability of different feature categories as a function of scan angle class 191

LISTE DES ABRÉVIATIONS

	Anglais	Français	
3D	Three dimensional	Tri dimensionnel	3D
ABA	Area Based Approach	Approche zonale	
ALS	Airborne Laser Scanning	Balayeur lidar aéroporté	BLA
BL	Broadleaved tree	Feuillu	
CHM	Canopy height model	Modèle de hauteur de la canopée	MHC
DTM	Digital terrain model	Modèle numérique de terrain	MNT
I	Intensity	Intensité	I
ITC	Individual Tree Approach	Approche par arbre individuel	
LAI	Leaf area index	Indice de surface foliaire	ISF
LAD	Leaf area density	Densité de la surface foliaire	
LiDAR	Light Detection and Ranging	Détection et estimation de la distance par la lumière	LiDAR
MSL	Multispectral lidar	Lidar multispectral	LMS
NA	Not Applicable	Non applicable	NA
NDVI	Normalized Difference Vegetation Index	Indice de végétation par différence normalisée	IVDN
NL	Needleleaf tree	Arbre à aiguilles (Conifère)	
OOB	Out-of-bag	Observations non utilisées à la suite du processus bootstrap	OOB
PRF	Pulse repetition frequency	Fréquence de répétition des impulsions	FRI
RGB	Red, green, blue	Rouge, vert, bleu	RVB
RF	Random forest	Forêt aléatoire	
SC	Scarborough, Ontario		
YRF	York Regional Forest, Ontario		

RÉSUMÉ

L'identification de l'espèce est cruciale pour l'inventaire forestier. L'automatisation de la séparation des arbres individuels, de l'identification de leur espèce et de l'évaluation de leurs propriétés, comme la hauteur, peut améliorer la prise de décision dans la gestion forestière. En télédétection, la technique standard pour l'identification des espèces utilise l'information spectrale obtenue avec les images des capteurs passifs multi ou hyperspectraux. Le balayeur laser aéroporté (BLA) monospectral à retours discrets, a une capacité de séparation d'un nombre limité d'espèces (souvent entre feuillus et conifères), avec des variables calculées à partir de la hauteur ou de l'intensité des retours. L'apparition des lidars multispectraux (LMS) offre l'opportunité d'utiliser une information spectrale améliorée par rapport aux balayeurs laser monospectraux, en permettant de réaliser des différences d'intensité entre les canaux, comme des ratios ou des indices normalisés. Le lidar multispectral Titan de Teledyne Optech Inc., issu en 2014, est le premier système aéroporté avec trois lasers intégrés (canaux C1, C2, C3) qui balayent avec des longueurs d'onde différentes (respectivement 1550, 1064, et 532 nm) et différents angles de balayage (respectivement inclinée de 3,5°, 0° et 7° par rapport au plan vertical).

L'objectif de cette étude est de tester l'exactitude de l'identification des espèces d'arbres en utilisant un LMS aéroporté. Les objectifs spécifiques sont d'évaluer : 1) l'amélioration de l'exactitude de l'identification des espèces par rapport à celle obtenue avec un lidar monospectral, 2) l'influence d'une caractéristique de l'arbre, la hauteur, sur l'exactitude de l'identification des espèces et 3) l'influence d'un paramètre de l'enregistrement, l'angle de balayage, sur l'exactitude de l'identification des espèces.

Deux enregistrements ont été acquis dans la région de Toronto, Canada, en différents type de milieux (arbres urbains, en plantation ou en forêt mixte). Pour le premier objectif dix espèces de feuillus et conifères ont été utilisés. Pour les deux derniers objectifs six espèces de conifères en plantation ont été utilisés. L'identification de l'espèce a été réalisée par l'algorithme de forêt aléatoire (*random forest*).

Pour l'objectif 1), les résultats de classification avec des variables 3D et d'intensité calculées à partir de chaque canal séparément (monospectral) ont été comparés à ceux

obtenus avec des variables calculées avec tous les canaux (multispectral). Le LMS a présenté une amélioration significative quand le nombre de classes a été élevé. L'erreur *out-of-bag* a été de 3-5% pour la classification feuillu-conifère, 13%-20% pour sept genres et 24% pour dix espèces. L'exactitude de l'identification de l'espèce peut être améliorée en utilisant le LMS par rapport aux systèmes BLA monospectral, surtout quand la diversité des espèces est assez grande (sept espèces ou plus).

Pour l'objectif 2), malgré la normalisation des variables 3D selon la hauteur de l'arbre, la corrélation de ces variables avec la hauteur de l'arbre reste encore élevée dans certains cas (r^2 jusqu'à 0.6). Pour réduire l'influence de la hauteur de l'arbre dans l'identification de l'espèce, plusieurs stratégies de classification ont été testées a) utiliser toutes les variables, sans stratification en fonction de la hauteur, b) considérer seulement les variables qui ne varient pas en fonction de la hauteur de l'arbre et c) entraîner des classificateurs différents par strate de hauteur. La précision de la stratégie b) a été plus faible, certaines variables utiles étant exclues à cause de leur variation en fonction de la hauteur de l'arbre. La stratégie c) offre une amélioration limitée par rapport à la stratégie a). L'exactitude de la classification a été évaluée en tenant compte de différentes approches pour traiter les arbres pour lesquels il y a des variables qui ne peuvent pas être calculées. Une approche hybride de classification est proposée pour utiliser des variables complexes pour les grands arbres et des variables plus robustes pour les petits arbres.

Pour l'objectif 3), l'influence de l'angle de balayage (jusqu'à 20°) sur l'exactitude de la classification des espèces d'arbres est limitée pour une faible variation d'élévation du terrain (40 m), entre 1% (toutes les variables) et 8% (variables 3D seulement). La normalisation de l'intensité selon la portée améliore l'exactitude avec 8% pour les classifications qui utilisent seulement des variables d'intensité monospectrales (canaux individuels). Cette amélioration décroît (2-4%) quand des variables qui ne changent pas de valeur après la normalisation ont été ajoutées, comme les variables 3D ou les variables d'intensité multispectrales (indices normalisés).

Le LMS est un système de télédétection prometteur, pour extraire de l'information utile pour l'identification des espèces.

Mots clés : identification d'espèce d'arbre, lidar multispectral, intensité, *random forest*, Titan, angle de balayage, hauteur de l'arbre.

Abstract

Species identification is important for forest inventories. Automatizing the isolation of tree crowns, the identification of tree species and the evaluation of tree properties like tree height, might improve decision making in forestry. In remote sensing, the standard technique in species identification uses spectral information from multi or hyperspectral passive sensors. The monospectral aerial lidar scanner with discrete returns (ALS) has a capacity to separate a limited number of species (often between broadleaf and needleleaf), with variables calculated from return heights or return intensities. The development of multispectral lidars (MLS) offers the opportunity to use an improved spectral information compared to monospectral ALS, by allowing to realise the difference of intensities between channels, like ratios and normalised indices. The multispectral Lidar Titan of Teledyne Optech Inc., issued in 2014, is the first system that incorporates three laser (channels C1, C2, C3) that scan with different wavelengths (respectively 1550, 1064 and 532 nm) and different scan angles (respectively 3.5°, 0° and 7°, compared to the vertical plane).

The objective of this study is to test the accuracy of tree species identification using an aerial MLS. The specific objectives are to evaluate: 1) the improvement of the accuracy of tree species identification compared to that obtained using a monospectral lidar, 2) the influence of a tree characteristic, the tree height, on the accuracy of tree species identification and 3) the influence of an acquisition parameters, the scan angle, on the accuracy of tree species identification.

Two datasets were acquired in the Toronto region, Canada, in different environments (urban trees, tree plantations or mixed forest). For the first objective, ten broadleaf and needleleaf species were used. For the two last objectives six needleleaf trees in a plantation were used. Species identification was realised through a random forest algorithm.

For the objective 1), the classification results with 3D and intensity features computed from individual channels (monospectral) were compared to those obtained from features computed with all channels (multispectral). The MLS presented a significant improvement when the number of classes was high. The out-of-bag error was 3-5% for the needleleaf/broadleaf classification, 13% - 20% for seven genera and 24% for 10 species. The tree species accuracy can be improved using a MLS compared to a monospectral ALS, mainly when the species diversity is fairly high (seven species or more).

For the objective 2), despite the normalisation of the 3D features for tree height, feature correlation to tree height remains elevated in certain cases (r^2 up to 0.6). To reduce the influence of tree height in species identification, several classification strategies were tested a) using all features, without stratification according to tree height, b) considering only features that do not vary according to tree height, and c) training several classifiers for each height stratum. The accuracy of b) strategy was low, because several useful features were discarded because of their correlation to tree height. The strategy c) offers a limited improvement compared to strategy a). The classification accuracy was evaluated considering different approaches to process trees that had incomputable features. A hybrid classification approach is proposed to use complex features for large trees and robust features for smaller trees.

For objective 3), the influence of scan angle (up to 20°) on the tree classification accuracy is limited for a small variation in terrain altitude (40 m), between 1% (all features) and 8% (3D features only). The intensity normalisation according to the range improved with 8% the accuracy for the classifications that used only monospectral intensity features (individual channel intensities). This improvement decreased (2-4%) when features that are not affected by intensity normalisation were added, like 3D features or multispectral intensity features (normalised indices).

The MLS is a promising remote sensing system to provide useful information to tree species identification.

Keywords: tree species identification, multispectral lidar, intensity, random forest, Titan, scan angle, tree height.

CHAPITRE 1

INTRODUCTION

1.1 Importance de l'identification de l'espèce

Dans un contexte de mondialisation, de pression accrue sur la ressource forestière et d'avancement technologique, la demande de précision de l'inventaire forestier ainsi que l'exigence de réduction de coûts de l'inventaire deviennent des enjeux majeurs.

Dans une perspective économique, l'identification de l'espèce d'arbre est une information essentielle dans l'industrie forestière pour l'évaluation de la possibilité forestière (Tompalski *et al.* 2014), pour une meilleure prédiction de la production forestière par modèle de croissance (Falkowski *et al.* 2010), pour la gestion et la planification des traitements forestiers et des coupes et pour une meilleure planification de l'utilisation appropriée du bois (Wulder *et al.* 2008). L'identification de l'espèce des jeunes arbres est très importante pour le suivi des plantations, pour distinguer entre les arbres plantés et la régénération naturelle et pour évaluer la régénération après le feu (Wing, Eklund et Sessions 2010) ou après une épidémie.

Dans une perspective environnementale et écologique, l'espèce est aussi très importante dans l'évaluation du stock du carbone (Jenkins *et al.* 2003 ; Koch 2010 ; Vesterdal *et al.* 2013), de la biodiversité et de l'habitat faunique (Bradbury *et al.* 2005 ;

Goetz *et al.* 2007). La connaissance de l’espèce d’arbre est importante pour pouvoir établir des mesures contre la propagation des épidémies d’insectes ou fongiques (McKenney *et al.* 2003 ; Solberg *et al.* 2006), pour contrer la prolifération des espèces invasives ou pour mieux prévenir les feux de forêt (Mutlu *et al.* 2008). Connaître l’espèce permet aussi d’évaluer d’autres propriétés plus complexes comme le stress de l’arbre relié à la sécheresse, à la déficience de nutriments ou aux effets pernicieux des insectes ravageurs. Enfin, la connaissance de l’espèce est importante pour prédire la résilience du peuplement forestier face aux changements climatiques et pour produire les rapports internationaux de gaz à effet de serre (Rosenqvist *et al.* 2003).

1.2 Utilisation de l’information spectrale ou structurale obtenue par télédétection pour l’identification de l’espèce par arbre individuel

Généralement, dans l’inventaire forestier, l’identification de l’espèce est réalisée sur le terrain. Malheureusement, cette méthode est trop onéreuse et peu pratique sur des surfaces forestières étendues ou difficilement accessibles. Dès lors, l’identification des espèces est réalisée seulement sur des placettes échantillon. Alors, pour réaliser les cartes forestières, on emploie différentes méthodes d’extrapolation. Généralement, les inventaires forestiers utilisent la stratification, soit la délimitation des zones homogènes (selon le peuplement, les conditions géomorphologiques ou climatiques) qui pourraient subir un même traitement. Il s’agit d’une identification au niveau du peuplement défini comme un pourcentage sur une certaine surface qu’elle soit définie comme polygone (Sasaki *et al.* 2012), comme placette (Van Ewijk *et al.* 2014) ou comme pixel (Dalponte, Bruzzone et Gianelle 2012). Le plus souvent, cette délimitation est réalisée par photo-interprétation ou par classification automatique des zones homogènes. La composition des espèces identifiées dans les placettes échantillon est attribuée alors à l’ensemble du peuplement délimité (Berger, Leboeuf et Pomerleau 2015). En conséquence, le plus souvent, les inventaires forestiers sur grandes surfaces enregistrent l'estimation de pourcentage des espèces dominantes dans un peuplement délimité spatialement par un polygone.

Avec l'augmentation de la résolution des données acquises par la télédétection, l'identification de l'espèce devient de plus en plus précise, en passant d'une identification au niveau du peuplement à une identification par arbre individuel. L'identification des espèces n'est univoque qu'au niveau de l'arbre individuel. Cependant, pour qu'une telle identification se fasse correctement, il faut suffisamment d'information pour chaque arbre.

L'identification par arbre individuel devient opérationnelle grâce aux progrès technologiques tant au niveau de la cueillette de données qu'à celui de leur traitement. En effet, l'augmentation de la résolution des données acquises par la télédétection sur différents types de plateformes (satellites, avions, drones ou terrestres), la diversification du type de capteurs utilisés (imagerie passive multispectrale ou hyperspectrale, imagerie active par lidar ou radar), l'augmentation de précision des systèmes de positionnement par satellite (Global Navigation Satellite System, GNSS) et des systèmes de navigation inertielle (INS), ainsi que la capacité des ordinateurs à stocker et à traiter de larges bases de données à l'aide d'algorithmes de classification (apprentissage par ordinateur, réseaux de neurones), permettent d'établir une cartographie de la ressource forestière de plus en plus détaillée et sur des territoires chaque fois plus vastes.

Même si la technologie actuelle permet d'envisager une cartographie à l'échelle de l'arbre individuel sur des territoires immenses (possiblement sur l'ensemble de la planète), il y a actuellement peu de régions où l'approche par arbre individuel est appliquée de manière opérationnelle dans l'inventaire forestier et peu d'études ont également pris en compte des surfaces vastes (Perron 2018). Si un tel inventaire à l'échelle de l'arbre individuel est techniquement possible, la principale limitation est financière. Techniquement, ces contraintes entraînent un compromis entre résolution spatiale, spectrale et temporelle, dimensions de la surface cartographiée et du temps de traitement. Puisque la couverture spatiale et la résolution d'un capteur sont inversement reliées, les acquisitions sur des surfaces étendues n'ont souvent pas la précision optimale requise pour l'identification des espèces des arbres individuels.

Pour l'identification des espèces, plusieurs études ont comparé les avantages et les désavantages entre l'approche par arbre individuel et l'approche zonale (Latifi *et al.* 2015 ; Næsset *et al.* 2004 ; Ørka *et al.* 2013). D'ailleurs, plusieurs variables utilisées dans l'approche par arbre individuel pour la reconnaissance des espèces ont été d'abord développées pour une approche zonale, optique ou lidar. Le passage de l'approche zonale à l'approche par arbre individuel s'est fait graduellement; surtout grâce à l'augmentation de la résolution et à l'accélération des processus de traitement.

Une grande diversité de variables a été utilisée pour identifier l'espèce d'arbres par télédétection, que ce soit à partir de l'information spectrale (différence de réflectance) ou structurale (forme de la couronne ou type, taille, densité et regroupement du feuillage). Ces variables ont été définies à partir de capteurs passifs (image multispectrale ou hyperspectrale) ou actifs (lidar, SAR), ayant différentes résolutions et ayant été acquis à partir de différentes plateformes (satellite, aéroporté, drone ou capteurs terrestres) (revue de littérature : Fassnacht *et al.* 2016).

En télédétection, les principales variables spectrales et structurales qui servent à l'identification des espèces ont été définies différemment en fonction de la méthode ou du type du capteur utilisé. Par exemple, pour la photo-interprétation, méthode qui a été longtemps la principale approche opérationnelle et qui reste encore une référence pour la validation (Parkan 2019), ces variables ont été définies pour servir à une reconnaissance visuelle (Avery 1978 ; Heller, Doverspike et Aldrich 1964 ; Hershey et Befort 1995 ; Sayn-Wittenstein 1960).

La signature spectrale des espèces a été définie par la réflectance dans chaque longueur d'onde du spectre visible et infrarouge. Les différences de réflectance dans chaque longueur d'onde servent à identifier les espèces. Les différents capteurs passifs ou actifs réalisent différents types d'échantillonnages du spectre. La résolution spectrale d'un capteur est donnée par le nombre de bandes ou de canaux et par la largeur spectrale de chaque bande ou canal. Une bonne résolution spectrale aide à distinguer les espèces qui présentent seulement de petites différences dans la signature spectrale. Mais la très grande variabilité spectrale d'une même espèce et un chevauchement des signatures spectrales entre les espèces pose des problèmes d'identification (Leckie *et al.* 2017). Pour des capteurs avec une faible résolution spectrale (quelques bandes à large spectre), par exemple pour les capteurs passifs panchromatiques (image noir et blanc) ou multispectraux (4 à 8 bandes), la capacité discriminative est limitée (Parkan 2019). Les images hyperspectrales ont l'avantage d'avoir une haute résolution spectrale (plusieurs bandes à un spectre étroit), ce qui permet de détecter des caractéristiques des espèces qui se distinguent juste dans des portions étroites du spectre (Pant *et al.* 2013 ; van Aardt et Wynne 2007).

Les capteurs actifs, comme le lidar, enregistrent une signature spectrale sur une portion très étroite du spectre parce qu'ils utilisent une seule longueur d'onde (lidar monospectral, le plus souvent 1064 nm), ou plusieurs longueurs d'onde (lidar multispectral, par exemple 1064 nm, 1550 nm, 553 nm dans le cas du Titan de Teledyne Optech, utilisé dans cette étude). Le désavantage est qu'il n'est pas possible d'isoler une information stricte sur la réflectance du feuillage parce que l'énergie réfléchie dépend aussi de la taille des feuilles par rapport à l'empreinte au sol. Cela rend difficile l'utilisation des bases de données préexistantes sur la signature spectrale. Par conséquent, il faut définir des « signatures » spécifiques pour le lidar, qui prennent en compte aussi bien la réflectance que la taille des feuilles.

Les acquisitions multi temporelles ont pour but de pallier à une résolution spectrale insuffisante, en profitant de la différence de phénologie (Bolyn *et al.* 2018 ; Liu *et al.* 2018b ; Persson, Lindberg et Reese 2018 ; Pu, Landry et Yu 2018 ; Sheeren *et al.* 2016). Les données lidar, enregistrées avec et sans feuillage, ont été utilisées conjointement pour la reconnaissance des espèces (Brandtberg 2007 ; Kim *et al.* 2009 ; Ørka, Næsset et Bollandsås 2010).

L'utilisation des images multi et hyperspectrales souffrent de quelques désavantages, reliés surtout à la nécessité de devoir réaliser des corrections radiométriques et géométriques pour pallier aux différentes conditions d'illumination (météo, élévation du soleil) et d'enregistrement (comme l'angle de vue) (Schaepman-Strub *et al.* 2006). Également, la présence des zones ombragées dans les images multi et hyperspectrales représente une des problématiques importantes pour l'utilisation de la signature spectrale dans la reconnaissance de l'espèce. Dans le cas du lidar, on considère qu'il s'affranchit de la variabilité des conditions extérieures d'illumination, parce qu'il illumine lui-même l'objet. En plus, le problème posé par les différences spectrales entre les zones ombragées et les zones ensoleillées des couronnes n'affecte pas les signatures obtenues avec des données lidar.

Chez les capteurs passifs, une partie de cette information est donnée par la texture de la couronne. Toutefois, cette information varie en fonction de l'angle de vue des images ou peut être déformée après le processus d'orthorectification. Dernièrement, avec les nouvelles technologies de stéréo correspondance, les nuages de points photogrammétriques obtenus à partir des images de l'optique passive nous donnent eux aussi une bonne information structurale de l'arbre.

Le désavantage des images des capteurs passifs est qu'elles fournissent une information seulement à partir de la partie supérieure et extérieure de l'arbre. Le pouvoir de pénétration de ces capteurs est limité et superficiel, il éclaire fort peu sur les aspects de l'arbre qui sont dissimulés sous le feuillage; spécialement si celui est dense. En revanche, l'impulsion laser a une plus grande capacité de pénétration à travers le feuillage. Par conséquent, elle fournit une information répartie sur l'ensemble de la couronne. Cependant, l'intensité de l'impulsion décroît progressivement en fonction de la densité du feuillage, ce qui rend difficile la calibration des deuxièmes et troisièmes retours dans le but de retrouver une valeur de réflectance (Okhrimenko, Coburn et Hopkinson 2019).

D'autre part, l'information structurale issue des capteurs actifs enregistre des variables représentatives concernant la forme de la couronne, ou la texture, la densité et le regroupement du feuillage. Aujourd'hui, avec l'augmentation de la résolution et du niveau de détail enregistré, alors que les différents capteurs actifs, comme le lidar, enregistrent des données avec un niveau de détail de plus en plus fin sur la structure de l'arbre, cette information gagne en importance aux dépens de l'information de type spectrale.

Le lidar n'est pas un capteur spécialement conçu pour l'identification des espèces. Toutefois, s'il existe un intérêt dans cette approche en foresterie, cela tient au fait qu'on estime qu'il est possible d'associer précisément les informations, qui peuvent être extraites par le lidar (localisation et délimitation des couronnes d'arbres, estimation des hauteurs), et l'espèce, sans pour cela recourir à des sources de données additionnelles (imagerie optique passive). Cela peut représenter une réduction des coûts et une réduction des erreurs de correspondance entre les identifications d'un même arbre à partir de sources de données différentes. Ces erreurs de correspondance sont principalement causées par des erreurs de géoréférencement et de corrections géométriques.

Parmi les premières études à mettre en évidence la possibilité de l'identification de l'espèce à partir du nuage de points lidar monospectral on peut citer celle de Brandtberg *et al.* (2003), de Holmgren et Persson (2004) et de Moffiet *et al.* (2005). L'augmentation de la précision et de la stabilité de l'information sur l'intensité du lidar monospectral améliore la classification, mais atteint aussi une limite. Parmi les premières études à mettre en évidence l'importance de l'intensité dans la reconnaissance de l'espèce on mentionne Holmgren et Persson (2004). Le lidar monospectral à retours discrets a été utilisé généralement pour classifier un nombre restreint d'espèces, le plus souvent entre deux (feuillus/conifères) et quatre. L'exactitude de l'identification entre 70% et 98% a été obtenue dans différentes études (Harikumar, Bovolo et Bruzzone 2017 ; Holmgren et Persson 2004 ; Holmgren, Persson et Söderman 2008 ; Kim *et al.* 2009 ; Ko, Sohn et Remmel 2013 ; Korpela *et al.* 2010b ; Li, Hu et Noland 2013 ; Lin et Hyyppä 2016 ; Ørka, Næsset et Bollandsås 2009 ; Ørka, Næsset et Bollandsås 2010 ; Suratno, Seielstad et Queen 2009 ; Vauhkonen *et al.* 2009). Peu d'études ont testé l'exactitude d'identification pour un nombre élevé d'espèces, en obtenant une plus faible exactitude, par exemple 63% pour 10 espèces (Rana *et al.* 2020). L'exactitude de classification varie en fonction du nombre d'espèces, de la densité de retours lidar, de la complexité des variables utilisées et de l'algorithme utilisé pour la classification. Pourtant, une limite est atteinte dans le nombre et l'exactitude de l'identification des espèces avec le lidar monospectral à retours discrets.

Certaines recherches se sont penchées vers le lidar à forme d'onde complète qui a l'avantage de conserver plus d'information structurale. Ce système enregistre toute l'énergie réfléchie d'un retour et permet d'avoir un échantillonnage complet du profil de la végétation. L'ajout de cette information peut améliorer l'identification des espèces. Néanmoins, elle nécessite beaucoup de prétraitement, avant de pouvoir appliquer un algorithme de détection de l'espèce (Blomley *et al.* 2017 ; Cao *et al.* 2016 ; Heinzel et Koch 2011 ; Heinzel et Koch 2012 ; Hovi *et al.* 2016 ; Li, Hu et Noland 2013 ; Lindberg *et al.* 2014 ; Vaughn, Moskal et Turnblom 2012 ; Yao, Krzystek et Heurich 2012 ; Yu *et al.* 2014 ; Zhou *et al.* 2018).

D'autres études ont cherché à améliorer l'identification des espèces par l'analyse combinée de plusieurs capteurs, entre l'information de haute qualité spectrale (images passives multi ou hyper spectrales) avec la précision de l'information structurale (lidar monospectral). Beaucoup d'études et des applications opérationnelles utilisent le lidar monospectral et la photographie multispectrale (Brandtberg 2007 ; Dalponte *et al.* 2014 ; Deng *et al.* 2016 ; Dinuls *et al.* 2012 ; Fang *et al.* 2018 ; Heinzel et Koch 2012 ; Holmgren, Persson et Söderman 2008 ; Kim *et al.* 2009 ; Korpela *et al.* 2009 ; Koukoulas et Blackburn 2005 ; Ørka *et al.* 2013 ; Ørka *et al.* 2012 ; Puttonen, Litkey et Hyyppä 2010 ; St-Onge, Audet et Bégin 2015 ; Sugumaran et Voss 2007 ; Suratno, Seielstad et Queen 2009 ; Törmä 2000 ; Vauhkonen *et al.* 2009 ; Zhang *et al.* 2016). Pour extraire encore plus d'information sur les espèces, certaines études proposent une analyse combinée entre lidar monospectral et imagerie hyperspectrale (Fricker *et al.* 2019 ; Liu *et al.* 2017 ; Marrs et Ni-Meister 2019 ; Shi *et al.* 2018a ; Sugumaran et Voss 2007). D'autres études récentes proposent d'utiliser le lidar multispectral et des nuages de points photogrammétriques issus des images multispectrales (Kukkonen *et al.* 2019a ; Kukkonen *et al.* 2019b). Les désavantages de ces techniques concernent principalement les erreurs issues des corrections géométriques des images passives et des erreurs de correspondance des couronnes d'arbres entre le lidar et l'imagerie passive. En plus, faire l'acquisition et le traitement d'information provenant de plusieurs capteurs différents accroit les coût considérablement.

1.3 Lidar multispectral

Le lidar monospectral est utilisé dans l'inventaire forestier de précision surtout pour l'extraction de l'information structurelle, issue de l'analyse de la distribution 3D du nuage de points. Le lidar multispectral répond à une tendance actuelle d'intégration de l'information spatiale et spectrale dans la reconnaissance de l'espèce. L'avantage d'obtenir de l'information spectrale à partir des données lidar pour la classification des espèces est d'avoir cette information associée avec une géolocalisation précise dans la canopée et indépendante des facteurs externes comme l'ensoleillement (sans ombrage). L'innovation technologique de ce type de système par rapport à un lidar monospectral consiste dans l'ajout d'un ou de deux canaux laser de longueurs d'onde différente, qui partagent tous le même système de géolocalisation par GPS et d'orientation par un système de navigation inertielle (SNI) (Figure 1.2). Ainsi, en plus d'augmenter la densité du nuage de points 3D, on améliore la qualité de l'information spectrale acquise. L'identification de l'espèce est bonifiée par la possibilité d'utiliser les différences entre les canaux ayant différentes longueurs d'onde et par le calcul des ratios, des indices de végétation normalisés ou par la réalisation d'images composées colorées. Le lidar à deux longueurs d'onde (1064 nm et 532 nm), le SHOALS (Guenther 1985), a été premièrement conçu pour la bathymétrie des zones côtières (Irish et Lillycrop 1999). Le VQ-1560i-DW de RIEGL (Riegl 2017), avec les deux mêmes longueurs d'onde, mais avec une configuration différente d'angle de balayage et de discrétisation du signal, a été utilisé davantage pour les applications en foresterie et notamment pour l'identification de l'espèce (Pilarska et Ostrowski 2019). Le Titan de Teledyne Optech, issu en 2014, a été conçu pour répondre à la fois aux besoins de la bathymétrie et de la topographie, ainsi que de cartographie forestière. Il partage des caractéristiques similaires avec les deux autres systèmes, mais possède en outre une troisième longueur d'onde. Ces trois canaux ont des plans de balayage différents, séparés par 3,5 degrés. Le canal 2 (C2), à 1064 nm balayant à la verticale est équivalent d'un lidar monospectral. Le plan de balayage du canal 1 (C1), à 1550 nm, est incliné vers l'avant à 3,5 degrés et celui du canal 3 (C3), à 553 nm, de 7 degrés (Figure 1.1). Cette configuration résulte dans une distribution de lignes de balayage couvrant le mieux la surface scannée (Figure 1.2). Mais, en même temps, elle ne permet pas d'avoir une information spectrale équivalente dans les trois canaux, c'est-à-dire à partir du même objet, avec une même perspective et avec la même résolution spatiale. La Figure 1.3 est un exemple de la différence entre les trois nuages de points issus des trois canaux du Titan, en vue latérale et verticale.

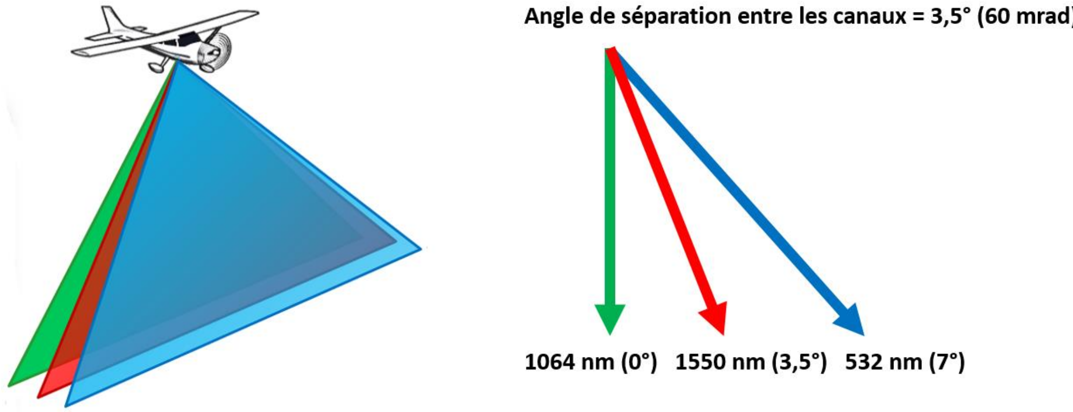

Figure 1.1 : Configuration des angles des plans de balayage des trois canaux laser du système Titan de Teledyne Optech.

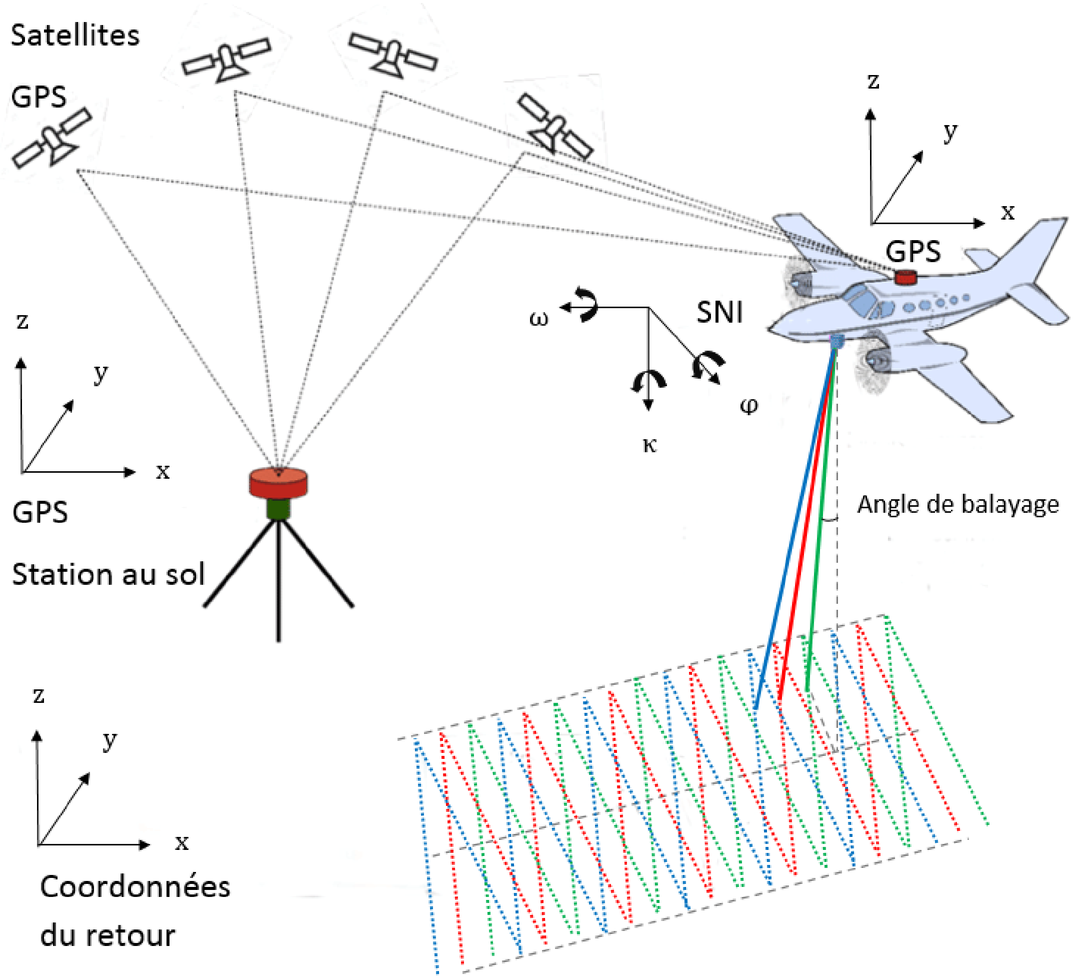

Figure 1.2: Configuration du système lidar multispectral, Titan de Teledyne Optech. GPS : Global Positioning System - Système de positionnement par satellites, SNI : système de navigation inertielle.

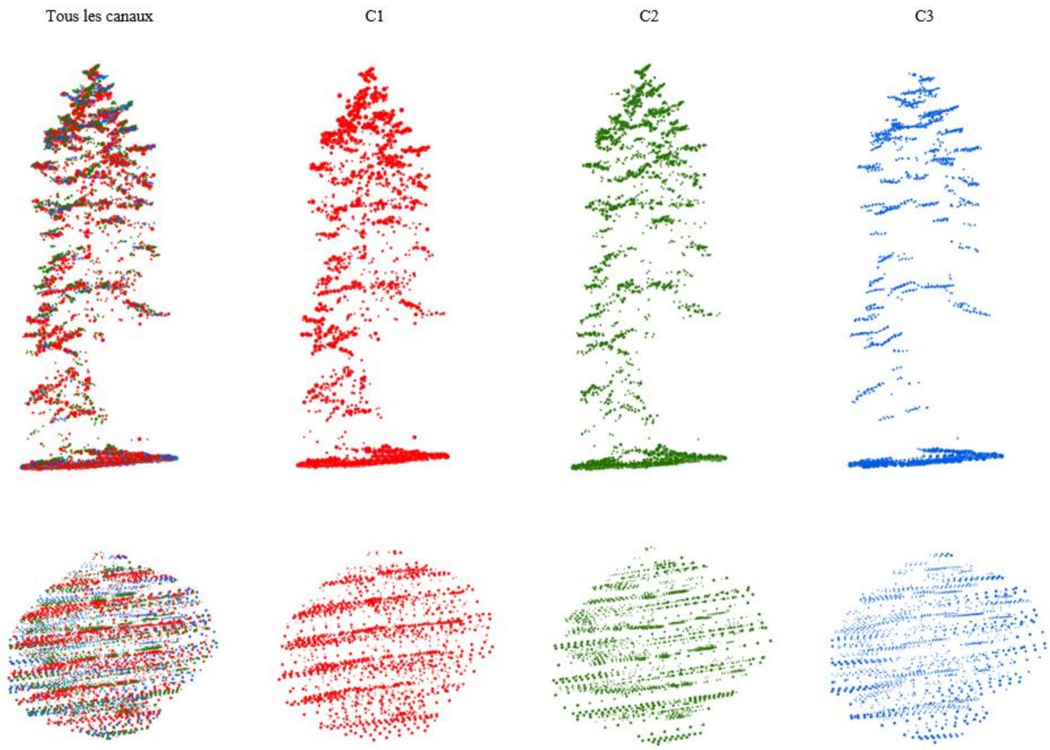

Figure 1.3 : Nuage de points lidar multispectral à partir de tous les canaux (1ère colonne) et à partir de canaux individuels. Les nuages de points sont représentés en vue latérale (en haut) et vue verticale (en bas).

La plupart des études faites avec les données recueillies par le capteur Titan se sont penchées sur la question de la classification de l'utilisation du sol (Matikainen, Hyyppä et Litkey 2016 ; Shaker, Yan et LaRocque 2019 ; Zou *et al.* 2016). Peu d'études ont testé les vertus de cette imagerie pour l'identification des espèces (Ahokas *et al.* 2016 ; Axelsson, Lindberg et Olsson 2018 ; Yu *et al.* 2017). Les Figures 1.4 et 1.5 représentent respectivement des exemples de nuages de points obtenus avec le lidar multispectral Titan pour des espèces de feuillus et des conifères.

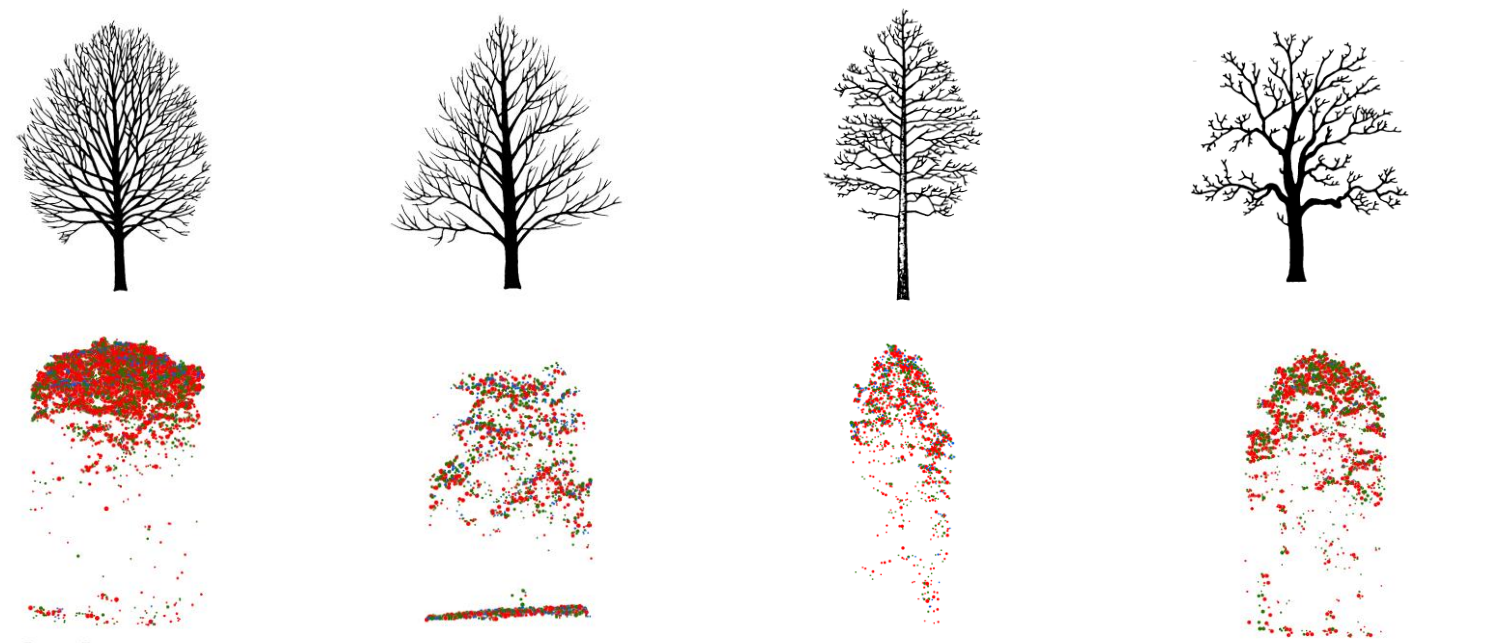

Érable à sucre *Acer saccharum* | Frêne d'Amérique *Fraxinus americana* | Peuplier faux-tremble *Populus tremuloides* | Chêne rouge *Quercus rubra*

Figure 1.4 : Exemple de variation du nuage de points en fonction des espèces de feuillus. La silhouettes des arbres en haut est tirées de Farrar (1995). Dans le nuage de points multispectral en bas, la taille des points est proportionnelle à l'intensité des retours.

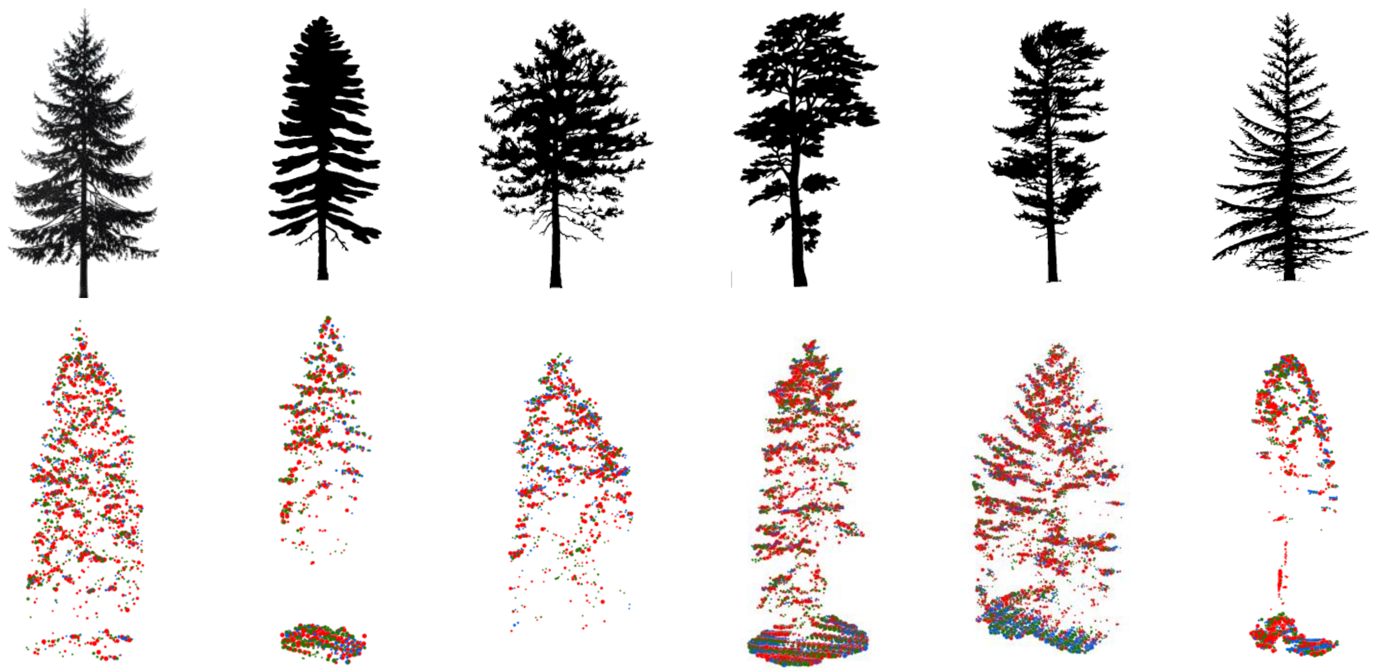

Figure 1.5 : Exemple de variation du nuage de points en fonction des espèces de conifères. Les silhouettes des arbres en haut sont tirées de Farrar (1995). Dans le nuage de points multispectral en bas, la taille des points est proportionnelle à l'intensité des retours.

.

1.4 Étapes méthodologiques utilisées pour l'identification de l'espèce par arbre individuel

L'identification de l'espèce par arbre individuel comporte généralement trois étapes, 1) la délimitation de l'espace occupé par la couronne et l'extraction de l'information correspondante, nuage de points ou pixels, 2) le calcul des variables représentatives des propriétés spectrales ou structurelles de l'arbre et 3) la classification des espèces par un algorithme automatique. Nous allons présenter ces trois étapes et comparer différentes techniques pour leur réalisation. Plusieurs revues de littérature au sujet des méthodes utilisées dans la délimitation et l'identification des espèces par arbre individuel, ainsi que des comparaisons entre différentes technologies ont été réalisées par Fassnacht *et al.* (2016) et par Lindberg et Holmgren (2017).

1.4.1 Étape 1 : Délimitation des couronnes

La délimitation des couronnes d'arbres individuels peut être modélisée à partir des données recueillies sur terrain à l'aide du GPS. Cependant, l'échantillonnage sur le terrain est un effort onéreux (temps et argent); il est, de plus, limité par l'accessibilité. La délimitation des couronnes d'arbres individuels par des moyens de télédétection peut être réalisée aussi manuellement par photo-interprétation de paires d'images stéréoscopiques suivie d'une numérisation 3D. Mais cette technique demande également beaucoup de temps de traitement et l'exactitude est tributaire de l'expertise du photo-interprète.

Certains algorithmes, comme la délimitation de bassins versants (Beucher et Meyer 1993), ont été appliqués pour la segmentation des couronnes à partir d'images multispectrales (Leckie *et al.* 2017). Néanmoins, ces algorithmes ont des limitations causées par les déformations géométriques dues au changement de l'angle de vue du capteur ou à la différence spectrale entre la zone ensoleillée et celle ombragée d'une même couronne. La précision de cette méthode est aussi largement influencée par la résolution de l'image.

La délimitation des couronnes peut être réalisée automatiquement à partir des données lidar, qui ne présentent pas les limitations mentionnées précédemment pour les capteurs passifs. Par contre, les algorithmes proposés et le taux de détection dépendent largement de la densité des points. Deux méthodes ont été principalement employées avec des données lidar, soit une segmentation en 2D à partir du modèle de hauteur de la canopée (MHC), soit une délimitation en 3D à partir du nuage de points.

La méthode la plus souvent utilisée est une délimitation 2D à partir du MHC (Persson, Holmgren et Söderman 2002). La première étape consiste à localiser la cime des arbres individuels à l'aide des algorithmes de détection des maxima locaux en utilisant le MHC (Popescu, Wynne et Nelson 2002), ou directement à partir du nuage de points (Vega *et al.* 2014). La deuxième étape délimite la couronne en employant des algorithmes par croissance de région (Brandtberg *et al.* 2003 ; Hyyppä et Inkinen 1999 ; Hyyppä *et al.* 2001 ; Maltamo *et al.* 2004), par délimitation de bassin versant (Heinzel et Koch 2012 ; Koch, Heyder et Welnacker 2006), ou par segmentation par la reconnaissance de forme (Brandtberg *et al.* 2003). Cette méthode prend seulement en compte les couronnes dominantes et ignore la complexité 3D des arbres dominés. Elle peut être appliquée à partir des densités relativement faibles comparées aux densités nécessaires pour une délimitation 3D. Par exemple, les premières études avec détections des arbres individuels ont commencé avec une densité de 0,5 premiers retours par m^2 pour les arbres matures (Popescu, Wynne et Nelson 2002). Une délimitation 2D a été aussi proposée directement à partir du nuage de points lidar (Lee *et al.* 2010).

Pour éliminer les retours au sol et sur la végétation de sous-bois, une approche largement utilisée est celle du seuillage (*threshold*) appliqué sur le nuage de points délimités en 2D. De cette façon est obtenue une délinéation plus proche de l'espace 3D occupé par la couronne de l'arbre. Le plus souvent, un seuil à hauteur fixe par rapport au modèle numérique de terrain (MNT) est utilisé, par exemple 2 mètres (Shi *et al.* 2018b ; Yu *et al.* 2017). Par ailleurs, certaines études proposent un seuil variable, comme pourcentage en fonction de la hauteur de l'arbre (Hovi *et al.* 2016 ; Korpela *et al.* 2010b).

Finalement, une délimitation 3D a l'avantage de prendre en compte la complexité du couvert forestier, mais demande beaucoup de ressources computationnelles, notamment en mémoire et en temps de calcul (Hamraz, Contreras et Zhang 2017 ; Holmgren, Persson et Söderman 2008 ; revue de littérature: Lindberg et Holmgren 2017). Avec une densité encore plus grande (170 points/m^2), il est possible de délimiter les arbres en 3D, tout en prenant en compte les petits arbres en dessous de la canopée (Hamraz, Contreras et Zhang 2017). Les approches de délimitation 3D utilisent soit une segmentation directement à partir du nuage de points, comme les *alpha-shapes* (Holmgren, Persson et Söderman 2008), soit des algorithmes d'agglomération (Lindberg *et al.* 2014), soit à travers un espace voxelisé (Reitberger *et al.* 2009).

Les principaux défis de la délimitation automatique des couronnes sont reliés à la différence de taille, de forme et de statut des arbres, ce qui empêche l'utilisation des mêmes paramètres de segmentations pour tous les cas. La forme de l'arbre est différente pour chaque espèce, donc appliquer un algorithme de délinéation avec les mêmes paramètres pour toutes les espèces pourrait créer des erreurs systématiques de délinéation pour une espèce donnée. Il est donc recommandé de choisir des paramètres capables de tenir compte de la diversité à l'intérieur d'une population. Ces erreurs s'ajoutent à celles de l'identification de l'espèce. Peu d'études ont testé le processus complet de délimitation automatique et d'identification des espèces (Leckie *et al.* 2017), parce qu'il est difficile de faire la distinction entre l'erreur qui provient de l'algorithme d'identification des espèces de celui qui provient de l'algorithme de délimitation des couronnes d'arbres.

La qualité de la délimitation de l'espace 3D occupé par les couronnes d'arbres a une influence considérable sur la valeur des variables calculés à partir des nuages de points extraits de cet espace. L'inclusion des retours provenant des arbres voisins, des petits arbres opprimés ou de la végétation de sous-bois peuvent produire un changement significatif dans les valeurs des variables et, par conséquent, influencer l'exactitude de l'identification de l'espèce.

1.4.2 Étape 2 : Calcul des variables

Les études sur la classification des arbres à l'aide du lidar aéroporté ont développé un nombre élevé de variables différentes à partir de la hauteur des retours (variables 3D) ou à partir de l'intensité (variables I). Ce chapitre présente les principaux types de variables et les facteurs qui influencent leurs valeurs ou leur possibilité de calcul, comme les caractéristiques de l'arbre ou les propriétés de l'enregistrement lidar.

Parmi les variables 3D, nous mentionnons principalement deux types. Les variables qui servent à retrouver les dimensions de l'arbre, comme sa hauteur, la dimension de sa couronne, la longueur de la cime, sont obtenues à partir des hauteurs des retours au-dessus du modèle numérique de terrain. Ces variables lidar sont très importantes pour calculer différentes variables forestières, comme le volume de bois, la biomasse, l'indice de surface foliaire. Cependant, utilisé pour l'identification de l'espèce, ce type de variables pourrait introduire un biais de classification en créant une association entre la hauteur de l'arbre et l'espèce. Ce biais pourrait être d'autant plus grand si, dans l'échantillon d'entraînement, les classes de hauteur d'arbres n'étaient pas équilibrées entre les espèces. Alors, pour éviter ce type de biais dans la classification, plusieurs études proposent une normalisation de ces variables en fonction de la hauteur de l'arbre (Ørka, Næsset et Bollandsås 2009). Ørka, Næsset et Bollandsås (2009) remarquent l'importance de vérifier si la normalisation des variables 3D par rapport à la hauteur de l'arbre produit réellement des variables indépendantes par rapport à la hauteur de l'arbre. Pourtant, même normalisées, plusieurs variables présentent une certaine corrélation avec la hauteur de l'arbre, justement parce que les caractéristiques morphologiques de l'arbre changent en fonction de la hauteur, selon ses étapes de développement (Millet 2012).

La sélection des variables dans un classificateur est influencée par la distribution des espèces par classe de hauteur (Ørka, Næsset et Bollandsås 2009). D'autre part, certaines études soulignent justement que l'information sur la hauteur de l'arbre est importante dans la classification parce qu'elle est significative pour ce changement structural et spectral de l'arbre dans son développement (Jones, Coops et Sharma 2010). Pourtant, il n'est pas du tout évident comment on peut utiliser l'information sur la hauteur de l'arbre pour améliorer la classification sans, en même temps, introduire de biais d'association hauteur-espèce. Plusieurs études ont proposé des solutions différentes, mais nulle n'a apporté de solution universellement acceptée.

La densité d'échantillonnage influence la qualité du nuage de points et permet ou non le calcul de certaines variables, en fonction aussi de leur complexité. Par exemple, une faible densité de points peut amener à l'impossibilité de calculer même des variables 3D très simples comme la dispersion des retours dans la couronne. En contrepartie, une haute densité de points permet de calculer des variables très complexes, par exemple, l'information sur l'angle et la structure des branches (Harikumar, Bovolo et Bruzzone 2017 ; Ko, Sohn et Remmel 2013). Néanmoins, la haute densité d'échantillonnage impose des limites en termes de coûts, stockage et temps de traitement.

Les premières études sur l'identification des espèces mettent en évidence la possibilité d'utiliser l'analyse de la distribution des points lidar et l'extraction de la forme extérieure du nuage de points lidar à retour discret pour distinguer entre un nombre limité d'espèces, principalement entre feuillu et conifères. Les études ultérieures, utilisant des densités des points plus élevées ont proposé des variables plus complexes, basées sur des algorithmes d'analyse de nuage de points. Certaines variables 3D donnent une évaluation de la pénétration de l'impulsion laser à travers la couronne par des statistiques sur la distribution des points dans l'ensemble de l'arbre ou en différentes parties de l'arbre. Parmi ces variables nous pouvons mentionner les percentiles de hauteur (Harikumar, Bovolo et Bruzzone 2017 ; Li, Hu et Noland 2013), les proportions de types de retours (par exemple entre premier et deuxième retour). D'autres variables enregistrent la forme extérieure de l'arbre, comme les rapports entre la hauteur et le diamètre de la couronne, les paramètres des équations polynomiales qui correspondent à la forme de l'arbre, l'enveloppe convexe (*convex hull*) ou formes alpha (*alpha shapes*) (Holmgren, Persson et Söderman 2008 ; Ko, Remmel et Sohn 2012 ; Ko, Sohn et Remmel 2013 ; Vauhkonen *et al.* 2009). Une classification des principales variables lidar utilisée pour la reconnaissance des espèces a été réalisée par Lin et Hyyppä (2016).

Les variables d'intensité sont calculées comme différentes statistiques à partir des valeurs d'intensité de chaque retour considéré. Cette valeur d'intensité représente une mesure de l'énergie rétrodiffusée. Mais il est difficile à savoir ce que cette valeur représente exactement, pour pouvoir faire une association entre l'intensité et une caractéristique de la couronne. L'information sur l'intensité de chaque impulsion laser émise n'est pas fournie pour les données à échantillonnage discret, ce que rend difficile une association précise entre la valeur de l'intensité du signal reçu et une valeur de réflectance. L'intensité des retours du lidar à retour discret dépend d'une multitude de facteurs, comme les caractéristiques de l'objet (réflectance dans la longueur d'onde du laser émetteur, taille, regroupement et orientation des feuilles), les caractéristiques de l'impulsion (intensité émise, divergence, angle de balayage, portée), ainsi que les algorithmes de détection (seuil de détection d'un signal au-dessus du niveau de bruit, laps de temps entre déclenchement du signal et l'enregistrement de l'intensité) et l'algorithme de discrétisation du signal reçu. Certains de ces paramètres ne sont pas connus du côté utilisateur, par exemple l'algorithme de discrétisation du signal reçu est propriétaire pour les systèmes de Optech Inc. Tous ces facteurs rendent la normalisation de l'intensité difficile pour retrouver une valeur de réflectance.

En plus des variables calculées à partir de chaque canal individuel, le lidar multispectral a l'avantage de pouvoir utiliser des ratios ou des indices normalisés à partir des différentes statistiques entre les canaux (Teo et Wu 2017 ; Yu *et al.* 2017). Une précision s'impose en ce qui concerne les indices normalisés de végétation calculés à partir du lidar multispectral, par rapport à ceux calculés à partir des images multispectrales passives. Les derniers ont été construits pour faire ressortir uniquement la différence de longueur d'onde entre les bandes d'une même image ayant la même résolution et géométrie de vue. Par contre, les canaux du lidar multispectral aéroporté, comme le Titan, ne respectent pas ces conditions de résolution et géométrie, donc une attention particulière doit être accordée à ces effets.

En plus de l'espèce, ces variables sont influencées par multiples facteurs qui influencent la configuration du nuage de points correspondant à une couronne. Ces facteurs sont reliés aux propriétés de l'arbre et de son environnement (a), aux paramètres d'enregistrement (b) et aux paramètres méthodologiques de délimitation du nuage de points et de normalisation des valeurs de hauteur et d'intensité de chaque retour (c).

Parmi les facteurs reliés aux propriétés de l'arbre et de son environnement (a), la hauteur de l'arbre a une influence essentielle sur la qualité du nuage de points. La hauteur de l'arbre est directement reliée avec le volume occupé par la couronne où peuvent être interceptées les impulsions laser. Cela influence le nombre de points disponibles pour calculer un certain type de variables, en fonction de sa complexité. En conséquence, certaines variables complexes ne peuvent pas être calculées pour les petits arbres, ce qui crée un biais de classification en fonction de la hauteur de l'arbre.

D'autre part, pour certaines variables, les valeurs sont très différentes en fonction de la taille des arbres, ce qui rend difficile leur identification comme appartenant à une même espèce d'arbres. La Figure 1.6 illustre la différence entre nuages de points d'une même espèce d'arbres ayant des hauteurs entre 3 et 30 mètres.

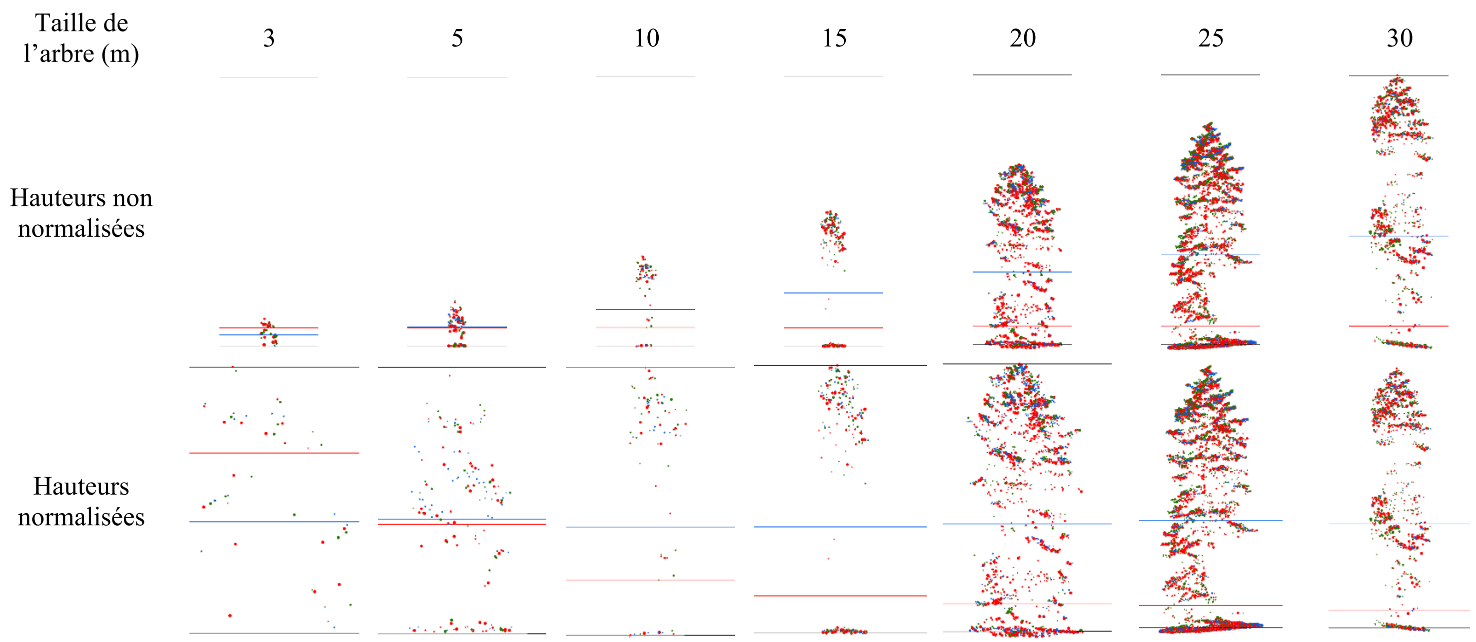

Figure 1.6 : Différence entre les nuages de points du lidar multispectral en fonction de la hauteur des arbres entre 3 et 30 mètres. L'impact relatif des seuils de délimitation des retours au sol est montré par des lignes bleues – seuil de 40% et lignes rouges –seuil de 2 mètres.

Les caractéristiques de l'environnement de l'arbre peuvent influencer la qualité du nuage de points. Elles ont un effet sur les zones d'occlusion. Ces caractéristiques se réfèrent au statut de l'arbre par rapport à ses voisins et à la densité de la forêt. D'autres caractéristiques sont reliées à la plasticité de la forme de l'arbre en réponse aux conditions de l'environnement, comme la densité des arbres voisins. Elles peuvent introduire une plus grande variabilité intra espèce. Plusieurs études ont testé l'influence de ces caractéristiques sur les variables des arbres individuels (Blair et Hofton 1999 ; Chen et Leblanc 1997 ; Goodwin, Coops et Culvenor 2006 ; Goodwin, Coops et Culvenor 2007 ; Hopkinson et Chasmer 2009 ; Richardson, Moskal et Kim 2009).

Les paramètres d'enregistrement (b) qui affectent la qualité des nuages de points de chaque arbre ont fait l'objet de plusieurs études (Goodwin, Coops et Culvenor 2006 ; Hopkinson 2007 ; Næsset 2004, 2009). De manière plus spécifique, certaines études ont abordé la densité d'échantillonnage (Gobakken et Næsset 2008 ; Lim, Hopkinson et Treitz 2008 ; Vauhkonen *et al.* 2008), l'altitude du survol (Morsdorf *et al.* 2008), la taille de l'empreinte au sol, l'angle de balayage (Holmgren, Nilsson et Olsson 2003b ; Morsdorf *et al.* 2008).

Les différents angles de balayage changent la distribution des points dans la couronne. Un exemple de cette différence de distribution des points dans la couronne est fourni dans la Figure 4.2. Les systèmes lidar actuels proposent un angle maximum de balayage très large, autour de 30-40 degrés, ce qui dépasse largement le standard de 15-20 degrés utilisé présentement en foresterie. Cette disponibilité ouvre la porte aux études concernant l'influence de l'angle sur les variables forestières, vu qu'une augmentation de l'angle maximum de balayage serait préférable pour la réduction des coûts de l'enregistrement (Wulder *et al.* 2012).

Parmi les paramètres méthodologiques (c), nous mentionnons ceux qui influencent la sélection des points considérés dans le calcul des variables par la délimitation de l'espace occupé par la couronne de l'arbre. Parmi ces paramètres, le type et la valeur de la hauteur du seuil à partir duquel les retours sur la végétation de sous-bois sont éliminés a une grande influence sur la valeur des variables. La Figure 1.6 est un exemple de différents impacts que les seuils à hauteur fixe ou les seuils à hauteur variables ont sur la délimitation du nuage de points en fonction de la hauteur de l'arbre.

D'autres paramètres méthodologiques changent les valeurs des variables. Par exemple, pour réduire la corrélation des variables avec la hauteur de l'arbre, les valeurs de hauteurs de chaque point ont été normalisées par rapport à la hauteur de l'arbre. Plusieurs choix méthodologiques concernent la manière de calcul de la hauteur des points au-dessus du MNT ou du calcul de la hauteur de l'arbre en tenant compte des 3 canaux ensemble ou par canal individuel. Ces choix peuvent influencer la valeur des variables.

D'autre part, les valeurs d'intensité ont été normalisées pour réduire l'influence de la différence de portée, elle-même influencée par les différences de relief et par l'angle de balayage. Plusieurs équations de normalisation de l'intensité ont été proposées dans la littérature. Certains, en plus de la portée, prennent en compte plusieurs facteurs qui déterminent une diminution de l'intensité, comme l'atténuation atmosphérique, l'angle d'incidence, la taille de l'objet. Le choix d'une équation et de ses paramètres peut changer significativement la valeur d'une variable.

1.4.3 Étape 3 : Classification par un algorithme automatique

Dans une troisième étape, un classificateur est appliqué pour construire un modèle utilisant les valeurs des variables calculées pour les couronnes de référence, pour ensuite l'appliquer à d'autres couronnes pour prédire l'espèce. Les algorithmes non paramétriques sont généralement préférés pour ces types de données, parce qu'ils sont moins affectés par la diminution de l'exactitude lorsque le nombre de dimensions est trop important par rapport aux couronnes d'entraînement, cet effet étant connu sous le nom de fléau de la dimensionnalité, ou effet de Hughes (Hughes 1968). Avec le développement actuel des algorithmes de classification dans le domaine de l'apprentissage automatique (*machine learning*), nous pouvons utiliser un grand nombre de variables, possiblement corrélées entre elles, sans affecter l'exactitude de classification. Certaines études ont comparé la performance de plusieurs algorithmes de classification (Fernández-Delgado *et al.* 2014), pour conclure sur la bonne performance de l'algorithme r*andom forest* (RF) (Breiman 2001). Cet algorithme effectue un apprentissage sur de multiples arbres de décision entraînés sur des sous-ensembles de données extraits aléatoirement (*bagging*) de la population et en utilisant une sélection aléatoire de variables à chaque nœud de décision. La décision finale de la classe (ici l'espèce de l'arbre) est réalisée par vote entre les résultats obtenus par chacun des arbres de décision. L'estimation de la performance du modèle est réalisée par validation croisée. L'algorithme RF a été souvent utilisé dans l'identification des espèces d'arbres (Korpela *et al.* 2010b ; Ørka *et al.* 2012). Parmi les avantages de cet algorithme, nous mentionnons sa capacité de traiter des données ayant une dimensionnalité élevée. Dans le cas du lidar multispectral, l'ajout des deux canaux supplémentaires multiplie le nombre des variables 3D et d'intensité. Le degré de corrélation entre les mêmes variables calculées à partir de deux canaux différents est très grand. L'avantage de pouvoir utiliser un algorithme comme RF qui accepte des variables corrélées est de pouvoir distinguer un nombre élevé d'espèces utilisant de petites différences entre les variables. L'algorithme RF est utilisé aussi pour identifier les variables les plus importantes pour une classification, selon la réduction en exactitude moyenne (*mean decrease in accuracy*).

Le lidar multispectral est un appareil prometteur pour l'identification de l'espèce d'arbre et pour l'inventaire forestier en général, parce qu'il ajoute une information spectrale très intéressante à une information structurale de haute qualité issue du lidar monospectral. Présentement, il y a très peu d'études qui ont examiné l'utilisation du lidar multispectral dans l'identification de l'espèce d'arbres. Cette thèse contribue ainsi à combler ce manque.

1.5 Objectifs

L'objectif principal de la thèse est d'évaluer l'exactitude de l'identification des espèces d'arbres en utilisant un balayeur lidar aéroporté multispectral, plus spécifiquement le Titan, de Teledyne Optech. L'objectif du Chapitre II est de réaliser une première évaluation globale de l'amélioration de l'identification des espèces utilisant le lidar multispectral par rapport au lidar monospectral. Les objectifs des chapitres suivants abordent de manière plus précise l'influence d'une caractéristique de l'arbre, la hauteur (Chapitre III), et d'un paramètre d'enregistrement, l'angle du balayage (Chapitre IV), sur l'exactitude de l'identification des espèces.

L'objectif du Chapitre II est d'évaluer l'augmentation en exactitude de l'identification de l'espèce que l'utilisation d'un balayeur multispectral à trois longueurs d'onde pourrait apporter par rapport à un balayeur monospectral. Pour répondre à cet objectif, une comparaison est faite entre l'exactitude obtenue avec une classification utilisant des variables 3D et d'intensité définies à partir des nuages de points provenant des trois canaux, par rapport à une classification utilisant des variables issues seulement d'un canal à la fois (considéré comme équivalent d'un balayeur lidar monospectral). Le lidar multispectral a l'avantage d'avoir des variables 3D calculées à partir d'une plus haute densité de points, des versions différentes des mêmes variables d'intensité calculées pour chacun des canaux, ainsi que des variables calculées comme rapports entre canaux.

L'exactitude de la classification a été évaluée sur un nombre élevé d'espèces (10) et à plusieurs niveaux (espèce, genre ou type de feuillage : feuillu/conifère).

Dans le Chapitre III, pour évaluer l'influence de la hauteur de l'arbre sur l'exactitude de l'identification de l'espèce, deux objectifs spécifiques ont été définis, 1) évaluer la sensibilité des variables 3D et d'intensité par rapport à la hauteur de l'arbre, et 2) évaluer l'exactitude obtenue par différentes stratégies de classification proposées pour diminuer l'effet de la hauteur de l'arbre sur la classification. Parmi ces stratégies, les deux premières proposent une classification unique sur tous les arbres, indifféremment de leur hauteur, en considérant a) toutes les variables et b) seulement les variables faiblement corrélées avec la hauteur de l'arbre. La dernière stratégie c) propose des classifications différentes pour les arbres en fonction de leur classe de hauteur, ce qui permet d'adapter les variables utilisées en fonction de la hauteur de l'arbre.

Vu la prise en compte des petits arbres qui vont intercepter moins d'impulsions laser, parfois insuffisants pour pouvoir calculer toutes les variables, il a été jugé nécessaire de vérifier l'impact des NA (non applicable) dans l'évaluation de l'exactitude de la classification. Cet impact a été évalué pour l'étape de la délimitation du nuage de points et pour l'étape de la classification. Trois approches sont évaluées pour diminuer l'impact des NA sur l'exactitude de l'identification.

Le Chapitre IV étudie l'influence de l'angle de balayage sur l'exactitude de l'identification des espèces. Une attention particulière a été accordée à l'efficacité de la normalisation de l'intensité de l'effet de la portée pour l'amélioration de l'exactitude d'identification des espèces. Les objectifs spécifiques sont 1) d'estimer l'effet de l'angle de balayage sur les variables 3D et d'intensité, 2) d'évaluer l'effet de la normalisation sur les variables d'intensité (réduction de la corrélation avec l'angle de balayage), 3) d'identifier les espèces pour lesquelles les variables sont les plus sensibles à la variation de l’angle de balayage, 4) de vérifier si l’angle de balayage a un impact sur l’exactitude de l’identification de l’espèce et 5) de vérifier si la normalisation des variables d’intensité a une influence sur l’exactitude de l’identification de l’espèce.

CHAPITRE 2

IDENTIFYING THE GENUS OR SPECIES OF INDIVIDUAL TREES USING A THREE-WAVELENGTH AIRBORNE LIDAR SYSTEM

Cet article a été publié :

Brindusa Cristina Budei, Benoît St-Onge, Chris Hopkinson, Félix-Antoine Audet, 2018, Identifying the genus or species of individual trees using a three-wavelength airborne lidar system, *Remote Sensing of Environment*, Volume 204, pages 632-647, DOI: 10.1016/j.rse.2017.09.037

Abstract

The identification of individual tree species is crucial for forest inventory, carbon stocks assessment as well as for habitat and ecosystem change studies. Previous studies have shown the potential of using both the geometrical information (proportions, shape of the crown profile, etc.) and return intensities of airborne laser scanning (ALS) point clouds to identify trees. So far, single wavelength (1064 nm or 1550 nm) ALS systems have been the most common. Teledyne Optech Inc. (Vaughan, Canada) introduced the Titan multispectral airborne lidar, the first three-wavelength system, equipped with 1550 nm, 1064 nm and 532 nm lasers. The objective of this study was to assess the accuracy of this discrete return multispectral lidar (MSL) for identifying the species of single trees, compared to standard discrete single wavelength lidar. Two distinct datasets were acquired in the Toronto region, Canada. The point clouds of single trees were extracted, and 3D and intensity classification features were computed. New intensity features were developed for this purpose, such as lidar NDVIs (normalized difference vegetation index). The species of each tree were identified with a random forest classifier using features calculated from 1) each channel separately and 2) all channels. A stringent selection strategy was employed to reduce the number of features down to 5-9, from 99-142. Trees were classified either as broadleaved (BL) or needleleaf (NL), by genus (4-7 classes), or by species (10 classes). When using all channels, the classification accuracy surpassed what was achieved with single channels, but this advantage was only significant when the number of classes was high, i.e. in the case of seven genera, or ten species. Using MSL data, the out-of-bag error was 3-5% for the BL-NL classification, 13% and 20% for respectively four and seven genera, and 24% for ten species. In the latter case, the best single-channel classification (based on 1550 nm data) resulted in an error of 35%. In the MSL classification, the most useful features were the NDVIs (Normalized Difference Vegetation Index, based on the intensity of infrared and green channels) and the 1550 nm intensities. We therefore conclude that species identification accuracy can be improved by using a three-wavelength ALS such as the Titan system compared to single channel ALS systems, especially when tree species diversity is fairly large (seven species or more).

Keywords: tree, species, genus, multispectral, LiDAR, intensity, identification, random forest, Titan

Résumé

L'identification de l'espèce est cruciale pour l'inventaire forestier, pour l'évaluation du stock de carbone, ainsi que pour les études de changement d'habitat et d'écosystème. Les études précédentes ont démontré le potentiel de l'utilisation de l'information géométrique (proportions, forme de la couronne, etc.) ainsi que l'intensité des retours des nuages de points du balayeur laser aéroporté (BLA) pour identifier les arbres. Jusqu'à présent, les systèmes BLA à une seule longueur d'onde (1064 nm ou 1550 nm) ont été les plus courants. Teledyne Optech Inc. (Vaughan, Canada) a introduit le lidar aéroporté multispectral Titan, le premier système à trois longueurs d'onde, équipé avec des lasers de 1550 nm, 1064 nm et 532 nm. L'objectif de cette étude a été d'évaluer l'exactitude de ce lidar multispectral (LMS) à retours discrets à identifier les espèces des arbres individuels, par rapport au lidar standard à une seule longueur d'onde. Deux enregistrements ont été acquis dans la région de Toronto, Canada. Le nuage de points des arbres individuels a été extrait et les variables 3D et d'intensité ont été calculées pour la classification. Des nouvelles variables d'intensité ont été développées pour ce but, comme les IVDNs lidar (indice de végétation par différence normalisée). L'espèce de chaque arbre a été identifiée avec un classificateur par forêt aléatoire utilisant les variables calculées à partir de 1) chaque canal séparément et 2) tous les canaux. Une stricte stratégie de sélection a été employée afin de réduire le nombre de variables de 99-142 à 5-9. Les arbres ont été classifiés soit selon le type de feuille, large (BL) ou aiguille (NL), par genre (4-7 classes), ou par espèce (10 classes). Quand tous les canaux ont été utilisés, l'exactitude de classification a dépassé ce qui a été obtenu avec les canaux individuels, mais cet avantage a été significatif seulement quand le nombre de classes a été élevé, i.e. dans le cas de sept genres, ou dix espèces. Utilisant les données LMS, l'erreur par validation croisée (out-of-bag) a été de 3-5% pour la classification BL-NL, 13% et 20% pour sept genres et 24% pour dix espèces respectivement. Dans le dernier cas, le résultat de la meilleure classification utilisant un seul canal (à partir des données 1550 nm) a eu une erreur de 35%. Dans la classification avec LMS, les variables les plus utiles ont été les IVDN (indice de végétation par différence normalisée, à partir de l'intensité dans les canaux infrarouge et vert). Nous concluons alors que l'exactitude de l'identification de l'espèce peut être améliorée en utilisant un BLA avec trois longueurs d'onde comme le système Titan par rapport aux systèmes BLA à un seul canal, surtout quand la diversité des espèces est assez grande (sept espèces ou plus).

Mots-clé : arbre, espèce, genre, multispectral, LiDAR, intensité, identification, *random forest*, Titan

2.1 Introduction

The identification of tree species is critical for forest inventory (Felbermeier, Hahn and Schneider 2010), carbon stocks assessment (Jenkins *et al.* 2003) as well as for habitat and ecosystem change studies (Bradbury *et al.* 2005 ; Vastaranta *et al.* 2014). While the advantages of precise species data for the latter studies are self-evident, it should be underlined that species-specific allometric models for predicting timber volume or above-ground biomass (e.g. as a function of diameter at breast height and height) are more accurate than more general ones (Lambert, Ung and Raulier 2005 ; Tompalski *et al.* 2014). For decades, researchers have sought automated remote sensing methods for identifying tree species to replace photo-interpretation, a traditional approach (e.g., in North America and Europe) considered as time-consuming and subjective. Interpreters use three-dimensional (3D) appearance, brightness and color cues to recognize species on aerial photography (Eid, Gobakken and Næsset 2004 ; Leckie *et al.* 1998), thus exploiting the architectural and reflectance differences between species. In boreal and temperate forests, important variations in structural characteristics indeed exist between species. The overall crown shape of most spruces (*Picea sp.*) and firs (*Abies sp.*), for example, is pointy and vertically elongated, compared to the roundish crowns of most broadleaved (BL) trees (such as *Acer*, *Betula*, *Populus*). Among needleleaf (NL) trees, branching patterns may differ. For example, white pines (*Pinus strobus*) and Norway spruces (*Picea abies*) seen from above exhibit a star-shaped outline, while white spruces (*Picea glauca*) and American larch (*Larix laricina*) have a smoother and more compact architecture. At least some of these 3D characteristics can be measured using airborne laser scanning (ALS) and used to identify species, by computing features, such as the height distribution of laser returns, features extracted using alpha shapes, or 3D textural properties (Li, Hu and Noland 2013 ; Vauhkonen *et al.* 2009). When using single channel ALS (usually 1064 nm or 1550 nm) for basic species identification tasks, such as distinguishing between NL and BL trees or between just two NL species, the achieved accuracies were as high as 95% (Holmgren and Persson 2004). Separating BL species, or distinguishing between a much larger number of species is however more challenging (Brandtberg 2007 ; Kim, Hinckley and Briggs 2011). Some studies have tried to improve the identification accuracies by using full-waveform ALS features, such as pulse echo width, waveform amplitude, waveform energy, number of echoes, etc. (review : Koenig and Höfle 2016). Accuracy improvements in species classification by about 6% (Vaughn, Moskal and Turnblom 2012) or 11% (Yu *et al.* 2014) were achieved by including full-waveform features, compared to identification based on discrete-return only.

The reflective properties of different species vary according to biochemical attributes of the foliage such as pigment concentration and nitrogen content (Ustin *et al.* 2009), structural attributes (leaf and stem structures, e.g., LAI and LAD), water content (Asner 1998) and stem reflectance (Asner *et al.* 2014). For example, compared to NL species, boreal or temperate BL deciduous trees have leaves with a high growth rate during the short warm season and, consequently, have a large photosynthetic capacity and high concentrations of chlorophyll and nitrogen (Wright *et al.* 2004). To some degree, these differences can be discriminated based on their spectral signature.

Some limited improvement in tree species identification had been achieved by adding intensity features from the monospectral ALS (Korpela *et al.* 2010b ; Ørka, Næsset and Bollandsås 2009). More recently, a larger number of feature types were derived in a systematic way from 3D and intensity information, with improved results for species classification (Lin and Hyyppä 2016). In general, approaches for capturing spectral radiometric data in addition to 3D information are comprised of a) using image matching to extract color photogrammetric point clouds from multispectral multi-view airborne images, b) combining single channel ALS to multi- or hyperspectral imagery, or c) combining airborne scanning lasers having different wavelengths. The first approach is still quite recent, but was used for example to identify three different tree boreal species with an accuracy of 89% (St-Onge, Audet and Bégin 2015). The second approach, which proceeds by extracting spectral information at the pixel locations corresponding to ALS first returns, either from multispectral (3-4 spectral bands) imagery (Holmgren, Persson and Söderman 2008 ; Ørka *et al.* 2012 ; Persson *et al.* 2004), or hyperspectral imagery (Dalponte, Bruzzone and Gianelle 2012 ; review : Ghosh *et al.* 2014), has brought improvements in the accuracy of species identification. However, coloring ALS points with image intensities requires joining two data sets usually obtained through distinct aerial surveys. Moreover, it is hindered by the complex directional reflectance anisotropy related to the changing sun-object-sensor geometry that influences intensities within and among images (Heikkinen *et al.* 2011). Considering these limitations, an emerging third approach was developed by using lidar sensors that transmit and receive at several wavelengths (Hopkinson *et al.* 2016 ; Wang, Tseng and Chu 2013). In addition to the increased density of the 3D component, the intensity of returns is measured in two or more wavelengths, allowing the creation of spectral signatures potentially useful for species recognition.

ALS intensities depend on the power of the backscattered laser pulses measured by the sensors. Instantaneous received power, explained by the radar equation (Jelalian 1992 ; Roncat *et al.* 2014 ; Wagner *et al.* 2006), is determined by acquisition parameters (beam width, aperture, range, etc.) and the effective backscatter cross-section (σ, in m^2) of the reflecting object:

$$\sigma = \frac{4\pi}{\Omega}\rho A \qquad \text{Eq. 2.1}$$

where $4\pi/\Omega$ is the scattering angle of the object relative to an isotropic scatterer, ρ its reflectance, and A the object's area within a footprint (silhouette area). A is logically related to leaf area index, and $4\pi/\Omega$ to leaf angle distribution (Asner 1998), two characteristics that vary between species, but that are wavelength independent. ρ owever varies with wavelength and can theoretically enhance species discrimination if multispectral intensity data are acquired. Intensity values are obtained through a process in which the received power at a given time is converted to digital values on an arbitrary scale. In the case of discrete return laser scanners, intensities should be approximately proportional to the power of the received energy at the instant a return is triggered. However, the methods by which intensity values are generated by a given sensor are sometimes proprietary (e.g., for Teledyne Optech sensors) and not disclosed by the ALS system vendors, making it difficult to know exactly how received power is translated to digital values in these cases. It is nevertheless expected that the intensities will be correlated to σ, i.e. at least partly influenced by the values of ρ, which is itself species dependent.

Using ALS multispectral intensities rather than the spectral signature of passive sensors has certain theoretical advantages. The measurements of ALS intensity have the advantage of being independent from external illumination conditions. Because they are all done using the same “hot spot” geometry, the intensity data is not influenced by variable shadowing, leading to lesser variations compared to the aerial imaging case (Woodhouse *et al.* 2011). In addition, tree and ground signals cannot be separated in passive sensors' measurements of reflectance, whereas the association of the 3D and intensity data in ALS allows this discrimination by imposing a height threshold. Moreover, normalization of the radiometric variations caused by range difference in ALS data can be corrected to some extent for power attenuation due to the travel distance of pulses and their reflection (Korpela *et al.* 2010a). Several strategies for more advanced radiometric normalization have also been proposed (review : Kashani *et al.* 2015 ; Yan and Shaker 2014).

The first attempts at using multispectral ALS data for land use, or vegetation classification usually had to rely on multiple airborne surveys, each using a single wavelength system. Wang, Tseng and Chu (2013) acquired two wavelength full-waveform ALS data in two separate flights using Optech ALTM Pegasus HD400 (1064 nm) and Riegl LMS-Q680i (1550 nm), and tested their performance in land cover classification. They highlighted the possibility of soil-vegetation separation, and the importance of moisture and physiological information of vegetation for species retrieval. Recently, Hopkinson *et al.* (2016) compared variation in intensity between discrete ALS point clouds acquired at three different wavelength, each with a different sensor on independent flights (Teledyne Optech's Aquarius - 532 nm, Gemini - 1064 nm, and Orion - 1550 nm). They found that the intensity-based foliage characterization was different for each sensor and was associated with both the sensor's wavelength and the survey sampling characteristics (flight altitude, system settings, etc.). Variations in the latter factors however makes it difficult to combine the intensities of different monospectral ALS to classify land cover or identify tree species using wavelength ratios as NDVI.

The operational advantages of integrating lasers of different wavelengths into a single system led to the development of multispectral laser (MSL) simulations and system prototypes. Some studies were conducted to analyze the variations of NDVI and photochemical reflectance index (PRI) along canopy profiles using a four wavelength airborne MSL (531, 550, 670 or 690, and 780 nm) simulated on virtual forest stands (Morsdorf *et al.* 2009) or tested in laboratory over living trees (Woodhouse *et al.* 2011). They demonstrated the possibility of capturing leaf-level physiological variations along vertical profiles and spatially distinguishing the photosynthetic active elements from bark material. Furthermore, different prototypes using a supercontinuum laser source were tested in laboratory. Chen *et al.* (2010) tested such a MSL prototype for NDVI estimation and collected range and intensity data at 600 nm and 800 nm. In another experiment, a full waveform hyperspectral terrestrial lidar using a supercontinuum laser was developed by Hakala *et al.* (2012) for the measurement of vegetation features at eight different wavelengths (542, 606, 672, 707, 740, 775, 878, and 981 nm). Nevalainen *et al.* (2014) used the same hyperspectral terrestrial lidar to test 27 vegetation indices and their relation with the chlorophyll amount. Furthermore Vauhkonen *et al.* (2013) tested this device for separating pines from spruces using intensity features and NDVI. For leaf nitrogen estimation and for different material classification, Gong *et al.* (2015) and Wei *et al.* (2012) tested a MSL with four wavelengths in the visible and infrared spectra (556, 670, 700, and 780 nm) transmitted from four semiconductor laser diodes. Gaulton *et al.* (2013) tested the possibility of estimating the vegetation moisture with a full-waveform dual wavelength terrestrial laser scanner system, operating at two wavelengths (1063 and 1545 nm). These studies proved that differences between lidar intensity in different wavelengths could be used to distinguish several characteristics of vegetation which could help in species identification.

The first operational three wavelength airborne laser scanning system was introduced by Teledyne Optech in 2014. The Titan system is comprised of lasers firing at three different angles at the respective wavelengths of 532, 1064 and 1550 nm (see Table 2.1 for details). The system is fundamentally a discrete return ALS (up to four discrete

XYZ returns per pulse), but each channel can be fitted with a waveform digitizer to generate full-waveform data. Compared to combining separate ALS surveys at different single wavelengths, a MSL system has the advantage of mitigating the differences in survey sampling characteristics (flight paths, atmospheric conditions, vegetation phenology, etc.) between the data from the three wavelengths, thus facilitating analysis (Hopkinson *et al.* 2016). As highlighted by Fernandez-Diaz *et al.* (2016), three wavelength and three-look angle design provides redundancy and diversity which is beneficial on technical and financial levels. According to the same study, the system can be flown up to 2000 m above ground level.

Table 2.1: Titan system's laser characteristics

Channel	**Wavelength**	**Divergence (1/*e*)***	**Forward tilt**	**Pulse width**
C1	1550 nm	0.35 mrad	3.5 º	3.0 – 3.5 ns
C2	1064 nm	0.35 mrad	0.0 º	3.0 – 3.5 ns
C3	532 nm	0.7 mrad	7.0 º	2.5 – 3.0 ns

* Paul LaRoque, Teledyne Optech., pers. comm.

Fernandez-Diaz *et al.* (2016) studied the pulse energy characteristics of the laser source as a function of the pulse repetition frequency (PRF). They concluded that the advantage of the Titan fiber laser sources is that the energy per pulse does not degrade significantly as the PRF increases, which used to be the case with the standard monospectral laser systems as Optech's Gemini or Aquarius. Differences in ground return density between channels was attributed to beam divergence, independent laser power between channels and look angles, which resulted in different energy densities at the footprint. Assessment of the range resolution of the Titan system by the same authors showed that its variation between channels is small and insignificantly affected by the PRF, compared to other monospectral systems like Aquarius and Gemini. This improved range resolution could be beneficial for studies about canopy structure.

To date, the majority of studies that tested the Titan system for land cover classification were based on raster images generated using intensity or return height data. For land cover classification, some studies used only intensity data from the three channels (Ahokas *et al.* 2016 ; Hopkinson *et al.* 2016 ; Morsy *et al.* 2016 ; Wichmann *et al.* 2015), or a combination of 3D and intensity information (Bakuła, Kupidura and Jełowicki 2016 ; Hu 2016 ; Matikainen, Hyyppä and Litkey 2016 ; Zou *et al.* 2016). In a first study using Titan data to identify a large number of tree species, St-Onge and Budei (2015) used the mean and standard deviation of the intensities extracted from manually delineated crowns. This allowed to identify BL vs. NL trees with a 4.6% error, and distinguish between 8 genera with a 24.3% error. Yu *et al.* (2017) used Titan data to discriminate between three species (pine, spruce and birch) of which crowns were automatically delineated. They calculated four types of features, respectively based on point cloud, single-channel intensity, multi-channel intensities, and the combined data from the three channels. The best accuracy (85.9%) was obtained using the combined dataset, but was not much higher than that reached using single channels. It appears probable that this limited performance increase could be attributed to the low number of species classes. A higher number of species in a classification model will normally decrease the accuracy of the identification (Baldeck and Asner 2014), creating a situation where enriched data would be beneficial. We therefore posit that using MSL system datasets in forests having much greater species diversity should lead to a larger accuracy increase compared to single channel ALS results.

The objective of the present study is to evaluate the magnitude of the accuracy gains provided by the three wavelength data of the Titan system compared to single wavelength ALS in the identification of tree species. Three classification levels were considered: species, genus, and BL vs. NL. This represents, to the best of our knowledge, the first attempt to separate a relatively large number of species (10) using an operational MSL system. The general hypothesis is that the combination of ALS data acquired in three wavelengths will markedly enhance the species identification capacity, in this situation characterized by a fairly high diversity of BL and NL species, due to the increased spectral resolution of the data.

2.2 Data and methods

2.2.1 Study regions

The MSL datasets used in this study were acquired in two different environments, with a mixture of indigenous and non-indigenous trees: a suburban site with individualized trees along streets, and a partly managed forest comprised of plantations and naturally growing trees. The first MSL dataset was acquired on October 2, 2014, during a test flight over a 38 ha area located in the district of Scarborough (SC), Ontario, Canada (centered on 79°68' W, 43°47' N), a low-density suburb of the city of Toronto. The most common BL genera found in this site are *Acer* and *Fraxinus*, and the most common NL genera are *Picea* and *Pinus*. Sampled trees are situated principally along the streets and are most often isolated so that neighbouring crowns do not interpenetrate. At the time of acquisition, the foliage color of the BL trees had not yet started to change significantly. The topography of this site is essentially flat (Table 2.1).

The second dataset was acquired on July 2, 2015, over a 2 546 ha site located in the York Regional Forest (YRF), in Ontario, Canada (centered on 79°19' W, 44°04' N). This site is characterized by a mix of natural forests (53%) and reforestation/plantation areas (47%), mostly NL trees, which creates a mosaic of various ecosystem types (Regional Municipality of York 2010). The main species are Norway spruce (*Picea abies*), white spruce (*Picea glauca*), red pine (*Pinus resinosa*), white pine (*Pinus strobus*), Scots pine (*Pinus sylvestris*), American larch (*Larix laricina*), sugar maple (*Acer saccharum*), white ash (*Fraxinus americana*), trembling aspen (*Populus tremuloides*), and red oak (*Quercus rubra*). Most tree stands are dense, with touching or interpenetrating crowns. The characteristics of each survey are summarized in Table 2.2.

2.2.2 Multispectral lidar data

Titan MSL discrete return XYZ position and intensity data quantized on a 12 bit scale for the two sites were obtained from Teledyne Optech. The recorded intensity values corresponded to the peak amplitude of each return. The relationship between the received power and the recorded intensities was said to be linear over the entire scale (pers. comm. Paul LaRoque, Teledyne Optech, 28 oct. 2015).

Table 2.2: Survey characteristics

	SC	**YRF**
Flight date	2 October 2014	2 July 2015
Pulse repetition frequency / channel (kHz)	200	100
System pulse repetition frequency (kHz)	600	300
Scan frequency (Hz)	52	52
Field of view (degree)	30	30
Mean flight altitude above ground (m)	360	800
Footprint diameter (cm) in C1, C2, C3	12.6, 12.6, 25.2	28, 28, 56
Number of flight lines	3	18
Lateral strip overlap	approx. 43%	approx. 50%
Mean number of first returns m^{-2} by channel (C1, C2, C3) of individual flight lines*	12.6, 12.8, 12.6	3.4, 3.4, 3.3
Mean number of first returns m^{-2} of all channels (C1, C2, C3) for aggregated flight lines*	53.7	20.2

*The mean number of first returns m^{-2} were calculated over the entire scanned area, i.e. including all surface types.

A quality assessment of the 3D data was performed using various visualization and quantitative strategies by St-Onge and Budei (2015). The inter-channel coregistration, and the inter-swath registration were checked, and no evidence of misregistration was found.

The MSL data have been provided with the range of each return, which allows correction of the intensities for attenuation. The equation of Korpela *et al.* (2010a) was used for this purpose:

$$I_n = (R/R_{ref})^a I_{raw} \qquad \text{Eq. 2.2}$$

Where I_n is the range-normalized intensity, I_{raw} is the raw intensity, R the range, and R_{ref} the reference range. The a exponent was set to 2.

2.2.3 Selection and identification of sample crowns

Sample crowns were selected at both sites for training and evaluating the species classifier. Only the trees having a height of 5 m or more, a minimum crown area of 1 m^2, and having at least one return from each channel were kept. At the SC site, the trees were identified based on a field census of tree species of the Scarborough area (City of Toronto 2010) and by using Google Street ViewTM. The latter terrestrial images were acquired in the summer of 2014. All trees that were visible from the streets were sampled. At the YRF site, a field survey conducted in August 2015 provided species observations at 400 geolocations. At these locations, observations of single recognizable trees, tree groups of the same species, or dominant species of a given plantation were made. The locations were chosen for their accessibility (along roads or trails) and, where possible, were well spatially distributed (for species found in several locations across the site) to account for potential variations in site conditions and ALS scan angles. Our aim was to select dominant trees stratified in three height classes for each species (5-10 m, 10-20 m, and >20 m). Because the pre-existing site documentation (stand map, species information, etc.) was fairly general, and many stands were mixed woods, strict stratification of the sample (i.e., *n* trees per height class) was operationally difficult (see Table 2.3 for height statistics). At this site, aerial photos were acquired at the same time as the MSL data, with the built-in CM-1000 RGB sensor of Teledyne Optech. The images had a ground resolution of approximately 10 cm, which allowed the photo-interpretation of several species with high certainty. These images were used by a photo-interpreter to ensure that the tree crowns delineated on the lidar CHM within groups or plantations were indeed of the species mentioned in the field notes (e.g., so that naturally regenerating BL trees within a pine plantation would not be included). Field observations on defoliated or dead trees were used to train the photo-interpreter to exclude them during the delineation stage, as recognizing trees from different species at various degrees of defoliation was outside the scope of this study. At the YRF site, NL trees were easier to identify by photo-interpretation than BL trees because they were often found in monospecific plantations. Photo-interpretation of BL species being more difficult, their identification came solely from field observations. For this reason, the BL classes had generally fewer individuals than the NL.

Sample trees were identified according to three classification levels: foliage type (BL and NL), genus and species. At the SC site a total of four tree genera were studied (3 BL and 1 NL, see Table 2.3). For this site, identification was limited to the genus level because there were too few sampled trees per species to have a reasonable minimum number of individuals per class (here established at 30), or because the exact species was sometimes difficult to ascertain due to the possible presence of various cultivars. At YRF site we studied a total of ten species from seven genera (4 BL and 3 NL). The sample contained some relatively isolated trees (crown not touching neighbours), as well as numerous trees growing in closed canopy conditions. Because many of the NL trees were sampled from plantation sites, they came from generally mature and even-aged populations. For red pine, samples were taken from several plantations having different ages. Even if the sample was dominated by mature trees, a relatively better representation of small trees compared to the other NL classes was achieved. The species with uneven-aged populations were mainly broadleaf trees like red oak, or trembling aspen. Height distributions varied between species, the modal height class being for example 20-26 m for Norway spruce, white pine, red pine or sugar maple, but 10-17 m for Scots pine, American larch or white ash (see Table 2.3).

Table 2.3: Number and height (m) statistics of sample crowns

	NL/BL	Genus	Species	N	Min	Max	Median	Mean	SD
SC									
	NL	*Picea*		71	7.7	19.2	13.0	12.9	2.6
	BL	*Acer*		184	5.3	23.3	10.3	10.8	3.5
		Fraxinus		71	7.2	23.5	13.8	13.3	3.1
		Gleditsia		36	5.4	19.7	10.6	10.6	3.1
Total				362					
YRF									
	NL	*Picea*	*abies* (Norway spruce)	204	9.5	30.6	26.3	25.7	3.6
			glauca (White spruce)	223	9.7	26.6	22.0	21.6	2.9
		Pinus	*sylvestris* (Scots pine)	194	6.1	23.3	13.7	14.1	3.2
			resinosa (Red pine)	192	5.6	29.6	23.6	21.8	5.8
			strobus (White pine)	189	9.9	28.8	22.8	22.0	3.6
		Larix	*laricina* (American larch)	186	10.1	29.2	16.7	18.1	4.5
	BL	*Acer*	*saccharum* (Sugar maple)	202	10.2	31.7	23.1	22.2	4.4
		Fraxinus	*americana* (White ash)	45	7.4	23.8	11.8	12.7	3.6
		Populus	*tremuloides* (Trembling aspen)	174	5.2	28.5	19.9	19.3	6.0
		Quercus	*rubra* (Red oak)	49	7.9	26.2	20.1	17.9	5.3
Total				1658					

2.2.4 Delineation of sample tree crowns

The crowns geolocated in the field or identified in the photo-interpretation were delineated manually using visual interpretation of 2D renderings of the canopy height model, the intensity images (color composite of intensity of the three laser channels) and, in the case of the YRF, the RGB images. Manual delineation was chosen to enable the assessment of species identification accuracy without significant uncertainty caused by automated delineation. Manual delineation however does not guarantee perfect results as, for example, closely growing trees of the same species could appear as being a single crown. This type of error could affect some of the 3D features used for species identification. Figures 2.1 and 2.2 show examples of delineated crowns overlaid on the CHM, multispectral intensity image, and a vegetation index.

Figure 2.1 : Canopy height model (top), color composite (red: C1, green: C2, blue: C3) of the three-channel MSL first-return intensities of the SC site with a sample of manually delineated crowns (a = Pinus, b = Fraxinus, c = Betula, d = Acer, e = Picea; crown f is severely defoliated), and NDVI of type 1 (NDG1, see Table 2.7)

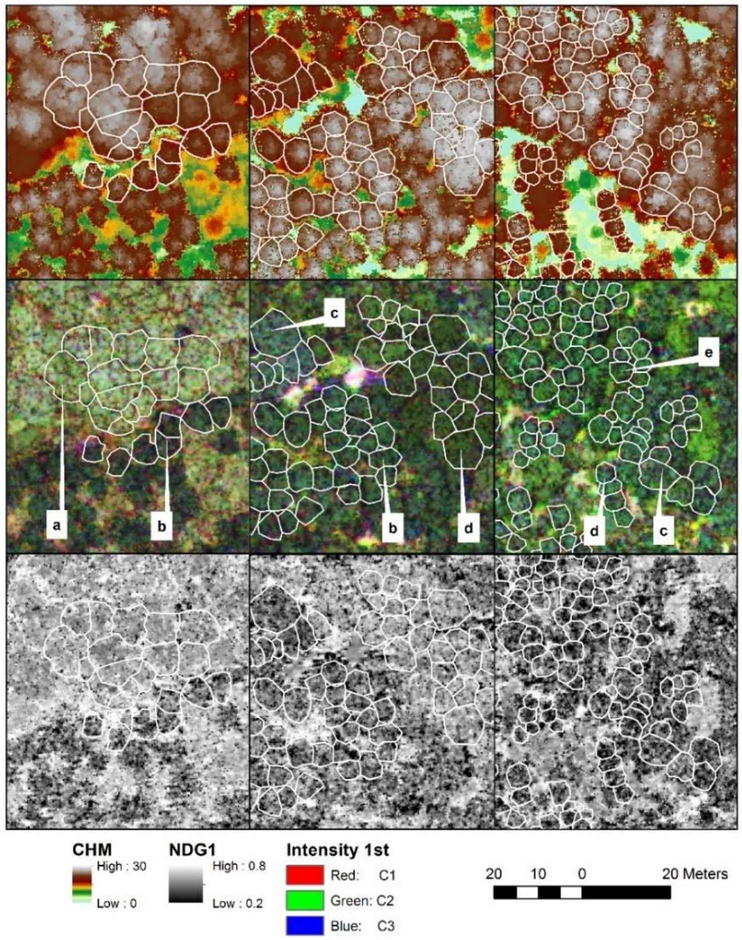

Figure 2.2: Canopy height model, color composite (red: C1, green: C2, blue: C3) of the three-channel MSL first-return intensities of the YRF site with a sample of manually delineated crowns (crowns : a = Acer saccharum, b = Pinus resinosa, c = Pinus strobus, d = Picea glauca, e = Picea abies), and NDVI of type 1 (NDG1, see Table 2.7).

2.2.5 Lidar point cloud statistics of tree crowns

Table 2.4 presents the density of returns, per channel and overall (C321), within the selected sample crowns and Table 2.5 gives a general view of the dynamic range of intensities.

Table 2.4: Return density (returns m^{-2}) above 2 m in tree crowns

	C1	C2	C3	C321
SC				
1st returns	19.8	19.7	19.6	59.1
all returns	29.5	34.8	32.1	96.3
YRF				
1st returns	7.8	7.5	6.1	21.3
all returns	13.4	13.2	8.2	34.8

Table 2.5: First return intensities above 2 m at different percentiles in tree crowns

	C1	C2	C3
SC			
5%	22	9	6
50%	218	431	44
95%	376	744	93
YRF			
5%	5	2	3
50%	29	18	9
95%	79	46	20

2.2.6 Computation of classification features

To identify tree class at each classification level (foliage type, species and genus), we developed two feature categories: 3D features based on the XYZ data (Table 2.6) and intensity features (Table 2.7). The 3D and intensity classification features were computed from MSL returns on a per-crown basis. Returns falling within the delineated polygons were attributed to the corresponding individual tree. Returns lower than 2 m above ground (i.e., above the ground elevation at the crown centroid) were discarded to eliminate signal from the understory or from the ground (i.e., non tree vegetation, exposed soil, road, etc.). Because each of the Titan's laser return is monospectral, the construction of spectral signatures was achieved through object-based binning. i.e. by computing crown-wise statistics. Using the average intensity in each channel theoretically allows the creation of crown spectral signatures. As the cross-section (A) and ρ variations are evened out by averaging crown-wise, the mean effective backscatter cross-section per crown parameter of σ (Eq. 2.1) should be obtained. Furthermore, distribution statistics such as standard deviation or intensity percentiles could also reflect species-specific characteristics (Vauhkonen *et al.* 2013).

A large number of ALS classification features for land use or species identification have been proposed in past studies (see introduction). In addition, these features are sometimes replicated for different categories of returns (single returns, first of many, all returns, etc.). Multispectral ALS offers the possibility of increasing the number of features, at least by a factor of three in the case of the Titan system. This can however lead to a situation in which an unreasonable number of features complicates analyses (the so-called "curse of dimensionality"). For a given number of training samples, the increase in feature number (dimensions) can lead to a reduction in predicting power (the so-called Hughes effect : Hughes 1968), and certainly, to difficulties in generalizing the results. For this reason, we have tried to limit the number of features at all stages of the analysis. Overall, the 3D and intensity features are not “complete” with regards to the full set of all features published in the existing literature, and cannot in any case be said to be “exhaustive”, as a very wide variety of new features can still be devised. However, we posit that they are sufficient to allow gaining significant knowledge on the new information provided by additional laser channels for the purpose of tree species classification.

Following preliminary tests performed on a wide range of features, we discarded those that did not perform well, were highly redundant, or for which it would be difficult to give a meaningful interpretation. For instance, we restricted the intensity feature computations to the first returns, either the single returns (as these should correspond to hits where the backscatter cross-section profile is highest and transmission losses are high enough to prevent the 2^{nd} echo) or the first of many, depending on the feature (see Table 2.6). Also, for classification models using intensity features from the three Titan channels, we did not include features computed using the pooled returns from the three channels (which would conflate intra- and inter-channel variances and mix different types of measurements), but kept only those computed separately on each of the three channels. On the contrary, when using the full discrete-return three-channel dataset, the 3D features were computed on the pooled returns from all channels (as the increased density can be advantageous), but not on the separate channels (highly redundant). Depending on the intended goal, 3D features were derived using either the first returns (e.g., for fitting a polynomial on a crown in the case of the SU feature), or all returns (e.g., for the coefficient of variation of return heights). We did not compute features using exclusively single or second returns. A second step in the *a priori* feature reduction consisted in discarding those that produced spurious or no data values for smaller trees having a low number of returns. When just a few problematic trees occurred, we deleted them instead of discarding the feature. We first present the general principles of the 3D and intensity features. We then explain their nomenclature and provide details on their calculation in Tables 2.6 and 2.7.

2.2.6.1 3D features

In the case of 3D features, we wanted to refrain from using absolute measurements, such as tree height or crown area, to ensure that the identification of species would in no case result from a chance association between a given species and specific sizes. For this reason, 3D features were normalized relative to the tree height. This type of normalization was also used for species identification in certain previous studies

(Holmgren and Persson 2004 ; Ørka, Næsset and Bollandsås 2009). Tree height itself (*H*) was defined as the difference between the elevation of the highest return in the crown and the elevation of the DTM pixel under the crown centroid (read on a 1 m resolution raster DTM). The height of each return within the crown was also computed relatively to this DTM pixel's value, thus avoiding any effect of underlying topography on the 3D shape of crowns (Vega *et al.* 2014). Different families of 3D features were designed (see Table 2.6 for details) to capture variations in tree proportions (e.g., AH: ratio of the crown area over the tree height), shape (e.g., SU: curvature of a 3D surface fitted to the crown envelope), slope of the crown profile (SL, or HR: different slope calculations between concentric rings), or porosity (e.g., D1_2: height difference between 1st and 2nd returns of the same pulse, RB: ratios accounting for point distribution in tree height), among other aspects.

2.2.6.2 Intensity features

Different families of intensity features (see Table 2.7) were designed to capture the intensity characteristics for the overall crown (mean, dispersion statistics, percentiles), along a vertical gradient (difference between intensity of 1st and 2nd returns), or along a radial gradient (mean intensity by concentric ring). As in the case of 3D features, some ratios between metrics of different return types were computed (RM). Normalized differences between channels were computed to produce NDVI-like features, similar to those used by Wichmann *et al.* (2015) and Zou *et al.* (2016).

2.2.6.3 Feature nomenclature

In Tables 2.6 and 2.7, the feature names are presented as a concatenation of type (3D, or intensity - I), followed by the feature family (e.g. SL, NDG1), type of return used, the statistic that was computed, and the channel. For clarification we provide the three following examples of feature names: *3D_SL_all_p50_C321* is a 3D feature that represents the median (p50) of the slope feature family (SL) calculated on all returns of all three channels (C321). *I_NDG1_1st_p75* is an intensity metric that represents the green NDVI of type 1 (NDG1) and is computed using the 75th percentile (p75) of the first returns values in the concerned channels (C3 and C2). *3D_RM_1st_mn_2nd_mn_C3* represents the ratio between the mean height of the first returns (1st_mn) and the mean height of the second returns (2nd_mn) of the third channel (C3).

In the equations found in Tables 2.6 and 2.7, the following definitions and symbols are used:

- *x, y, z* represent the three-dimensional coordinate system;
- *i* designates each of the *n* returns within a crown (*i* = 1, *n*) depending on return type:
  - i_{1st} = first returns,
  - i_{si} = single returns,
  - i_{2nd} = second returns,
  - i_{all} = returns of all types (first, second, etc.), *i* may also designate any of the possible return types when it appears in a generic equation;
- *max* is the highest point in a crown;
- d_i represents the horizontal distance between the i^{th} return and the highest point in the crown and calculated as:

$$d_i = \sqrt{(x_i - x_{max})^2 + (y_i - y_{max})^2} \qquad \text{Eq. 2.3}$$

- H_{max} is the height of a tree defined as:

$$H_{max} = z_{max} - z_{DTM} \qquad \text{Eq. 2.4}$$

  where z_{DTM} is the lidar raster DTM height at crown centroid.

  H_i corresponds to the height of the i^{th} return within a crown and is given by:

$$H_i = z_i - z_{DTM} \quad \text{Eq. 2.5}$$

- H_{i1} and H_{i2} are the respective heights of the first and second returns of the same pulse.
- I_{i1} and I_{i2} are the respective intensities of the first and second returns of the same pulse.
- R_{max} represents the crown radius defined as the horizontal distance between *max* and the farthest return from it;
- A_j corresponds to each of concentric ring (annulus) of equal width ($R_{max}/4$, with $j = 1,4$) centered on the location of *max*. A_1 is the core circle containing *max*, and A_4 the outside ring.
- *m* is the slope between *max* and the i^{th} return as given by:

$$m_i = \frac{z_{max} - z_i}{d_i} \quad \text{Eq. 2.6}$$

- V_{chull} represents the volume of the convex hull of the crown computed with the function *chullLiDAR3D* from the R package *rLidar*.

In the "Statistics" column of Tables 2.6 and 2.7, *mn* designates the mean, *sd* the standard deviation, *cv* the coefficient of variation (*sd/mn*), *p5, p10, p25, p50, p75, p90, p95* respectively the 5th, 10th, 25th, 50th, 75th, 90th and 95th percentiles, and *lm* is a linear model fit calculated with the *lm* function from the *stats* R package. Moreover, the function *surf.ls* from the R package *spatial* was used to perform a least square fit of a trend surface of the form:

$$\widehat{H} = ax^2 + by^2 + cxy + dx + ey + f \quad \text{Eq. 2.7}$$

For conciseness, the "Equation" column in Tables 2.6 and 2.7 gives only a few examples of the several possible combinations of return types and feature statistics.

Table 2.6: Description of 3D features (prefix = 3D_)

Symbol	Description	Return types	Statistics	Equation
AH	Ratio of crown **A**rea over tree **H**eight	-	-	$AH = Crown\ area\ /H_{max}$
DI	**DI**spersion: coefficient of variation of return heights	all, 1st	cv	$DI\_1st\_cv = cv(H_{i_{1st}})$ $DI\_all\_cv = cv(H_{i_{all}})$
PE	Intensity value at **PE**rcentiles: 5th, 10th, 25th, 50th,75th, 90th, 95th	1st, all	p5, p10, etc.	$PE\_p95 = p95(H_i)$
SL	The **SL**ope of the lines connecting the highest return to each other returns	all, 1st	mn, sd, cv, p25, p50, p75	$SL\_mn = \sum_{i=1}^{n-1} m_i \Big/ (n-1)$ where $(max \neq i)$; $SL\_p50 = p50(m_i)$; etc.
HR	**H**eight by **R**ings. HR_lm: the slope of a linear model fit (lm) on the H_{Aj} and d_{Aj} values. HR_cv: the coefficient of variation of the H_{Aj} values.	all, 1st	cv	$H_{A_j} = \sum_{i=1}^{nj} H_i \Big/ n_j$ where n_j is the number of returns in ring j. d_{Aj} is the ring radius at mid-width. $HR\_cv = cv(H_{Aj})$
RB	**R**atio of the number of points in different height **B**ins defined in % of tree height over the total number of points (e.g., 60_80 is the ratio of the number of points in the 60–80% bin over all the points in a crown).	all	Counts: 60_80, 80_90, 90_100, 95_100	$RB_{90\_100} = n_{90-100}/\ n$ etc.
CH	Ratio of the **C**onvex **H**ull volume over the maximum height cubed.	all	-	$CH = V_{chull}/H_{max}^3$

Symbol	Description	Return types	Statistics	Equation
SU	Sum of the two quadratic coefficients (coef) of a least square **SU**rface fit (eq. 2.7) on the H_i values, and average of absolute vertical residual values of the above fit divided by the height of tree (rs).	1st	-	$\text{SU\_coef} = a + b$ where a and b are coefficients of eq. 2.7. $rs = \sum_{i=1}^{n} \lvert H_i - \widehat{H}_i \rvert$ $\text{SU\_rs} = rs/H_{max}$
D1_2	Height **D**ifference between **1**st and **2**nd return of the same pulse, in the same channel, divided by the height of tree.	-	mn, sd, cv, p25, p50, p75	$\Delta H_{i1\_2} = (H_{i_1} - H_{i2})/H_{max}$ $D1\_2\_mn = mn(\Delta H_{i1\_2})$ etc.
RM	**R**atio between different statistics.	all, 1st, 2nd		$RM\_1st\_mn = mn(H_{i_{1st}}) \,/\, H_{max}$ $RM\_1st\_p50 = p50(H_{i_{1st}}) \,/\, H_{max}$ $RM\_all\_mn = mn(H_{i_{all}}) \,/\, H_{max}$ $RM\_all\_p50 = p50(H_{i_{all}}) \,/\, H_{max}$ $RM\_1st\_p50\_1st\_mn = p50(H_{i_{1st}}) / mn(H_{i_{1st}})$ $RM\_1st\_p50\_all\_mn = p50(H_{i_{1st}}) / mn(H_{i_{all}})$ $RM\_1st\_mn\_all\_mn = mn(H_{i_{all}}) / mn(H_{i_{1st}})$ $RM\_1st\_mn\_2nd\_mn = mn(H_{i_{1st}}) / mn(H_{i_{2nd}})$

Table 2.7: Description of intensity features (prefix = I_)

Symbol	Description	Return types	Statistics	Equations
MI	**M**ean **I**ntensity; Mean intensity of returns between interval of percentiles (5–95, 10–90); Mean intensity between interval of percentile normalized by the overall mean intensity	1st, si	mn	$MI\_mn = mn(I_i)$ $MI\_10\_90\_mn = mn(I_{i_{10\_90}})$ $MI\_10\_90\_n\_mn = mn(I_{i_{10\_90}})\ /mn(I_i)$
DI	**DI**spersion: Standard deviation, coefficient of variation	1st, si	sd, cv	$DI\_cv = cv(I_i)$ $DI\_sd = sd(I_i)$
PE	Intensity value at **PE**rcentiles: 5^{th}, 10^{th}, 25^{th}, 50^{th},75^{th}, 90^{th}, 95^{th}	1st, si	p5, p10, etc.	$PE\_p95 = p95(I_i)$
IR	Standard deviation of the mean **I**ntensity by **R**ing.	1st	sd	The mean return intensity is calculated from returns in each ring $I_{A_j} = \sum_{i=1}^{n_j} I_i \Big/ n_j$ Where n_j is the number of returns in ring j. $IR\_sd = sd(I_{A_j})$
D1_2	**D**ifference of intensity between **1**st and **2**nd returns of the same pulse, in the same channel.	-	mn, sd, p25, p50, p75	$\Delta I_{i1\_2} = (I_{i1} - I_{i2})$ $3D\_D1\_2\_mn = mn(\Delta I_{i1\_2})$
RM	**R**atio between different statistics.	all, 1st, 2nd	-	RM_1st_ mn_all_ mn $= mn(I_{i_{1st}})/\ mn(I_{i_{all}})$ RM_1st_ mn_2nd_ mn $= mn(I_{i_{1st}})/\ mn(I_{i_{2nd}})$

Symbol	Description	Return types	Statistics	Equation
NDG1	**G**reen (type **1**) **N**ormalized **D**ifference vegetation index	1st, si	mn, p50, p75	$I\_NDG1\_mn = \frac{mn(I_{i_{C2}}) - mn(I_{i_{C3}})}{mn(I_{i_{C2}}) + mn(I_{i_{C3}})}$
NDG2	**G**reen (type **2**) **N**ormalized **D**ifference vegetation index	1st, si	mn, p50, p75	$I\_NDG2\_mn = \frac{mn(I_{i_{C1}}) - mn(I_{i_{C3}})}{mn(I_{i_{C1}}) + mn(I_{i_{C3}})}$
NDIR	**I**nfra**R**ed **N**ormalized **D**ifference vegetation index	1st, si	mn, p50, p75	$I\_NDIR\_mn = \frac{mn(I_{i_{C1}}) - mn(I_{i_{C2}})}{mn(I_{i_{C1}}) + mn(I_{i_{C2}})}$

2.2.7 Random forest classification and feature selection

The species class of each tree was identified, at each classification level, using Breiman and Cutler's Random Forests for Classification (RF) approach (Breiman 2001). This classification method has various advantages, or is sometimes at least equivalent in terms of performance, compared to other methods (Fernández-Delgado *et al.* 2014). It has been proved to be adequate for species classification in other studies (Korpela *et al.* 2010b ; Ørka *et al.* 2012). RF does not rely on the assumptions of normality and homoscedasticity. Normality tests (Shapiro-Wilk) on our data revealed that a large proportion of the features did not follow a normal distribution. Also, tests of variance equality between classes (Levene test) indicated that the assumption of homoscedasticity was not fulfilled either. Therefore, some widely used methods such as linear or quadratic discriminant classification could not be directly applied in this case. In addition, RF can handle a very large set of predictors, has a low sensitivity to collinearity between features (Immitzer, Atzberger and Koukal 2012), and should not overfit (Breiman 2001). However, RF is sensitive to unbalanced data (large discrepancies in the number of samples per class). Down- or up-sampling strategies to equalize the class frequencies should be applied when the training set itself is unbalanced (Chen, Liaw and Breiman 2004).

In accordance with our objectives, we developed classification models using 3D and intensity features *i*) for each of the three Titan channels taken separately (C3, C2, C1), and *ii*) for all channels taken together (C321), including features from two channels in the case of normalized differences. These four options are thereafter referred to as "channel sets". The first group *i*) served to demonstrate the achievable accuracies using single channel ALS, with particular attention to the common 1064 nm and 1550 nm channels. The role of second group was to highlight potential gains brought about by multispectral ALS data.

Despite precautions taken at the design stage, the number of features remained large, varying from 50 to 142. For this reason, we considered different approaches of feature selection. Our goal was to identify a small number of features that jointly provided good species separability using RF classification. Dimensionality reduction strategies through selection or extraction of synthetic features (e.g. principal component analysis) are numerous, and are still the object of active research in the field of pattern recognition where high dimensionality classification problems abound. In ALS-based land-use or species classification, dimensionality reduction was performed for example by testing the classifier using all possible feature combinations (Hovi *et al.* 2016), an approach that may create a combinatorial burden, or based on the influence of each feature in an initial random forest classification (Yu *et al.* 2017). Other studies used different algorithms implemented in RF for variable selection and ranking, prior to final species classification (Korpela *et al.* 2010b ; Vauhkonen *et al.* 2010). We proceeded by first selecting the most useful variables, and then discarded those that were highly inter-correlated. This selection procedure was performed for each site only on the highest available level of classification (genera for SC and species for YRF). A RF trial using all features (Tables 2.6 and 2.7) was used to generate an initial accuracy value (mean decrease accuracy) for each feature. The parameter values used in RF were *ntree* = 1501 (RF results do not improve significantly over 300 trees, and odd numbers were preferred to avoid voting ties), *mtry* = 11 (we chose a median *mtry* value to apply for all classification models, after testing the best *mtry* for each level and channel set), and balanced with *sampsize* parameter equal to the minimum number of individuals in a class at a given classification level (36 in the lowest case). The *sampsize* parameter ensures that, at each iteration, the number of sampled crowns was the same in each class. Only features that had a mean decrease accuracy value larger than 0.01 in this initial RF classification were kept. Based on the correlation matrix of the remaining features, we discarded features which had an absolute correlation value larger than 0.9 with another one that had a greater usefulness (larger value of mean decrease accuracy).

Consequently, the number of retained features was different for each channel set, depending on the joint usefulness of features and the degree of inter-correlation.

Once the reduced set of features was determined, a RF classification was rerun using only the remaining features. This allowed testing these parsimonious models through the evaluation of their out-of-bag error (for OOB estimate error rate see Belgiu and Drăguţ 2016 ; Liaw and Wiener 2002), with *ntree* = 501, *mtry* = 3 and 100 times randomization for each classification level, and each channel set. For each of these combinations, a confusion matrix was calculated and expressed in percentages, summing up all the resulting confusion matrices of the 100 iterations of RF. The feature selection obtained at the highest classification level for each site was applied at the lower levels. All RF procedures were implemented in the “randomForest” R package (Liaw and Wiener 2002). Finally, the role of the individual features in class separability was examined through box and whisker plots.

2.3 Results

The two-step procedure of variable selection using accuracy and inter-correlation criteria produced a number of features much smaller than the initial set (Tables 2.8 and 2.9). The number of retained features was equal, or lower, in the case of C321, compared to those of the separate channels. Moreover, even if the initial number of features was greater for SC than for YRF (due to features computed from the difference between 1^{st} and 2^{nd} returns), more features were retained for YRF than for SC. The number of selected features for each combination of site and channel set depended largely on the degree of inter-correlation between features. Those belonging to the same family (e.g. NDG2) were in general strongly inter-correlated as they represented different statistics (e.g. mn, p50, p75) of the same calculated property. The initial number of features in Table 2.9 was slightly variable because a few features causing no data occurrences for several trees were discarded.

Table 2.8: Number of features retained at each step of selection (SC)

Elimination step	**C3** (532 nm)	**C2** (1064 nm)	**C1** (1550 nm)	**C321**
Initial	68	68	68	142
Accuracy filter	16	20	18	19
Correlation filter	7	5	5	5

Table 2.9: Number of features retained at each step of selection (YRF)

Elimination step	**C3** (532 nm)	**C2** (1064 nm)	**C1** (1550 nm)	**C321**
Initial	51	49	51	99
Accuracy filter	23	22	23	33
Correlation filter	11	11	14	9

Tables 2.10 and 2.11 list the features retained for classification for each region by channel set, by decreasing importance (based on the mean decrease accuracy). For each classification model, selected variables were comprised of intensity and 3D features, except for the C321 of the SC region, which included only intensity features. Features based on normalized differences (NDG) stood out as the most important ones at the two sites for the C321 channel sets. C1 intensity-based features were the single channel features most useful in the C321 feature sets. At YRF, only two out of nine selected features were based on 3D data. They also had low ranks (7^{th} and 8^{th}). For the two sites, the proportion of 3D features was higher in the single channel sets compared to the C321 channel sets. In all cases the first feature was always an intensity feature. The 3D features were more represented at YRF than at SC, and were the more frequent type for channels considered separately.

Table 2.10 : Selected features (SC)

C3 (532 nm)	**C2** (1064 nm)	**C1** (1550 nm)	**C321**
I_RM_1st_mn_all_mn_C3	I_PE_1st_p95_C2	I_PE_1st_p95_C1	I_NDG2_si_mn
I_CT_si_mn_C3	3D_PE_1st_p50_C2	I_D1_2_sd_C1	I_PE_1st_p95_C1
I_D1_2_p75_C3	I_DI_si_sd_C2	3D_SL_1st_p50_C1	I_PE_si_p75_C2
I_D1_2_mn_C3	I_D1_2_sd_C2	3D_SL_all_p25_C1	I_D1_2_sd_C1
3D_RM_1st_mn_all_mn_C3	I_RM_1st_mn_all_mn_C2	3D_SL_all_p50_C1	I_NDG1_si_mn
3D_SL_all_p75_C3			
3D_SL_1st_mn_C3			

Table 2.11: Selected features (YRF)

C3 (532 nm)	**C2** (1064 nm)	**C1** (1550 nm)	**C321**
I_PE_si_p75_C3	I_PE_1st_p90_C2	I_PE_1st_p75_C1	I_NDG1_1st_p75
3D_CH_all_C3	3D_SL_all_p75_C2	I_DI_1st_sd_C1	I_NDG2_1st_mn
3D_PE_all_p25_C3	3D_CH_all_C3	3D_CH_all_C1	I_DI_1st_sd_C2
3D_PE_all_p50_C3	3D_RM_1st_mn_all_mn_C2	3D_SL_1st_p75_C1	I_NDIR_1st_p75
I_DI_si_sd_C3	3D_SL_all_p25_C2	3D_RM_1st_mn_all_mn_C1	I_PE_1st_p75_C1
I_IR_1st_C3	3D_SL_all_p50_C2	3D_HR_all_lm_C1	I_PE_si_p75_C3
I_DI_1st_cv_C3	3D_SL_1st_p50_C2	I_RB_05_95_1st_C1	3D_RM_1st_mn_2nd_mn_C321
3D_MI_all_mn_C3	3D _RM_1st_mn_2nd_mn_C2	3D_RM_1st_mn_2nd_mn_C1	3D_SL_all_mn_C321
I_PE_1st_p50_C3	3D_HR_all_lm_C2	3D_SL_all_mn_C1	I_DI_1st_sd_C1
3D_PE_all_p75_C3	I_RM_1st_mn_all_mn_C2	3D_SL_all_p50_C1	
I_PE_1st_p25_C3	3D_RM_all_p50_all_mn_C2	3D_SL_all_p25_C1	
		3D_SL_1st_mn_C1	
		3D_RM_all_mn_C1	
		I_PE_1st_p25_C1	

Figures 2.3 and 2.4 illustrate the class separability at the highest classification level for each selected feature of C321 at both sites. No two classes were perfectly separated using any given single feature, but some stood out as having only a small overlap with the rest, such as the *Picea* genus at SC using NDG1 and NDG2 features, or sugar maple at YRF with I_PE_1st_p75_C1. Other features that contributed most to the separability of some classes should also be highlighted. The normalized green vegetation indices (NDG) generally had higher value for BL species than for NL ones, as in the case of optical imagery. Ash was however confounded with NL species at YRF, based on NDG values. The infrared-based index (NDIR) provided less separability power, but was useful for example in separating white pines from other BL species. The two 3D features at species level brought limited discriminative power, but helped for example

in isolating Norway spruce from the rest of the BL species. Overall, it is clear that combining all features results in a good level of separability. For example, while Scots pines and white pines are confused with NDG-based features, but distinct from red pines, white pines can be partly isolated from the two other pine species using other features, such as I_PE_1st_p75_C1.

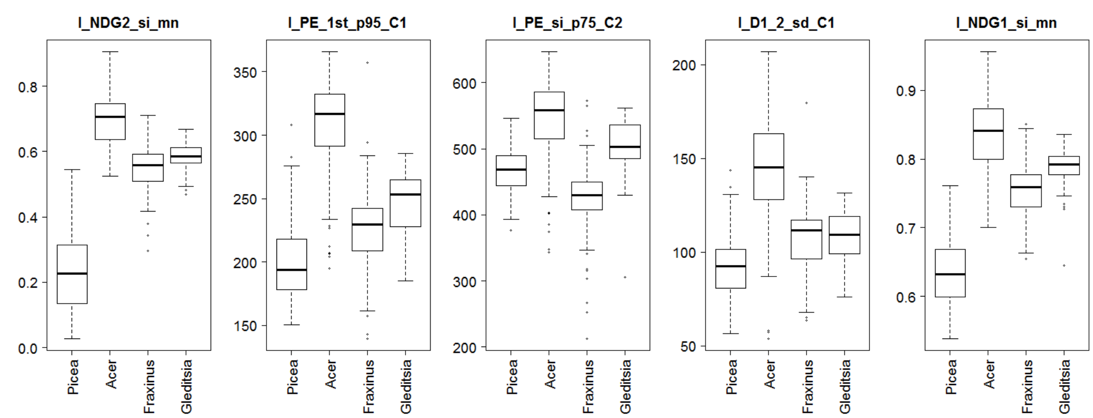

Figure 2.3: Variation of selected variables at the genus level (SC)

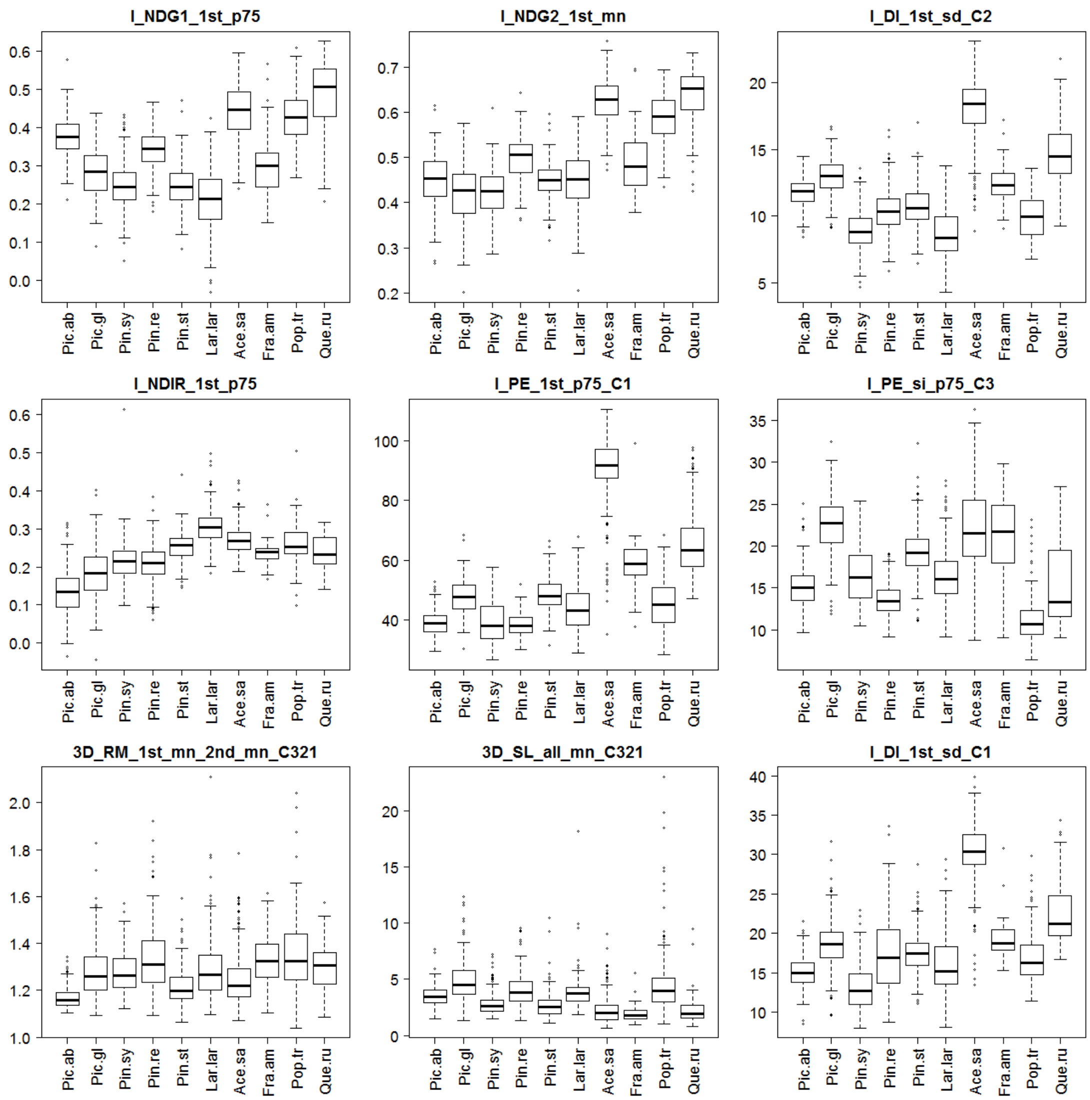

Figure 2.4: Variation of selected variables at the species level (YRF)

Tables 2.12 and 2.13 show the species identification OOB errors of random forest classifications for the different channel sets and sites. The values reported in these tables represent the means of the different OOB values obtained for a given model through 100 random iterations. The standard deviation of these OOB error values never exceeded 0.55% per classification model. The best results at all levels of classification were obtained using the pooled data from the three channels (C321). Interestingly, this was achieved using a number of features lower or equal to that of the single channels. The contrast between C321 results on the one hand, and single channel results on the other hand, became greater as the number of classes increased. The difference between the best single channel classification model (most often C1) and the corresponding C321 model became appreciable only when classifying into seven genera, or 10 species at the YRF site. Except for the BL vs. NL classification level at SC, C3 results were the least accurate.

Table 2.12: Identification OOB error rate (SC)

Laser channels	**C3** (532 nm)	**C2** (1064 nm)	**C1** (1550 nm)	**C321**
Number of features	7	5	5	5
BL vs. NL	3.0%	6.6%	5.3%	2.8%
4 genera	24.6%	21.8%	15.8%	13.3%

Table 2.13: Identification OOB error rate (YRF)

Laser channels	**C3** (532 nm)	**C2** (1064 nm)	**C1** (1550 nm)	**C321**
Number of features	11	11	14	9
BL vs. NL	14.2%	12.3%	10.2%	4.6%
7 genera	36.7%	29.9%	31.3%	19.9%
10 species	38.4%	35.9%	34.7%	23.6%

Confusion matrices for the C321-based species identification presented in Tables 2.14 to 2.17 are calculated as a weighted mean error of the 100 random iterations. Confusion matrices presenting absolute counts for a single iteration are given in the appendix (Table A.1 to A.4). At the most general classification level (Table 2.14), omission and commission errors behave somewhat differently between the two study regions, but the errors are so low that this may be simply anecdotal. At the genus level, the accuracies do not vary sharply between classes, with intervals of 78.9% to 91.6% for SC, and 63.3% to 90.6% at YRF. No marked performance differences were seen between the BL and NL genera accuracies. At both sites, maples had the highest accuracy among BL trees, while oaks at the YRF site had the highest error.

Table 2.14: Confusion matrix in % for C321 at the BL/NL level

	SC			**YRF**	
	NL	**BL**		**NL**	**BL**
NL	**94.4**	5.6	**NL**	**96.4**	3.6
BL	2.1	**97.9**	**BL**	7.2	**92.8**

Table 2.15: Confusion matrix in % at the genus level (SC)

	Picea	***Acer***	***Fraxinus***	***Gleditsia***
Picea	**91.6**	1.4	7.0	0.0
Acer	0.0	**88.0**	7.1	4.9
Fraxinus	7.0	5.6	**78.9**	8.5
Gleditsia	0.0	0.0	13.9	**86.1**

Table 2.16: Confusion matrix in % at the genus level (YRF)

	Picea	***Pinus***	***Larix***	***Acer***	***Fraxinus***	***Populus***	***Quercus***
Picea	**85.7**	7.7	4.2	0.5	0.5	1.2	0.2
Pinus	7.8	**73.4**	9.9	0.2	4.3	3.7	0.7
Larix	1.1	9.7	**81.7**	0.0	2.7	4.8	0.0
Acer	0.0	0.5	0.5	**90.6**	1.5	2.5	4.5
Fraxinus	4.4	6.7	2.2	2.2	**68.9**	11.1	4.4
Populus	1.1	8.0	2.3	0.0	2.9	**82.2**	3.4
Quercus	0.0	6.1	0.0	20.4	4.1	6.1	**63.3**

The confusion matrix at species level (Table 2.17) contains results that could be expected based on the more general classification levels, i.e. higher confusion rates occur among NL species, or among BL species, but rarely between a NL and a BL species. Notable exceptions were the higher levels of confusion between poplars and red pines, and between red oaks and white pines. The highest rate of confusion is the commission error of 20.4% of red oaks towards sugar maples, while the overall highest accuracy was achieved for sugar maple.

Table 2.17: Confusion matrix in % at the species level (YRF)

	Pic.ab	***Pic.gl***	***Pin.sy***	***Pin.re***	***Pin.st***	***Lar.lar***	***Acer.sa***	***Fra.am***	***Pop.tr***	***Que.ru***
Pic.ab	**83.8**	2.9	1.5	7.8	1.5	1.0	0.0	0.0	1.5	0.0
Pic.gl	0.9	**86.1**	1.8	0.9	6.3	3.1	0.4	0.0	0.4	0.0
Pin.sy	0.5	4.1	**63.4**	10.8	11.3	5.2	0.0	3.6	1.0	0.0
Pin.re	6.3	0.0	13.5	**72.9**	0.5	3.6	0.0	0.0	3.1	0.0
Pin.st	3.2	7.9	6.3	2.1	**64.6**	10.1	0.0	3.7	1.1	1.1
Lar.lar	0.5	3.2	8.1	0.5	7.5	**73.1**	0.0	2.7	4.3	0.0
Acer.sa	0.0	0.0	0.0	0.0	0.5	0.5	**90.6**	1.5	2.5	4.5
Fra.am	0.0	4.4	0.0	0.0	8.9	2.2	2.2	**66.7**	11.1	4.4
Pop.tr	0.0	1.1	0.0	8.0	1.7	1.7	0.0	2.9	**81.0**	3.4
Que.ru	0.0	0.0	0.0	0.0	8.2	0.0	20.4	6.1	8.2	**57.1**

Pic.ab = Picea abies, Pic.gl = Picea glauca, Pin.sy = Pinus sylvestris, Pin.st = Pinus strobus, Lar.lar = Larix laricina, Fra.am = Fraxinus Americana, Pop.tr = Populous tremuloides, Que.ru = Quercus rubra.

2.4 Discussion

2.4.1 Feature selection

For reducing the large number of initial 3D and intensity features, especially in the multispectral case, we selected the most useful and less redundant ones based on thresholds of mean decrease accuracy and inter-correlation between features. The final selection of features varied between study sites, and classification levels. We consider futile to discuss minute details of the feature selection results, such as the fact that the 75th intensity percentile was the first variable in the C1 channel set while the 90th came out first for C2 (species level at YRF, see Table 2.11). However, general trends are quite informative on the usefulness of the broad categories of variables. Firstly, for all channel sets and sites, intensity-based features ranked first, and in the case of the C321 set, normalized differences were the most useful. This behaviour was also observed by

Yu *et al.* (2017) in a study using Titan ALS data for identifying two NL and one BL species where an intensity feature and a normalized difference feature were respectively the first and second most important variables in the three-channel set, and a channel ratio was first among the combined intensity variables. In our study, seven out of the nine most useful related features were intensity-based, while four out of the five best features in Yu *et al.* (2017) were also computed from intensity. These trends indicate that, regardless of the relationship between species and architectural traits of trees, and despite tripling the density of the 3D data in the case of the C321 channel set, variations in monospectral, but especially multispectral intensities, carry more information on species than 3D data. In searching for explanations for these findings, it should be remembered that the intensity values depend not only on the reflectance of the foliage, but also on its orientation and on the area of its cross-section within each laser footprint. Differences in this regard between NL and BL species are expected to be large. This fact was confirmed, among other observations, by sugar maples having the highest intensities in all but one of the single intensity plots of Figures 2.3 and 2.4. Sugar maples have large and overlapping leaves, a planophile leaf angle distribution, and a high infrared reflectance, thus generating powerful returns. They had the largest ratio of number of single returns over number of first returns (not presented). NDVI-like features were very useful for species identification probably because they capture, in the case of NDG1 and NDG2, the variations between the green (linked to the chlorophyll contents) and the infrared (related to the foliar structure and water content) parts of the spectrum. C1-based features (1550 nm) were also quite frequent among the most useful variables, showing the utility of this wavelength. C3-based single-channel features seldom appeared (but C3 was present in most normalized differences). The wider divergence and longer ranges due to the 7° firing angle in C3 resulted in a lower incidence power at leaf level, and thus, the laser irradiance at canopy level in this channel should be lower than in the infrared channels. In addition, the reflectance of foliage at 532 nm is much lower than in the infrared. For these reasons, it is expected that the signal to noise ratio in C3 should be much smaller than in the other channels. Nevertheless, a C3 intensity-based feature ranked first, i.e. above 3D features, in both regions when classification was carried out using the C3 channel set.

2.4.2 Accuracy improvements in species identification

The results presented above demonstrate that the additional information provided by the two extra wavelengths of the Titan MSL, compared to single channel ALS sensors, improved species classification at all classification levels and sites, with an effect strongly proportional to the number of classes. Because there have been very few studies on species identification with three wavelength ALS, we are quite limited when trying to compare our results to those of other researchers. Even in the case of single-wavelength ALS species identification studies, comparing the respective accuracies reported in previous studies is quite arduous because the number of species, the size of trees, and different acquisition parameters vary between them. Such research efforts were so far presented by Hopkinson *et al.* (2016) and Yu *et al.* (2017). The former researchers were able to separate tree classes (broadleaf, larch and pine/spruce trees at plot level, Titan data acquired at a height of 800 m above ground level) with an accuracy between 66% and 80%, but did not compare to single channel results. Yu *et al.* (2017) obtained an accuracy of 86% when combining features from all three channels for identifying three species (pine, spruce and birch at individual tree level, data acquired at 400 m above sea level), which was not significantly different from the best performance using single channel. In our study, the advantages of three-channel ALS became significant for classifications with seven or more classes. Even in the case of the identification of four genera, gains relative to single-wavelength ALS were marginal, a result that is compatible to those of Yu *et al.* (2017). Evidently, having a greater number of species brings more variability in the shape, size and reflectance of leaves, and in tree architecture, creating a more difficult identification task. In this case, the added information contents of the Titan data allowed us to identify as many as 10 species with an accuracy superior to 75% using as little as nine features from MSL only. To the best of our knowledge, such results had not yet been reported in the scientific literature.

2.4.3 Limitations and generalizability

The error levels reported in this paper apply to manually delineated crowns. It is probable that these levels would rise in the case of automatically delineated crowns due to unavoidable random or systematic segmentation errors. Moreover, it can be expected that species identification of smaller trees is more difficult than that of larger ones, simply because the number of returns (at a given point density) will then be lower. The 3D characteristics would then be less well defined and the per-crown intensity statistics noisier. The majority of classification studies limit their research to trees having commercially valuable sizes. Having a diversity of tree ages in the sampled crowns comparatively increase the intra-species variability and the classification error probability because of the changes in tree architecture, leaf shapes and reflectance with tree age. Further research must be done to understand if stratification by tree height or age could improve classification performance, as remarked also by Hovi *et al.* (2016). Furthermore, the random forest model trained with a limited sample coming from a specific region is difficult to apply on a broader scale without additional training samples to account for site variation.

Both datasets used in the present study covered rather small areas and were each surveyed over a short period of time during which no significant changes occurred in the atmospheric or surface conditions that could have affected pulse attenuation. Furthermore, the sampling density (crown samples/km^2) was relatively high, creating very good conditions for training a classifier, at the cost however of numerous hours of field work and interpretation. Deploying this approach over larger territories, using surveys carried out on different days, i.e. encompassing varying surface and atmospheric conditions, could certainly lead to complications. While it can be assumed that basic 3D features, such as tree proportions or overall shape for a given species at a given age, would be relatively stable over a larger region, intensities might be affected by variations in foliage humidity (especially in the 1550 nm channel), or in atmospheric transmissivity between survey days. While the latter can be corrected to some extent (Yan and Shaker 2014), the effects of foliage humidity variations might be difficult to model. This in turn could create the obligation of gathering costly training data for each flight. On a broader level, variations for example in tree architecture with age or site characteristics (Hovi *et al.* 2016), or changes in foliage reflectance caused by leaf maturation during the leaf-on season (Hakala *et al.* 2015 ; Kim 2010) or by stress (Gaulton *et al.* 2013 ; Gong *et al.* 2015), would affect the results of any ALS-based species identification, whether in the single or multi-channel case. Further methodological or technological developments are required before a truly robust approach can come about. Nevertheless, our study, by comparing the respective species identification accuracy of single-channel and three-channel lidar data has clearly demonstrated the advantages of using multispectral ALS data for a single tree crown classification. This will hopefully provide better forest data for informing management decisions, as well as a clearer picture of the complex mosaic of species of mixed forest ecosystems.

2.5 Conclusion

The additional laser channels in airborne MSL, compared to single channel ALS, were shown to be useful for increasing the accuracy in species identification. A significant increase was achieved only when the number of species classes was relatively high. Discrimination between broadleafs and needleleaf species (two classes) did not significantly benefit from MSL data. The additional intensities, and especially channel ratios like NDVIs, were the features that improved most the classification accuracy.

3D features performed well for a limited number of species and for single channels, but their discrimination power was surpassed by intensity features.

Considering the usefulness of MSL intensities, future efforts are needed to improve lidar intensity standardization within large areas. Finally, the features' sensitivity to the intra-species variability caused by tree age, height and growth conditions will need to be further researched.

2.6 Acknowledgements

We express gratitude to Teledyne Optech Incorporated (Vaughan, Canada) for graciously providing the Titan MSL datasets used in this study. We also thank the authorities of the York Regional Forest (namely Kevin Reese) for granting permission and facilitating access to the YRF study area. We acknowledge the collaboration of CarboMap (Edinburgh, Scotland) in field logistics and data collection. This study was partly funded by the National Science and Engineering Council of Canada, through the AWARE project. We acknowledge the reviewers for the useful comments which help us improve our work.

CHAPITRE 3

VARIABILITY OF MULTISPECTRAL LIDAR 3D AND INTENSITY FEATURES WITH INDIVIDUAL TREE HEIGHT AND ITS INFLUENCE IN TREE SPECIES IDENTIFICATION

Cet article a été publié :

Brindusa Cristina Budei, Benoît St-Onge, 2018, Variability of multispectral lidar 3D and intensity features with individual tree height and its influence on needleleaf tree species identification, *Canadian Journal of Remote Sensing*, Volume 44, Issue 4, pages 263-286, DOI: 10.1080/07038992.2018.1478724

Abstract

Tree species identification is important in forest management. The multispectral lidar Titan of Teledyne Optech Inc. can improve tree species separation by providing classification features computed from the three-channel intensities, ratios and normalized differences. However, the value of features used in classification algorithms (e.g., random forest, RF) may vary with tree size. The focus of the present study is to show how tree height influences the 3D and intensity features, how this relationship may affect the species classification accuracy, and how different classification strategies may circumvent this problem. Six needleleaf species (*Pinus resinosa*, *Pinus strobus*, *Pinus sylvestris*, *Larix laricina*, *Picea abies* and *Picea glauca)*, found in plantations of different ages, were sampled to train classifiers. Some features yielded a good discriminatory power for species identification, despite their relation to tree height (r^2 up to 0.6). Two random forest (RF) classification strategies—a) using only size-invariant features (SIF) and b) training separate classifiers per tree height strata (HSC)—were compared to a standard classification (STD: all features, without height stratification). The accuracy of the SIF approach was lowest, useful variables being removed due to their relationship to tree height. The HSC provided only a minor improvement over the STD results.

Keywords: tree species; tree height; multispectral lidar; intensity; Titan; *random forest*; forestry

Résumé

L'identification des espèces est importante dans la gestion forestière. Le lidar multispectral Titan, de Teledyne Optech Inc. peut améliorer l'identification des espèces en utilisant les variables calculées à partir des intensités des trois canaux, de leurs ratios, ou des différences normalisées (NDVI). Pourtant, les variables utilisées dans l'algorithme de classification peuvent varier en fonction de la taille de l'arbre. L'objectif de cette étude a été de tester comment la hauteur de l'arbre influence les variables 3D et d'intensité, comment cette relation affecte la précision de la classification et comment différentes stratégies de classification peuvent contourner ce problème. Six espèces de conifères (*Pinus resinosa*, *Pinus strobus*, *Pinus sylvestris*, *Larix laricina*, *Picea abies* et *Picea glauca*), se trouvant dans des plantations de différents âges, ont été échantillonnées pour entraîner le classificateur. Certaines variables apportent un bon pouvoir discriminant pour l'identification des espèces malgré leur variation en fonction de la hauteur de l'arbre (r^2 jusqu'à 0.6). Deux stratégies de classification utilisant *random forest* (RF) – a) considérant seulement les variables qui ne varie pas en fonction de la taille de l'arbre (SIF) et b) entraîner des classificateurs différents par strate de hauteur (HSC) - ont été comparées avec la classification standard (STD : toutes les variables, sans stratification en fonction de la hauteur). La précision de la stratégie SIF a été plus faible, certaines variables utiles étant exclues à cause de leur variation en fonction de la hauteur de l'arbre. La stratégie HSC offre une amélioration limitée par rapport à STD.

Mots clés : espèce de l'arbre; hauteur de l'arbre; lidar multispectral; intensité; Titan; *random forest*; forestrerie

3.1 Introduction

Information on tree species is very important in forest management, be it for planning timber harvesting, scheduling silvicultural treatments or planning ecological assessment for conservation. However, data on species in boreal and temperate forests often lack the required precision, especially where species diversity is relatively high (e.g., North America) and existing forest stand maps are fairly general or infrequently updated (Beaudoin *et al.* 2014 ; Brosofske *et al.* 2014 ; Hudak *et al.* 2016 ; Thompson *et al.* 2007). To solve this problem, a wide variety of methods were developed for identifying species using airborne or satellite imagery (see review by White *et al.* 2016). More recently, the usefulness of airborne laser scanning (ALS) for extracting structural information on forests led several researchers to test the use of ALS data for identifying species, focusing on individual tree level (see reviews by Fassnacht *et al.* 2016 ; Koenig and Höfle 2016 ; Vauhkonen *et al.* 2014). In this approach, features (sometimes called "metrics") are extracted for each tree, and a classifier (e.g., discriminant analysis, support vector machine, random forest, etc.) is trained to identify species. Features are derived from the three-dimensional (3D) ALS data, or from the discrete return or full waveform laser intensities (Holmgren, Persson and Söderman 2008 ; Hovi *et al.* 2016 ; Kim *et al.* 2009 ; Korpela *et al.* 2010b ; Li, Hu and Noland 2013 ; Li *et al.* 2010 ; Lin and Hyyppä 2016 ; Ørka, Næsset and Bollandsås 2009 ; Van Ewijk *et al.* 2014 ; Vaughn, Moskal and Turnblom 2012 ; Vauhkonen *et al.* 2010). A large number of such features were developed in the context of studies and, for this reason, different feature selection approaches were proposed. Among the most useful features, the ones based on intensity often appeared in the top ranks of the selections (Budei *et al.* 2018 ; Korpela *et al.* 2010b ; Ørka, Næsset and Bollandsås 2009).

Recently, multispectral lidar (MSL) technologies were developed. The first operational MSL lidar system with three channels—the Titan—was introduced by Teledyne Optech in 2014 (Fernandez-Diaz *et al.* 2016). This system collects 3D and intensity data in the green, near-infrared (NIR) and short wave infrared (SWIR) portions of the spectrum. MSL offers the possibility to enhance the intensity-based tree identification features by using intensity statistics from the two additional channels (compared to monospectral lidar) or from channel combinations, such as ratios between channels or vegetation indices such as the Normalized Difference Vegetation Index (NDVI) (Ahokas *et al.* 2016 ; Axelsson, Lindberg and Olsson 2018 ; Budei *et al.* 2018 ; St-Onge and Budei 2015 ; Yu *et al.* 2017). This could put MSL on par with multispectral imagery regarding its capacity to distinguish species using spectral signatures. What is more, the simpler acquisition geometry of ALS (viewing and incidence angle coincide) theoretically gives it an advantage over passive imagery (Woodhouse *et al.* 2011).

The training of species identification classifiers requires that a representative sample of trees be visited in the field to ascertain their species and to then attribute the species to the corresponding crown point cloud in the ALS dataset. One element of representativeness is the correspondence between the tree height distribution in the sample and in the population. Indeed, several studies have indicated that tree size (height or crown area, both strongly linked to tree age) may influence the values of 3D classification features (Hovi *et al.* 2016 ; Korpela *et al.* 2010b ; Ørka, Næsset and Bollandsås 2009). Moreover, very little is known on the possible influence of tree size on intensity feature values. The latter are considered to be indirectly influenced by tree height, and at a smaller degree, compared to 3D features (Brandtberg 2007 ; Hovi *et al.* 2016 ; Ørka, Næsset and Bollandsås 2009). Ørka, Næsset and Bollandsås (2009) concluded that species identification based on features that varied with tree size is problematic. In the following section we examine biological factors linked to tree size that could influence the 3D point characteristics within crowns as well as possible determinants of the ALS return intensities. We also look at the relationship between tree size, ALS point density and feature computation.

3.1.1 Changing tree architecture with height / age

The crown structure of individual trees is a result of two levels of response to the environment. At the species level, the adaptation to the environment results in a specific tree architecture and growing modality. At the individual level, each tree has a certain capacity to surpass the pre-established organization plan for its species in order to respond to specific environmental conditions (Millet 2012). Crown structure is therefore also influenced by local growing conditions, (e.g., illumination, local soil conditions) (Larcher 2003 ; Messier *et al.* 1999 ; Valladares and Niinemets 2007).

It is well known that tree architecture also changes with age. In that regard, two main stages of tree development may be distinguished (Millet 2012). During its expansion stage (from young to mature), a tree increases in volume and exploits most of its resources in developing its trunk and its branch hierarchy. Once it reaches sexual maturity, it will devote more resources to flowering. In the regression stage (senescence), a slowdown in tree and branch growth occurs, and an eventual decrease of biomass (Millet 2012).

During the first development stage of *Picea abies* or *Pinus sylvestris*, for example, axes (trunk and branches) reach the fourth order and tree organization is similar to the Rauh model (Hallé, Oldeman and Tomlinson 1978 ; Millet 2012). In the second stage for *Picea abies*, initial axes of third and fourth orders, which can live 8 to 10 years, are progressively replaced by partial reiteration, forming drapery. In the case of *Pinus sylvestris*, there is abundant partial reiteration in the crown that leads to a supplementary axis order (Millet 2012).

3.1.2 Variability of crown-wise lidar point cloud quality

The number, density and 3D spatial distribution of lidar returns in a given crown, which determine the crown-wise point cloud quality, depends on the ALS acquisition parameters, such as flying altitude, beam divergence, pulse repetition and scan frequencies (Fernandez-Diaz *et al.* 2016 ; Goodwin, Coops and Culvenor 2006 ; Hopkinson 2007 ; Næsset 2009). For given acquisition parameters, crown area will obviously determine the number of lidar returns within a crown. The high correlation between crown area and tree height implies that taller trees have a greater probability of intercepting lidar pulses. As the properties of individual pulses are subject to random variation (Hovi *et al.* 2016), the features computed from a larger number of returns are more accurate than those computed from a reduced number of returns. This signifies that classification features computed for smaller trees, having fewer returns, would have a greater variability. In this regard, Hovi *et al.* (2016) found that the feature variance attributable to individual tree structure increased with a decreasing number of returns per crown. However, large trees may also present more structure variability. For example, Hovi *et al.* (2016) found that, for pines and birches, identification accuracy of the bigger trees was lower despite the larger number of pulses per crown, a fact attributable to the more complex architecture of large trees.

Tree height will also influence the number of returns for the same pulse in a discrete return dataset (Ørka, Næsset and Bollandsås 2009). Given tree height and the vertical resolution of lidar pulses (the minimum time or distance between consecutive returns), there is a higher probability that small trees do not contain many second or third returns for example (Ørka, Næsset and Bollandsås 2009). This negatively affects the possibility of computing some features that require a minimum number of returns of a specific type (see methods section for examples). Thus, small trees are more problematic in terms of the variety of features that can be correctly computed, possibly having "no-data" values for several features. Such missing data often complicates training and classification.

3.1.3 Lidar penetration depth in tree crown

Many factors may impact the lidar pulse penetration depth in a crown. For example, scan angle and the pulse repetition rate influence the power of lidar pulse at target level, which in turn can determine penetration depth (Chasmer *et al.* 2006 ; Disney *et al.* 2010). Tree characteristics such as gapiness, leaf area index or foliage reflectance are also determinant. For a given species, the latter crown characteristics vary with age, crown architecture, stress or senescence (Gaveau and Hill 2003) as well as with tree density or tree status as either dominant or suppressed (Chasmer *et al.* 2006). During the first stage of tree architectural development (expansion), internodes have a greater length and a fast growth rate. When a tree reaches the peak of its expansion, branch growth segments become smaller, with a slower growth rate, and are concentrated at the uppermost surface of the tree crown. A higher leaf density in the upper canopy determines a higher pulse interception at this level and a lower power available for the succeeding returns, thus influencing the pulse penetration probability. Branch orientation can also evolve with age (Millet 2012). Combined with lidar scan angle, branching layout could influence the lidar penetration depth probability. The relation between tree size or age, and lidar penetration depth, may change lidar classification feature values for a given species. The combined effect of the lidar penetration depth in tree crowns and the threshold value used to exclude low points during ALS point cloud processing (explained in the following section) should result in very different 3D feature values for small trees compared to larger ones.

3.1.4 Minimum return height threshold

Before computing 3D or intensity classification feature values per crown, researchers commonly exclude low returns that may belong to the ground or understorey by selecting only points above a vertical threshold. The height of this threshold determines the number of available returns for calculating features. Small trees are obviously more affected by this threshold (Ørka, Næsset and Bollandsås 2009). It is therefore important to carefully choose the threshold height, because this may influence the calculated feature values, the number of computable features, and thus the number of removed trees due of no-data values. Overall, threshold selection will affect species identification accuracy.

There are two possible ways of defining height thresholds. The first is to choose a fixed height above ground, usually above the ALS digital terrain model (DTM). The threshold of 2 m above ground, first introduced by Nilsson (1996), is the most commonly used threshold for area-based analysis of forest structure (Maltamo, Suvanto and Packalén 2007 ; Næsset and Økland 2002 ; Packalén and Maltamo 2008) and is sometimes also used in individual tree crown (ITC) analysis (Shi *et al.* 2018b ; Yu *et al.* 2017). The second method is to determine threshold height as a proportion of tree height. This has the advantage of always using the same "part" of the tree (Budei *et al.* 2018 ; Hovi *et al.* 2016 ; Korpela *et al.* 2010b). In most studies that focus on identifying commercial-size trees, a high fixed threshold is advisable because this allows eliminating almost all understorey returns without removing crown returns. However, when considering a larger range of tree heights, including small trees, the threshold choice becomes critical. For example, a fixed threshold of 2 m may leave too few returns for reliably calculating feature values of short trees. Some studies tried to use a very low threshold to preserve as much data as possible for smaller trees, for example a threshold 1.3 m was used by Ørka, Næsset and Bollandsås (2009), 0.5 m by Næsset and Bjerknes (2001), 0.3 m by García *et al.* (2010) or 0.17 m by Hudak *et al.* (2006).

Næsset and Bjerknes (2001) compared the 0.5 m, 1.3 m and 2 m thresholds, and Gorgens, Valbuena and Rodriguez (2017) tested 13 threshold values ranging from 0 to 7 m. A high percentage threshold of 60% was chosen by Korpela *et al.* (2010b) to reflect the most frequent height of the crown base, recognizing that it may not be adequate for all trees. Gorgens, Valbuena and Rodriguez (2017) considered that the threshold should be adapted to each specific feature because some features (e.g., central tendencies, density metrics) are more sensitive to the threshold height and benefit from a low cut-off level. Others are more robust and benefit from a high threshold (e.g., upper percentiles). The method used to choose the optimal threshold is always adapted to the use of the feature, for example for predicting stand volume (Gorgens, Valbuena and Rodriguez 2017) or above-ground biomass (Næsset 2011). No specific method for choosing the best threshold for tree species identification was found in the literature. The specific challenge is to determine the optimal threshold that can be applied to a broad range of tree sizes while at the same time diminishing the intra-species feature variability.

3.1.5 Effects of the normalization of return height by tree height

To ensure the independence of feature values relative to tree height, several scaling approaches have been proposed, such as normalizing 3D feature by tree height or by penetration depth, or using features that are invariant to tree height, such as those describing shapes or using different ratios of returns (e.g., mean height of first returns over the mean height of all returns). The first scaling approach, consisting of using the ratio of return height to tree height or, similarly, the ratio of the calculated 3D feature value to tree height, were used in several studies (Brandtberg 2007 ; Holmgren and Persson 2004). Alternatively, Ørka, Næsset and Bollandsås (2009) proposed a normalization strategy based on canopy penetration depth. Features capturing different aspects of the crown shape, such as those produced by adjusting a parabolic surface to the returns (Holmgren and Persson 2004), or those measuring slopes between the highest return in the crown and other returns, are supposed to be scale-invariant (Budei *et al.* 2018). The ratios of different return types and the ratios of the number of returns in different height bins, also called density features (Ørka, Næsset and Bollandsås 2009), are also designed to be scale-invariant.

Whatever the strategy for avoiding correlations between tree size and feature values, a certain variation related to tree height still remains because of changing tree architecture as a tree develops from young to mature. Such variations affect for example crown shape (i.e., allometry) or the internal crown structure (Brandtberg 2007 ; Ørka, Næsset and Bollandsås 2009). Ørka, Næsset and Bollandsås (2009) remarked that the effect of normalization for the production of scale-invariant features has not yet been specifically researched, leaving a knowledge gap that we here wish to fill.

3.1.6 Variation of intensity features with tree age and height

Intensity features proved to be useful in tree species classification, even in the case of monospectral lidar (Holmgren, Persson and Söderman 2008 ; Kim *et al.* 2009 ; Korpela *et al.* 2010b ; St-Onge, Audet and Bégin 2015). More recently, intensity features derived from MSL gained a lot of importance in such classifications (Budei *et al.* 2018 ; Yu *et al.* 2017), a situation that warrants a closer analysis of the potential relationship between tree size and intensity.

The intensity of a return from the canopy depends on the incident pulse power, the proportion of that power that penetrates through the canopy until it hits a sufficient area of vegetation material for a return to be triggered (in the discrete return case), and the reflective properties of the intercepting object. Penetration is influenced by the transmissivity of the crown, while the backscattered power is determined by the reflectance at specific wavelengths, and the area and orientation of the surfaces (Gaveau and Hill 2003). Pulse power at target level is influenced by ALS acquisition parameters such as pulse incidence angle, which may have a double impact. First, a greater scan angle results in a larger pulse range, which translates into a greater pulse power attenuation. Second, the penetration through a tree crown may be different for a vertical pulse compared to an oblique pulse due to the interaction with the branch and leaf orientations. Because range affects incident power, several approaches of intensity normalization have been proposed in the literature. The most common is based on the radar equation, but was proposed in several versions depending on additional information considered, such as scan angle or object size (leaf size in the case of trees) (Gatziolis 2011 ; Korpela *et al.* 2010a). Improvements in tree species classification after intensity normalization appear more difficult to ascertain than improvements on classification of other surface types. Some studies considered that even without normalization, intensity features help improving tree species classification (Brandtberg 2007 ; Holmgren, Persson and Söderman 2008). Others reported some limited improvements after intensity normalization (Korpela *et al.* 2010b). However, Ørka, Næsset and Bollandsås (2009) concluded that the proportion of the (non-standardized) intensity variance associated to differences between species was relatively small.

On one hand, some studies mentioned a certain relation between intensity and tree size, and the fact that this relation could affect species separability (Hovi *et al.* 2016 ; Korpela *et al.* 2010b). Tree architecture, leave shape and size, and reflectance changes with age may all influence lidar intensity. Korpela *et al.* (2010b) showed that intensity features are influenced by tree height or age, with different tendencies in pines or spruces. Hovi *et al.* (2016) demonstrated stronger intensities for trees that had reached a stage where the growth of the apex has ceased, because of the associated larger leaf density in the upper crown. Moreover, senescent trees often show stress in the upper crown, which changes leaf reflectance and thus the intensity or lidar returns. Defoliation in highly stressed trees generates more returns from bark and branches, which has a very different reflectance compared to leaves. Hovi *et al.* (2016) and

Korpela *et al.* (2010b) remarked that defoliated pines or spruces had a lower mean intensity but a larger coefficient of variation in comparison to normal trees. Moreover, Ørka, Næsset and Bollandsås (2009) found that the intensity of dominant trees was about 5% higher than that of intermediate trees. This was attributed to the deeper crown and higher density and foliage mass in dominant trees compared to suppressed trees.

The relation between intensity feature and tree height does not affect features computed from different return types in the same way. Ørka, Næsset and Bollandsås (2009) found that the intensity of first returns are influenced by biomass to a lesser degree than subsequent returns, and that features derived from first returns are not correlated to tree height, at least for tall trees. Moreover, they found that the single returns were the least correlated to the structural crown characteristics, but were useful for identifying species, in comparison to first returns (including first of many or single returns). On the contrary, features computed from the other return types (e.g., all returns, last returns) seemed to be more dependent to tree height.

On the other one hand, some studies like Hovi *et al.* (2016) concluded that the majority of the within-species variance in intensity is due to differences between individual trees that are not related to height, age, site type or mean scan angle.

3.1.7 Constant species characteristics

Notwithstanding the above considerations, there are some properties that, even if varying somewhat with tree height/age, are more constant within species than between species. For example, even though the branching pattern may change with height/age, the interspecies differences with regard to branching pattern are still more important. Moreover, branch and needle types within species are constant characteristics even if their sizes or complexity may change with age. For example, spruce branches grow horizontally with densely packed needles, creating compact scattering surfaces. Pine or larch crowns, for their part, do not exhibit this compactness and produce a different pattern of laser returns (Hollaus *et al.* 2009 ; Hovi *et al.* 2016). For these reasons, among all the possible 3D and intensity features, there may be some that are less sensitive to the variable characteristics of trees within a single species. Furthermore, when MS ALS is used, it is possible to choose among a great variety of intensity-based features, in addition to 3D features. Studying the correlation of 3D and intensity features with tree height may reveal those that are less influenced by tree size and, for this reason, potentially more useful for species identification because of the reduced intraspecific variance.

3.1.8 Strategies for handling ALS feature variations with height in tree species classification

The problem of variation of lidar features with tree height can be addressed in different ways during the classification process.

(1) Trees can be divided in separate categories, depending on a minimum number of returns required to compute the lidar features used in the classification algorithm. Ørka, Næsset and Bollandsås (2009) divided trees into two datasets, the first containing trees having at least three returns in each return category, and the second containing small trees that have at least three single returns.

(2) A stratification by tree height could improve the classification, as suggested by Hovi *et al.* (2016). This consists of training a different classifier for each height stratum.

(3) Several strategies of feature selection that take into account the variability related to tree height before training a classifier had been proposed in the literature. Tree height could be included in a variance analysis as a way to highlight the influence of height (Brandtberg 2007). Ørka, Næsset and Bollandsås (2009) analyzed the covariance of each feature with height, species

and interaction between height and species in order to allow selecting candidate features with high proportion of variability explained by tree species before species classification. Another strategy would consist of identifying features with a low intraspecific variance despite a large size range while being useful for discriminating between species. This would simplify sample collection for training the classifier because no special attention would have to be devoted to the height distribution within the sample. It would also avoid having to stratify the classification. However, Ørka, Næsset and Bollandsås (2009) remarked that the large impact of tree height on feature values in the case of small trees left but a few selected candidate features.

3.1.9 Objectives

The main goal of this study is to assess whether lidar feature variability related to tree height may influence the accuracy of tree species classification. We address this goal through the following two objectives.

The first objective was to assess the sensitivity of a wide variety of 3D and intensity features computed from a three-wavelength ALS system (Titan) to changes in tree size. The second objective was to test whether different classification strategies, varying selections of trees by height strata, or selection of features by degree of correlation with tree height would have an effect on classification accuracy. The strategies considered are: 1) standard classification (all features considered for trees of all sizes); 2) restricting features to those who have a weak correlation with tree sizes; and 3) classifying trees by height strata with all features. We hypothesized that a stratified classification by tree height would improve accuracy compared to a classification without stratification under the condition that it is impossible to identify very good features that do not vary a lot with tree height within species but are very good discriminant between species. Before we proceeded with the analysis on size and classification, we deemed it necessary to examine the effect of the height threshold used to exclude low returns from the point cloud of individual crowns, as this has an effect on the feature values. Finally, throughout the analyses we have devised approaches to address the problem of missing data (due to some features being uncomputable in certain cases) and to verify the effect of these strategies on the success of the classification.

3.2 Data and methods

3.2.1 Study site

The study site is located in the York Regional Forest (Ontario), a managed forest, comprised of different monospecific plantations as well as plantations combining two or more species and naturally growing forests. Predominant plantations are composed of needleleaf species such as red pine (*Pinus resinosa)*, white pine (*Pinus strobus*), Scots pine (*Pinus sylvestris*), American larch (*Larix laricina*), Norway spruce (*Picea abies*) and white spruce (*Picea glauca*). Broadleaved trees (maples, oaks, aspen and ash), which are located mainly in natural-growing stands or interspersed in pine plantations (aspen), were not included in analyses.

3.2.2 Field and reference data

Tree species of different plantations were verified in the field in August 2015. Forest inventory maps, last updated in 2015, were used to identify stands corresponding to monospecific plantations or to combinations of species easily distinguishable by photo interpretation. Monospecific plantations were nevertheless verified by photo interpretation because naturally competing species or understorey trees may have grown since the plantation establishment.

3.2.3 Multispectral ALS data

The multispectral ALS data were obtained with a Titan system from Teledyne Optech on 2 July 2015 at a mean flight altitude of 800 m above ground. The mean number of first returns/m^2 was 3.3 per flight line for each individual channel, while the overall first return density was about 20.2 returns/m^2 when the three channels from overlapping flight lines were aggregated. Lidar intensities were corrected for range attenuation, using the equation of Korpela *et al.* (2010a). For more details on the survey characteristics and range correction, see Budei *et al.* (2018).

Two raster elevation models and one false colour intensity image were interpolated from the ALS data and used in the process of tree crown delineation. The DTM was generated from returns classified as ground using the "lasground" and "las2dem" functions of LAStools (Isenburg 2014) with a resolution of 1 m. The canopy height model (CHM) was computed from the highest returns above the DTM in each pixel of 0.25 m. A colour composite intensity image was prepared using the interpolated intensities of the first returns in each channel, with a resolution of 0.25 m.

Moreover, during the Titan survey, high resolution images (ground sample distance of approx. 0.1 m) were collected with a CM-1000 RGB sensor from Teledyne Optech and used in the photo-interpretation of species.

3.2.4 Selection and delineation of sample crowns

Several thousands of trees over a wide height interval (2 m up to ≈35 m, Figure 3.1) were manually delineated. We focused the analysis on the main species found in plantations, in other words, needleleaves. This facilitated the delineation and identification of a large number of trees per species and limited the random impacts of factors affecting the growth and architecture of trees found in natural stands. Overall, six species were used in the analyses: *Pinus resinosa* (red pine, the most abundant species), *Pinus strobus* (white pine), *Pinus sylvestris* (scots pine), *Picea abies* (Norway spruce), *Picea glauca* (white spruce) and *Larix laricina* (American larch). The age of plantation establishment according to forest maps ranged from 23–88 years old for *Pinus sylvestris* (nevertheless, regeneration and new plantations of trees about ten years old are also found interspersed in old growth stands), 28–75 years for *Pinus strobus*, 26–89 years for *Picea abies*, 28–86 years for *Picea glauca*, and 27–63 years old for *Larix laricina*. It should be mentioned that these establishment ages do not correspond exactly to the ages of the trees.

Trees were manually delineated to ensure that erroneous crown outlines from an automated process would not alter the ALS feature values. Delineation was done by photo-interpreting the CHM, RGB aerial images taken from different points of view, and the MSL intensity image composite. The latter type of imagery also proved useful for the automated delineation of densely stocked trees (Naveed and Hu 2017).

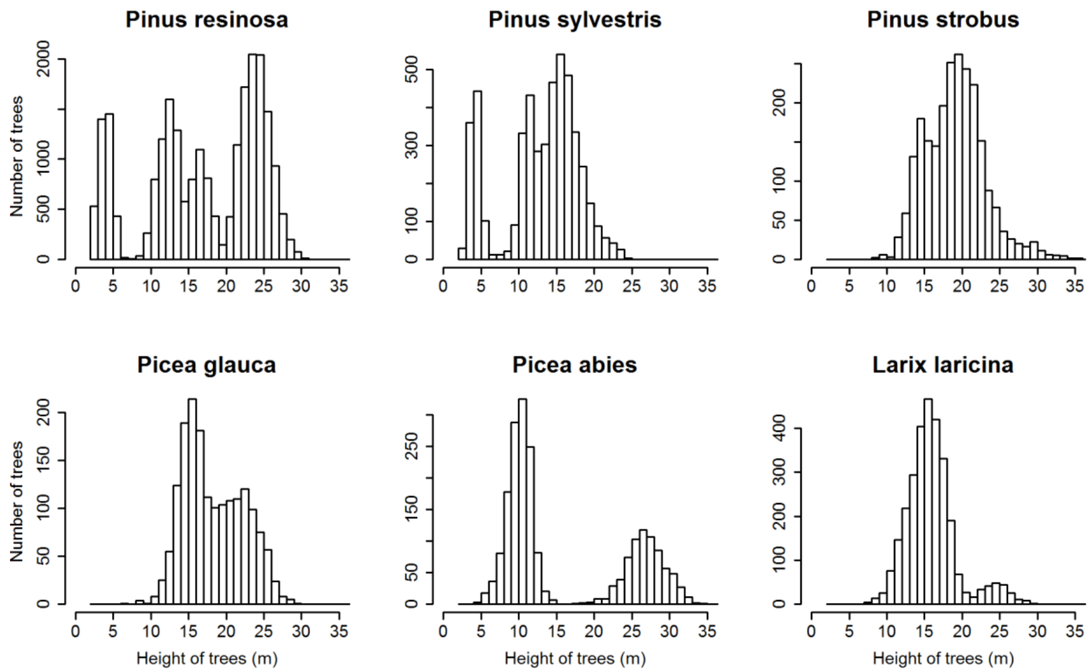

Figure 3.1: Height distribution of trees per species in the training samples.

3.2.5 MSL features used in species identification

For the purpose of identifying species through a classifier, features were derived from the XYZ and intensity data of the point cloud of each individual training crown, leading to two respective subsets: 3D and intensity features. Different families of 3D features were designed (see Table 3.1 for details) to capture interspecific variations in tree proportions (e.g., AH: ratio of the crown area to the tree height), shape (e.g., SU: curvature of a 3D surface fitted to the crown envelope), slope of the crown (SL: slope of the lines connecting the highest return to each other returns, or HR: slope calculation from returns aggregated by concentric rings) or porosity (e.g., RB: ratios accounting for return distribution in tree height or different statistics of height of returns, such as mean, standard deviation, percentiles, skewness), among other aspects. See (Budei *et* *al.* 2018) for full details on the computation of these features. In addition, the ratios of the number of first returns to all returns as well as the ratio of the number of single returns to all first returns (RP) were calculated.

All 3D features were designed to be scale-invariant or normalized by tree height, in other words, none depended on the absolute height values of returns. For example, the average slope, or the curvature of the crown surface, are inherently scale-invariant. When height percentiles were used, they were computed using normalized heights: $h_n = h / H_{max}$, where h is the height of a return above ground (ground elevation for the entire crown being the single DTM value at the XY position of the crown centroid, thus preserving the original 3D spatial distribution of returns), and H_{max} is the greatest return height, taken as the height of the tree. In theory, if tree architecture (e.g., proportions) of a given species does not vary with tree size, the proposed 3D features should take values that are independent of tree size. Moreover, each family of features was comprised of variants determined by return types (first returns or all returns). In all cases, the 3D features were computed from the combined returns of the three Titan channels.

Table 3.1: Description of 3D features

Symbol	Description
AH	Ratio of crown **A**rea to tree **H**eight
DI	**DI**spersion: coefficient of variation (cv), skewness (skew) and kurtosis (kurt) of return heights
HR	The slope coefficient of a linear model fit on the values of mean **H**eight of returns that XY position fit in each of four concentric and equidistant **R**ings, centred on the highest return location (lm), and coefficient of variation of the mean height by ring (cv)
MH	**M**ean of normalized **H**eight
PE	**PE**rcentiles of normalized height
RB	**R**atio of the number of returns in different height **B**ins defined in % of tree height to the total number of returns (e.g., 60_80 is the ratio of the number of returns in the 60–80% bin to all the returns in a crown)
RM	**R**atio between different statistics: - 1st returns mean height / tree height (1st_mn) - 1st returns median height / tree height (1st_p50) - 1st returns median height/1st returns mean height (1st_p50_1st_mn) - all returns mean height / tree height (all_mn) - all returns median height / tree height (all_p50) - all returns median height/1st returns mean height (all_p50_mn) - 1st returns median height/all returns mean height (1st_p50_all_mn) - 1st returns mean height/all returns mean height (1st_mn_all_mn) - 1st returns mean height/2nd returns mean height (1st_mn_2nd_mn)
RP	Ratio of first returns to all returns. **R**atio of single returns to first returns
SL	The average **SL**ope of the lines connecting the highest return to each other returns
SU	Sum of the two quadratic coefficients (coef) of a least square **SU**rface fit, and average of absolute vertical residual values of the above fit divided by the height of tree (rs)

Abbreviations: mn = mean, cv = coefficient of variation, p = percentile, lm = linear model fit, 1st = first returns, all = all returns, 2nd = second returns).

Intensity features such as the mean and standard deviation, coefficient of variation, percentiles, skewness and kurtosis of the intensity value distribution per crown were computed from the values of first or single returns over the entire crown, or along a radial gradient (IR: mean intensity by concentric rings around the centre of the tree). As in the case of 3D features, some ratios between features of different return types were computed (RM: difference between the respective mean intensities of 1^{st} and 2^{nd} returns). Furthermore, all possible multispectral band ratios (e.g., mean of the 532 nm intensity to the mean of the 1064 nm intensities, etc.) have been calculated. Finally, normalized differences between channels were derived to produce NDVI-like features (e.g., [1064 nm - 532 nm] / [1064 nm - 532 nm]). In all cases, the range-normalized intensities were used. Table 3.2 summarizes all intensity feature families. The symbol in the first column is further used in feature name aggregation, together with information concerning the return type selection (all returns, first returns or single returns) and the calculated statistic (mean, percentiles, dispersion). For examples of feature name aggregation see (Budei *et al.* 2018). The computation of all 3D and intensity metrics were done using R (R Core Team 2015) scripts and functions.

Table 3.2: Description of intensity features

Symbol	Description
DI	**DI**spersion: Standard deviation, coefficient of variation, skewness, kurtosis
IR	**I**ntensity by concentric **R**ing centered on the highest return
MI	**M**ean of **I**ntensity
NDG1	**G**reen (type 1) **N**ormalized **D**ifference Vegetation Index: [C2-C3]/[C2+C3]
NDG2	**G**reen (type 2) **N**ormalized **D**ifference Vegetation Index : [C1-C3]/[C1+C3]
NDIR	**I**nfra**R**ed **N**ormalized **D**ifference Vegetation Index: [C1-C2]/[C1+C2]
PE	**P**ercentiles
RCG1	**G**reen **R**atio of **C**hannels (type **1**) **:** C3-C2
RCG2	**G**reen **R**atio of **C**hannels (type **2**) **:** C3-C1
RCIR	**I**nfra**R**ed **R**atio of **C**hannels**:** C3-C1
RM	**R**atio between different statistics. - 1^{st} returns mean intensity/all returns mean intensity (1st_ p50_all_ p50) - 1^{st} returns mean intensity/2^{nd} returns mean intensity (1st_ p50_2nd_ p50)

Abbreviations: 1st = first returns, all = all returns, 2nd = second returns, p = percentile).

3.2.6 Effect of the height threshold

As in several other studies, removal of low height returns was done to avoid the effect of ground and small vegetation on the values of 3D and intensity features. Because one of our key objectives was to find features that do not significantly vary with tree size, including for smaller trees, the choice of a height threshold was critical. The strategy for selecting a proper threshold was based on a systematic analysis of its effect on the variability of feature values (per species). Three groups of threshold scenarios were tested: 1) no threshold: all returns considered, ground level included, with negative values included down to -5 m in the case of steep relief, 2) fixed thresholds (0.0, 0.5, 1.0, 1.5 and 2.0 m) and 3) percentages of H_{max} (10%, 20%, 30% and 40%). In the case of the first group, negative height values may occur on sloping terrain when ground or very low vegetation returns are located below the level of the ground elevation at the crown centroid. In the case of very small trees, the removal of points below a relatively high threshold (e.g., removing returns below 2 m from a 3 m high tree) might leave an insufficient number of returns for the computation of certain features. In this case, the feature was considered non-applicable (NA), leading to a missing value that forced the removal of the tree. In a random forest classification, NA fields normally lead to skipping the problematic sample. In the present case, this amounts to removing trees from the training dataset. Alternatively, it is also possible to discard a feature that causes numerous NA values for smaller trees, at a given height threshold. Imputing the median values of a feature to replace the NA, as a way of addressing the problem of NA values in a random forest (RF), was not here considered as an adequate option because it would create a bias in the classification: the median would be calculated mostly with larger trees but imputed to smaller ones.

We first checked for each threshold option the number of trees that didn't have at least one return per channel, and that needed to be removed for this reason. This very low number of returns per channel was chosen to keep the largest possible number of small trees, which was in turn needed to test the lower height limit of species identification. The second step consisted of considering the number of NA cases (number of trees for which a feature could not be computed) and choosing a bypass method. The main focus of these first two steps in choosing an optimal threshold was to verify which one would preserve the largest number of trees, or the largest number of features computable for all trees. The optimal threshold in that regard should correspond to the best compromise between the number of removed trees, or removed features; in other words, it should be the threshold that generates the fewest NAs.

The third step consisted of analyzing the intra-species variability of each feature per threshold value. The objective was to identify the height threshold value that kept feature variability at its minimum, potentially allowing for a better classification. For example, a low-height threshold value may cause features to be influenced by the presence of an understorey, and may thus introduce variation in feature values that is not related to the tree. For representing variability, we computed the standard deviation (SD) of each feature-threshold set (for example, the SD of the mean NIR intensity of red pines using returns above a 2 m height threshold). Only the trees common to all thresholds were selected. This prevented dissimilarity in the variability comparison that arose because of the larger number of small trees considered (not discarded) at lower height thresholds compared to higher threshold values. For each feature, the set of SD values across all thresholds were ranked from smallest to largest, with rank #1 (lowest SD) being considered the best. The average rank of each threshold across all features was then calculated. The threshold with the smallest average rank should minimize intra-species variability of feature values and was for this reason selected. Also, the mean percentage of a standard deviation decrease between the "no threshold" case (including all returns) and each of the other thresholds tested was calculated using the following equation:

$$\mathrm{P\_SD\_dec} = \mathrm{mean}(100 - \frac{\mathrm{SD_{thr}} * 100}{\mathrm{SD_{no\_thr}}}) \qquad \text{Eq. 3.1}$$

Despite recent research such as a study conducted by Gorgens, Valbuena and Rodriguez (2017) suggesting that the threshold should be optimized for each feature individually, we preferred for simplicity's sake to choose a unique threshold for all features. After applying this threshold, we proceeded to study the relationship between tree height and feature values.

3.2.7 Relationship between tree height and feature values

The relationship between tree height (H_{max}) and the feature values were analyzed using graphical and statistical procedures. Boxplots of feature values, per species, and per 5 m height classes, as well as scatterplots were produced. Moreover, the Pearson correlation (r) as well as the coefficient of determination (r^2) and the p-value of the linear regression between H_{max} (used as a proxy for tree height) and feature values were computed, for each feature. All statistical calculations were performed using the R statistical package (R Core Team 2015). It is assumed that very low values of r^2 would indicate that the effect of tree size on the feature value is weak, provided the relationship is approximately linear. Linearity was assessed graphically based on the scatterplots. Histograms of r^2 values were also computed per species and per class of features (3D *vs*. intensity). These values were computed for the entire tree dataset, and also on a subset of trees higher than 7 m. The latter subset was used because prior examination of the data showed that small trees (< 7 m in general) often had very different feature values from the taller ones. The risk existed that this may create spurious correlations between height and feature values when none existed for most of the range (7–30 m). The removal of small trees to create this second subset mainly concerned two species, *Pinus resinosa* and *Pinus sylvestris*, that had a large number of trees in the 2–5 m stratum.

3.2.8 Species classification strategies

To estimate what the potential effect of tree size has on classification performance (random forest classification in the present case), three different strategies were devised. The "standard" classification strategy, employed in most species classification studies, used all features across all tree sizes for identifying species, whether they were correlated to size or not. This strategy was employed as a reference to evaluate the other ones. The second strategy consists of using only features that are weakly correlated to height. Although based on a logical rationale, it may lead to the selection of features that are poor discriminators for species, which could result in high inter-species confusion rates. The third strategy availed itself of the stratification of trees in height strata, under the assumption that within each of these height classes the correlation between feature values and height would be negligible due to the low variance of height itself. Training was thus carried out independently for each height stratum, resulting in separate RF models. However, this would call for more intensive field sampling, in other words, the acquisition of reference data for numerous trees for each species-size class. To summarize, the three classification strategies were:

- Standard (STD): all features were considered regardless of their correlation to size.
- Size-invariant features (SIF): only features having a relationship to height with a r^2 <=0.2 were retained.
- Height stratum classes (HSC): all features were considered regardless of their correlation to size, but were used per height strata. Following an evaluation of several stratification schemes, we opted for the following ones: *i*) seven 5 m classes (2–5 m, and six 5 m strata from 5 to 35 m); *ii*) three broader classes: 2–15 m, 15–25 m, and 25–35 m. After training each RF separately for each height stratum, the classification results were compiled and the accuracy evaluated on

the aggregated classes. This option allowed for the selection of different sets of features for each stratum, and for the use of a different value of the RF *sampsize* parameter per stratum, depending on the abundance of samples in each stratum.

Moreover, for small trees, some features could not be computed due to the insufficient number of returns per crown in certain MSL channels. Solving this shortcoming required either to remove the problematic trees or the uncomputable features. Three selection approaches were assessed: 1) remove any tree that has at least one NA occurrence, 2) remove any feature that produces an NA for at least one tree, and 3) combine the first two approaches in a hybrid one. In the third approach, only the non-classified trees that had been left out of the first approach (tree removal) were subsequently classified, namely by using the remaining features of the second approach (feature removal).

Finally, to minimize the risk of overfitting, a parsimonious classification with the hybrid selection approach was tested using only the ten best features among those available for each classification strategy. We then assessed the decrease in accuracy caused by using only this limited number of features. This classification was also useful to understand whether the automatic ordering by mean decrease accuracy resulting from the RF classification algorithm had a tendency to promote size-invariant features or not. Another use of this final classification was to estimate the usefulness of MSL lidar compared to monospectral lidar, by estimating the ratio of 3D features to intensity features (using the two additional channels). All RF classifications were balanced, in other words, had an equal number of samples per species.

3.3 Results

3.3.1 Effect of height threshold

The first step of the analysis consisted of counting the trees removed because they did not have at least one return in each channel after the thresholds were applied. There were no removed trees using the "no threshold" case, or using any of the percentage threshold cases (Table 3.3, "Step 1" column). By contrast, a progressively increasing number of trees were removed as the fixed thresholds were increased, up to 154 trees (0.41%) in the case of the 2 m threshold (Table 3.3, "Step 1" column). The majority of the removed trees were less than 5 m high. Due to their small crown area, some of these trees could fit between scan lines of a specific channel but nevertheless be correctly covered by the two other channels, thus making their delineation possible. The rare cases of larger trees removed in this step are mainly suppressed trees, shadowed by their taller neighbours, or stressed trees with a very low reflectance (causing a low number of returns).

The second step of this analysis consisted of counting the NA occurrences in feature calculation caused by the number of returns being insufficient for meeting the computational requirements of each feature. The number of trees or features removed in the second step was calculated on all remaining trees available for each thresholding method, in other words, using the trees having passed the first step. The number of trees removed because of NA values increased with increasing threshold height, from a minimum of 1578 trees for the "no threshold" case to a maximum of 5770 trees for the 2 m threshold (Table 3.3, *Step 2*, *No. of trees removed*). The trees for which all features could be computed were used in RF classification, in the tree removal approach. The features being correctly calculated for any tree were used in RF classification, in the feature removal approach. The number of removed features (Table 3.3, *Step 2*, *No.

of features removed) did not vary in a strictly proportional fashion with the threshold size because the trees considered by threshold were not the same (many potentially problematic trees were removed at step 1). However, when calculated with the common trees to all thresholds, the number of features with NA increased according to threshold height for fixed thresholds (87 for no threshold; 88 for 0.5 and 1 m; 92 for 1.5 and 2 m; not reported in Table 3.3) and remained constant for percentage thresholds (88). For 3D features, the majority of NA occurred for trees less than 5 m high. For intensity features, NAs are more widespread across tree height categories but more frequent for small trees. No NA values were generated for trees taller than 25 m for 3D features, and 30 m for intensity features.

Except for the “no threshold” case, the height threshold which had the least NAs was 10% of tree height, with about 0.01% NA for 3D and 0.20% NA for intensity features. The largest proportion of NA was found for the 2 m threshold, with 0.06% for 3D and 0.60% for intensity features.

The third step of the analysis for choosing a threshold was ranking thresholds by comparing the SD of each feature value per threshold. The mean rank obtained per threshold is presented in Table 3.3 (*Step 3, mean rank*) and indicates that the 40% threshold caused the minimum intra-species feature variation. When testing by 5 m strata, the 40% threshold was also the threshold which ranked first for the majority of strata. The mean percentage of SD decrease (P_SD_dec in Eq. 3.1, Table 3.3, *Mean % SD decrease*) also indicates that the largest variability reduction compared to the “no threshold” (*no_thr* in Eq. 3.1) situation occurred in the 40% threshold.

The 40% threshold was chosen for further calculations because of the significant reduction in feature variability it brought, and for the relatively low number of removed trees compared mainly with 2 m and 1.5 m thresholds, especially in the 2–5 m strata.

Table 3.3: Threshold selection

	Step 1	Step 2			Step 3	
Threshold	**No. of trees removed**	**No. of trees removed**	**No. of 3D features with NA (total of 50)**	**No. of intensity features with NA (total of 114)**	**Mean rank**	**Mean % SD decrease (P_SD_dec, Eq. 3.1)**
no thr.*	0	1578	5	87	9.74	0.00
0.0 m	0	1818	5	87	8.26	3.51
0.5 m	1	4515	5	92	6.80	17.11
1.0 m	4	4697	5	92	5.26	18.81
1.5 m	16	5176	11	106	5.52	19.05
2.0 m	154	5770	11	106	5.89	17.97
10%	0	4386	5	88	5.40	19.00
20%	0	4611	5	88	3.83	21.24
30%	0	4753	5	92	3.13	23.34
40%	0	5123	5	92	2.77	24.91

* no thr.: no thresold (all points)

3.3.2 Relation between tree height and features

When feature values per species were linearly regressed against tree height, r^2 values between 0.0 and 0.6 were obtained (

Figure 3.2). For individual species, the relationship between tree height and feature values was generally weak ($r^2 < 0.2$), although some features were highly correlated to tree height. The per-species frequencies of r^2 values were relatively similar between 3D and intensity features. When very small trees (< 7 m) were excluded from the regression, the r^2 values dropped for species that had more trees in this size category, such as *Pinus resinosa* and *Pinus sylvestris* (Figure 3.3).

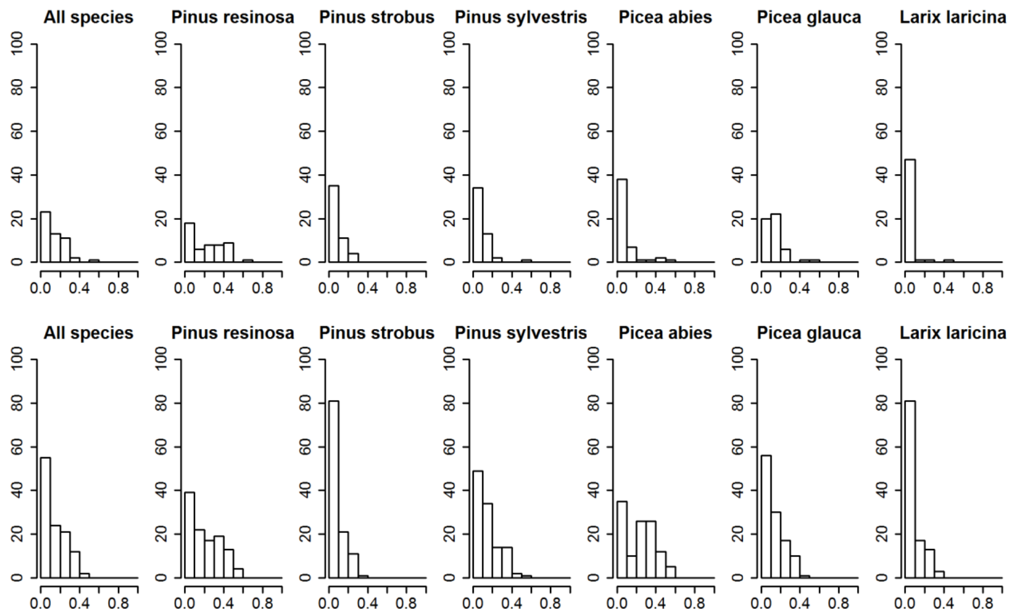

Figure 3.2: Frequency of r^2 values from regressions between height and features (3D features in the first row, and intensity features in the second row) for trees of all heights (>= 2 m).

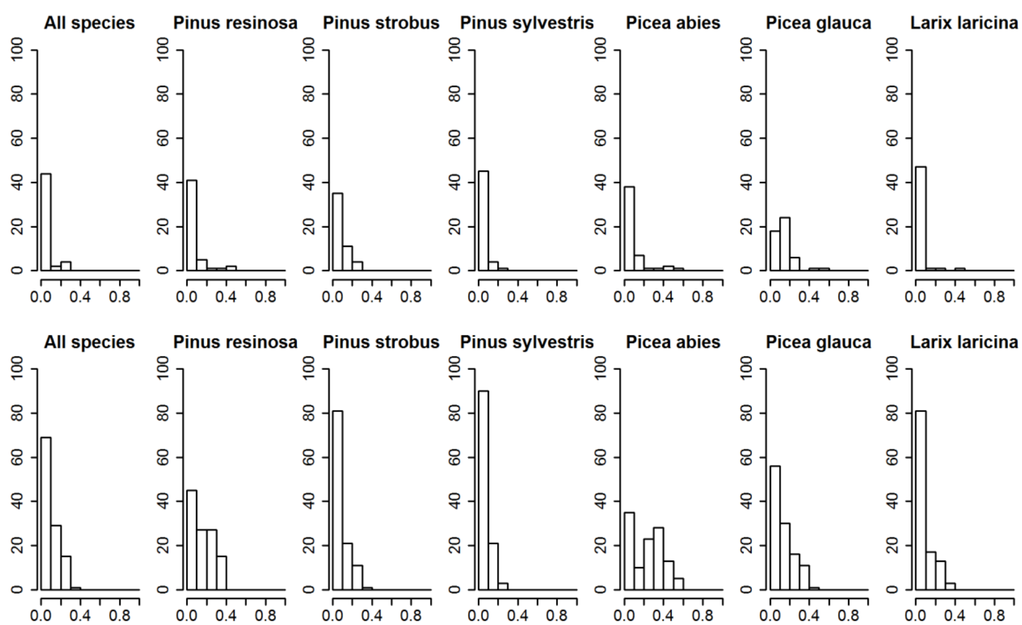

Figure 3.3: Frequency of r^2 values from regression between height and features (3D features in first line and intensity features in second line), excluding trees less than 7 m high.

The box plots by species and by height strata allowed a better understanding of the feature–tree height relationship. The number of features being high, only a few examples (Figures 3.4 to 3.10) are shown. Examples of highly correlated features are the ratio of first return to all returns (3D_RP_1st_all_C321, Figure 3.4), the sum of the quadratic coefficients of a fitted surface polynomial on the first returns of all channels (3D_SU_1st_coef_C321, Figure 3.5), or the type 2 NDVI calculated on single returns (I_NDG2, Figure 3.6). In the case of some 3D features like the standard deviation of the slope (3D_SL_1st_sd_C321, Figure 3.7), or intensity features like the skewness value of single returns (I_DI_si_skew_C3, Figure 3.8), the relationship between feature values and tree height is very weak, leading to low r^2. At the same time, these features offered little discriminatory power. For other features, the relation to the tree height is complex (3D_PE_1st_p75_C321, Figure 3.9 and I_MI_1st_95_5_mn_C1, Figure 3.10). Moreover, Figure 3.9 illustrates the large differences between the feature values of smaller trees in the first two height strata and the other larger trees that occur for some features or some species. In some cases, the small tree values contributed to raising the r^2 value. Overall, the correlation between feature values and tree height is sometimes direct (Figure 3.6) and sometimes inverse (Figure 3.5) for all tree species considered. Other times, the correlation is more complex, with direct relations for some species and inverse for others (Figure 3.10). The complete values of correlation between each feature and tree height are given in Table 3.4 for 3D features and in Table 3.5 for intensity features. The correlation was preferred to the r^2 because it shows the direction of the relation.

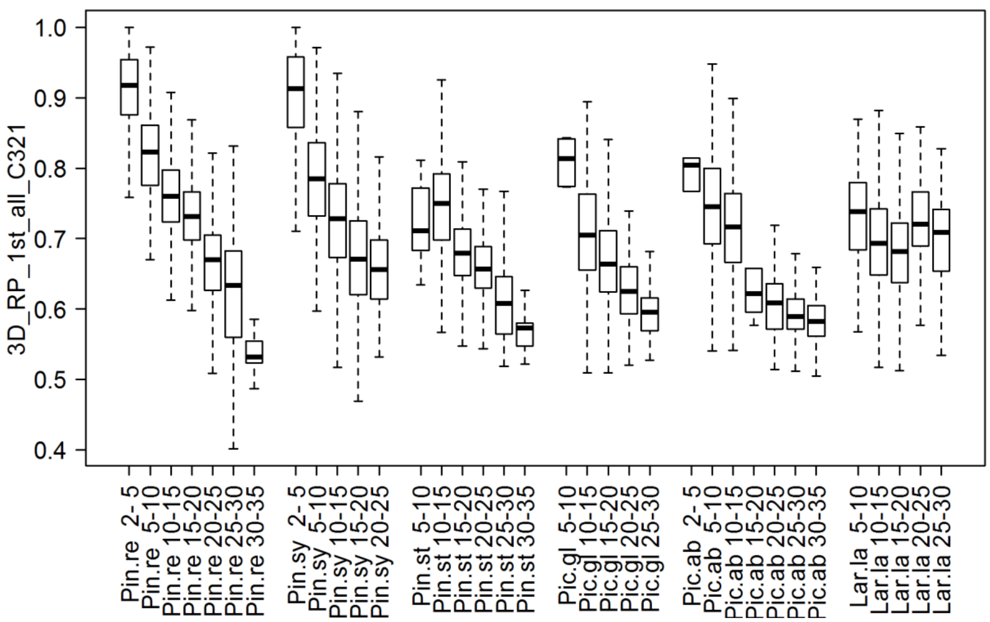

Figure 3.4: Relationship between tree height and the ratio of first returns to all returns, all channels merged.

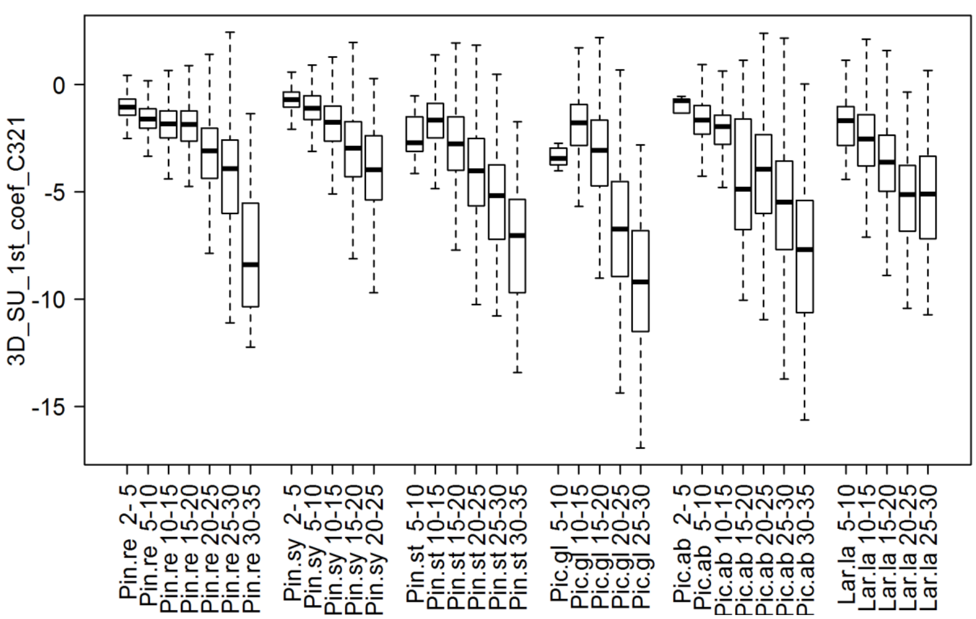

Figure 3.5: Relationship between tree height and the sum of the quadratic coefficients of a fitted surface polynomial on the first returns of all channels.

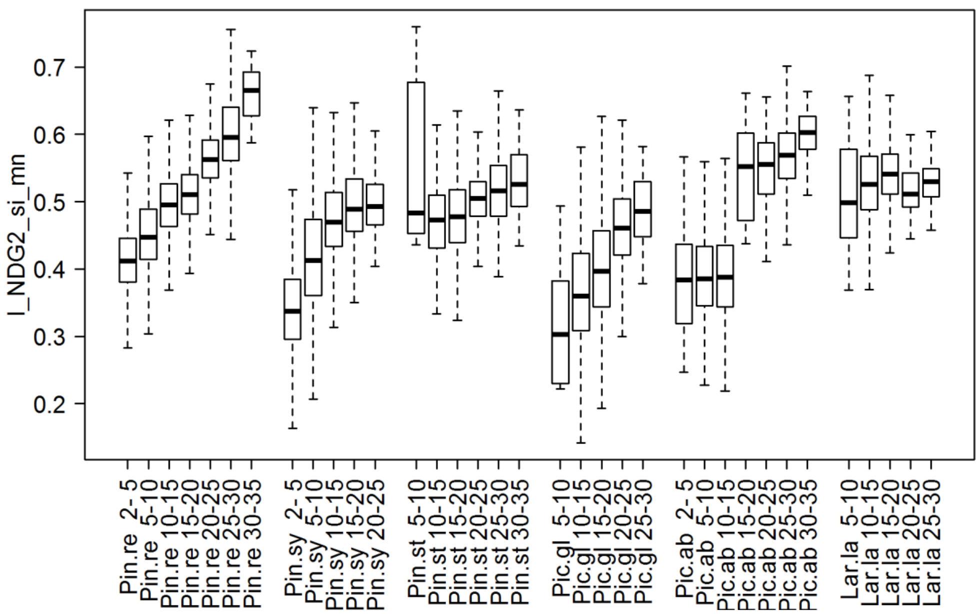

Figure 3.6: Relationship between tree height and the NDVI calculated between the green and the middle IR channels.

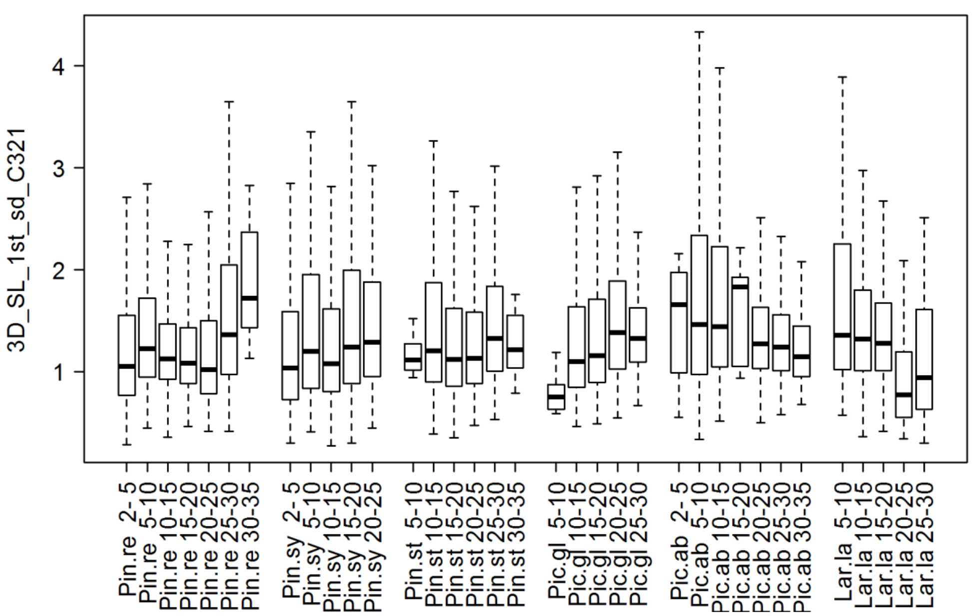

Figure 3.7: Relationship between tree height and the standard deviation of the slope calculated on the first returns.

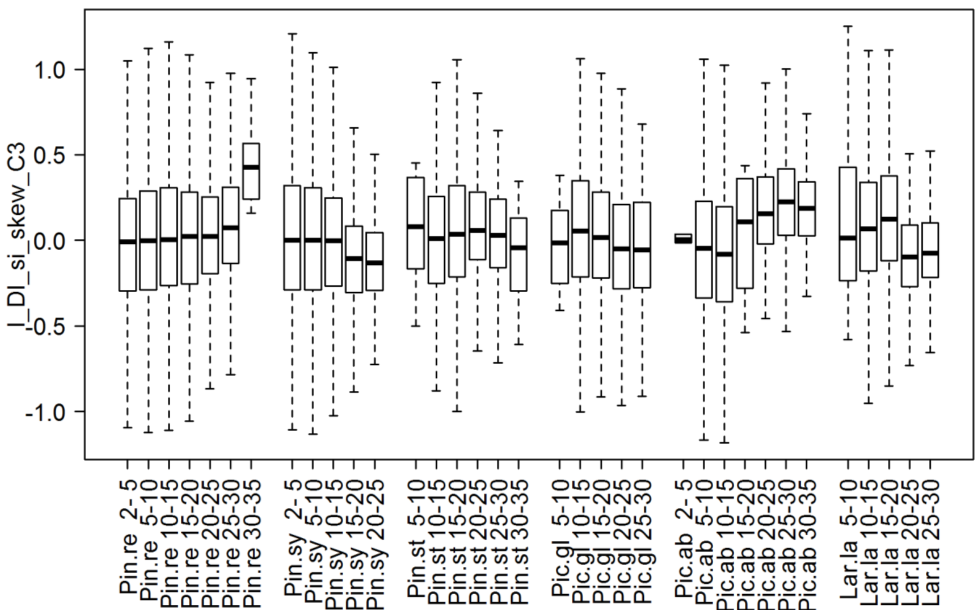

Figure 3.8: Relationship between the skewness of the intensity distribution of the single returns.

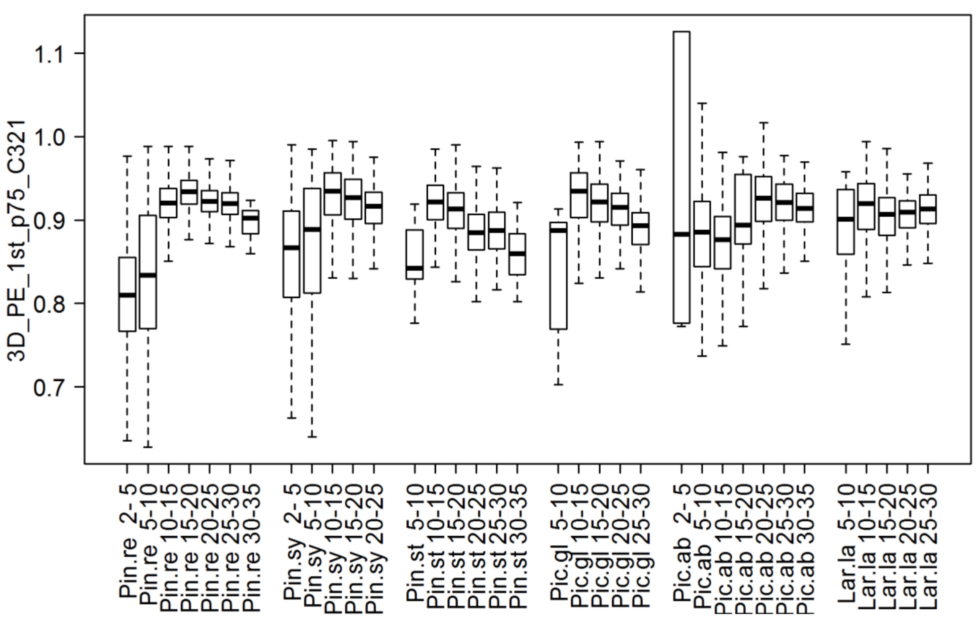

Figure 3.9: Example of a complex relationship (between tree height and the 75th percentile of the normalized return heights).

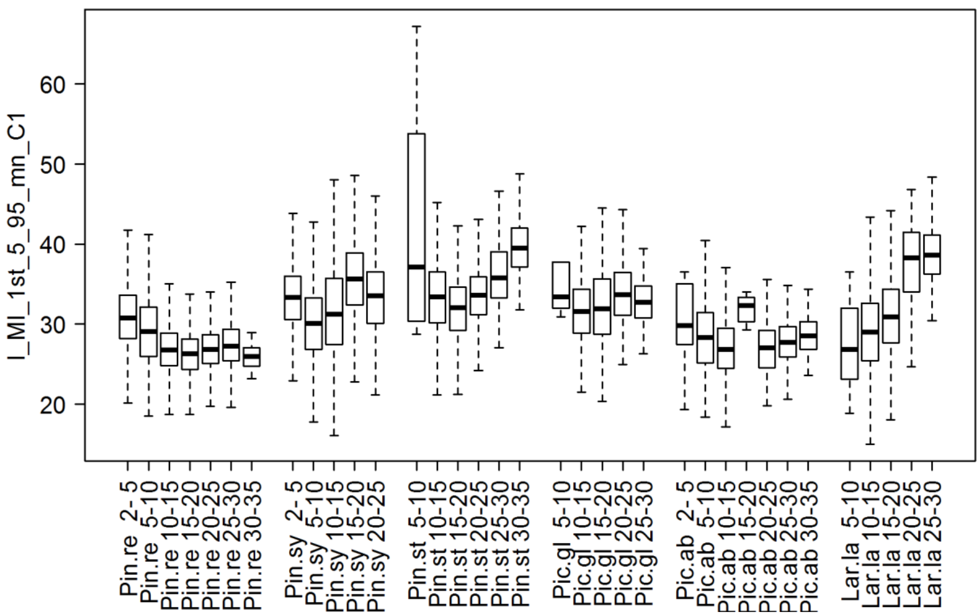

Figure 3.10: Example of a complex relationship (between tree height and the mean intensity between the 5th and 95th intensity percentile).

Every aspect of feature value computations appears to have impacted the height-feature correlation: the feature family; the type of return (all, first, single, etc.); the selected channel (in the case of intensity features); as well as the statistic (e.g., mean, SD, percentile, etc.). These trends are obvious also in Tables 3.4 and 3.5. Moreover, in many cases, features that are weakly correlated to height also tend to offer a low power for discriminating between species. However, some features having a low correlation to tree height, such as the ratio of metrics (3D_RM_1st_mn_all_mn_C321), slope (3D_SL_all_p50_C321) or NDVI (I_NDG1_1st_p75), nevertheless appeared among the first ten features in the RF mean decrease accuracy (see classification results section and Table 3.7). The 75th percentile of intensity from first returns in the C1 (I_PE_1st_p75_C1) feature constitutes a case where the variability within species is limited and a relatively good contrast between *Pinus resinosa* and *Pinus strobus* or *Picea glauca* was achieved. These types of features, while potentially very useful, were relatively rare. Overall, 3D features were slightly less correlated to height than intensity features.

The mean and the maximum of the absolute correlations (|r|) of lidar features with tree height vary across species (see the last two rows of Tables 3.4 and 3.5). For 3D features, the higher mean and maximum absolute correlations apply to *Picea abies* and *Picea glauca*, while the lower mean and maximum absolute correlations apply to *Larix laricina*. For intensity features, the higher mean and maximum absolute correlations still apply to *Picea abies*, followed by *Pinus resinosa* and *Picea glauca*, while the lower mean and maximum correlations apply to *Pinus sylvestris* and *Larix laricina*. Some feature families are generally more correlated with height than others. The mean correlation by feature family, calculated from mean absolute correlation value by species, is reported in Tables 3.4 and 3.5 (column *Mean of absolute correlations by feature family*). The 3D feature families in descending order of correlation to tree height were: ratio between area and height (AH); ratios of return types (RP); coefficients and residuals of a fitted surface (SU); mean height (MH); ratio of returns by height bin (RB), ratios of metrics (RM); percentiles (PE); dispersion (DI); height by ring (HR); and slopes (SL). The intensity features in descending order of correlation to tree height were: percentiles (PE); channel ratios (RC…); NDVIs (ND…); means of intensity (MI); dispersion (DI); SD of the mean intensity by ring (IR); and ratios of metrics (RM).

Table 3.4: Correlation between 3D features and tree height (trees less than 7 m high excluded)

3D features	**Pinus resinosa**	**Pinus sylvestris**	**Pinus strobus**	**Picea abies**	**Picea glauca**	**Larix laricina**	**Mean of absolute correlations**	**Mean of absolute correlations by feature family**
3D_AH_C321	**0.63**	0.39	0.50	0.37	**0.54**	**0.64**	0.51	0.51
3D_DI_1st_cv_C321	0.10	0.25	0.30	-0.09	0.48	-0.16	0.23	
3D_DI_1st_kurt_C321	0.34	0.23	0.16	0.25	0.00	0.11	0.18	
3D_DI_1st_sd_C321	0.11	0.27	0.30	-0.04	0.49	-0.16	0.23	
3D_DI_1st_skew_C321	-0.42	-0.29	-0.13	-0.41	-0.09	-0.07	0.24	
3D_DI_all_cv_C321	0.14	0.34	0.34	-0.14	0.41	-0.27	0.27	
3D_DI_all_kurt_C321	0.13	-0.18	-0.01	0.20	-0.19	0.14	0.14	
3D_DI_all_sd_C321	0.13	0.33	0.32	-0.09	0.40	-0.29	0.26	
3D_DI_all_skew_C321	-0.21	0.09	-0.05	-0.34	0.14	-0.08	0.15	0.21
3D_HR_1st _cv_C321	0.01	0.13	0.29	0.12	0.44	-0.03	0.17	
3D_HR_all _cv _C321	-0.06	0.17	0.26	0.05	0.32	-0.08	0.16	
3D_HR_1st _lm_C321	0.15	-0.07	-0.20	**-0.51**	-0.48	0.09	0.25	
3D_HR_all _lm _C321	0.19	-0.11	-0.13	-0.43	-0.32	0.10	0.22	0.20
3D_MH_1st_mn_C321	0.03	-0.16	-0.34	0.29	-0.43	0.04	0.21	
3D_MH_all_mn_C321	-0.07	-0.30	-0.37	0.27	-0.41	0.11	0.26	0.23
3D_PE_1st_p25_C321	0.16	-0.06	-0.27	0.24	-0.41	0.08	0.20	
3D_PE_1st_p50_C321	0.14	-0.06	-0.30	0.32	-0.35	0.03	0.20	
3D_PE_1st_p75_C321	0.00	-0.10	-0.35	0.38	-0.24	-0.06	0.19	
3D_PE_all_p25_C321	-0.07	-0.31	-0.32	0.23	-0.39	0.15	0.25	
3D_PE_all_p50_C321	0.09	-0.12	-0.30	0.28	-0.37	0.11	0.21	
3D_PE_all_p75_C321	-0.05	-0.13	-0.36	0.30	-0.32	-0.01	0.20	0.21
3D_RB_all_pt_0_60 _C321	0.24	0.30	0.29	-0.18	0.36	-0.23	0.27	
3D_RB_all_pt_60_80 _C321	-0.33	-0.01	0.24	-0.29	0.30	0.04	0.20	
3D_RB_all_pt_80_90 _C321	0.28	-0.03	-0.12	0.15	-0.24	0.28	0.18	
3D_RB_all_pt_90_100 _C321	-0.05	-0.18	-0.38	0.30	-0.33	-0.08	0.22	
3D_RB_all_pt_95_100 _C321	-0.23	-0.23	-0.34	0.15	-0.33	-0.17	0.24	0.22
3D_RM_1st_mn_2nd_mn_C321	-0.40	0.09	-0.18	**-0.63**	-0.40	-0.46	0.36	
3D_RM_1st_mn_all_mn_C321	0.21	0.30	0.25	0.00	0.03	-0.25	0.17	
3D_RM_1st_mn_C321	0.03	-0.16	-0.34	0.29	-0.43	0.04	0.21	
3D_RM_1st_p50_1st_mn_C321	0.25	0.18	0.07	0.16	0.20	-0.04	0.15	
3D_RM_1st_p50_C321	0.14	-0.06	-0.30	0.32	-0.35	0.03	0.20	
3D_RM_all_mn_C321	-0.07	-0.30	-0.37	0.27	-0.41	0.11	0.26	

3D features	Pinus resinosa	Pinus sylvestris	Pinus strobus	Picea abies	Picea glauca	Larix laricina	Mean of absolute correlations	Mean of absolute correlations by feature family
3D_RM_all_p50_all_mn_C321	0.32	0.28	0.20	0.14	0.07	0.02	0.17	
3D_RM_all_p50_C321	0.09	-0.12	-0.30	0.28	-0.37	0.11	0.21	0.22
3D_RP_1st_all_C321	**-0.65**	-0.38	**-0.54**	**-0.72**	**-0.50**	-0.03	0.47	
3D_RP_si_1st_C321	**-0.56**	0.14	-0.48	**-0.68**	**-0.67**	-0.08	0.43	0.45
3D_SL_1st_cv_C321	0.12	0.09	-0.08	-0.18	-0.08	-0.05	0.10	
3D_SL_1st_mn_C321	-0.17	0.01	0.08	-0.05	0.30	-0.17	0.13	
3D_SL_1st_p25_C321	-0.18	0.08	0.27	0.07	0.39	-0.01	0.16	
3D_SL_1st_p50_C321	-0.30	0.00	0.19	0.03	0.38	-0.13	0.17	
3D_SL_1st_p75_C321	-0.31	-0.03	0.09	-0.01	0.31	-0.24	0.16	
3D_SL_1st_sd_C321	0.05	0.02	-0.04	-0.15	0.01	-0.11	0.06	
3D_SL_all_cv_C321	0.17	0.05	-0.04	-0.02	-0.03	0.09	0.07	
3D_SL_all_mn_C321	0.04	0.05	0.07	0.12	0.22	-0.20	0.12	
3D_SL_all_p25_C321	-0.11	0.09	0.29	0.16	0.43	-0.06	0.19	
3D_SL_all_p50_C321	-0.14	0.04	0.19	0.20	0.37	-0.20	0.19	
3D_SL_all_p75_C321	0.00	0.10	0.10	0.19	0.30	-0.26	0.16	
3D_SL_all_sd_C321	0.09	0.03	-0.04	-0.01	0.00	-0.04	0.03	0.13
3D_SU_1st_coef_C321	-0.46	-0.45	-0.48	**-0.69**	**-0.71**	-0.41	0.53	
3D_SU_1st_rs_C321	0.10	0.17	0.28	-0.18	0.47	-0.21	0.24	0.38
Mean of absolute values	0.19	0.16	0.24	0.24	0.32	0.14	0.22	
Maximum of absolute values	0.65	0.45	0.54	0.72	0.71	0.64	0.53	

Numbers in bold represent strong correlations (greater than 0.5 or lower than -0.5).

Table 3.5: Correlation between intensity features and tree height (trees less than 7 m high excluded)

Intensity features	**Pinus resinosa**	**Pinus sylvestris**	**Pinus strobus**	**Picea abies**	**Picea glauca**	**Larix laricina**	**Mean of absolute correlations**	**Mean of absolute correlations by feature family**
I_DI_1st_cv_C1	**0.61**	0.29	0.47	**0.69**	**0.60**	0.08	0.46	
I_DI_1st_cv_C2	**0.61**	0.13	0.43	**0.62**	0.48	0.01	0.38	
I_DI_1st_cv_C3	**0.58**	0.46	**0.58**	**0.56**	**0.56**	0.21	0.49	
I_DI_1st_kurt_C1	0.29	0.37	0.04	-0.12	-0.14	-0.02	0.16	
I_DI_1st_kurt_C2	0.17	0.25	-0.18	-0.29	-0.23	-0.05	0.19	
I_DI_1st_kurt_C3	0.26	0.02	0.04	0.35	0.20	0.20	0.18	
I_DI_1st_sd_C1	**0.58**	0.44	**0.53**	**0.70**	**0.63**	**0.51**	0.56	
I_DI_1st_sd_C2	0.42	0.30	0.47	0.33	0.36	0.48	0.39	
I_DI_1st_sd_C3	0.39	0.45	0.49	0.02	0.25	0.37	0.33	
I_DI_1st_skew_C1	0.45	0.27	0.28	0.44	0.40	-0.07	0.32	
I_DI_1st_skew_C2	**0.52**	0.01	0.29	**0.56**	0.38	-0.09	0.31	
I_DI_1st_skew_C3	0.22	0.03	0.37	**0.53**	0.40	0.04	0.26	
I_DI_si_cv_C1	0.30	0.30	0.18	0.13	0.13	-0.06	0.18	
I_DI_si_cv_C2	0.26	0.07	0.09	0.01	-0.08	-0.08	0.10	
I_DI_si_cv_C3	0.41	0.33	0.41	**0.62**	0.28	-0.04	0.35	
I_DI_si_kurt_C1	0.32	0.45	0.27	0.05	0.13	0.31	0.25	
I_DI_si_kurt_C2	0.31	0.43	0.24	0.12	0.17	0.29	0.26	
I_DI_si_kurt_C3	0.34	0.30	0.02	0.23	0.17	0.40	0.24	
I_DI_si_sd_C1	0.41	0.35	0.39	**0.50**	0.44	0.20	0.38	
I_DI_si_sd_C2	0.35	0.16	0.30	0.14	0.08	0.19	0.20	
I_DI_si_sd_C3	0.36	0.42	**0.51**	0.26	0.31	0.23	0.35	
I_DI_si_skew_C1	0.27	0.37	0.11	0.04	0.02	-0.05	0.14	
I_DI_si_skew_C2	0.11	0.20	0.00	-0.17	-0.10	-0.06	0.11	
I_DI_si_skew_C3	0.05	-0.13	0.03	0.32	-0.10	-0.06	0.11	0.28
I_IR_1st _sd_C1	0.01	-0.10	-0.19	-0.02	0.25	0.02	0.10	
I_IR_1st _sd_C2	-0.14	-0.23	-0.26	-0.09	0.07	0.05	0.14	
I_IR_1st _sd_C3	-0.22	0.00	-0.16	-0.14	0.10	0.10	0.12	0.12
I_MI_1st_90_10_mn_C1	0.05	0.30	0.13	-0.04	0.11	0.39	0.17	
I_MI_1st_90_10_mn_C2	-0.41	0.13	-0.08	-0.50	-0.26	0.37	0.29	
I_MI_1st_90_10_mn_C3	-0.36	0.18	-0.09	**-0.61**	-0.41	0.26	0.32	
I_MI_1st_90_10_n_mn_C1	-0.46	-0.19	-0.28	**-0.53**	-0.43	0.06	0.33	
I_MI_1st_90_10_n_mn_C2	**-0.52**	-0.02	-0.28	**-0.57**	-0.36	0.08	0.31	
I_MI_1st_90_10_n_mn_C3	-0.23	-0.08	-0.40	-0.47	-0.36	-0.03	0.26	
I_MI_1st_95_5_mn_C1	0.08	0.31	0.14	-0.01	0.14	0.39	0.18	
I_MI_1st_95_5_mn_C2	-0.40	0.13	-0.07	-0.49	-0.25	0.38	0.28	
I_MI_1st_95_5_mn_C3	-0.35	0.19	-0.07	**-0.61**	-0.39	0.27	0.31	
I_MI_1st_95_5_n_mn_C1	-0.47	-0.24	-0.30	-0.49	-0.38	0.04	0.32	
I_MI_1st_95_5_n_mn_C2	**-0.53**	-0.07	-0.30	**-0.55**	-0.35	0.06	0.31	
I_MI_1st_95_5_n_mn_C3	-0.19	-0.06	-0.37	-0.41	-0.27	0.00	0.22	

Intensity features	**Pinus resinosa**	**Pinus sylvestris**	**Pinus strobus**	**Picea abies**	**Picea glauca**	**Larix laricina**	**Mean of absolute correlations**	**Mean of absolute correlations by feature family**
I_MI_1st_mn_C1	0.18	0.34	0.18	0.06	0.19	0.41	0.23	
I_MI_1st_mn_C2	-0.35	0.14	-0.04	-0.47	-0.21	0.39	0.27	
I_MI_1st_mn_C3	-0.34	0.20	-0.04	**-0.59**	-0.38	0.28	0.30	
I_MI_si_mn_C1	**0.58**	0.34	0.47	**0.69**	**0.62**	**0.57**	0.54	
I_MI_si_mn_C2	0.30	0.18	0.36	0.20	0.32	**0.52**	0.31	
I_MI_si_mn_C3	-0.13	0.24	0.23	**-0.52**	0.04	0.42	0.26	0.29
I_NDG1_1st_mn	-0.10	-0.05	0.00	0.28	0.16	0.23	0.14	
I_NDG1_1st_p50	-0.17	0.04	0.09	0.18	0.15	0.22	0.14	
I_NDG1_1st_p75	-0.03	-0.18	0.02	0.44	0.22	0.19	0.18	
I_NDG1_si_mn	0.35	-0.09	0.04	**0.64**	0.22	0.07	0.23	
I_NDG1_si_p50	0.30	-0.13	0.06	**0.64**	0.17	0.07	0.23	
I_NDG1_si_p75	0.26	-0.20	-0.05	**0.55**	0.13	0.06	0.21	
I_NDG2_1st_mn	0.47	0.23	0.22	**0.65**	0.48	0.18	0.37	
I_NDG2_1st_p50	0.35	0.23	0.27	**0.60**	0.44	0.19	0.35	
I_NDG2_1st_p75	0.46	0.09	0.21	**0.68**	**0.50**	0.15	0.35	
<u>I_NDG2_si_mn</u>	**0.62**	0.18	0.19	**0.77**	0.48	0.04	0.38	
I_NDG2_si_p50	**0.56**	0.09	0.20	**0.75**	0.44	0.04	0.35	
I_NDG2_si_p75	**0.53**	0.06	0.10	**0.72**	0.45	0.04	0.32	
I_NDIR_1st_mn	**0.54**	0.29	0.27	**0.58**	0.37	-0.09	0.36	
I_NDIR_1st_p50	0.46	0.19	0.21	**0.53**	0.30	-0.06	0.29	
I_NDIR_1st_p75	**0.50**	0.29	0.24	**0.55**	0.40	-0.07	0.34	
I_NDIR_si_mn	**0.50**	0.32	0.26	**0.61**	0.45	-0.04	0.36	
I_NDIR_si_p50	0.41	0.26	0.22	**0.54**	0.42	-0.05	0.32	
I_NDIR_si_p75	0.42	0.29	0.22	**0.59**	0.46	-0.04	0.34	0.29
I_PE_1st_p05_C1	**-0.52**	-0.27	-0.43	-0.48	-0.46	-0.15	0.38	
I_PE_1st_p05_C2	**-0.55**	-0.33	-0.43	-0.45	-0.36	-0.10	0.37	
I_PE_1st_p05_C3	**-0.61**	-0.37	-0.47	**-0.59**	**-0.56**	-0.20	0.47	
I_PE_1st_p10_C1	**-0.50**	-0.15	-0.41	**-0.51**	-0.48	-0.08	0.36	
I_PE_1st_p10_C2	**-0.56**	-0.25	-0.44	-0.49	-0.41	-0.04	0.36	
I_PE_1st_p10_C3	**-0.59**	-0.29	-0.45	**-0.61**	**-0.56**	-0.12	0.44	
I_PE_1st_p25_C1	-0.37	0.13	-0.26	-0.49	-0.41	0.13	0.30	
I_PE_1st_p25_C2	**-0.55**	0.00	-0.36	**-0.58**	-0.43	0.15	0.35	
I_PE_1st_p25_C3	**-0.51**	-0.07	-0.37	**-0.63**	**-0.55**	0.05	0.37	
I_PE_1st_p50_C1	0.04	0.32	0.14	-0.07	0.08	0.39	0.17	
I_PE_1st_p50_C2	-0.40	0.17	-0.05	**-0.52**	-0.24	0.37	0.29	
I_PE_1st_p50_C3	-0.35	0.17	-0.14	**-0.61**	-0.42	0.25	0.32	
I_PE_1st_p75_C1	0.39	0.38	0.36	0.36	0.46	**0.52**	0.41	
I_PE_1st_p75_C2	-0.15	0.21	0.19	-0.25	0.01	0.48	0.21	
I_PE_1st_p75_C3	-0.13	0.31	0.14	**-0.53**	-0.21	0.34	0.28	
I_PE_1st_p90_C1	0.46	0.38	0.42	**0.55**	**0.55**	**0.54**	0.48	
I_PE_1st_p90_C2	0.09	0.24	0.29	-0.08	0.15	0.50	0.22	
I_PE_1st_p90_C3	0.04	0.36	0.30	-0.38	-0.05	0.39	0.26	

Intensity features	Pinus resinosa	Pinus sylvestris	Pinus strobus	Picea abies	Picea glauca	Larix laricina	Mean of absolute correlations	Mean of absolute correlations by feature family
I_PE_1st_p95_C1	0.48	0.41	0.45	**0.58**	**0.56**	**0.52**	0.50	
I_PE_1st_p95_C2	0.22	0.28	0.33	0.00	0.19	0.49	0.25	
I_PE_1st_p95_C3	0.14	0.39	0.36	-0.28	0.04	0.42	0.27	
I_PE_si_p25_C1	**0.55**	0.23	0.38	**0.62**	**0.56**	**0.52**	0.48	
I_PE_si_p25_C2	0.15	0.09	0.28	0.17	0.27	0.47	0.24	
I_PE_si_p25_C3	-0.28	0.08	0.05	**-0.62**	-0.06	0.34	0.24	
I_PE_si_p50_C1	**0.55**	0.30	0.45	**0.67**	**0.62**	**0.56**	0.53	
I_PE_si_p50_C2	0.26	0.15	0.35	0.22	0.31	**0.52**	0.30	
I_PE_si_p50_C3	-0.12	0.24	0.21	**-0.52**	0.07	0.39	0.26	
I_PE_si_p75_C1	**0.50**	0.32	0.47	**0.68**	**0.64**	**0.57**	0.53	
I_PE_si_p75_C2	0.33	0.20	0.38	0.23	0.32	**0.52**	0.33	
I_PE_si_p75_C3	0.02	0.33	0.33	-0.40	0.13	0.42	0.27	0.34
I_RCG1_1st_mn	0.09	0.04	-0.02	-0.29	-0.12	-0.24	0.13	
I_RCG1_1st_p50	0.16	-0.06	-0.10	-0.19	-0.10	-0.23	0.14	
I_RCG1_1st_p75	0.02	0.16	-0.04	-0.43	-0.17	-0.21	0.17	
I_RCG1_si_mn	-0.34	0.07	-0.06	**-0.63**	-0.22	-0.09	0.24	
I_RCG1_si_p50	-0.29	0.11	-0.08	**-0.62**	-0.18	-0.10	0.23	
I_RCG1_si_p75	-0.26	0.18	0.03	**-0.54**	-0.14	-0.09	0.21	
I_RCG2_1st_mn	-0.46	-0.24	-0.24	**-0.64**	-0.48	-0.19	0.38	
I_RCG2_1st_p50	-0.35	-0.24	-0.28	**-0.58**	-0.44	-0.20	0.35	
I_RCG2_1st_p75	-0.46	-0.10	-0.22	**-0.67**	**-0.50**	-0.16	0.35	
I_RCG2_si_mn	**-0.62**	-0.19	-0.21	**-0.75**	-0.49	-0.05	0.39	
I_RCG2_si_p50	**-0.56**	-0.10	-0.22	**-0.74**	-0.45	-0.06	0.35	
I_RCG2_si_p75	**-0.54**	-0.07	-0.12	**-0.70**	-0.46	-0.05	0.32	
I_RCIR_1st_mn	**-0.54**	-0.31	-0.28	**-0.57**	-0.35	0.07	0.35	
I_RCIR_1st_p50	-0.46	-0.21	-0.22	**-0.52**	-0.29	0.04	0.29	
I_RCIR_1st_p75	**-0.51**	-0.30	-0.25	**-0.55**	-0.41	0.05	0.35	
I_RCIR_si_mn	**-0.51**	-0.34	-0.27	**-0.60**	-0.47	0.02	0.37	
I_RCIR_si_p50	-0.42	-0.28	-0.23	**-0.54**	-0.43	0.02	0.32	
I_RCIR_si_p75	-0.43	-0.31	-0.23	**-0.59**	-0.47	0.02	0.34	0.29
I_RM_1st_mn_2nd_mn_C1	-0.23	-0.15	-0.03	-0.05	-0.08	0.18	0.12	
I_RM_1st_mn_2nd_mn_C2	-0.14	-0.16	-0.04	0.04	-0.05	0.12	0.09	
I_RM_1st_mn_2nd_mn_C3	-0.22	-0.01	-0.12	-0.17	-0.25	0.00	0.13	0.11
Mean of absolute values	0.35	0.21	0.24	0.44	0.31	0.21	0.29	
Maximum of absolute values	0.61	0.46	0.58	0.70	0.63	0.57	0.56	

Numbers in bold represent strong correlations (greater than 0.5 or lower than -0.5).

3.3.3 Classification results

Random forest classification models were trained to recognize the six tree species using three strategies, each one dealing with the occurrence of NA by either removing problematic trees or features, or by combining these two approaches into a hybrid one. Table 3.6 summarizes all classification results.

Because of the different strategies for managing the NA occurrences, two different classification success calculations were used in Table 3.6. The first is simply the accuracy of the random forest classification for trees without NA values (either because problematic trees, or problematic features, were removed). The second represents the ratio of correctly classified trees to all trees (including trees with NA values). In this case, a classification failure occurred either because a tree was assigned to a wrong species class or because a tree could not be classified due to at least one NA value. For clarity, these two types of classification success calculations are presented respectively in equations 3.2 and 3.3:

$$\mathbf{Pcct} = \frac{\mathbf{Ntc} * \mathbf{100}}{\mathbf{Nt} - \mathbf{Nt\_NA}} \qquad \text{Eq. 3.2}$$

$$\mathbf{Pcct\_NA} = \frac{\mathbf{Ntc} * \mathbf{100}}{\mathbf{Nt}} \qquad \text{Eq. 3.3}$$

where

- Pcct = percent of correctly classified trees excluding trees with at least one NA
- Pcct_Na = percent of correctly classified trees including trees with at least one NA
- Ntc = number of trees considered in classification (without NA)

- Nt = total number of trees (including NA)
- Nt_NA = number of trees presenting at least one NA

For all strategies, the percentage of classification success without taking into account the removed trees (Pcct, Eq. 3.2, Table 3.6, fourth column) was higher for the tree removal approach than for the feature removal approach (i.e., 88% compared to 82% for STD strategy) because the total number of trees considered in the respective classification models differed.On the contrary, when calculating the percentage of classification success taking into account all the trees (Pcct_NA, Table 3.6, fifth column), including the removed (non-classified) trees, the tree removal approach systematically produced a lower percentage of classification success than the feature removal approach (i.e., 76% compared to 82% for STD strategy).

The next comparisons used the percentage of classification success calculated for all trees (fifth column). When comparing classification accuracy using only features with a weak correlation to tree height ($r^2 < 0.2$) calculated from all trees (SIF) versus trees higher than 7 m (SIF 7 m), the species identification accuracy was 2% higher for the latter. However, they did not surpass the accuracy of STD strategy. Moreover, the identification of species per height strata (HSC 7 or HSC 3) did not lead to improved accuracy compared to the STD strategy with the tree removal approach (about 87%–88%), but offered some limited improvements for the feature removal approach (84%–85% compared to 82%). Overall, the HSC strategy performed better than the SIF strategy. The last two columns of Table 3.6 present the results of the hybrid approach calculated with all features (sixth column: *Accuracy hybrid all features*) and with only the ten best features ordered by random forest mean decrease accuracy (seventh column: *Accuracy hybrid reduced no of features*). The best accuracy calculated from all features was equal for the STD and HSC 3 strategies (87%), and lower for the others. The best accuracy calculated from reduced features was almost the same for HSC 3 (83%) and

STD (82%), but lower for the other strategies. When considering the results of the two approaches separately, the stratified RF (HSC strategy) with the features removal approach gave the highest percentage of well-classified trees (about 84%–85%). By contrast, when combining the two approaches into a hybrid classification, the biggest improvement occurred in the non-stratified RF (from 76%–82% to 87% for STD) compared to stratified RF (from 75%–85% to 86%).

Figure 3.11 represents the classification performance of all combinations of classification strategies and approaches, given in total number of trees for which the species prediction was correct, incorrect or not applicable. Figure 3.12 represents the detailed results of tree classification, given in absolute tree numbers and by strata of 5 m. The distribution of non-classified trees by strata (with a large percentage in the 2–15 m stratum) is obvious for the tree removal approach. In the 2–10 m stratum, the important number of trees removed resulted overall in less accurate results for the tree removal approach compared to the feature removal approach. The same tendency is observed in the 10–20 m stratum, only for the HSC and STD strategies. For the SIF strategy in the 10–35 m stratum, and for the STD strategy in the 20–35 m stratum, keeping the largest number of features seemed to benefit the accuracy of classification, since the number of incorrectly classified trees in the feature removal approach surpassed the sum of incorrectly and non-classified trees in the tree removal approach.

Table 3.6: Random forest classification results

Classification type	NA elimination approach	No. trees classified	% classif success without NA (Pcct, variable no. of trees)	% classif success with NA (Pcct_NA, 37225 trees)	% classif success hybrid (all features)	% classif success hybrid (10 best features)
STD	tree removal	32102	88	76	87	82
STD	feature removal	37225	82	82		
SIF	tree removal	32102	83	71	80	76
SIF	feature removal	37225	69	69		
SIF 7 m	tree removal	32102	85	73	83	78
SIF 7 m	feature removal	37225	71	71		
HSC 7	tree removal	32102	87	75	86	79
HSC 7	feature removal	37225	85	85		
HSC 3	tree removal	32102	88	76	87	83
HSC 3	feature removal	37225	84	84		

STD = standard, SIF = Size invariant features (r^2 calculated with all trees), SIF 7 m = Size invariant features (r2 calculated with trees higher than 7 m), HSC 7 = Height stratum classes (7 strata of 5 m), HSC 3 = Height stratum classes (3 strata of 10 m)

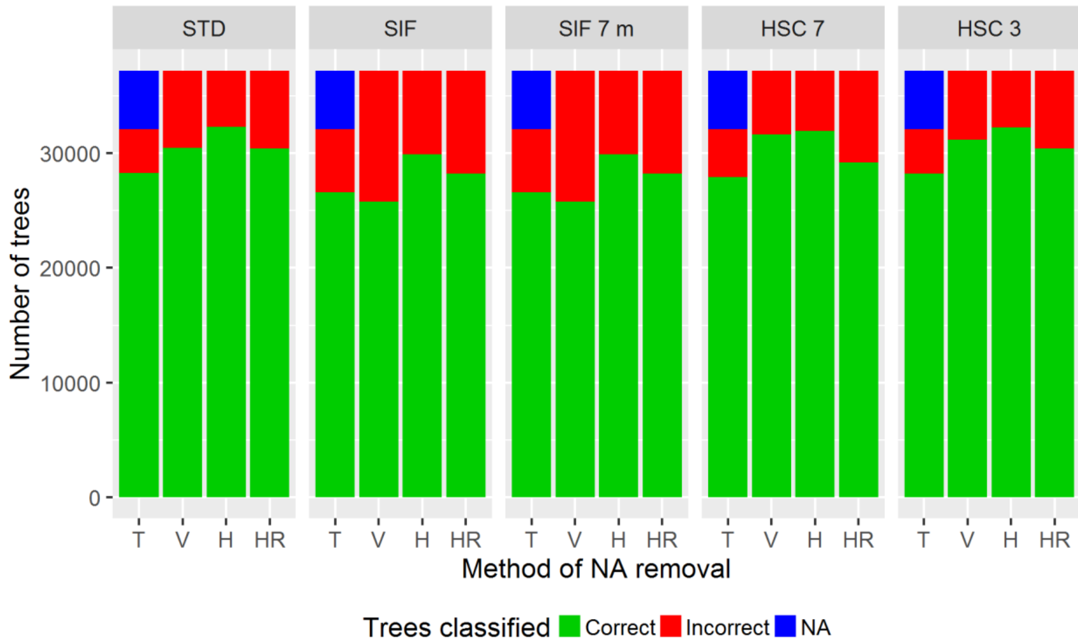

Figure 3.11: Performance of different classification strategies (STD, SIF, SIF 7 m, HSC 7, HSC 3) and approaches (T = tree removal, V = variable removal, H = hybrid, HR = hybrid with reduced number of variables).

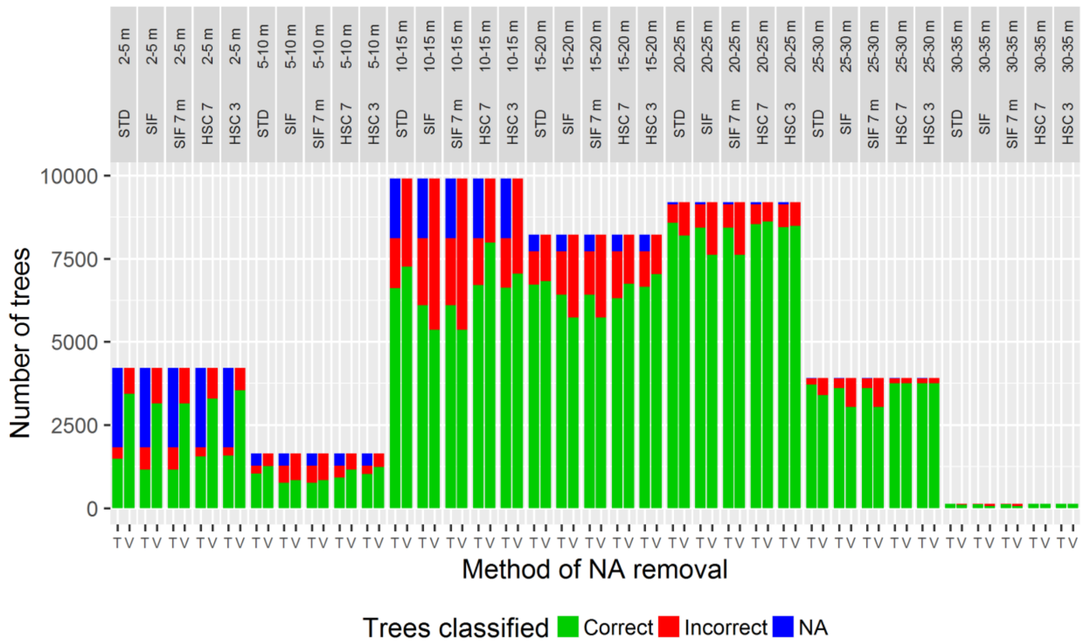

Figure 3.12: Performance of different classification strategies (STD, SIF, SIF 7 m, HSC 7, HSC 3) and approaches (T = tree removal, V = variable removal) calculated by 5 m strata.

Table 3.7: Feature selection for the STD, SIF and SIF 7 m classification strategies

Approach	Tree removal			Features removal		
Strategy	**STD**	**SIF**	**SIF 7 m**	**STD**	**SIF**	**SIF 7 m**
10 first variables from RF mean decrease accuracy	I_PE_1st_p95_C3	I_PE_1st_p95_C3	I_PE_1st_p90_C3	3D_RP_1st_all_C321	3D_DI_all_cv_C321	I_MI_1st_mn_C1
	3D_RP_1st_all_C321	I_MI_1st_mn_C1	I_MI_1st_95_5_mn_C1	3D_RM_1st_mn_all_mn_C321	I_MI_1st_mn_C1	3D_RM_1st_mn_all_mn_C321
	3D_RM_1st_mn_2nd_mn_C321	I_NDG1_1st_p75	3D_RM_1st_mn_all_mn_C321	3D_RP_si_1st_C321	3D_SL_all_p50_C321	3D_PE_all_p25_C321
	I_RCIR_si_mn	I_RCG1_1st_p75	I_NDG1_1st_p75	3D_DI_all_sd_C321	3D_DI_all_kurt_C321	3D_DI_all_sd_C321
	3D_RM_1st_mn_all_mn_C321	3D_SL_all_p50_C321	I_RCG1_1st_p75	I_PE_1st_p90_C1	3D_SL_1st_p50_C321	3D_RB_pt_80_90_all_C321
	I_NDG1_si_mn	3D_DI_all_cv_C321	3D_DI_all_sd_C321	I_PE_1st_p75_C1	3D_HR_lm_all_C321	3D_DI_all_kurt_C321
	I_NDIR_si_mn	3D_SL_all_p25_C321	I_NDG1_1st_mn	I_PE_1st_p95_C2	3D_SL_all_p75_C321	3D_SL_all_p50_C321
	I_RCG1_si_mn	I_NDG1_1st_mn	I_RCG1_1st_mn	I_NDIR_1st_p75	3D_RM_all_p50_all_mn_C321	3D_HR_lm_all_C321
	3D_RP_si_1st_C321	I_RCG1_1st_mn	3D_SL_all_p50_C321	3D_AH_C321	3D_RB_pt_90_100_all_C321	3D_RB_pt_60_80_all_C321
	I_PE_si_p75_C2	3D_HR_lm_all_C321	3D_HR_lm_all_C321	I_RCIR_1st_p75	3D_DI_1st_kurt_C321	3D_SL_all_p25_C321
Mean *r*	0.36	0.22	0.21	0.37	0.21	0.23

Table 3.8: Feature selection per height stratum for the HSC7 classification strategy, tree removal approach

Strategy	Stratum 2-5 m	Stratum 5-10 m	Stratum 10-15 m	Stratum 15-20 m	Stratum 20-25 m	Stratum 25-30 m	Stratum 30-35 m
10 first variables from RF mean decrease accuracy	3D_AH_C321	I_RCIR_si_mn	I_PE_1st_p95_C3	I_DI_1st_sd_C3	I_PE_1st_p90_C3	I_PE_1st_p95_C3	I_MI_si_mn_C3
	I_NDG1_si_p50	3D_RP_1st_all_C 321	I_NDIR_si_mn	I_RCIR_si_mn	I_DI_1st_sd_C2	I_DI_1st_kurt_C1	I_NDG1_si_mn
	3D_MH_1st_mn_ C321	I_NDIR_1st_p75	I_RCIR_si_mn	I_PE_1st_p75_C1	I_PE_si_p75_C1	3D_HR_1st _lm_C321	I_NDG1_1st_p75
	3D_DI_1st_cv_C 321	3D_AH_C321	I_DI_1st_sd_C3	I_NDG1_1st_p75	I_PE_1st_p90_C1	I_NDIR_si_mn	3D_RM_1st_mn_ all_mn_C321
	I_MI_si_mn_C3	I_NDIR_1st_p50	I_MI_si_mn_C1	I_RCG1_1st_p75	I_PE_1st_p75_C1	3D_RM_1st_mn_ all_mn_C321	I_DI_si_skew_C2
	I_NDG1_1st_mn	I_RCIR_1st_p75	I_MI_si_mn_C2	I_MI_si_mn_C1	I_NDG1_si_mn	3D_SL_all_p50_ C321	I_RCG1_1st_mn
	I_RCG1_si_p75	I_NDIR_si_p75	I_NDIR_1st_p75	3D_RM_1st_mn_ 2nd_mn_C321	3D_SL_1st_p75_ C321	I_PE_1st_p90_C2	I_DI_1st_kurt_C2
	I_NDG1_1st_p75	I_RCIR_1st_p50	I_RCIR_1st_p75	I_NDIR_1st_p75	I_RCG1_si_p75	I_PE_si_p50_C2	I_DI_1st_kurt_C1
	I_MI_1st_90_10_ mn_C3	I_RCIR_1st_mn	I_NDIR_1st_mn	I_RCIR_1st_p75	3D_HR_1st_lm_C 321	I_PE_1st_p75_C2	I_DI_1st_skew_C 1
	I_RCG1_1st_p50	I_NDIR_1st_mn	I_RCIR_1st_mn	I_NDIR_si_p50	3D_HR_all_lm _C321	I_PE_si_p25_C2	3D_RB_all_pt_0_ 60_C321
Mean *r* all strata	0.24	0.37	0.36	0.34	0.31	0.24	0.20
Mean *r* by stratum	0.34	0.22	0.14	0.16	0.16	0.14	0.17

Table 3.9: Feature selection per height stratum for the HSC7 classification strategy, feature removal approach

Strategy	Stratum 2-5 m	Stratum 5-10 m	Stratum 10-15 m	Stratum 15-20 m	Stratum 20-25 m	Stratum 25-30 m	Stratum 30-35 m
10 first variables from RF mean decrease accuracy	3D_AH_C321	I_RCIR_1st_p75	I_PE_1st_p95_C3	I_DI_1st_sd_C3	I_PE_1st_p90_C3	I_DI_1st_kurt_C1	I_MI_si_mn_C3
	3D_DI_1st_cv_C321	3D_AH_C321	I_NDIR_1st_p75	I_PE_1st_p90_C1	I_PE_1st_p75_C1	I_PE_1st_p95_C3	I_NDG1_si_mn
	3D_SU_1st_rs_C321	I_NDIR_1st_p75	I_RCIR_1st_p75	I_RCIR_1st_p75	I_PE_1st_p90_C1	I_DI_1st_kurt_C2	I_NDG1_1st_p75
	3D_PE_all_p25_C321	I_NDIR_1st_p50	I_PE_1st_p95_C2	I_NDIR_1st_p75	I_PE_1st_p95_C2	3D_HR_all _lm_C321	3D_RM_1st_mn_all_mn_C321
	3D_RB_all_pt_0_60 _C321	I_RCIR_1st_p50	I_PE_1st_p75_C2	I_NDG1_1st_p75	3D_SL_all_p50_C321	I_PE_1st_p90_C2	I_DI_si_skew_C2
	3D_RM_1st_mn_C321	I_NDIR_1st_mn	I_PE_1st_p75_C1	3D_RM_1st_mn_2nd_mn_C321	I_IR_1st _sd_C3	3D_SL_all_p50_C321	I_RCG1_1st_mn
	I_PE_1st_p05_C1	I_PE_1st_p95_C2	I_NDG1_1st_p75	3D_HR_all _lm _C321	I_DI_1st_cv_C3	3D_RP_1st_all_C321	I_DI_1st_kurt_C2
	I_DI_1st_sd_C2	I_RCG2_1st_p75	I_RCG1_1st_p75	I_RCG1_1st_p75	3D_SL_all_p75_C321	I_PE_1st_p75_C2	I_DI_1st_kurt_C1
	3D_HR_1st_cv_C321	I_PE_1st_p75_C2	I_NDIR_1st_mn	I_DI_1st_sd_C2	3D_HR_1st_lm_C321	I_DI_1st_sd_C2	I_DI_1st_skew_C1
Mean *r* all strata	0.30	0.33	0.29	0.30	0.28	0.25	0.20
Mean *r* by stratum	0.25	0.22	0.14	0.15	0.15	0.15	0.17

Table 3.10: Feature selection per height stratum for the HSC3 classification strategy

Approach	**Trees removed**			**Features removed**		
Strategy	**Stratum 2-15 m**	**Stratum 15-25 m**	**Stratum 25-35 m**	**Stratum 2-15 m**	**Stratum 15-25 m**	**Stratum 25-35 m**
10 first variables from RF meand decrease accuracy	I_PE_1st_p95_C3	I_PE_1st_p95_C3	I_PE_si_p75_C3	3D_RP_1st_all_C321	I_PE_1st_p90_C3	I_PE_1st_p95_C3
	I_RCIR_1stu_mn	I_RCG1_si_mn	I_DI_1st_kurt_C1	3D_DI_all_cv_C321	I_PE_1st_p75_C1	I_DI_1st_kurt_C1
	I_NDIR_1stu_mn	I_NDG1_si_mn	I_PE_1st_p90_C2	3D_RM_1st_mn_C321	I_RCG1_1st_p75	I_PE_1st_p90_C2
	3D_RM_1st_mn_C321	3D_RM_1st_mn_2nd_mn_C321	3D_HR_lm_1st_C321	3D_AH_C321	3D_RM_1st_mn_2nd_mn_C321	3D_HR_lm_all_C321
	3D_SU_rs_1st_C321	I_MI_si_mn_C2	I_DI_1st_kurt_C2	3D_SU_rs_1st_C321	I_NDG1_1st_p75	3D_RM_1st_mn_all_mn_C321
	3D_RP_1st_all_C321	I_NDIR_si_mn	3D_SL_all_p50_C321	I_PE_1st_p90_C2	I_PE_1st_p95_C2	I_DI_1st_kurt_C2
	3D_RB_pt_0_60_all_C321	I_RCIR_si_mn	I_PE_1st_p75_C2	I_PE_1st_p90_C1	3D_HR_lm_1st_C321	3D_RP_1st_all_C321
	I_MI_si_mn_C1	3D_SL_all_p50_C321	I_PE_si_p75_C2	I_NDIR_1st_p75	3D_HR_lm_all_C321	3D_SL_all_p50_C321
	I_NDIR_1st_p75	3D_HR_lm_all_C321	I_PE_si_p50_C2	I_RCIR_1st_p75	I_NDIR_1st_p75	I_PE_1st_p75_C2
	I_RCIR_1st_p75	3D_HR_lm_1st_C321	3D_RB_pt_60_80_all_C321	I_NDIR_1st_mn	I_RCIR_1st_p75	3D_RB_pt_60_80_all_C321
Mean *r* all strata	0.34	0.28	0.23	0.35	0.28	0.23
Mean *r* by stratum	0.25	0.19	0.15	0.24	0.19	0.17

With regard to the non-stratified classification (Table 3.7), it should be noted for the tree removal approach that only four of the best classification variables were 3D features, and that an intensity feature always ranks first. By contrast, when using the feature removal approach, 3D features had a greater significance, mainly for the SIF classification, where they were more dominant (9/10 features) than the STD classification (5/10 features). The larger presence of 3D features in non-stratified classifications, using the feature removal approach, resulted from the reduced choice of intensity features that could be used for all trees, because of the presence of small trees that generated NA.

For the stratified approach HSC7 (Tables 3.8 and 3.9), the intensity features were always dominant (0/10 to 3/10 3D features), except for the 2–5 m stratum in the feature removal approach (7/10 3D features). The advantage of the stratified classification is that the uncomputable intensity features for small trees did not affect the feature selection in the other higher strata. For the stratified approach HSC3 (

Table 3.10), there was more balance between the 3D and intensity features (3/10 to 5/10 3D features) than in HSC 7.

The mean correlation of the first 10 features taken by order of mean decrease accuracy was still higher for the STD strategy than for the SIF strategy (Table 3.7). This was obvious since in the SIF strategy the highly correlated features were removed. This also highlights the fact that RF did not lead to higher rank features with a low correlation to tree height, even if they were available. Despite this higher mean correlation, the classification accuracy was also higher than what can be achieved with the SIF strategy. Generally, stratification strategies (HSC7 and HSC3) managed to reduce correlation with tree height for each classification in each individual stratum (Tables 3.8 - 3.10). However, the accuracy of the classification was similar to that of the STD strategy.

3.4 Discussion

3.4.1 Variation of 3D features with tree height

The correlations of all features with tree height were examined to assess the magnitude and direction of the influence of tree size. Because all 3D features were scale-invariant by design, significant positive or negative correlations were likely caused by the changing architecture and morphology of the trees with age as well as by the relative difference in laser penetration in the crown. Tree allometry, or other factors correlated to height or age (e.g., the leaf area index, LAI), might create a correlation between height and feature values. What is more, 3D features, including crown shape or return proportions, are generally better defined for large trees because of the larger number of returns in the corresponding point clouds. In the case of small trees that intercept fewer lidar pulses, the 3D features have a larger variation with atypical values and do not allow a high definition of the tree structure. Figure 3.5, for example, illustrates that all six needle-leaved species appear to have a stronger crown curvature

(3D_SU_coef_1st_123) as they become larger, in other words, as their "pointiness" becomes better defined.

The threshold used to eliminate returns from the ground affected the smaller trees more than the taller ones, as expected. Depending on the chosen threshold, the remaining portion of the upper tree crown differs. For some small trees, only the upper extremity of the crown is left in the case of larger absolute thresholds (e.g., 2 m). This part of the tree only includes a few returns that are not sufficient in number to be representative of a species' trait. For very small trees, the influence of the threshold is very strong. For this reason, it is advisable to stratify by height as a way to allow choosing adequate features for this tree category separately. This would limit the influence of possibly atypical feature values during the training based on the bulk of the tree sample, in other words, on all trees that are not very small.

3.4.2 Variation of intensity features with tree height

On the ALS intensity image, the spectral signature of pixels often varied from the centre to the periphery of the crowns. Low values were typically found at the edge of the crowns. This is most likely due to the lower peripheral leaf density where branches spread out. Peripheral returns are thus often triggered by branch extremities, which bear less foliage within a laser footprint and therefore yield a lower intensity (Hovi *et al.* 2016). This change in intensity and higher variability from tree centre to the crown edge was captured by features using mean intensity by radial sections of tree (rings), such as I_IR_sd_1st or, in a more general way, the SD of intensities. Advanced features accounting for this variation have been proposed by Axelsson, Lindberg and Olsson (2018). Tree size, in other words, crown area in this case, plays a role because in small trees the proportion of peripheral laser returns to crown core returns is higher than for larger ones. This change may affect the mean and SD of crown intensities for a given species. The large variance in intensity features for small trees can also be associated to the reduced number of returns, as remarked by (Hovi *et al.* 2016).

Moreover, ratios of channels and NDVI-based features, only available for multispectral lidar, were not expected to be correlated to tree size because of the inherent normalization effect of ratios or normalized differences. Our study demonstrated that they nevertheless varied with tree height. This is likely due to differential effects of tree size on intensity depending on the laser channel. Overall, the relationship between intensity feature values and height differed from feature to feature, taking the form of direct or inverse, non-linear (i.e., resembling a second-degree curve) or even more complex relationships. Despite these changing correlation patterns, intensity features retained high ranks in the tree classification feature importance (according to the mean decrease accuracy). It also needs to be remembered that only needleleaf species were studied. Intensity features could have gained more importance should broadleaf trees been included.

3.4.3 Classification strategies

The NA problem had to be handled prior to running the classifier, here the R version of random forest, which does not handle missing data. This led us to try different NA management approaches for the different classification strategies. The features removal approach resulted in an overall lower classification success compared to the tree removal approach but was able to make a species prediction for all trees. With the goal of keeping the best species prediction for all trees, we created a hybrid approach for dealing with NA. Compared to the tree removal approach, the hybrid classification success was higher (*hybrid all features* and *hybrid 10 best features* compared to *Pcct_NA* in Table 3.6) mainly because all trees could be classified. The hybrid results yielded a slightly higher success rate than those of the feature removal approach, except when employing the hybrid approach with HSC 7 and the ten best features.

The error was not uniform across the height strata. For large trees, there was generally a very good rate of well-classified trees, and very few trees removed, compared to the case of smaller trees.

The HSC classification strategy revealed that different combinations of features were more adapted to identify species for given height strata. Some features needed a high number of returns to produce an adequate value, and were therefore more useful for identifying the species of larger trees. For thinner height strata (5 m, in the HSC 7 strategy), the intensity features were predominant except for the small trees for which there existed uncomputable intensity features. For thicker strata (approx. 10 m in the HSC 3 strategy), the respective 3D and intensity feature numbers among the 10 selected ones were more balanced.

The classification strategy that eliminates features that are correlated to tree height (SIF) overall resulted in less accurate results than those using all features. Possibly, the 0.2 limit of r^2 was too low and eliminated too many useful features. On the other hand, features that were highly correlated to tree height proved to be very useful in species classification, as NDVIs or ratios of return types. It appears that the RF classification algorithm was able to overcome this limitation. Moreover, the RF may well have become trained to recognize patterns associated with species, regardless of whether trees are small or tall. In other words, it recognizes a specific pattern of feature values (over *n* useful features) for a given species within a certain size range, and a different pattern for the same species in another size range—but can in both cases associate these patterns to the proper species.

During the RF classification, the *sampsize* parameter, which affects accuracy, corresponded to the minimum number of trees in each species. For example, a low *sampsize* of 2 in the 2–5 m stratum (HSC 7), used because of the very low number of *Picea abies* in this stratum, affected the classification performance. The main advantage of the thicker height strata (HSC 3) is that they benefit from a larger *sampsize* per stratum. Finally, the thickness of the height strata must be adapted to the characteristics of the training sample and to the specific distribution of trees by height strata in order to have sufficient trees by species in each stratum. Otherwise, this could force the *sampsize* to be too low, resulting in a poor classification accuracy for strata having few samples.

In this study, we tried to retain most small trees in the classification, assuming that this could eventually be useful for identifying the small trees that regenerate naturally after a disturbance (fire, clear cut). However, the higher the number of small trees to be considered, the more difficult it is to perform a general classification (STD or SIF), because of the larger number of features that cannot be computed for all trees. Therefore, when applying such an approach for mapping tree species, a compromise should be made on the minimum size of the trees considered (a higher minimum simplifies the classification) and on the utility of a species map (a lower minimum will include more trees in the results). Using high density lidar (e.g., 25 returns/m^2) could solve a portion of the problems caused by small trees as a sufficient number of points would be attained, albeit at a much higher cost.

The significant costs of field sampling, and the logistics of working in regions with difficult access, brings us to design classification strategies that need as little field sampling as possible. The STD and SIF strategies fall into this category because trees from all height strata are considered together in the RF algorithm. This reduces the need of having to find a good number of trees of given species-size classes in the field. However, care should nevertheless be taken to include trees of all sizes in the sample, to avoid bias. In this regard, the HSC strategy is the most demanding as a minimum number of dominant trees must be sampled in each stratum. This requirement is more difficult to accomplish for small trees as the majority are found in understorey strata or are suppressed trees, and may not be visible in the ALS point cloud or be difficult to separate from the crown of dominant trees.

3.5 Conclusion

A significant number of lidar features were found to be correlated to tree height. Despite efforts of normalization, especially for 3D features, some degree of correlation to tree height indeed still remained, most likely because of changes in tree architecture that occur during the tree development. Coefficients of determination between tree height and feature values as high as 0.6 were found. Moreover, intensity features tended to be highly correlated to tree height, even in the case of ratios or NDVIs.

Small trees generated more NA features that are problematic in an RF classification (R implementation). The trees that generated NA need to be treated differently in order to profit from the maximum information available from MSL. The classification problem consisted of either finding a solution for using more complex and potentially useful features not available for all trees or for using robust features available for all trees but having a low-information discriminatory power for species classification. Three classification strategies with three different approaches of NA treatment were tested. The hybrid approaches improved classification results for all strategies. This approach is in fact another type of stratification approach. It is based not on tree properties such as height but on the lidar point cloud quality that allows for the computation of complex features from high-quality point clouds as well as for robust features from low-quality point clouds. With this hybrid approach, the results yielded by the HSC were similar to those of the STD. Finally, the hypothesis proposed in this study, namely that the HSC should yield the best results, was not confirmed when the hybrid approach was considered. However, for a simple application of RF, this hypothesis was adequate because results are similar for HSC and STD in the case of tree removal approach and better in the case of feature removal approach. For each stratum, results were affected by tree distribution (minimum number of trees by species in each stratum). The SIF yielded the worst results, due namely to an aggressive variable reduction that lowered the overall classification accuracy. Some very good features for species separation, which were also correlated to tree height, were in this case discarded. Some higher-correlated features were also ranked as better for species identification by the RF classifier (in STD or HSC strategies), which appeared to be capable of recognizing species-specific patterns across the range of tree sizes. We conclude that it is not essential to apply a height stratification when identifying species using a random forest classifier. However, due to the frequent correlation between tree height and the feature values, any sample used to train the classifier must be representative of the tree height range within a given area of interest.

3.6 Acknowledgements

We express our thanks to Teledyne Optech Incorporated (Vaughan, Canada) for graciously providing the Titan MSL datasets used in this study. We thank the authorities of the York Regional Forest (namely Kevin Reese) for granting permission and facilitating access to the forest’s study area. We acknowledge the collaboration of CarboMap (Edinburgh, Scotland) in field logistics and data collection. We thank the reviewers for their useful comments which help us in improving our work. Finally, we acknowledge Chris Hopkinson for providing us field measurements. This study was partly funded by the National Sciences and Engineering Research Council of Canada, through the AWARE project.

CHAPITRE 4

EFFECTS OF VIEWING GEOMETRY ON MULTISPECTRAL LIDAR-BASED NEEDLE-LEAVED TREE SPECIES IDENTIFICATION

Cet article est à soumettre :

Brindusa Cristina Budei, Benoît St-Onge, Richard A. Fournier, Daniel Kneeshaw, Effects of viewing geometry on 3D and intensity classification features used for ALS-based tree species identification, à soumettre à *Canadian Journal of Remote Sensing*

Abstract

The ability to automate tree species identification with remote sensing techniques, such as lidar, would improve forest management decision making. The multispectral lidar Titan of Teledyne Optech Inc., with three integrated lasers (channels C1, C2, C3) scanning with different wavelengths (respectively 1550, 1064, and 532 nm), and different scan angle planes (respectively tilted 3.5°, 0° and 7° relative to a vertical plane), improves tree species separation compared to monospectral lidar, by providing classification features computed from intensities in each channel, or from pairs of channels (ratios and normalized indices). The objective of the present study is to evaluate whether scan angle (up to 20°) influences the 3D and intensity feature values and if this influence affects species classification accuracy. In our study region located in Ontario, Canada, six needleleaf species were sampled to train classifiers with different feature selection. The feature correlation with scan angle was mainly below |±0.2| and influenced tree species classification accuracy between 1% (all features) and 8% (3D features only). The intensity normalization for range improved accuracy by 8% for classifications using only single channel intensities, but this improvement decreased to 2-4% when features unaffected by normalization were added, as 3D features or normalized indices.

Keywords: tree species; multispectral lidar; scan angle; intensity; Titan; *random forest*; forestry

Résumé

La capacité d'automatiser l'identification des espèces d'arbres avec les techniques de télédétection, comme le lidar, peut améliorer la prise de décision dans la gestion forestière. Le lidar multispectral Titan de Teledyne Optech Inc., avec trois lasers intégrés (canaux C1, C2, C3) qui balayent avec des longueurs d'onde différentes (respectivement 1550, 1064, et 532 nm) et différents angles de balayage (respectivement inclinée de 3,5°, 0° et 7° par rapport au plan vertical), améliore la séparation des espèces d'arbres par rapport à un lidar monospectral, en permettant le calcul des variables à partir des intensités de chacun des trois canaux, ou par paire de canaux (ratios et des indices normalisés). L'objectif de cette étude est d'évaluer si l'angle de balayage (jusqu'à 20°) influence les variables 3D et d'intensité et si cette influence affecte l'exactitude de la classification des espèces. Dans la zone d'étude localisée en Ontario, Canada, six espèces de conifères ont été échantillonnés pour entraîner le classificateur avec différentes sélections de variables. La corrélation des variables avec l'angle de balayage est généralement inférieure à |±0.2| et influence l'exactitude de la classification des espèces d'arbres entre 1% (toutes les variables) et 8% (variables 3D seulement). La normalisation de l'intensité selon la portée améliore l'exactitude pour les classifications qui utilisent seulement les intensités des canaux individuels par 8%, mais cette amélioration décroît vers 2-4% quand des variables non affectées par la normalisation ont été ajoutées, comme les variables 3D ou les indices normalisés.

Mots clés : espèce de l'arbre; lidar multispectral; angle de balayage; intensité; Titan; *random forest*; forestrerie

4.1 Introduction

Individual tree species identification is important for precise forest management, and several studies have tested identification methods from discrete small footprint airborne lidar alone (Harikumar, Bovolo and Bruzzone 2017 ; Ko, Sohn and Remmel 2013 ; Lin and Hyyppä 2016 ; Ørka, Næsset and Bollandsås 2009 ; Suratno, Seielstad and Queen 2009 ; Vauhkonen *et al.* 2010 ; Vauhkonen *et al.* 2009) or in combination with passive multispectral imagery (Deng *et al.* 2016 ; Liu *et al.* 2017 ; Ørka *et al.* 2013 ; Ørka *et al.* 2012 ; Shi *et al.* 2018a). Recently, airborne multispectral lidar was proposed as an improvement over single sensor technology to identify tree species (Axelsson, Lindberg and Olsson 2018 ; Budei *et al.* 2018 ; Yu *et al.* 2017).

Single tree species identification using lidar data has generally been performed through three steps. First, single tree crowns are delineated and then the corresponding lidar point clouds are extracted. Second, for each single tree point cloud, features are calculated from return heights (3D features), and from return intensities (intensity features). Third, a classifier (e.g., random forest, RF) is trained using reference tree crowns of known species to compute a classification model, which is then applied to target tree crowns to identify the species. The scan angle of the laser pulses on the trees may affect the values of the computed features, and consequently influence the accuracy of species identification. Understanding the effect of scan angle is an increasingly important issue as some airborne laser scanning systems, as the multispectral lidar, have several lasers scanning the same tree at different angles. Multispectral airborne lidar that collects intensities at different wavelengths should improve tree species separation compared to single laser systems. The advantage is thus that it provides intensity classification features computed separately from each of the channel intensities, but also ratios and normalized differences, as well as 3D features enhanced by the greater point density (Ahokas *et al.* 2016 ; Axelsson, Lindberg and Olsson 2018 ; Budei and St-Onge 2018 ; Budei *et al.* 2018 ; St-Onge and Budei 2015 ; Yu *et al.* 2017). The inconvenient is that, while providing richer spectral information, this system produces data with variable acquisition geometries between channels (i.e. larger net scan angles and no vertical view for two of the three channels). This potentially increases the scan angle influence on 3D and intensity features compared to monospectral lidar (i.e. vertical scanning plan only).

Tree level 3D and intensity features are highly variable because they are influenced by multiple elements, some depending on tree characteristics (species, height, stress, tree shape, vertical and horizontal distribution of vegetation within the crown, clumping and occlusion, leaf density, leaf angles), on tree environment (tree status, tree density, season, topography, understorey), on laser properties (pulse power, pulse divergence, wavelength, range, scan angle), and on survey configuration (pulse density, flight altitude, lateral overlap, flight lines configuration, maximum scan angle). Because it is very difficult to distinguish between the respective influences of these families of characteristics (Hopkinson 2007), the majority of studies choose to ignore the scan angle effect, even if its influence on forest feature accuracy is often mentioned (Zheng *et al.* 2017). The studies specifically addressing this subject are mainly based on simulation models using geometric representations of trees (Disney *et al.* 2010 ; Goodwin, Coops and Culvenor 2007 ; Holmgren, Nilsson and Olsson 2003b). So far, we could not find any studies that specifically assessed the influence of scan angle on multispectral features at the individual tree level, using real (non simulated) airborne lidar data.

Large scan angles (large deviation from the vertical) produce at least three effects. Firstly, large angles cause a decrease in return intensity because the increase in laser range and in the footprint size. Consequently, the pulse energy per unit area reaching the top of the canopy decreases (Disney *et al.* 2010 ; Hopkinson 2007). The effect of this attenuation (effect #1) is more important for beams having a large divergence.

Secondly (effect #2), large scan angles cause a decrease in the number of returns per emitted pulse (i.e., receiving multiple returns from a given pulse becomes less likely) and produces a higher proportion of single returns. Thirdly (effect #3), large scan angles cause a change in the distribution of returns through the forest canopy along the pulse trajectory. A decrease in the peak pulse power concentration at the top of the canopy alters the shape and amplitude of the signal, because more vegetal material is needed to trigger a return. Thus the pulse penetrates deeper, and the height of returns will be shifted down (Hopkinson 2007).

The decrease in return intensity at larger scan angles changes the values of intensity percentiles (effect #1). The change in return proportions (effect #2) affects also these features, especially when computed from all returns, because the number of second and third returns with reduced intensity is larger at nadir than at larger scan angles. Even if intensity normalization should compensate for the intensity decrease (effect #1), in practice rigorous calibration is very difficult for lidar intensity. Intensity normalization for vegetation returns through physical modelling is very complex because many factors have to be accounted for, as range related factors (laser spreading loss and air attenuation), or tree related factors (leaf reflectance, leaf size and orientation). Different physical equations have been proposed to empirically normalize return intensities to compensate for range variations (Coren and Sterzai 2006 ; Gatziolis 2011 ; Korpela *et al.* 2010a). The efficiency of intensity normalisation for range has been tested relatively to the reduction of feature variability (Kukkonen *et al.* 2019b ; Yan and Shaker 2017 ; You *et al.* 2017), or relatively to the improvement in tree species classification accuracy (Korpela *et al.* 2010a). Even if more advanced calibration methods were used to retrieve radiometric characteristics that could help building active species spectral signatures and help improving classification accuracy (Kaasalainen *et al.* 2009 ; Kaasalainen *et al.* 2011 ; Okhrimenko, Coburn and Hopkinson 2019 ; Okhrimenko and Hopkinson 2019), this type of calibration exceeds the objectives of this study.

Moreover, even the range normalisation applied here is also technically difficult on data that is distributed in the widely used LAS format because of the lack of information on pulse range. Therefore, it will also be useful to evaluate if intensity normalisation is necessary to improve species identification accuracy or could be omitted without significant loss of accuracy.

There are no corrections proposed for effects #2 and #3 because these effects concern mainly second or third returns that issued from a complex species specific interaction of the laser pulse with leaves and branches. The effect #2 affecting mainly lidar features computed from return proportions (e.g. ratio of single to multiple returns, ratio of canopy to ground returns or ratios of returns above a threshold to all returns) was highlighted in several studies using the Area Based Approach – ABA (*i.e.,* at the plot level) concerning canopy cover (Arumäe and Lang 2018 ; Holmgren, Nilsson and Olsson 2003b ; Korhonen *et al.* 2011 ; Korhonen and Morsdorf 2014 ; Morsdorf *et al.* 2008), or gap fraction (Hopkinson *et al.* 2016 ; Korhonen *et al.* 2011 ; Korhonen and Morsdorf 2014 ; Liu *et al.* 2018a ; Zheng *et al.* 2017).

The change in return distributions (effect #3) was highlighted by changes in lidar features such as the height percentiles (Bater *et al.* 2011 ; Disney *et al.* 2010 ; Holmgren, Nilsson and Olsson 2003a ; Hopkinson *et al.* 2016 ; Korhonen *et al.* 2011 ; Lovell *et al.* 2005 ; Magnussen and Boudewyn 1998 ; Montaghi 2013 ; Næsset 1997 ; Roussel *et al.* 2018). Some of these studies show the two opposite effects of scan angle (shifting upward or downward the height percentiles) is not only related to forest density and occlusions, but is also species specific. The height percentiles varied more for species with longer tree crowns relative to crown diameter, like spruce, compared to species with a shorter crown, like pines, because of the probability of intercepting oblique pulses. Simulation studies explained the upward shift also by an increased distance the beams travel through the canopy, thus producing an increase in the interception probability of pulses at large incidence angles (Disney *et al.* 2010 ;

Goodwin, Coops and Culvenor 2007 ; Roussel *et al.* 2017). The upward shift is also related to the effect #2, a decrease in number of returns per pulse influence the height percentiles calculated from all returns (Roussel *et al.* 2018). These three effects that are difficult to correct will influence features values, which, in turn, will affect species identification accuracy.

The main objective of this study is to identify the effect of scan angle on tree identification, from feature calculation to classification, using real tree data and to evaluate the improvement brought about by range normalization of intensity. This was accomplished through five specific objectives: (i) investigate the effect of the scan angle on 3D and intensity features used to identify species, (ii) evaluate the effect of intensity normalization per feature type and per mean scan angle, (iii) identify the species for which features are most sensitive to scan angle, (iv) evaluate whether the scan angle affects the accuracy of species classification and (v) verify if feature normalization, to correct for the intensity effect of scan angle, has any influence on the accuracy of species identification.

4.2 Data and methods

4.2.1 Reference data on tree species

The study area is located in the York Regional Forest (YRF), Ontario, Canada (centered on 79°19' W, 44°04' N), in the Great Lakes–St. Lawrence forest region (Rowe 1972), specific for mixedwood plains ecozone. The topography is almost flat, with a maximum terrain altitude difference of approximatively 43 m (approximatively from 240 to 303 m). The forest stands in the study area are either mixed natural growing stands or needleleaf reforested/planted stands. We sampled six needleleafs species found in plantations having different ages: red pine (*Pinus resinosa)*, white pine (*Pinus strobus*), Scots pine (*Pinus sylvestris*), American larch (*Larix laricina*), Norway spruce

(*Picea abies*) and white spruce (*Picea glauca*). Tree species identification was carried out in the field in August 2015 to produce a reference database of individual trees within the plantations. High resolution (10 cm) images acquired during the Titan survey with CM-1000 RGB camera were used to identify additional reference trees or to verify the tree species in plantations by photo-interpretation.

The trees in this study are sampled mainly from needleleaf plantations. Trees in plantations, typically have similar characteristics as they are even aged, grew in similar conditions. Our data thus represent rather an opportunity to isolate scan angle effect from other tree characteristics. For example, in more complex environments, like natural stands or mixed stands composed of both needleleaf and broadleaf species, trees grow with a wider variety of shapes and sizes, in dominant, sub-dominant or supressed positions. Thus, isolating scan angle effect would be more difficult. A large sample tree dataset is required to highlight statistical trends, because tree characteristics, occlusions and other flight parameters might have greater effects on lidar features than the scan angle. This study took advantage of multiple overlapping flight lines and high return density of the Titan dataset that allowed computing advanced features for multiple single flight line views of each tree.

4.2.2 Lidar data and intensity correction for range

The multispectral lidar was acquired with Titan system of Teledyne Optech Inc.. This system has three integrated lasers (hereafter referred as channels: C1, C2, C3), that sends pulses having different wavelengths (respectively 1500, 1064, and 532 nm for C1-C3), and different scan angle planes, respectively tilted at 3.5°, 0° and 7° relative to a vertical plane. The data was acquired at the study area in July 2015, over 2,546 ha, at a mean altitude of approximately 800 m above ground. The mean number of first returns per m^{-2}, by channel and by individual flight lines was 3.4 for C1 and C2 and 3.3 for C3, which is equivalent of a total of 10 returns m^{-2} for all channels in single flight line. A total of 19 flight lines were acquired, with an average lateral overlap of 50%, thus providing two views of each tree, from different angles. Most flight lines were acquired following parallel centerlines, but in one area, additional flight lines were acquired perpendicularly with the existing ones. These two orientations (north-south and east-west) locally increased the number of views per tree.

Manual delineation of sampled crowns was performed on the canopy height model (CHM), generated using the highest return of the three channels above the digital terrain model (DTM) using 10 cm pixel size. The color composite image, interpolated from first returns intensity of each of the three channels was used to verify species and disambiguate delineation when two trees of different species were difficult to separate from the 3D information only, following the procedure proposed by Budei *et al.* (2018). The DTM was calculated from all ground returns gathered from all channels and all flight lines. This allowed producing one DTM (ground reference) for all three channels and for all flight lines. A similar approach was taken for tree height calculation: individual tree heights were calculated using all the first returns.

The lidar data acquired with Titan system were obtained both in LAS 1.3 and ASCII formats. The latter contained additional information on laser range and gave precise scan angle data, compared to integer precision level scan angle values provided in usually used LAS files. The laser range information allowed us to normalize intensity. The equation proposed by Korpela *et al.* (2010a) was used for this purpose:

$$\mathrm{I_n} = (\mathrm{R}/\mathrm{R_{ref}})^{\mathrm{a}}\mathrm{I_{raw}} \qquad \text{Eq. 4.1}$$

Where I_n is the range-normalized intensity, I_{raw} is the raw intensity, R the range, and R_{ref} the reference range. The a exponent was set to 2.

4.2.3 Net pulse scan angles

The maximum scan angle (mirror) for each of the three channels was approximately ±15°. The tilt of the sensor scanning planes of the three Titan lasers, respectively at 3.5° forward (C1), vertical (C2) and 7° forward (C3), increase the net scan angle. The net scan angle was calculated from the angle along the scanning plane (mirror angle), and the angle of the sensor scanning plane (tilt) (Figure 4.1). The high precision data of mirror scan angles (5 decimals) is provided in ASCII files. However, the information concerning the sensor orientation for each pulse (roll, pitch and yaw) or flight trajectories were not provided. Therefore, the roll and pitch of the aircraft were considered to be equal to zero. These assumptions are considered to be reasonable since the wind speed during the flight was under 11 km/hour, and there are no visual asymmetries in return distributions along the flight path. The yaw does not influence the scan angle value. The equation used to calculate the net angle (γ) from the mirror scan angle (α) and the scanning plane tilt (β) was:

$$\gamma = \text{atan}\sqrt{\tan^2(\alpha) + \tan^2(\beta)} \qquad \text{Eq. 4.2}$$

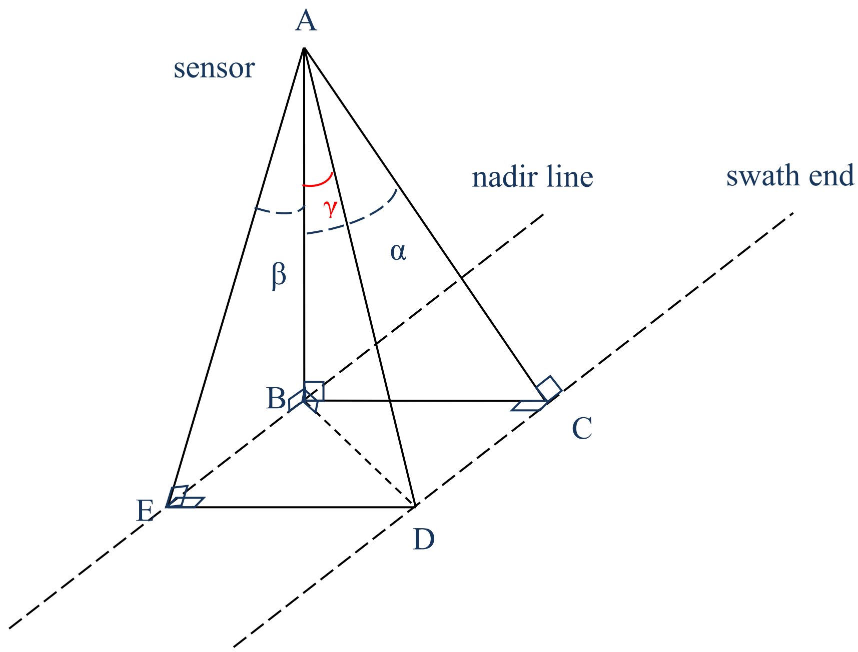

Figure 4.1: Calculation of net scan angle γ ($\widehat{BAD}$). β represents the inclination of scanning plane for C1 or C2. BC = ED represents the distance between the nadir line and the interception position (C or D), when mirror scan angle = α.

The "scan angle" refers from hereafter to the net angle, as calculated in Eq. 4.2, which applies for Titan channels 1 and 3. The "incidence angle", largely used in studies concerning basckscattering signals from a scanned object (Disney *et al.* 2010 ; Hopkinson 2007 ; Morsdorf *et al.* 2008 ; Pang *et al.* 2011) assume an accurate measure of scan angle and of local surface normal (often calculated from the DTM). However, the use of "incidence angle" was considered inappropriate in this study, since the exact aircraft attitude parameters (roll, pitch and yaw) were not known, and consequently the true incidence angle relative to the horizontal plane at tree level could not be calculated, and finally the local normal of the tree crown is difficult to define.

Across overlapping flight lines, each tree was scanned from multiple angles. For clarity, the scan of a single tree from a single flight line (point of view) is hereafter named a "tree view" and comprises the three point clouds corresponding to each Titan channels. For each tree view, several mean scan angles were calculated from the individual pulse scan angles of each point cloud used in a feature calculation (see details in section "Tree views selection"). First, different mean scan angle values were used to calculate correlation with lidar features, taking into account correspondence between respective channels or ratios of channels. Second, these mean scan angles were used in defining two class limits for each of the feature type selection (individual channel, pair of channels or all channels) used in species identification. The accuracy was compared afterwards between scan angle classes divided by these defined class limits. Figure 4.2 highlights the difference in point cloud configuration according to mean scan angle in C2 for a *Pinus resinosa* tree.

We evaluated what was the intensity normalisation effect on the correlation of features to scan angle (*objective ii*) and on classification accuracy (*objective v*). For the *objective ii,* the percentage of features presenting a Pearson correlation with mean scan angle higher than 0.2 was compared between intensity features calculated respectively from raw as well as normalized intensity. For the *objective v*, each instance of random forest classification that used intensity features was applied twice for raw and normalized intensities respectively.

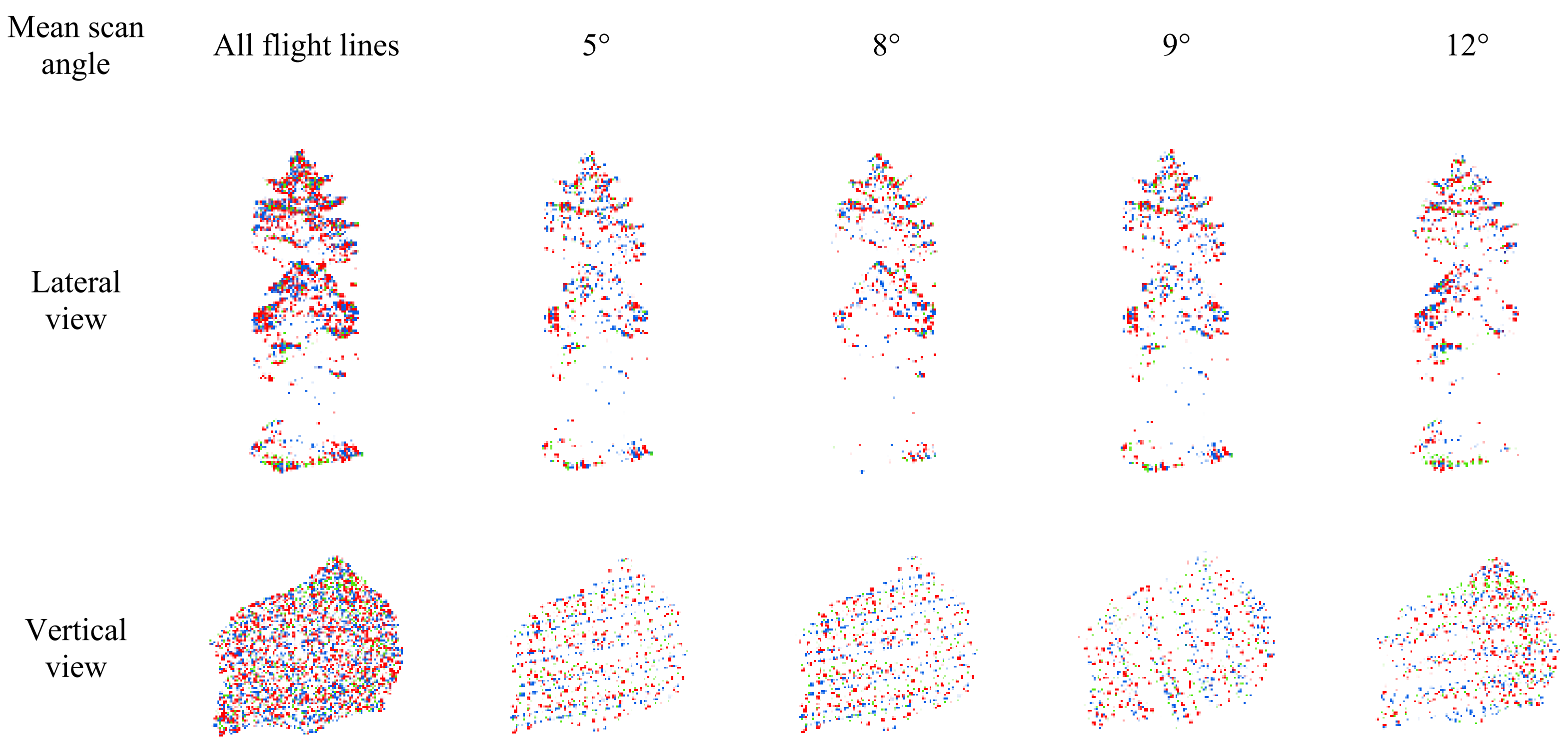

Figure 4.2: Example of three point clouds (red : C1, blue: C2, green: C3, intensity: point size) of one Pinus resinosa tree, seen by all four flight lines (first column) and its corresponding four tree views in each of the individual flight line (columns 2 to 5) seen with specified mean scan angle in C2.

4.2.4 Multispectral lidar features

3D and intensity features were computed for each reference tree. Several versions of each feature were computed from the point cloud extracted from each flight line and channel combination. A feature version corresponds to one of three potential return types: all returns (all), first returns (1st) and single returns (si). A variable threshold for each tree was used to remove points associated with the ground and understory, keeping only returns higher than 40% of the height of the reference trees.

The 3D features were calculated using the normalized height above ground of returns in the crown. A unique value of ground, the DTM pixel value at the tree crown centroid, was used to calculate return heights for all returns of the tree, to avoid changing return height distribution in the crown according to the terrain slope. The returns heights were then normalized with the maximum return height in the crown, considered as equivalent of tree height. The same DTM was used for the calculation of all features. 3D features were calculated for each single channel as well as for the three channels together (C1, C2, C3, C321). The features used include the mean (mn), the relative height at certain percentiles (PE, e.g. 5^{th}, 10^{th}, 25^{th}, 50^{th}, 75^{th}, 90^{th} and 95^{th} percentiles: p05, p10, p25, p50, p75, p90, p95), the return height distribution (DI, e.g. standard deviation: sd, coefficient of variation: cv, skewness: skew, and kurtosis: kurt), the ratios of features calculated from different return types (RM), the shape of the crown (e.g. mean of the slope (SL) between each return and the highest return within a tree). We also computed the ratios of number of returns of different type (RP, e.g., ratios of first returns over all returns, etc.), which were included with 3D features.

The intensity features were computed from raw intensities as well as from the range-normalized intensities. Most intensity features were computed from individual channels (e.g., mean intensity, intensity percentiles). Other intensity features were produced by using simple ratios of intensities from two different channels (ratios of channels: RC), two ratios using the green (G) channel: RCG1 from C2/C3 channels combination, RCG2 from C1/C3, and the third ratio using only infra-red (IR) channels: RCIR from C1/C2, or normalised differences (ND) e.g. NDG1 as (C2+C3)/(C2-C3), NDG2 and NDIR from consequently channels. For complete description of features and features' name composition see Budei *et al.* (2018) and Budei and St-Onge (2018).

4.2.5 Tree views selection

Some features need a high number of returns to be calculated. Depending on tree characteristics (tree height), tree environment (neighbour occlusion) or flight configuration (return density or position of the tree near the swath end), the number of returns by channel in individual flight line could be insufficient to calculate some features, and would produce "non applicable" (NA) values. The presence of NA could create bias in comparisons between correlation coefficients of features calculated with different scan angles, or between classification accuracies for different groups of tree views with similar scan angle. Several criteria were used to discard trees that would cause NA values in the features. For example, trees that were severely defoliated were not considered. Furthermore, only trees taller than 10 m were selected, because below this threshold, the number of NA increases progressively as the trees become shorter. Selected trees were sufficiently well scanned from at least two flight lines in order to allow computation of all features in all three channels of these flight lines. This selection is intended as to reduce the probability of outliers (e.g. tree height, stress) affecting only a specific scan angle class, because of being scanned by a single flight line.

Tree views located at the extremity of the scan swath (that had a mean scan angle larger than ± 14° in C2) were discarded. The main reason for this choice was that returns near the end of scan lines of an oscillating mirror, here 15°, have a less precise geolocation and are less evenly distributed. They are closer together at the end of scan line when the oscillating mirror slows before reaccelerating in the opposite direction. What is more, the space between scan lines is greater at wider scan angles, leaving bigger gaps. Common practice is therefore to eliminate returns at the extremities of scan lines. However, in order to avoid computing features from point clouds that would be cut in the middle of tree views (i.e., in the middle of a tree crown) at the 14° scan angle threshold, we have retained all tree views that had a mean scan angle of 14° in C2 or less, but kept the returns therein having a scan angle above 14° if any. From a total of 37,063 candidate trees that had been manually delineated (Budei and St-Onge 2018), 13,325 trees were selected because they met all the above criteria. This resulted in 27,922 tree views that were used for computing the correlation between feature values and mean scan angle, and for the RF classification. The distributions of the mean scan angle of the tree views by channel are different for each species (

Figure 4.3). We pay attention to have a minimum of 30 tree views in each mean scan angle class and apply a balanced RF algorithm to compensate for the difference in sample size for different species.

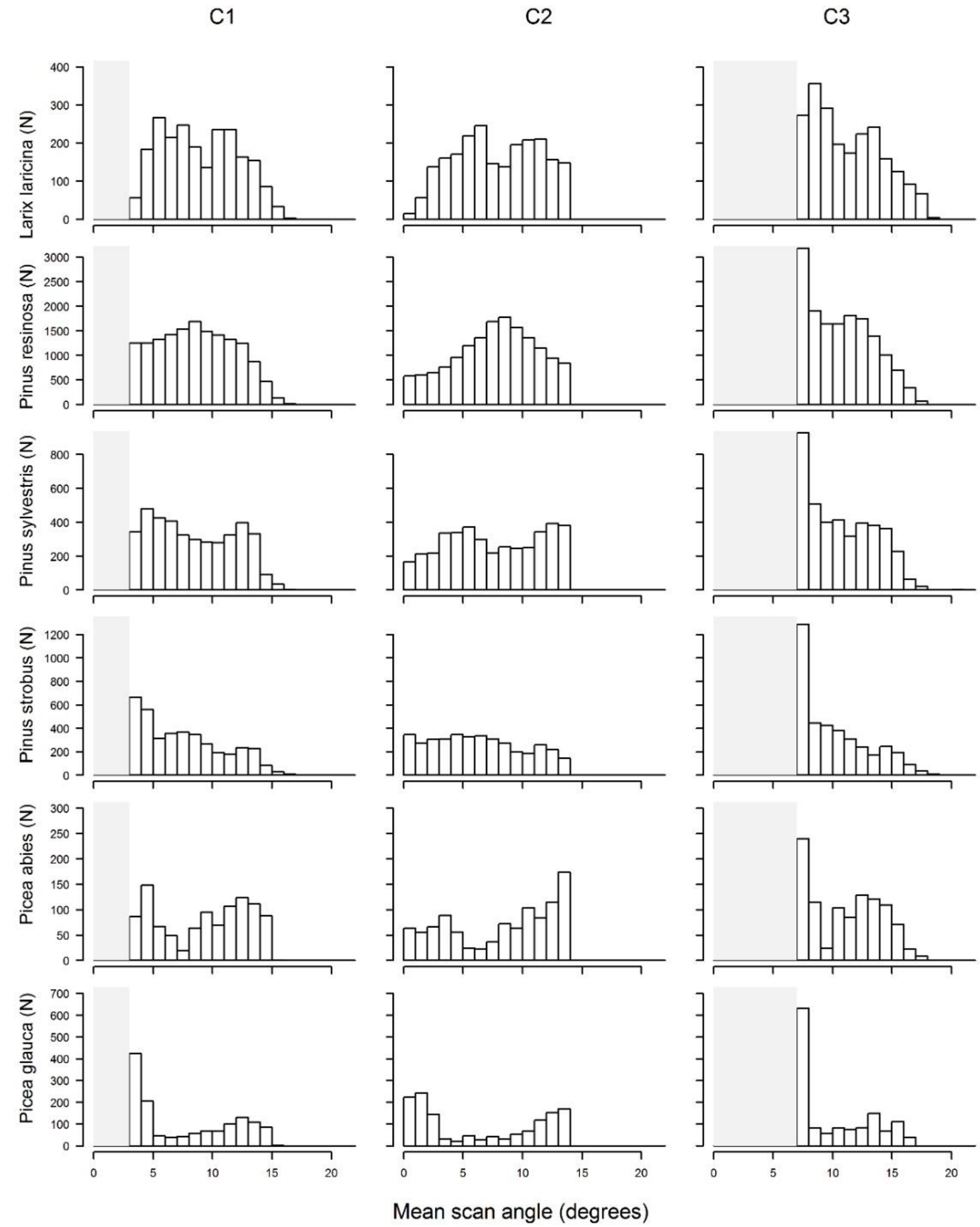

Figure 4.3: Distributions of mean scan angle of the tree views by channels (C1, C2 and C3) and species. The gray areas represent mean scan angles not achievable in the respective channel due to the Titan system's configuration.

4.2.6 Feature correlation to mean scan angle

Each feature was computed from a specific combination of point clouds seen with different geometries. For this reason, different mean scan angles were considered for each tree view, depending on the specific combination of point clouds extracted from different channels (C1, C2, C3, C321, C1_C2, C2_C3, and C1_C3), specific to each feature. The last three combinations of two channels were calculated to study the effect on multi-channel features such as channel ratios or normalized indices. These additional mean scan angles were necessary to calculate the correlation between feature values and the corresponding mean scan angle. Mean scan angle always took into account all return types of concerned channels. This was used also for features computed from first or single returns. These computed means were then used to calculate coefficients of correlations or to divide tree views into groups to balance classification samples, and to compare the resulting accuracy.

For single channel features, the mean scan angle value of a tree view was computed using the absolute scan angle value of all returns in that channel. For features constructed as channel ratios or NDVIs, the mean scan angle was first computed for each channel's point cloud and then the overall mean was calculated using:

$$m\_ang_l = \frac{\left|mean\left(ang_{C_1}\right)\right| + \left|mean\left(ang_{C_2}\right)\right|}{2} \qquad \textit{Eq. 4.3}$$

where m_ang_l is the absolute mean angle of points in flight line l; ang_{C1} and ang_{C2} are the return scan angles of the point cloud of a tree, respectively for the first and second channel of a ratio feature.

Boxplots of 3D features and intensity features calculated for each channel and species were used to compare feature variations with mean scan angle.

4.2.7 RF classification

Trees were first divided into three classes based on the corresponding mean scan angle presented in Table 4.1. This allowed determining if mean scan angle has any effect in species classification (objective *iii*) for each evaluated feature combination. The model was trained with a balanced sample according to each species – scan angle class combination, in order to avoid bias in the RF classification. The same value was used for the *nsize* parameter of the *rf* function from *randomForest* R library (Liaw and Wiener 2002). This value was equal to 20 for all classifications, which was somewhat less than the smallest tree view group of species – scan angle class. This choice lowers the accuracy results for all classifications, compared to using the minimum *nsize* for each specific RF classification set, but ensures that differences between classification accuracies did not come from a difference of *nsize* parameter. However, the main objective of these classifications was not to compare performance between different types of features or channels used, but to see if there were differences in results as a function of the three scan angle classes within the same RF classification model.

A particular attention was paid to the mean scan angle class limits to allow having an acceptable minimum *nsize* value in each group of species – scan angle class. There is not a perfect correspondence of mean scan angle in C1 and C3 compared to C2. On the contrary, the large variation can be seen from Figure 4.4 that compares the mean scan angles in C1 and C3 to the mean scan angles in C2. The last are represented in increasing order. Because of this large variation, the use of the mean scan angles calculated only from C2 is not adequate to split classes of tree views for the purpose of RF classification when only features from C1 or C3 channel are used. Therefore, different scan angle class delimitations were defined for each channel, or combination of channels, according to feature selection used in each classification. Also, we observed that linearly dividing the range of mean scan angle in each channel did not ensure a sufficient minimum number of trees in each group of species – scan angle class, for an acceptable *nsize* value. For C2, scan angle class limits were set to cover the range of mean scan angle values with equal class intervals: 0-5, 5-10 and 10-15 degrees. For the other channels, the values of mean scan angles were not evenly distributed, so the class limits were calculated as the equivalent of the class limits in C2, according to Eq. 4.2. The rounded value to nearest integer of class limit was used. Some minor adjustments were also done in order to ensure that a sufficient number of trees in each group was attained. The class limit was set as the mean of the class limits in the concerned channels for the feature sets that use two or three channels. For example, for 3D features computed from returns from all the three channels (C321), the first mean scan angle class limit was the mean of the first class limit in C1, C2 and C3 respectively. For NDIR features, mean scan angle class limits were calculated as the mean scan angle class limit in C1 and C2. All limits of the scan angle classes are presented in Table 4.1.

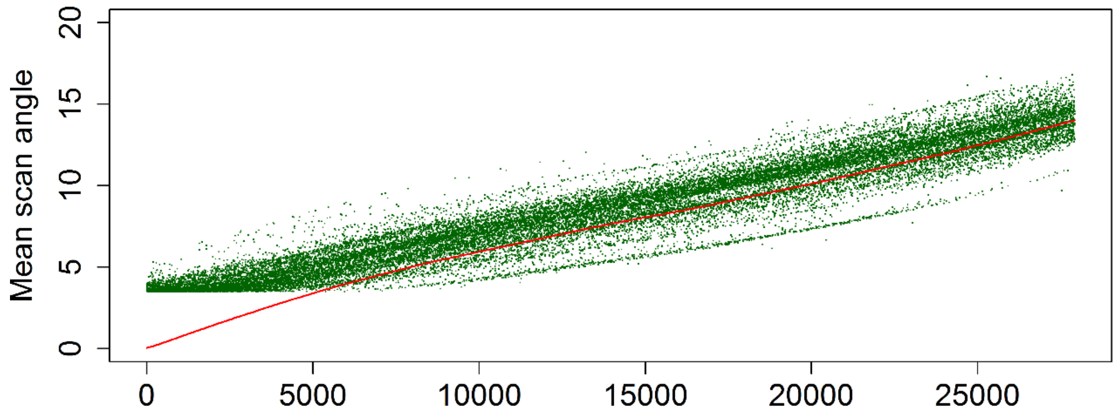

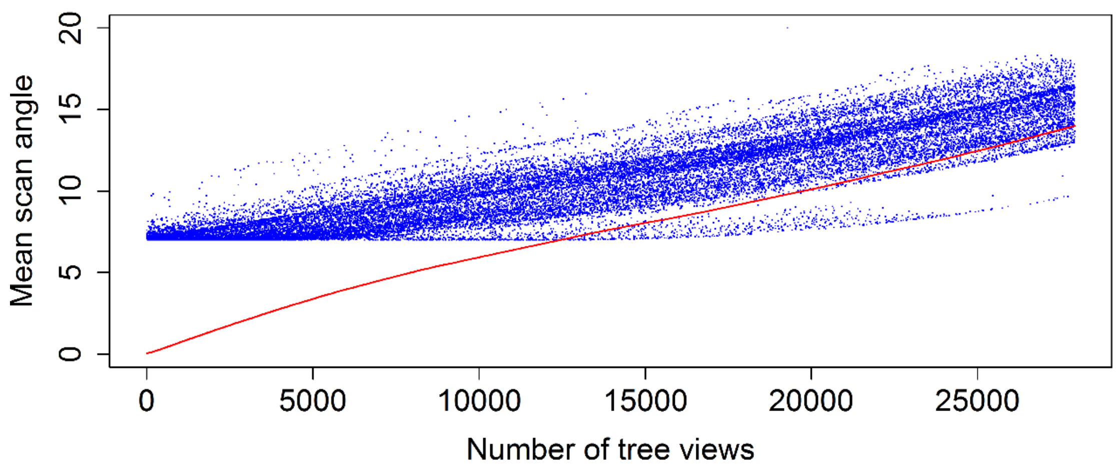

Figure 4.4: Difference in mean scan angle between C1 (green points), C3 (blue points) and C2 (red points) for the same tree view. Mean scan angles in C2 were increasingly ordered.

RF classifications were run for each individual channel and run separately for 3D features and for intensity features (raw and normalized), as well as with the combined 3D and intensity features. First, for each of these RF classifications, the model was trained once with all tree views. The out-of-bag accuracy was reported for the overall accuracy, when all tree views were used. The accuracy for each of the scan angle class was then calculated separately, by comparing the individual tree species predictions to the known species. The accuracy in each scan angle class of RF trained with different types of features were not completely comparable, as the number of trees in each scan angle class used to train the model was different depending on the channel.

Table 4.1: Tree views mean scan angle statistics in each channel and corresponding scan angle class limits used in the balanced RF classification (all units are degrees).

Channels	Min	Mean	Max	Class 1	Class 2	Class 3
C1	3.50	8.3	16.80	3-6	6-11	11-17
C2	0.02	7.17	13.00	0-5	5-10	10-15
C3	7.00	10.56	20.01	7-9	9-12	12-20
C321	2.12	8.48	16.53	2-7	7-11	11-17
C1-C2	1.78	7.69	15.38	1-5	5-10	10-16
C1-C3	5.25	9.36	17.20	5-8	8-12	12-18
C2-C3	3.53	8.83	16.16	3-7	7-11	11-17

4.3 Results

4.3.1 Feature correlation to scan angle

Results generally show a weak influence of the mean scan angle on feature values, but also showed large feature values variability with scan angle. Correlations between feature values and mean scan angle, as expressed by Pearson's r were generally less than $|\pm 0.2|$, with the largest correlation being 0.55. Figure 4.5 provides an example of the variability of a 3D feature, the 75th percentile value of the slope between the highest point in the crown and the other first returns (3D_SL_1st_p75), with viewing angle.

Similarly, Figure 4.6 allows appreciating typical variability of an intensity feature with viewing angle, namely the 95th percentile of intensity of the first returns (I_PE_1st_p95).

The correlation between feature values with mean scan angle, calculated for all trees and by species, is presented in three tables for 3D features (Table B.1), for raw and normalized intensities (Tables B.2 and B.3). The last column counts the occurrences when the correlation exceeds |±0.2| in the individual species columns. This information identifies features that are generally influenced by mean scan angle, affecting several species (*objective i*). The last row reported the number of features for which the correlations exceeds |±0.2| for each species. This information identifies the species for which features were more sensitive to mean scan angle (objective *iii*).

The most sensitive 3D features to scan angle were identified with correlations values above |±0.2| in Table B.1. The features characterising the crown shape, as the standard deviation of slope (SL) between the highest return and the other returns (e.g., 3D_SL_1st_sd_C1) were among the most correlated. The species with the highest number of correlations above 0.2 for SL features was *Larix laricina*. For the features based on ratios of return numbers (RP, e.g., #single returns / #1st returns, 3D_RP_si_1st_C3), the highest correlations were obtained for *Picea abies*, especially in C3, up to 0.55. Even if correlations of percentiles of return heights with mean scan angle are very low, some trends could be discerned. First, the percentile shift is not the same for all species. There is a downward shift for all height percentiles for *Picea abies*, generally an upward shift for *Pinus strobus*, an upward shift for *Pinus resinosa* except percentiles from single returns, and variable shift for *Pinus sylvestris* and *Larix laricina*, with upward for higher percentiles and downward for lower percentiles.

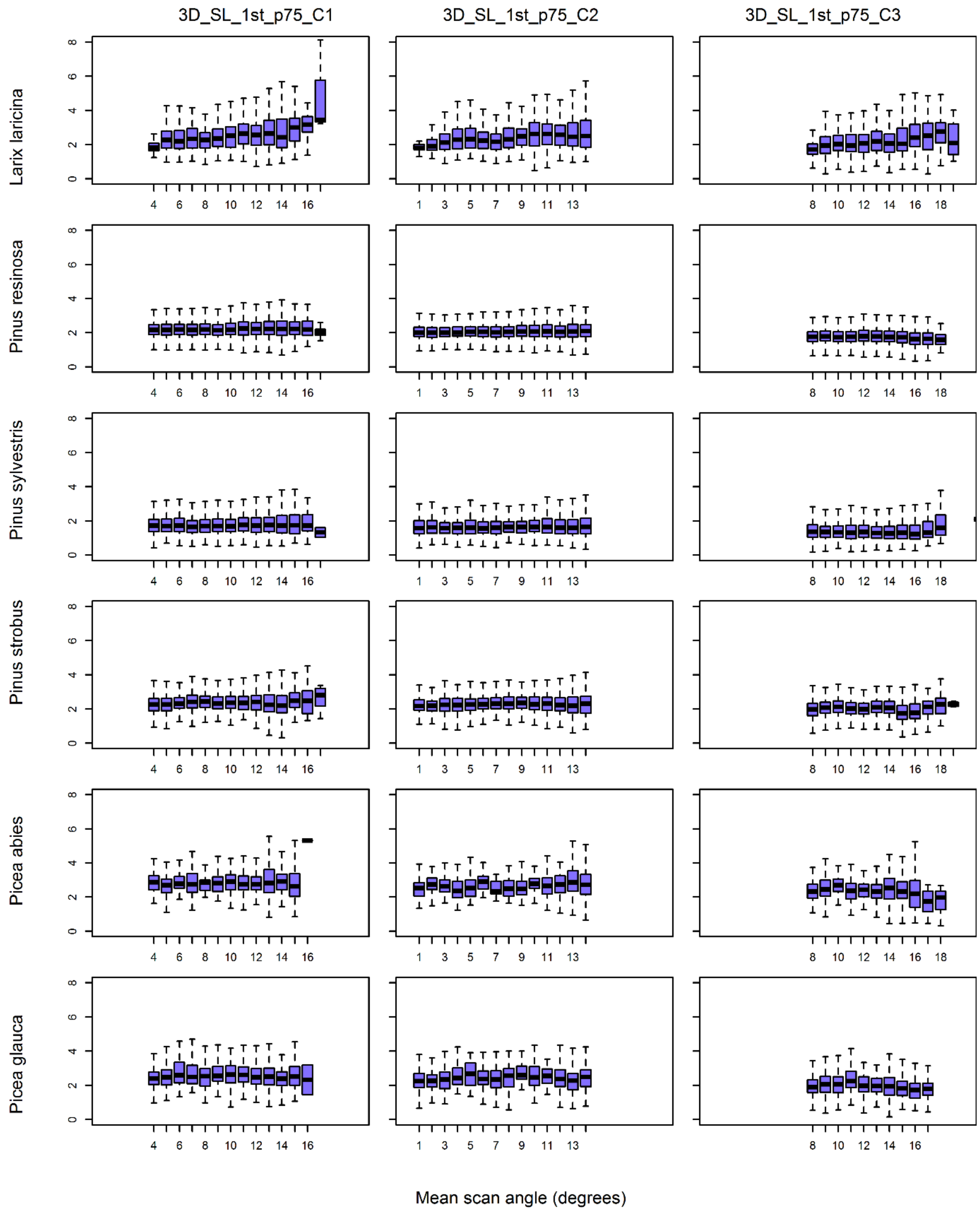

Figure 4.5: Variations of the feature 3D_SL_1st_p75 (75th percentile of the slope of the first returns in each of the three channels) according to scan angle, and per species.

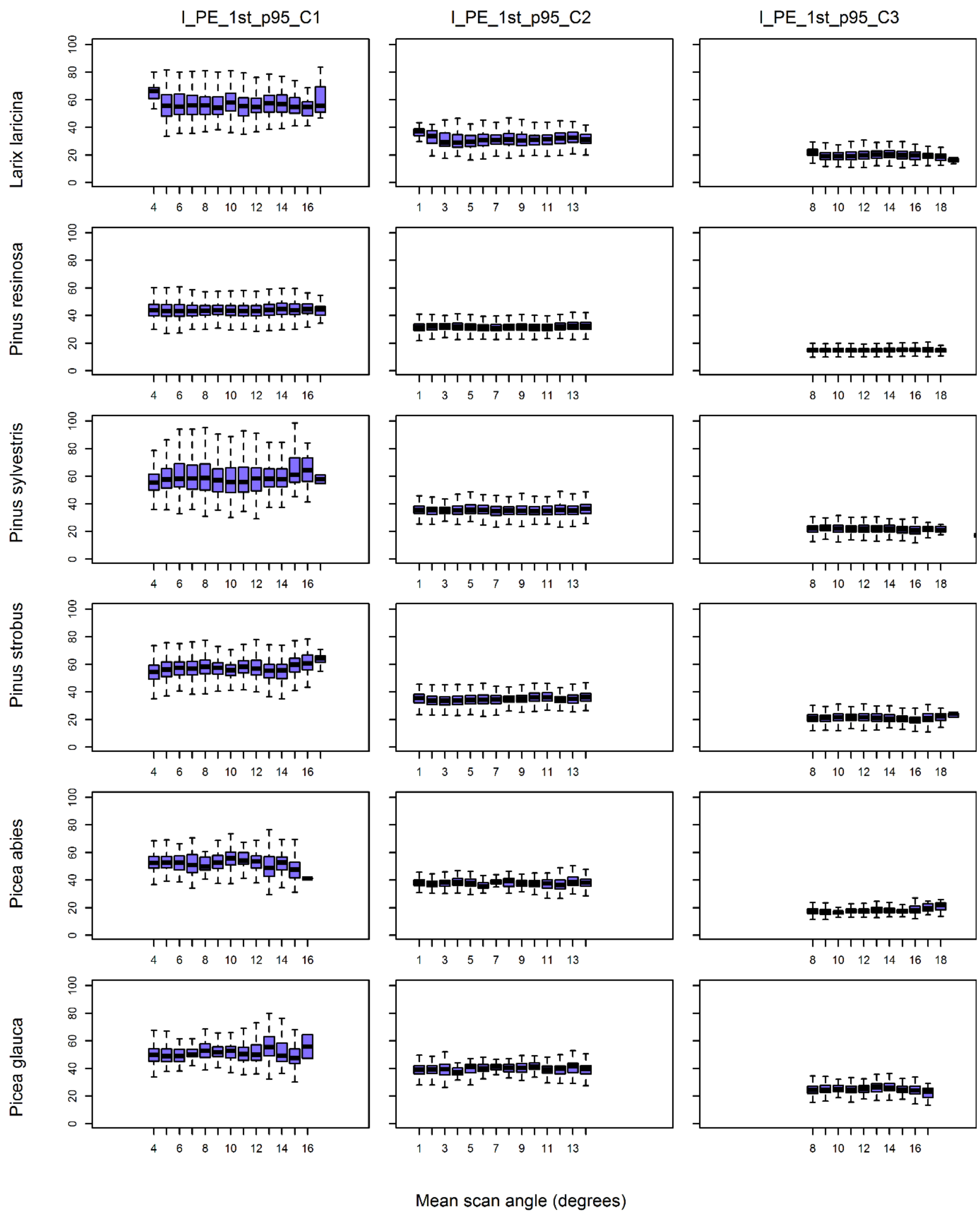

Figure 4.6: Variations of the feature I_PE_1st_p95 (95th percentile of the normalized intensity of the first returns in each of the three channels) according to scan angle, and per species.

The raw intensity features were the most correlated with mean scan angle and it affected three species, namely *Picea abies*, *Picea glauca* and *Pinus sylvestris* (Table B.2). These intensity features that stand out were the intensity percentiles (PE), the normalized mean intensities (MI) and the dispersion of intensities (DI). The intensity features values decreased in intensity with mean scan angle, therefore leading to a negative correlation. The intensity normalization reduced feature correlation to mean scan angle, but species were not affected evenly. Only intensity features for one species, *Picea abies*, remain correlated to mean scan angle (Table B.3). Intensity normalization for range changed the values of the intensity features calculated on single channels, and slightly decreased their variability as well as their correlation with mean scan angle. See Figure 4.7 for an example of the variation of an intensity feature calculated on single channels before and after normalization. On the contrary, intensity features based on channel ratios (RM), normalized indices (NDG1, NDG2, NDIR) or features describing dispersion (DI properties, like coefficient of variation, skewness or kurtosis), were not affected by intensity normalization. Figure 4.8 provides an example of raw and normalized values from 90th percentiles of first returns for the three normalized vegetation indices as a function of scan angle. We observed a decrease in variability of intensity features with increasing scan angles. This could be observed from the negative values in intensity dispersion features (DI), with the larger negative values for *Picea abies* for both raw and normalized intensities. The intensity features in C3 had lower values and also lower variability compared to intensity features in C1 and C2. For example see the 95e intensity percentile in the three channels in Figure 4.6. Regardless, these observations do not allow to isolate the scan angle effect from the wavelength and divergence differences between channels. The extended results on the correlation of each individual feature, presented in Table B.2 for raw intensities and Table B.3 for normalized intensities, are summarized in Table 4.2. For Tables 4.2 and 4.3, the percentage of cases having $r > |\pm 0.2|$ was calculated:

$$\mathrm{Np} = \frac{\mathrm{Nr} * 100}{\mathrm{Nf} * \mathrm{Ns}} \qquad \text{Eq. 4.4}$$

where *Nr* = number of cases having r > |±0.2|, *Nf* = number of features and *Ns* = number of species. Table 4.2 presents the reduction of correlation brought about by intensity normalization (*objective ii*). We see that the number of cases having a correlation > |±0.2| is reduced by more than half from 15.19%, to 6.02%, by applying the intensity normalization.

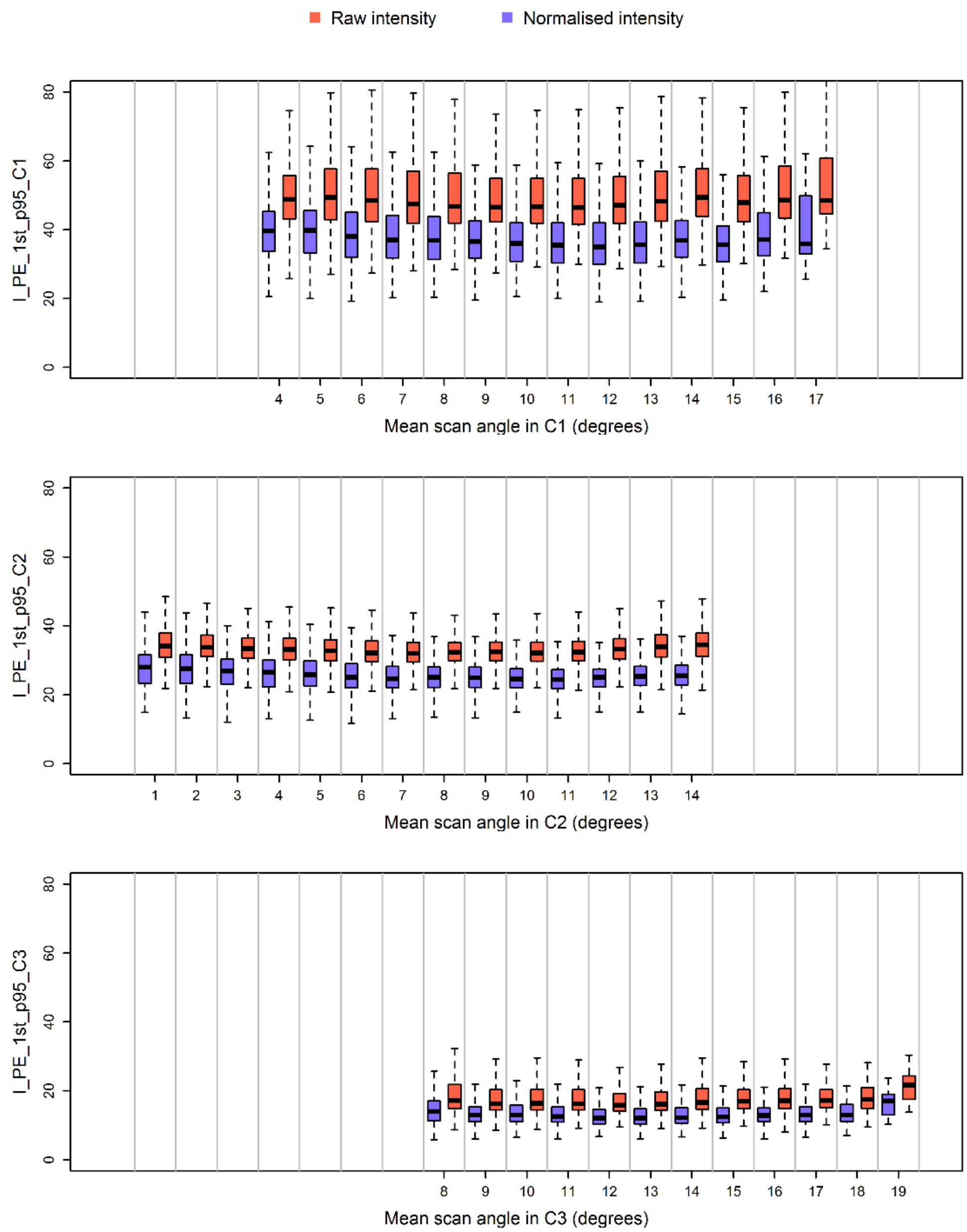

Figure 4.7: Raw and normalized values for the 95th percentile of intensity in the three channels as a function of mean scan angle.

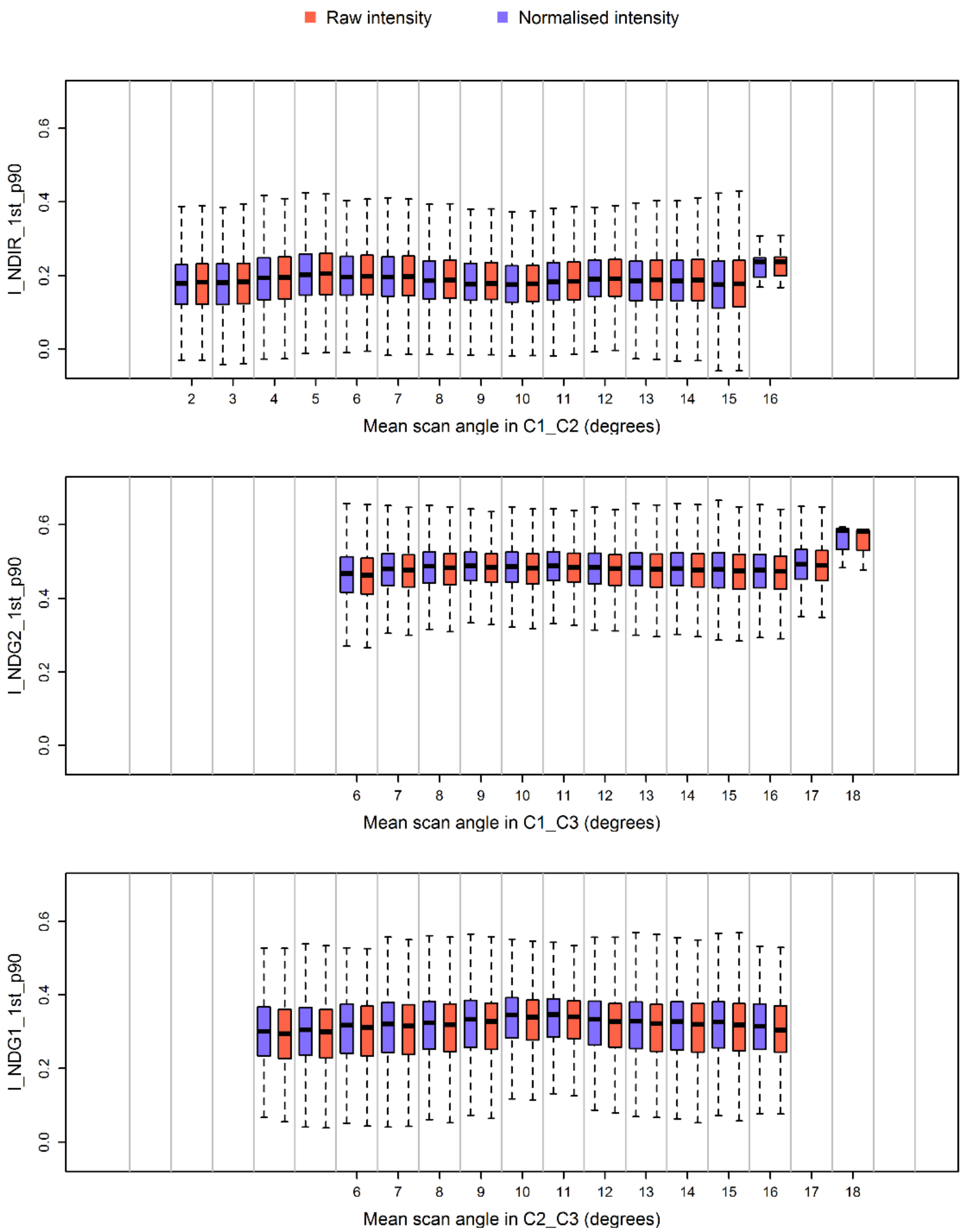

Figure 4.8 : Raw and normalized values from 90th percentiles of first returns for the three normalized vegetation indices as a function of mean scan angle.

Table 4.2: Number and percentage of cases having a correlation (*r*) greater than |±0.2| between mean scan angle and features.

Feature type	Number of features	Number of cases having r > |±0.2|	Percent cases having r > |±0.2|
3D	192	84	7.29%
Raw intensity	249	227	15.19%
Normalized intensity	249	90	6.02%

A summary of correlations between feature values and mean scan angle by species is presented in Table 4.3, based on the detailed results reported in Tables B.1 to B.3. The species for which the 3D features varied most with scan angle were *Larix laricina* and *Picea abies*, while the species for which the raw intensity features varied most with scan angle were *Picea abies*, *Picea glauca* and *Pinus sylvestris*. The species which showed a large reduction in the number of correlated intensity features after normalization were *Pinus sylvestris* and *Picea glauca*. After intensity normalization, only one species, *Picea abies*, still present more than two correlations above 0.2 between intensity features and mean scan angle. (see Table 4.2). This species has a different behaviour since there are some features for which correlation slightly increases after normalization, mainly lower intensity percentiles (5^{th}, 10^{th}, 25^{th}) and features calculated as normalized mean intensity (MI), see Tables B.2 and B.3 :

Table 4.3: Number and percentage of cases having a correlation (*r*) greater than |±0.2| between mean scan angle and feature values, by species.

	Number of cases having r > |±0.2|			Percent cases having r > |±0.2|		
Species	**3D**	**Raw intensity**	**Normalized intensity**	**3D**	**Raw intensity**	**Normalized intensity**
All	5	0	0	2.60%	0.00%	0.00%
Pinus resinosa	11	0	0	5.73%	0.00%	0.00%
Pinus strobus	9	0	0	4.69%	0.00%	0.00%
Pinus sylvestris	2	56	0	1.04%	22.49%	0.00%
Picea abies	21	88	89	10.94%	35.34%	35.74%
Picea glauca	12	83	1	6.25%	33.33%	0.40%
Larix laricina	29	0	0	15.10%	0.00%	0.00%

Table 4.4 compared the percentage of features that have correlations above |±0.2| with scan angle, depending on return type considered (all, 1st or single returns) and species. Only features that have been calculated for all these three return types category were considered. We observed that in addition to the general decrease in percentage of correlation between raw and normalized intensity features, the trends between features types were different. For raw intensity, the most correlated were the single return features and the least correlated were the all return features. The opposite was observed for the normalized intensity features. This is due to a single species, *Picea abies*, which presents an increase in correlation for first and all returns after normalization.

Table 4.4: Percent of features with a correlation (r) greater than $|\pm0.2|$ between mean scan angle and feature values, by return type and by species.

Intenisty features	**Return type**	**Pinus resinosa**	**Pinus strobus**	**Pinus sylvestris**	**Picea abies**	**Picea glauca**	**Larix laricina**	**All species**
Raw	all	0.00	0.00	19.51	32.93	29.27	0.00	13.62
	1st	0.00	0.00	20.73	34.15	30.49	0.00	14.23
	si	0.00	0.00	28.05	36.59	36.59	0.00	16.87
Normalized	all	0.00	0.00	0.00	53.66	0.00	0.00	8.94
	1st	0.00	0.00	0.00	40.24	0.00	0.00	6.71
	si	0.00	0.00	0.00	10.98	1.22	0.00	2.03

4.3.2 Classification accuracy

The overall accuracies and the accuracies for each of the scan angle classes are presented in Figure 4.9. The accuracies are given for different selections of features, depending on their type (3D or intensity), intensity normalization or number of channels. The numerical values of classification accuracies are provided in Figure 4.9 and in Table B.4. The changes in classification accuracy were small between scan angle classes. Generally, there was no clear or systematic decrease in classification accuracies with increasing scan angle (*objective iv*). The middle scan angle class gives sometimes slightly better results than the others. Even if the classification accuracies for individual feature groups might be low, the main interest here is to understand how classification accuracy in each feature group may vary with scan angle class and consequently may influence the overall accuracy (all scan angle classes and/or all features). The number of tree views in a class vary according to features used in classification. However, even if classification accuracies may be influenced by the variation in number of tree views in each class, we consider that the large number of tree views in each scan angle class may allow a comparisons between corresponding scan angle classes, without significant error.

In the case of classifications using only single channel 3D features, there was a difference between accuracy variations between the scan angle classes of the three channels. There is not a systematic decrease in accuracy from the first class to the third class. The exceptions concern the second class in C2, the third class in C3 and the second class in C321. The accuracy in the first scan angle class was very similar between channels: it varied by only 1%. However, the accuracy varied by 6% for the two other scan angle classes. Surprisingly, the best accuracy obtained from single channel 3D features was in C3, in the large scan angle class. The accuracy obtained from 3D features from C321 was generally a bit higher by 3-5% than the accuracy obtained from single channel 3D features, with the higher accuracy for the second class. In the case of intensity features, all the accuracies obtained with single channel normalized intensity were higher than their raw intensity counterpart, with an improvement between 5% and 10%. The accuracy of all two-channel combinations remained almost the same after normalization, ±1% (Table 4.5). In general, the accuracy of the second scan angle class was the highest. Conversely, the lowest accuracy was in the first scan angle class with raw intensities of C1 and C3. For almost all intensity features groups, the accuracy decreased from class 2 to class 3. Once the intensities were normalized, the lowest accuracy was seen in the 3rd scan angle class. When combining all features (3D plus intensity), the accuracies were the highest, even more so when the 3D features were combined to the normalized intensity. Accuracy variations with scan angle class was very weak (3%). Within this weak margin, the highest variations were recorded in the middle scan angle class.

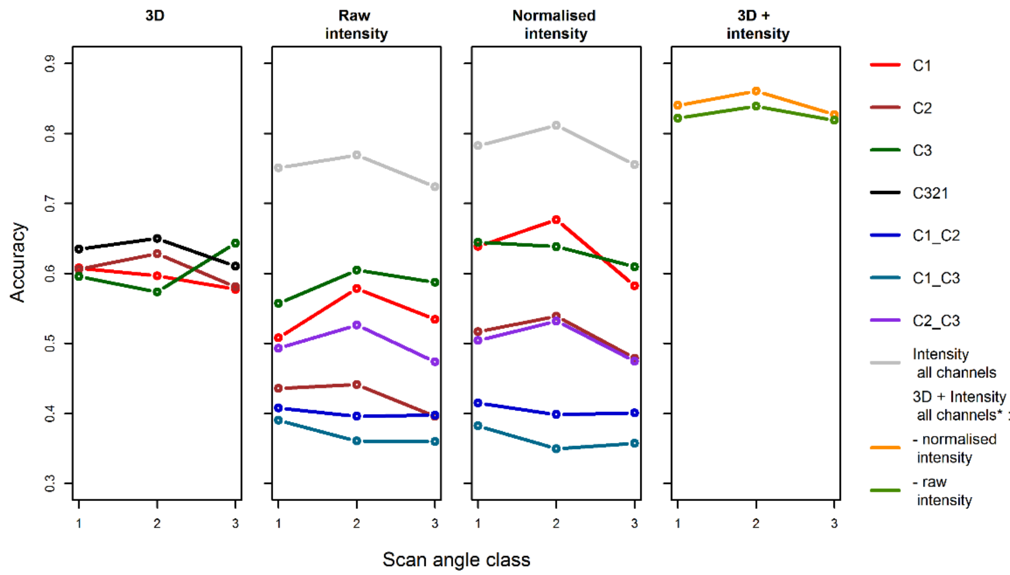

Figure 4.9: RF species identification accuracy by scan angle class. * Channels used in "3D+intensity" are C321 for 3D and C1, C2, C3, C1_C2, C1_C3, C2_C3 for intensity.

A summary of classification accuracy improvement after intensity normalisation is given in Table 4.5. The larger improvement was obtained for classifications using only single channel intensities, with a mean of 8%. It is highest for the first scan angle class (around 10%) and it decreases for the last class (around 5%). The accuracy improvement with the single channel intensities decreased according to proportion of features affected by intensity normalization (single channel features) compared to features that were not affected by intensity normalisation (channel ratios or 3D features) that were used in classification. For example, when adding the channel ratios and the normalized indices features, the overall improvement was half the mean of single channel improvement (4%). The overall improvement was even lower when 3D and intensity features were used together (2%).

Table 4.5: Improvement in accuracy between classifications using normalized intensity features compared to classifications using raw intensity features. Results are presented as overall (2nd column) and by mean scan angle class (columns 3 to 5), for classifications with different feature selection (rows).

Features	**Overall accuracy improvement**	**Accuracy improvement in class angle 1**	**Accuracy improvement in class angle 2**	**Accuracy improvement in class angle 3**
C1	0.10	0.13	0.10	0.05
C2	0.09	0.08	0.10	0.08
C3	0.06	0.08	0.04	0.02
Mean single chanel	*0.08*	*0.10*	*0.08*	*0.05*
C1-C2	0.00	0.01	0.00	0.00
C1-C3	0.00	-0.01	-0.01	0.00
C2-C3	0.01	0.01	0.00	0.00
Mean chanel ratios	*0.00*	*0.00*	*0.00*	*0.00*
all intensity	0.04	0.03	0.04	0.04
3D+intensity	0.02	0.02	0.02	0.01

4.4 Discussion

This study highlights that for net scan angles between 0° and 20°, and for a study area with low topographic variation, the correlation between individual tree feature values and scan angle was low, (<|±0.2|) (*objective i*). The general trends of correlations of individual tree feature values with scan angle were on the same order of magnitude as those reported in the literature for plot level features, such as mean tree height, canopy cover or gap fraction (Næsset 1997, Holmgren, Nilsson et al. 2003, Morsdorf, Frey et al. 2008, Montaghi 2013, Liu, Skidmore et al. 2018). At the same time, the variability in individual tree feature values for a given species of tree measured from any one scan angle (see boxplots in Figures 4.5 to 4.8) was very large. It is thus expected that even larger values of scan angle (i.e., 20-30 degrees) would induce larger variations in the feature values. The inherently large feature variability dampens the ability to highlight relative effect of scan angle. A similar situation was observed for plot level features. For example, Morsdorf, Frey et al. (2008) found that there was not a significant difference between percent canopy cover at larger scan angles than at lower scan angles, because the standard deviations were larger than the differences. This large variability might be explained by other tree properties, tree growth environment or flight configuration that have a larger influence on feature values than scan angle. For example, see the influence of tree height on feature values in Budei and St-Onge (2018) or that of tree density in Holmgren, Nilsson and Olsson (2003b). The advantage of our study is the large number of sample trees and the similar tree growing conditions, because the majority of them were planted. These conditions should allow us to detect whether there is an effect of scan angle on feature values.

Our analysis highlighted several effects due to scan angles. The different upward or downward shifts in height percentile depending on tree species was in line with simulation studies e.g. Holmgren, Nilsson et al. (2003). For example, features calculated for species with an elongated tree crown length, (e.g. spruces) were more affected by scan angle than those calculated for species with shorter crown length and more compact crown width (e.g. pines) (*objective iii*). The features most affected by scan angle were those related to crown shape, return proportions and single channel intensity. The effect # 2 of scan angle (decrease in the number of returns per emitted pulse) explains the higher correlations of features such as return proportions (RP), because the number of second and third returns are reduced at larger scan angles. Also, features related to crown shape (SL and SU) are highly sensitive to return distribution in the crown, being equally influenced by scan angle effects #2 and #3 (change in the distribution of returns) (Table B.1). The single channel intensity features computed from first or single returns were related mainly to the effect #1 (intensity attenuation), compared to those computed from all returns, which are influenced equally by effects

#1 and #2. Thus range normalization had a larger efficiency in reducing correlation for intensity features from first and single returns, and less for features computed from all returns (Table 4.4). Okhrimenko, Coburn and Hopkinson (2019) explained how the reduction of number and intensity of second and third returns could influence intensity features computed from all return types.

The features least sensitive to scan angle were the normalized intensity indices and the channel ratios. The reason is likely that scan angle effects like intensity attenuation and changes in return proportions are compensated when calculating the ratio between channels. However, configuration differences between Titan channels must be accounted for when considering the ratios of channels and normalized indices. Usually, normalized indices are computed from two channels of the same image. This implies that each corresponding pixel registers reflectance from the same object, with the same viewing geometry and the same resolution, so that the difference comes only from the wavelength. Instead, the different viewing geometries between the three Titan channels does not allow us to isolate only difference coming from channel wavelengths. In each channel the signal is returned from a different height in the crown. This effect can be seen in the shift in height percentiles (Hopkinson *et al.* 2016). Each channel sees different parts of the same tree due to changing occlusion patterns. Moreover, the three channels have different resolutions, because beam divergence, and consequently the footprint, is larger for C3 than C1 and C2. The stability of the intensity features is important for tree species identification. We reached classification accuracy as high as 0.5 using only ratios and normalized indices (Table 4.5). The stability of channel ratios and normalized intensity indices at different flight heights was shown to have a similar but higher influence on return intensity and return proportions as did scan angle, because of the range variation. Okhrimenko and Hopkinson (2019) even suggested a method to evaluate the recommended flight height in order to obtain stable normalized indices. A similar recommendation for a maximum scan angle could be considered.

However, this does not seem necessary for scan angles lower than 20° and for needle-leaved species classification with RF.

Intensity normalization changed features values calculated from single channels, such as percentiles of intensity. However, intensity normalization did not significantly change the features values calculated as ratios of channels, normalized indices or dispersion characteristics. Normalization contributes to the improvement of classification accuracy, when using only individual channel intensity features, between 6% and 10% (Table B.4). However, we did not observe an improvement when using only features based on channel ratios or normalized indices. Instead we observed only a limited improvement (2%) when using all 3D and intensity features, since the accuracy was already high (0.83). The classification improvement according to intensity normalization depends on the percentage of features that are affected by intensity normalization. So, using a high percentage of feature that are not affected by intensity normalization (ratios, normalized indices or 3D features), can be considered as an alternative solution to circumvent normalization.

Two limitations remain unexplored in our study and need further assessment. The first limitation relates to exclusion of trees at large scan angles. One of the most important differences between studies on scan angle using the ABA compared to the individual tree level (ITC) is due to tree occlusions. For ABA studies, a general value can be attributed to the plot feature, even if not all trees are seen. However, for single trees, occlusions related to scan angle can lead to the impossibility of calculating all features for each tree. The uneven point spacing at swath end or a low return density (in this study a single flight line) may also lead to the impossibility to calculate all features. These effects concern especially small or suppressed trees. Such trees have to be discarded because RF classification does not allow for missing data. The impact of scan angle on the number of discarded trees was limited in this study by choosing only trees grater than 10 m in height. As a consequence, the real possibility of tree species identification may be overestimated by the classification accuracy at larger scan angles because of the discarded trees. This aspect is thus worth considering in future studies. The second limitation unexplored relates to the gradual importance of occlusion effects and interception with large scan angles, which in turn influences the variability and the correlation of feature values to scan angle. These effects would also be enhanced by greater variation in topography (Goodwin, Coops et al. 2007). For large scan angles, occlusions from taller trees or self-occlusion tends to generate lateral asymmetry of return distribution in the crown. However, our experimental design did not allow us to evaluate the amplitude of this effect previously highlighted at the plot level for canopy cover studies (Holmgren, Nilsson et al. 2003, Korhonen, Korpela et al. 2011, Arumäe and Lang 2018).

We tested intensity normalization applied for individual returns. Other types of corrections for scan angle have been proposed in the literature for ABA features values. However, it is not evident to apply such corrections for tree level feature values. Holmgren, Nilsson and Olsson (2003b) suggested that such corrections are difficult to perform because lidar feature values are influenced by the same forest characteristics (i.e., tree height, tree density and species) that we try to predict, therefore creating a circular problem.

Generally, there was not a large variation in classification accuracies between the three scan angle classes when all features (3D + intensity) used and for a survey that did not use scan angles greater than 20º. Of course, an extension of our study would be needed to verify the effect of larger scan angles (e.g., from 20º to 30º), or of much hillier terrain. Airplane flight lines are typically planned to overlap lidar scanning swath from at least two flight lines. Therefore, tree point clouds are usually composed of points from several scanning angles in order to reduce occlusions and to mitigate the scan angle effects.

4.5 Conclusion

This is the first study involving a large number of individual trees to assess the effects of scan angle on multispectral lidar features. The large number of trees sampled highlights subtle trends induced by scan angle. The correlation of individual tree features with scan angle between 0º and 20º was below 0.2, with a high variability (*objective i*). The intensity normalization reduced feature correlation to scan angle for single channel intensities, but did not change values for features like intensity ratios or normalised indices (*objective ii*). For species such as *Picea abies,* the scan angle effects were highest (*objective iii*). Classification accuracy varied between scan angle classes up to 10%. There was not a systematic decrease in identification accuracy from nadir to higher scan angle classes. The best accuracy for classification using all features was obtained in the second scan angle class (between 5 and 10 degrees) (*objective iv*). The largest improvement in classification accuracy after intensity normalisation was obtained using only single channel intensity features. This improvement is less important when features non affected by intensity normalisation were also used.

4.1 Acknowledgements

We express our thanks to Teledyne Optech Incorporated (Vaughan, Canada) for graciously providing the Titan MSL datasets used in this study. We thank the authorities of the York Regional Forest (namely Kevin Reese) for granting permission and facilitating access to the forest's study area. We acknowledge the collaboration of CarboMap (Edinburgh, Scotland) in field logistics and data collection. Finally, we acknowledge Chris Hopkinson for providing us field measurements. This study was partly funded by the National Sciences and Engineering Research Council of Canada, through the AWARE project.

CHAPITRE 5

CONCLUSION

L'objectif principal de la thèse était d'évaluer l'exactitude de l'identification des espèces d'arbres en utilisant un balayeur lidar aéroporté multispectral, le Titan de Teledyne Optech. Les objectifs spécifiques étaient d'évaluer l'amélioration que le lidar multispectral apporte par rapport à un lidar monospectral (1) et d'évaluer l'influence des caractéristiques de l'arbre, comme la hauteur (2), ou des paramètres de l'enregistrement, comme l'angle de balayage (3), sur l'exactitude de l'identification de l'espèce d'arbres.

Dans ce chapitre nous allons faire une synthèse des principaux acquis méthodologiques à partir de l'ensemble des trois chapitres précédents. Premièrement, nous allons mettre en évidence certains aspects méthodologiques concernant les défis et les limites de l'identification des espèces d'arbres individuels par lidar multispectral. En ce sens, nous mentionnons d'abord les facteurs qui influencent la possibilité de l'application de cette méthode, notamment les facteurs qui influencent la possibilité du calcul de l'ensemble des variables utilisées dans l'identification de l'espèce de chaque arbre. Ensuite, nous mentionnons les facteurs qui influencent les valeurs des variables et influencent, en conséquence, l'exactitude de l'identification. Finalement, nous mentionnons les paramètres du classificateur *random forest* qui influencent directement l'exactitude de l'identification. Deuxièmement, nous allons revoir les principales conclusions à retenir concernant l'application de cette méthode. Troisièmement, nous allons revoir les principales perspectives dans l'identification de l'espèce par arbre individuel en comparant l'application du lidar multispectral avec d'autres méthodes utilisées présentement en télédétection.

5.1 Défis et limites méthodologique de l'identification des espèces d'arbres par lidar multispectral

De multiples facteurs influencent l'exactitude de l'identification de l'espèce. Ces facteurs sont présents à toutes les étapes méthodologiques, depuis l'enregistrement des données jusqu'à l'évaluation de l'exactitude de l'identification, en passant par l'extraction du nuage de points par arbre, la définition des variables 3D et d'intensité et l'identification des espèces par un algorithme de classification. Ces facteurs peuvent affecter la possibilité du calcul des variables, générant ainsi des non applicables (NA), la valeur des variables, ou impacter la performance du classificateur. Plusieurs essais ont été réalisés dans cette thèse pour trouver les meilleurs paramètres qui permettent de garder le plus grand nombre d'arbres dans le processus d'identification. Les exactitudes de l'identification des espèces varient beaucoup en fonction de ces choix de paramètres. Plusieurs questions corollaires ont été soulevées durant ce processus, concernant notamment la taille minimale des arbres que nous pouvons classifier, le nombre minimal de retours dans un nuage pour calculer chaque variable et le degré de signification des variables calculées à partir de petits nuages de points.

5.1.1 Facteurs qui influencent l'applicabilité de la méthode ou la possibilité de calcul des variables

Nous avons accordé une attention particulière aux NA, parce que le plus souvent les exactitudes rapportées pour l'identification des espèces ne tiennent pas compte des arbres pour lesquels il y a des variables qui ne peuvent pas être calculées. Pourtant, si les arbres exclus étaient considérés dans le pourcentage d'arbre pour lesquelles l'espèce n'a pas été identifiée correctement, le taux de réussite serait revu à la baisse (par exemple 88% contre 76% pour une classification standard, Table 3.6). Une comparaison entre l'exactitude obtenue en tenant compte ou en excluant les NA a été réalisée dans le Chapitre III (qui traite spécialement l'influence de la hauteur de l'arbre sur l'exactitude de l'identification de l'espèce). Les petits arbres sont plus sujets à être exclus de la classification (par exemple environ 40% pour les petits arbres de 2-5m, 25% pour 20-25m et 0% pour le 25-35m, Figure 3.12). Cela génère un biais du taux de réussite de l'identification en fonction de la hauteur de l'arbre. Dans les deux autres chapitres, les exactitudes rapportées ne prennent pas en compte les arbres pour lesquels il n'a pas été possible de calculer toutes les variables, ce qui augmente légèrement le taux réel d'identification. Dans ce cas, nous avons choisi le meilleur compromis entre a) l'élimination des arbres pour lesquels il y a au moins une variable qui ne peut pas être calculée ou b) l'élimination des variables qui ne peuvent pas être calculées pour tous les arbres, afin de garder le plus grand nombre d'arbres.

Le calcul de toutes les variables suppose qu' un nombre suffisant de retours de chaque type est disponible (tous les retours, premiers retours, retours uniques ou deuxièmes retours). Plusieurs facteurs peuvent influencer la possibilité du calcul d'une variable en limitant le nombre de retours dans le nuage de points correspondant à une couronne d'arbre. Dans ce sens, nous pouvons rappeler trois sources concernant 1) les caractéristiques de l'arbre comme la hauteur, 2) les paramètres d'enregistrement comme la densité de points ou l'angle de balayage, 3) les paramètres méthodologiques concernant le seuil choisi pour éliminer les retours au sol, le type de retours utilisé dans le calcul des variables ou le degré de complexité des variables, nécessitant un nombre minimal de retours.

1) Parmi les caractéristiques de l'arbre, la hauteur a une influence significative sur le nombre de NA, notamment sur la probabilité d'avoir un nombre suffisant de retours de chaque type. Le nombre de retours par impulsion est influencé par la hauteur de l'arbre (par exemple distance suffisante pour enregistrer un deuxième retour dans la couronne), mais aussi par l'espèce (type d'aiguilles et arrangement des branches). La sélection d'arbres en fonction de leur hauteur minimale influence largement l'exactitude de l'identification. Différentes limites de hauteur minimale de l'arbre ont été appliquées dans cette étude, adaptée aux objectifs spécifiques, par exemple une limite base de 2 m dans le Chapitre III pour étudier la possibilité d'identifier l'espèce des petits arbres, une limite modérée de 5 m dans le Chapitre II, pour une évaluation générale, et une limite plus élevée de 10 m dans le Chapitre IV, pour réduire l'influence relative de la hauteur de l'arbre par rapport à celle de l'angle de balayage.

2) Parmi les paramètres d'enregistrement, la densité de points a une influence majeure sur le nombre de NA. Les variables calculées aux Chapitres II et III utilisent une densité de points plus élevée en prenant en compte toutes les lignes de vol. En revanche, les variables calculées pour le Chapitre IV utilisent une densité de points moins élevée, parce qu'elles sont calculées à partir d'une seule ligne de vol. Par conséquent, davantage de variables sont susceptibles de produire des NA. L'utilisation d'une limite plus élevée de hauteur minimale de l'arbre (10 m dans ce chapitre) répond aussi à cette plus faible densité de points.

3) Parmi les paramètres méthodologiques, le choix du seuil (*threshold*) utilisé pour éliminer les retours au sol et sur la végétation basse a une influence particulière sur le nombre de NA, parce qu'il réduit le nombre de retours disponibles pour le calcul des

variables. Il affecte de manière significative les nuages de points correspondant aux petits arbres. Pour cette raison, une attention particulière a été accordée à ce sujet dans le Chapitre III. Un des tests pour choisir le type et la valeur optimale du seuil a été de réduire le nombre de NA. Dans le Chapitre II, nous avons utilisé un seuil à hauteur fixe de 2 m, souvent utilisé dans la pratique. Pour les Chapitres III et IV, le seuil retenu a été de 40% par rapport à la hauteur de l'arbre, ce qui permet de conserver une partie importante des nuages de points des petits arbres contrairement à ce qui arrive quand on emploie un seuil à hauteur fixe.

Certaines variables sont plus susceptibles à générer des NA, parce qu'elles sont calculées à partir de types de retours qui forment des nuages de points plus réduits, comme les retours uniques ou les deuxièmes retours, par rapport à d'autres sélections comme tous les retours ou les premiers retours, qui représentent des nuages de points plus grands. De plus, certaines variables complexes nécessitent un nombre élevé de points, comme les variables représentant les caractéristiques de dispersion des retours (DI), comme le coefficient de variation, skewness ou kurtosis ou les variables évaluant la forme de la couronne (SU ou HR).

5.1.2 Facteurs qui influencent le résultat de l'identification par changement des valeurs des variables

Plusieurs facteurs qui influencent les valeurs des variables ont été évalués dans cette étude. Certains ont été étudiés de manière approfondie comme la hauteur de l'arbre et l'angle de balayage. D'autres ont fait plutôt l'objet d'étude pour le choix de certains paramètres méthodologiques, comme ceux concernant la délimitation du nuage de points ou la normalisation des valeurs de hauteur et d'intensité des retours.

Nous avons cherché à diminuer la variabilité intra espèce des variables en accordant une grande attention à la sélection des retours représentatifs de la couronne, en considérant la meilleure délimitation de la couronne, la meilleure estimation de la hauteur d'arbre, ainsi qu'un choix optimal du seuil de sélection des retours au sol. Pour la sélection des retours dans la couronne, les avantages du lidar multispectral par rapport à un lidar monospectral sont reliés principalement à la plus haute densité de points. Dans cette étude, une seule délimitation de la couronne et une seule estimation de la hauteur de l'arbre ont été réalisées à partir des données ayant la plus haute densité (tous les trois canaux et toutes les lignes de vol). Ces informations ont été utilisées pour extraire les points et pour normaliser la hauteur des points dans chacun des canaux individuels. Par ailleurs, certaines évaluations des exactitudes d'identification concernent des variables issues des nuages de points avec une densité plus faible, par exemple un seul canal (Chapitre II), ou une seule ligne de vol (Chapitre IV). Dans des conditions réelles d'application où juste un canal ou juste une ligne de vol seraient disponibles, une augmentation de l'erreur de délimitation de la couronne ou de l'erreur de l'estimation de la hauteur de l'arbre augmentera l'erreur de l'identification, en comparaison avec l'erreur obtenue dans cette étude. Le choix d'avoir ignoré cette partie de l'erreur pourrait limiter l'évaluation des avantages du lidar multispectral par rapport au lidar monospectral ou sous-évaluer les erreurs reliées aux occlusions causées par un angle de balayage en provenance d'une seule ligne de vol.

Une autre source d'erreurs qui devrait être considérée dans une application opérationnelle sur des surfaces étendues est celle reliée à l'utilisation d'une délimitation automatique des couronnes d'arbres. Elle n'a pas fait l'objet de cette étude et ce choix a été fait pour pouvoir isoler seulement les erreurs reliées à l'étape de l'identification de l'espèce et mieux mettre en évidence l'apport de l'information multispectrale dans cette étape. Le cumul des erreurs entre l'étape de délimitation et l'étape de l'identification devrait être évalué pour une application opérationnelle, car il risque d'être important. Dans un premier temps, nous avons isolé les couronnes d'arbres sur tout l'espace d'étude avec un algorithme de croissance de région utilisé dans St-Onge, Audet et Bégin (2015). Nous avons pu constater alors la très grande variabilité de l'exactitude de l'identification en fonction des erreurs de délimitation qui causent une altération significative des valeurs des variables.

5.1.3 Paramètres du classificateur *random forest* qui influencent l'exactitude de l'identification

Plusieurs paramètres du classificateur *random forest* influencent l'exactitude de l'identification, comme le nombre de classes, le nombre minimal des arbres dans une classe, le processus de sélection des variables, la distribution des échantillons par espèce (*random forest* équilibrée). Puisque nous avons utilisé une approche guidée par les données, ces paramètres doivent être adaptés pour chacune des classifications. Ils varient donc d'un chapitre à l'autre, en fonction des différentes versions de classification qui ont été comparées, notamment en fonction du canal (variables provenant d'un seul canal par rapport aux variables provenant des trois canaux, Chapitre II), différents choix de variables (en fonction de la corrélation avec la hauteur de l'arbre ou le nombre de NA, Chapitre III), en fonction de la hauteur de l'arbre (Chapitre III) ou de l'angle du balayage (Chapitre IV). Pour répondre à cette diversité de classifications, les paramètres de *random forest* ont dû être adaptés en fonction du nombre d'arbres par espèce (Chapitre II), par espèce et classe de hauteur (Chapitre III) et par espèce et classe d'angle de balayage (Chapitre IV). Un judicieux choix de limites de classes a été nécessaire pour permettre d'avoir un nombre suffisant d'arbres dans chaque classe de hauteur ou d'angle. Ce nombre détermine la valeur de *nsize* qui peut être utilisée, soit le nombre d'arbres utilisés pour entraîner le classificateur. Dans le cas d'un faible nombre, l'utilisation de tous les arbres d'une classe pour entraîner le classificateur pourrait produire du surapprentissage (Chapitre II).

Le *random forest* équilibré a été employé, donc le même nombre d'arbres par espèce et par classe a été considéré pour entraîner le classificateur et afin d'éviter un débalancement du succès d'identification, qui serait plus élevé préférentiellement pour l'espèce la plus fréquente. Si *random forest* équilibré pouvait être efficace dans les conditions où les espèces sont plutôt également représentées, il peut aussi créer une surévaluation dans le cas des espèces rares.

Le nombre de NA influence le nombre d'arbres qui peuvent être considérés pour la classification, ainsi que l'évaluation de l'exactitude. La méthode hybride de classification proposée dans le Chapitre III permet d'améliorer l'exactitude réelle de classification en incluant des arbres qui seraient autrement exclus de la classification. Elle permet d'utiliser des variables plus robustes pour des petits arbres et des variables plus complexes pour les grands arbres. Elle propose une stratification de la classification en fonction de la possibilité de calculer toutes les variables.

Considérant le nombre élevé de variables prédictives, deux méthodes de sélection ont été proposées dans les Chapitres II et III. Ces méthodes utilisent l'algorithme de *random forest* pour un premier triage décroissant des variables en fonction de la valeur de dégradation moyenne de prédiction (*mean decrease accuracy*). En plus de la sélection des meilleures variables en fonction de cette valeur, dans le Chapitre II les variables hautement corrélées ont aussi été éliminées.

L'exactitude d'identification obtenue avec une deuxième classification utilisant cette dernière sélection de variables a alors été analysée pour mettre en évidence quel type de variable a été évalué pour avoir un meilleur pouvoir de discrimination. Dans le Chapitre III, l'exactitude d'identification obtenue avec les dix premières variables a été appliquée seulement sur la stratégie hybride (stratégie qui a produit les meilleurs résultats), afin d'évaluer l'augmentation d'erreur que cette réduction de variables pourrait engendrer par rapport à une classification utilisant toutes les variables. Dans le Chapitre IV, aucune sélection des variables n'a été effectuée.

Pour le Chapitre II, l'importance des variables retenues (par canal ou pour les trois canaux ensemble) a été analysée en fonction de l'exactitude obtenue par niveau de classification (espèce, genre et feuillu/conifère), pour mettre en évidence l'importance des variables multispectrales, comme les indices de végétation par différence normalisée (IVDN), dans l'augmentation de l'exactitude de l'identification de l'espèce.

Dans le Chapitre III, les dix variables retenues pour chacune des stratégies et des approches d'élimination des NA ont été analysées. La part des variables 3D en fonction de l'intensité a été mise en évidence par strate de hauteur d'arbre.

Dans le Chapitre IV, l'influence de l'angle de balayage sur la classification a été évaluée en comparant les exactitudes obtenues pour trois groupes d'arbres séparés en fonction de l'angle moyen de balayage. La mise en classe des arbres selon l'angle moyen de balayage, correspond à chaque sélection de variables. Finalement, l'influence de la normalisation de l'intensité pour l'effet de la portée, qui est étroitement relié à l'angle de balayage, a été évaluée pour mettre en évidence la baisse de corrélation des variables d'intensité avec l'angle de balayage, ainsi qu'une amélioration de la classification.

5.2 Conclusions à retenir

De façon générale, cette étude a mis en évidence que le lidar multispectral est souhaitable pour la reconnaissance des espèces. L'information spectrale issue de trois longueurs d'onde permet d'améliorer l'identification des espèces par rapport à un lidar monospectral, surtout parce qu'il devient possible de calculer des IVDN. La plus grande amélioration apportée par le lidar multispectral par rapport à un lidar monospectral dans l'identification des espèces d'arbres est enregistrée lorsque le nombre d'espèces est élevé (Chapitre II). La majorité des études sur l'identification des espèces avec le lidar monospectral ont pris en compte généralement 2 jusqu'à 4 espèces.

Avec le lidar multispectral, nous avons pu identifier entre 10 et 14 espèces avec des exactitudes comparables avec les études sur l'identification des espèces utilisant des images multi ou hyperspectrales.

En conséquence, l'intérêt et l'efficacité de l'utilisation du lidar multispectral augmentent en fonction de la complexité de l'écosystème, notamment avec une grande diversité d'espèces. La faible différence pour un nombre réduit d'espèces, par exemple feuillus/conifères, est due au fait que les variables 3D performent suffisamment bien dans ce cas, mais seront insuffisantes pour un nombre plus élevé d'espèces. Les variables qui peuvent être calculées avec le lidar multispectral, comme les IVDN, sont celles qui contribuent le plus à l'augmentation de l'exactitude de classification.

La hauteur de l'arbre influence les résultats de l'identification de l'espèce. Cela pose un problème pour les écosystèmes complexes où l'on retrouve aussi bien des zones de forêt mature que des zones de forêt en régénération. Dans le processus d'identification, un biais a été observé dans la répartition des erreurs, affectant surtout les petits arbres. Ce biais est dû premièrement à l'élimination des petits arbres du processus de classification lorsque le nombre de points était insuffisant pour calculer des variables complexes. Deuxièmement, le biais peut être dû à la corrélation des variables avec la hauteur de l'arbre (jusqu'à 0.6), qui persiste malgré la normalisation des variables 3D par rapport à la hauteur de l'arbre, normalisation appliquée spécialement pour réduire cette corrélation. De plus, en prenant en compte la densité du nuage de points, la distribution des hauteurs des arbres dans l'échantillon et la complexité des variables utilisées, le taux d'élimination des petits arbres qui généraient des NA était élevé. Donc, pour l'exactitude de l'identification des espèces, l'aspect concernant l'élimination des petits arbres s'est avéré, dans ce cas, plus important que le problème de la corrélation des variables avec la hauteur. Après l'évaluation de trois stratégies pour diminuer l'effet de la corrélation des variables avec la hauteur de l'arbre et de trois approches pour traiter les NA, la conclusion est que la stratification par tranche de hauteur de l'arbre ne présente un avantage que dans le cas d'une application simple de *random forest* avec une élimination des arbres qui ont des variables NA. Cependant, une approche hybride par une stratification qui prend en considération la qualité du nuage de points, plutôt que la hauteur de l'arbre, amène une amélioration plus importante, parce qu'elle permet d'utiliser des variables complexes pour les grands arbres et des variables plus robustes pour des petits arbres. Donc, une approche hybride est recommandée dans le cas de l'identification de l'espèce d'arbres de hauteurs très différentes où le pourcentage de NA est important.

Nous avons vu dans le Chapitre IV, que la corrélation des variables avec l'angle de balayage entre 0 et 20 degrés est faible, généralement en dessous de $|\pm 0.2|$. L'ajout des variables multispectrales, comme les IVDN et les ratios de canaux rendent l'effet de la normalisation de l'intensité marginal. Par leur construction, intégrant un rapport entre deux canaux, ces variables compensent partiellement les variations dues à la différence de portée. La corrélation avec l'angle de balayage pourrait alors être ignorée pour des angles de balayages en dessous de 20 degrés et des petites variations de relief, particulièrement si les IVDN sont utilisés ou si les intensités sont normalisées. La normalisation selon l'intensité améliore significativement la classification avec des variables utilisant les intensités monospectrales, mais pas celles de type IVDN.

Du point de vue méthodologique, cette étude démontre que l'influence de deux des facteurs qui pourraient affecter l'identification des espèces, notamment la hauteur de l'arbre et l'angle de balayage, peuvent être réduites avec une méthodologie adaptée.

Il faut aussi souligner la capacité de l'algorithme de *random forest* à obtenir des résultats satisfaisants, même avec des variables corrélées avec différents propriétés de l'arbre, comme la hauteur de l'arbre. En plus, cet algorithme permet d'obtenir des résultats satisfaisants même en utilisant des variables avec une très large variabilité et une très faible capacité de séparation entre espèces. C'est important de démontrer la capacité de *random forest* à réduire l'écart de classification entre l'utilisation des variables d'intensité normalisées pour l'effet de la portée et non normalisées, quand toutes les variables d'intensité et 3D sont utilisées. Cela est important, car, la plupart du temps, les fichiers LAS ne contiennent pas l'information sur la portée, rendant impossible la normalisation.

5.3 Perspectives dans l'identification des espèces par arbre individuel

Le lidar multispectral est une technologie prometteuse pour l'identification des espèces, même si elle n'est pas une technologie spécialement conçue à cette fin. Cette étude a démontré que le lidar multispectral peut compétitionner avec les technologies traditionnellement utilisées dans la reconnaissance des espèces, comme l'imagerie multispectrale ou hyperspectrale. Son avantage consiste dans la possibilité d'associer précisément l'information sur l'espèce avec une information structurale de très haute qualité concernant les propriétés de l'arbre. Cette association précise entre l'information spectrale et la localisation de cette information dans la couronne offre des perspectives multiples dans l'identification des espèces. Dans cette étude, nous avons identifié surtout les espèces d'arbres dominants ou en plantation qu'il est possible d'identifier par une délimitation en 2D de la couronne. Toutefois, le lidar ouvre une perspective très intéressante avec la possibilité d'une délimitation 3D de la couronne, par exemple l'identification des espèces d'arbres en position intermédiaire ou opprimée, qui n'ont pas fait l'objet de cette étude, car leur identification nécessite une délimitation 3D de leur couronne. L'intégration de cette précision de délimitation de la couronne ouvre des possibilités très intéressantes dans l'identification des espèces dans des écosystèmes avec un grand degré de complexité concernant la stratification des arbres et le nombre d'espèces. Si, pour le moment, une telle délimitation est encore difficile à appliquer sur de grandes surfaces, à cause des ressources nécessaires en temps de calcul et capacité de stockage de l'information, elle sera probablement applicable dans un futur proche.

Une autre perspective pour améliorer l'identification des espèces avec le lidar multispectral consiste dans une amélioration de la compréhension de l'interaction du lidar avec la canopée par l'utilisation de données de haute qualité issues d'autres capteurs. La tendance actuelle dans le développement est orientée vers des capteurs intégrant plusieurs technologies et pouvant enregistrer une diversité d'informations, par exemple lidar multispectral, caméras multi/hyperspectrales, thermiques (Marrs et Ni-Meister 2019). Le système utilisé dans cette étude est un capteur intégré, enregistrant à la fois le signal laser à retours discrets (trois canaux) et à forme d'onde complète (deux canaux) et de l'imagerie multispectrale RVB. Cette étude est limitée à l'utilisation des données à retour discret. Cependant, la capacité réelle du système à distinguer les espèces serait beaucoup plus grande si l'ensemble de l'information était exploitée. Ces informations pourraient également améliorer la compréhension que nous avons sur le lidar multispectral. Les données à forme d'onde complète peuvent être utilisées pour une compréhension approfondie de l'interaction de l'impulsion laser avec le feuillage de chaque espèce. Davantage d'informations peuvent être extraites et comparées avec le nuage de points photogrammétriques issus des photos de haute résolution acquises en même temps.

Le développement des algorithmes de classification comme *random forest* et *deep learning* offre des voies de recherches très intéressantes dans l'identification des espèces avec le lidar multispectral. *Random forest* a l'avantage de pouvoir utiliser un très grand nombre de variables, possiblement corrélées. En plus, il propose un outil de sélection des variables les plus significatives pour la classification. Cependant, cette approche guidée par les données est très sensible à la qualité et au nombre de couronnes utilisées pour l'entraînement du modèle. La limite d'une telle approche tient à la nécessité d'être calibrée en fonction des données. Une calibration de la méthode est nécessaire pour appliquer cette méthode à des écosystèmes différents, aux arbres poussant en différentes conditions ou à une diversité plus large d'espèces ou encore, si différents paramètres d'enregistrement étaient utilisés, comme l'altitude de vol, la densité des retours, l'angle de balayage, ou une grande différence dans la topographie. Alors, le processus de standardisation devrait faire l'objet d'une attention particulière, surtout pour des applications sur des surfaces étendues. Parmi ces efforts de standardisation, une place centrale est accordée à la normalisation de l'intensité, notamment aux corrections radiométriques pour retrouver une valeur de réflectance (Okhrimenko, Coburn et Hopkinson 2019). Dans le futur, ces corrections permettront le développement de modèles de classification plus facilement transférable entre différentes régions ou entre enregistrements acquis avec différents paramètres. En revanche, le signal lidar est difficile à normaliser et à interpréter à cause des multiples facteurs qui interviennent dans l'interaction entre l'impulsion émise et le signal reçu. D'autres efforts dans le processus de standardisation étudient la transférabilité des modèles entre régions différentes en utilisant des algorithmes statistiques pour uniformiser les valeurs des variables (Rana *et al.* 2018). Avec davantage d'études sur la transférabilité des modèles et sur la sélection des variables robustes, le lidar multispectral pourra être utilisé de manière opérationnelle sur de larges espaces pour identifier une diversité d'espèces d'arbres dans différents écosystèmes.

Enfin, le lidar multispectral est une technologie prometteuse pour l'amélioration de l'inventaire forestier. Le lidar multispectral permet d'obtenir une multitude d'informations utiles à la gestion forestière, comme la localisation des arbres individuels, leurs dimensions, la densité du feuillage. L'ajout d'une meilleure identification de l'espèce d'arbre à ces informations est un gain très intéressant qui fera du lidar multispectral un outil puissant dans la mise en place d'un inventaire de précision.

APPENDICE A : CONFUSION MATRICES

Table A.1: Confusion matrix for C321 at the BL/NL level

	SC				YRF		
	NL	**BL**	**Class error**		**NL**	**BL**	**Class error**
NL	**69**	2	0.03	**NL**	**1161**	27	0.02
BL	5	**286**	0.02	**BL**	29	**441**	0.06

Table A.2: Confusion matrix at the genus level (SC)

	Picea	***Acer***	***Fraxinus***	***Gleditsia***	**Class error**
Picea	**71**	0	0	0	0.00
Acer	1	**164**	13	6	0.11
Fraxinus	5	5	**57**	4	0.20
Gleditsia	1	2	5	**28**	0.22

Table A.3: Confusion matrix at the genus level (YRF)

	Picea	***Pinus***	***Larix***	***Acer***	***Fraxinus***	***Populus***	***Quercus***	**Class error**
Picea	**388**	16	12	0	3	8	0	0.09
Pinus	43	**468**	32	1	14	17	0	0.19
Larix	3	11	**167**	0	1	3	1	0.10
Acer	1	5	2	**182**	1	4	7	0.10
Fraxinus	1	1	0	2	**34**	4	3	0.24
Populus	2	7	3	0	7	**149**	6	0.14
Quercus	0	2	1	12	2	3	**29**	0.41

Table A.4: Confusion matrix at the species level (YRF)

	Pic.ab	***Pic.gl***	***Pin.sy***	***Pin.re***	***Pin.st***	***Lar.lar***	***Acer.sa***	***Fra.am***	***Pop.tr***	***Que.ru***	**Class error**
Pic.ab	**177**	8	4	3	7	1	0	0	4	0	0.13
Pic.gl	5	**202**	1	2	8	1	0	2	2	0	0.09
Pin.sy	3	6	**139**	13	15	9	1	5	3	0	0.28
Pin.re	11	2	27	**143**	3	2	0	2	2	0	0.26
Pin.st	5	13	16	6	**133**	9	0	3	4	0	0.30
Lar.lar	1	8	3	3	13	**155**	0	0	3	0	0.17
Acer.sa	0	2	2	3	1	0	**181**	1	4	8	0.10
Fra.am	0	1	0	1	1	0	2	**34**	2	4	0.24
Pop.tr	1	1	3	4	2	3	0	4	**149**	7	0.14
Que.ru	0	0	1	0	1	0	12	2	3	**30**	0.39

Pic.ab = Picea abies, Pic.gl = Picea glauca, Pin.sy = Pinus sylvestris, Pin.st = Pinus strobus, Lar.lar = Larix laricina, Fra.am = Fraxinus Americana, Pop.tr = Populous tremuloides, Que.ru = Quercus rubra.

APPENDICE B : CORRELATIONS BETWEEN FEATURES AND MEAN SCAN ANGLE

Table B.1: Correlations between 3D features and mean scan angle

Feature*	All trees	Pinus resinosa	Pinus strobus	Pinus sylvestris	Picea abies	Picea glauca	Larix laricina	Count of correlations ≥ 0.2 or < -0.2
3D_DI_all_cv_C1	0.03	0.03	0.00	0.02	0.04	0.00	**0.22**	1
3D_DI_all_cv_C2	0.02	0.01	-0.02	0.03	0.08	0.06	0.15	0
3D_DI_all_cv_C3	-0.03	-0.06	-0.05	-0.03	-0.01	-0.05	0.12	0
3D_DI_all_sd_C1	0.04	0.04	0.00	0.02	0.03	0.00	**0.21**	1
3D_DI_all_sd_C2	0.03	0.02	-0.02	0.03	0.06	0.07	0.15	0
3D_DI_all_sd_C3	-0.03	-0.06	-0.05	-0.03	-0.03	-0.05	0.11	0
3D_HR_all_cv_C1	-0.14	-0.16	-0.18	-0.06	-0.10	-0.16	-0.08	0
3D_HR_all_cv_C2	-0.17	**-0.20**	-0.16	-0.14	-0.11	-0.11	-0.12	1
3D_HR_all_cv_C3	-0.03	-0.06	-0.08	0.03	-0.05	-0.04	0.06	0
3D_HR_all_lm_C1	0.19	**0.23**	**0.22**	0.12	**0.24**	**0.22**	0.14	4
3D_HR_all_lm_C2	**0.21**	**0.25**	0.19	**0.20**	**0.25**	**0.23**	0.14	5
3D_HR_all_lm_C3	0.04	0.09	0.10	0.02	**0.22**	0.06	-0.08	1
3D_MH_si_mn_C1	0.00	-0.03	0.02	-0.05	**-0.21**	-0.01	-0.08	1
3D_MH_si_mn_C2	0.01	-0.02	0.02	-0.05	**-0.21**	-0.04	-0.12	1
3D_MH_si_mn_C3	-0.01	-0.01	0.02	-0.04	-0.14	0.01	-0.18	0
3D_PE_all_p05_C1	-0.03	-0.04	0.00	0.00	-0.04	0.00	**-0.20**	1
3D_PE_all_p05_C2	-0.01	0.00	0.02	-0.01	-0.07	-0.06	-0.12	0
3D_PE_all_p05_C3	0.04	0.06	0.05	0.04	0.00	0.05	-0.11	0
3D_PE_si_p25_C1	-0.01	-0.02	0.02	-0.07	**-0.21**	-0.03	-0.09	1
3D_PE_si_p25_C2	0.01	-0.01	0.02	-0.07	-0.18	-0.05	-0.11	0
3D_PE_si_p25_C3	-0.02	-0.02	0.02	-0.04	-0.10	-0.02	-0.19	0

Feature*	All trees	Pinus resinosa	Pinus strobus	Pinus sylvestris	Picea abies	Picea glauca	Larix laricina	Count of correlations ≥ 0.2 or < -0.2
3D_PE_si_p50_C1	0.00	-0.03	0.01	-0.04	**-0.21**	0.01	-0.07	1
3D_PE_si_p50_C2	0.02	-0.02	0.02	-0.02	**-0.20**	-0.01	-0.08	1
3D_PE_si_p50_C3	-0.01	-0.03	0.02	-0.03	-0.16	0.04	-0.17	0
3D_RB_all_pt_0_60_C1	0.04	0.03	0.01	0.02	0.09	0.01	**0.22**	1
3D_RB_all_pt_0_60_C2	0.03	0.02	0.00	0.03	0.11	0.07	0.16	0
3D_RB_all_pt_0_60_C3	0.00	-0.04	-0.01	-0.01	0.06	0.00	0.12	0
3D_RM_1st_mn_all_mn_C1	0.02	0.02	0.02	-0.03	-0.16	-0.05	0.17	0
3D_RM_1st_mn_all_mn_C2	0.01	-0.01	-0.02	-0.04	-0.07	-0.01	0.13	0
3D_RM_1st_mn_all_mn_C3	-0.11	-0.12	-0.09	-0.13	**-0.21**	-0.17	0.00	1
3D_RP_1st_all_C1	0.00	-0.02	0.00	0.05	**0.39**	0.05	-0.11	1
3D_RP_1st_all_C2	0.02	0.01	0.05	0.06	**0.36**	0.02	-0.12	1
3D_RP_1st_all_C3	0.16	0.14	0.06	0.18	**0.52**	**0.22**	0.03	2
3D_RP_si_1st_C1	0.07	0.09	0.08	0.08	**0.40**	0.08	0.06	1
3D_RP_si_1st_C2	0.06	0.07	0.10	0.09	**0.40**	0.08	0.09	1
3D_RP_si_1st_C3	**0.21**	**0.22**	0.09	**0.23**	**0.55**	**0.25**	0.13	5
3D_SL_1st_cv_C1	0.18	**0.20**	**0.21**	0.13	**0.20**	**0.24**	0.20	4
3D_SL_1st_cv_C2	0.19	0.19	**0.25**	0.16	**0.23**	**0.25**	**0.20**	4
3D_SL_1st_cv_C3	0.05	0.05	0.07	0.03	0.14	0.06	0.07	0
3D_SL_1st_mn_C1	0.13	0.14	0.13	0.09	0.11	0.11	**0.24**	1
3D_SL_1st_mn_C2	0.11	0.12	0.13	0.12	0.17	0.11	**0.21**	1
3D_SL_1st_mn_C3	0.02	0.00	0.02	0.02	-0.05	-0.06	**0.25**	1
3D_SL_1st_p75_C1	0.09	0.09	0.07	0.06	0.08	0.07	**0.24**	1
3D_SL_1st_p75_C2	0.08	0.07	0.07	0.08	0.14	0.09	**0.21**	1
3D_SL_1st_p75_C3	0.02	-0.01	0.00	0.02	-0.04	-0.05	**0.25**	1
3D_SL_1st_sd_C1	0.19	**0.21**	**0.23**	0.12	**0.21**	**0.26**	**0.26**	5
3D_SL_1st_sd_C2	0.18	0.18	**0.22**	0.16	**0.23**	**0.21**	**0.28**	4
3D_SL_1st_sd_C3	0.05	0.04	0.08	0.03	0.05	0.01	**0.21**	1
3D_SL_all_cv_C1	0.20	**0.21**	**0.22**	0.10	0.15	**0.23**	**0.27**	4
3D_SL_all_cv_C2	**0.26**	**0.29**	**0.26**	0.19	**0.24**	**0.32**	**0.23**	6
3D_SL_all_cv_C3	0.04	0.03	0.07	0.03	0.14	0.03	0.06	0

Feature*	All trees	Pinus resinosa	Pinus strobus	Pinus sylvestris	Picea abies	Picea glauca	Larix laricina	Count of correlations ≥ 0.2 or < -0.2
3D_SL_all_mn_C1	0.19	**0.20**	0.16	0.11	0.04	0.13	**0.34**	2
3D_SL_all_mn_C2	0.19	0.20	0.17	0.15	0.14	0.18	**0.28**	1
3D_SL_all_mn_C3	-0.02	-0.05	0.01	-0.02	-0.13	-0.13	**0.25**	1
3D_SL_all_p50_C1	0.04	0.03	-0.01	0.02	-0.07	-0.01	**0.21**	1
3D_SL_all_p50_C2	0.01	0.00	-0.01	0.02	-0.05	-0.01	0.16	0
3D_SL_all_p50_C3	-0.05	-0.08	-0.04	-0.03	-0.17	-0.13	**0.21**	1
3D_SL_all_p75_C1	0.13	0.13	0.11	0.08	-0.01	0.08	**0.29**	1
3D_SL_all_p75_C2	0.10	0.08	0.08	0.09	0.07	0.10	**0.25**	1
3D_SL_all_p75_C3	-0.02	-0.06	-0.02	-0.03	-0.12	-0.11	**0.25**	1
3D_SL_all_sd_C1	**0.21**	**0.21**	**0.22**	0.12	0.12	**0.23**	**0.35**	5
3D_SL_all_sd_C2	**0.25**	**0.26**	**0.24**	0.20	**0.23**	**0.28**	**0.29**	6
3D_SL_all_sd_C3	0.02	0.00	0.07	0.02	-0.02	-0.07	0.20	0
3D_SU_1st_rs_C1	0.04	0.02	0.01	0.06	0.11	0.10	**0.26**	1
3D_SU_1st_rs_C2	0.05	0.02	0.01	0.11	0.16	0.14	**0.21**	1
3D_SU_1st_rs_C3	-0.02	-0.05	-0.03	0.00	0.01	0.00	**0.21**	1
Count of correlations ≥ 0.2 or > -0.2	5	11	9	2	21	12	29	84

*3D features which did not have a correlation value larger than |±0.2| with the mean scan angle in all the three channels and for all species are not presented in the table. They are listed here : AH, DI_1st_cv, DI_1st_kurt, DI_1st_sd, DI_1st_skew, DI_all_kurt, DI_all_skew, DI_si_kurt, DI_si_sd, DI_si_skew, HR_si_cv, HR_si_lm, MH_1st_mn, MH_all_mn, PE_1st_p05, PE_1st_p10, PE_1st_p25, PE_1st_p50, PE_1st_p75, PE_1st_p90, PE_1st_p95, PE_all_p10, PE_all_p25, PE_all_p50, PE_all_p75, PE_all_p90, PE_all_p95, PE_si_p50, RB_all_pt_60_80, RB_all_pt_80_90, RB_all_pt_90_100, RB_all_pt_95_100, RM_1st_mn, RM_1st_p50_1st_mn, RM_1st_p50, RM_all_mn, RM_all_p50_all_mn, RM_all_p50, SL_1st_p25, SL_1st_p50, SL_all_p25, SU_1st_coef

Table B.2: Correlations between raw intensity features and mean scan angle

Feature*	All trees	Pinus resinosa	Pinus strobus	Pinus sylvestris	Picea abies	Picea glauca	Larix laricina	Count of correlations ≥ 0.2 or < -0.2
I_DI_1st_cv_C1	-0.05	-0.04	-0.05	-0.02	**-0.33**	-0.04	-0.02	1
I_DI_1st_cv_C2	-0.01	-0.02	-0.03	0.04	**-0.21**	0.02	0.03	1
I_DI_1st_cv_C3	-0.08	-0.06	-0.04	-0.09	**-0.37**	-0.08	-0.02	1
I_DI_1st_sd_C1	-0.11	-0.10	0.03	-0.14	**-0.49**	**-0.26**	0.05	2
I_DI_1st_sd_C2	-0.12	-0.10	0.04	-0.18	**-0.44**	**-0.31**	0.14	2
I_DI_1st_sd_C3	-0.13	-0.12	0.00	**-0.28**	**-0.29**	**-0.30**	0.00	3
I_DI_1st_skew_C1	-0.05	-0.05	-0.10	-0.02	**-0.26**	-0.07	-0.03	1
I_DI_1st_skew_C2	-0.02	-0.01	-0.08	0.02	**-0.21**	-0.02	0.01	1
I_DI_1st_skew_C3	-0.07	-0.06	-0.09	-0.05	**-0.24**	-0.04	-0.05	1
I_DI_all_cv_C1	-0.05	-0.05	-0.02	-0.05	**-0.39**	-0.05	-0.02	1
I_DI_all_cv_C2	0.01	0.01	0.00	0.00	**-0.34**	0.04	0.07	1
I_DI_all_cv_C3	-0.09	-0.07	-0.01	-0.12	**-0.38**	-0.09	-0.01	1
I_DI_all_sd_C1	-0.12	-0.12	0.05	-0.16	**-0.49**	**-0.30**	0.04	2
I_DI_all_sd_C2	-0.13	-0.11	0.06	**-0.23**	**-0.37**	**-0.36**	0.13	3
I_DI_all_sd_C3	-0.12	-0.13	0.02	**-0.28**	**-0.23**	**-0.30**	0.01	3
I_DI_all_skew_C1	-0.03	-0.03	-0.07	-0.02	**-0.31**	-0.04	0.01	1
I_DI_all_skew_C2	0.00	0.00	-0.07	0.00	**-0.33**	0.04	0.05	1
I_DI_all_skew_C3	-0.09	-0.07	-0.10	-0.10	**-0.30**	-0.07	-0.07	1
I_DI_si_sd_C1	-0.08	-0.06	-0.06	-0.06	**-0.32**	-0.20	0.03	1
I_DI_si_sd_C2	-0.07	-0.05	-0.02	-0.09	-0.16	-0.18	0.17	0
I_DI_si_sd_C3	-0.09	-0.08	0.00	**-0.21**	**-0.33**	-0.16	0.08	2
I_IR_all_sd_C1	-0.07	-0.10	0.06	-0.05	-0.12	**-0.20**	-0.06	1
I_IR_all_sd_C2	-0.09	-0.10	0.03	-0.11	-0.05	**-0.23**	-0.05	1
I_IR_all_sd_C3	-0.06	-0.07	0.04	-0.14	-0.05	**-0.22**	-0.04	1
I_IR_si_sd_C1	-0.03	-0.05	0.05	-0.04	-0.13	-0.16	0.02	0
I_IR_si_sd_C2	-0.03	-0.04	0.04	-0.04	-0.01	-0.19	0.03	0
I_IR_si_sd_C3	-0.06	-0.07	0.04	-0.14	-0.09	**-0.22**	-0.02	1
I_MI_1st_10_90_mn_C1	-0.10	-0.12	0.10	-0.20	**-0.22**	**-0.31**	0.09	2
I_MI_1st_10_90_mn_C2	-0.11	-0.10	0.08	**-0.24**	-0.07	**-0.34**	0.13	2
I_MI_1st_10_90_mn_C3	-0.10	-0.09	0.06	**-0.29**	0.10	**-0.28**	0.06	2

Feature*	All trees	Pinus resinosa	Pinus strobus	Pinus sylvestris	Picea abies	Picea glauca	Larix laricina	Count of correlations ≥ 0.2 or < -0.2
I_MI_1st_5_95_mn_C1	-0.11	-0.12	0.10	-0.20	**-0.24**	**-0.32**	0.09	2
I_MI_1st_5_95_mn_C2	-0.11	-0.10	0.08	**-0.24**	-0.08	**-0.35**	0.13	2
I_MI_1st_5_95_mn_C3	-0.11	-0.09	0.05	**-0.30**	0.08	**-0.29**	0.05	2
I_MI_1st_mn_C1	-0.11	-0.13	0.09	-0.20	**-0.28**	**-0.34**	0.09	2
I_MI_1st_mn_C2	-0.12	-0.10	0.07	**-0.25**	-0.10	**-0.36**	0.14	2
I_MI_1st_mn_C3	-0.11	-0.10	0.04	**-0.32**	0.07	**-0.31**	0.05	2
I_MI_all_10_90_mn_C1	-0.11	-0.13	0.08	-0.18	-0.08	**-0.28**	0.08	1
I_MI_all_10_90_mn_C2	-0.11	-0.10	0.07	**-0.20**	0.07	**-0.32**	0.11	2
I_MI_all_10_90_mn_C3	-0.08	-0.06	0.05	**-0.26**	0.15	**-0.24**	0.08	2
I_MI_all_10_90_n_mn_C1	0.04	0.04	0.05	0.04	**0.25**	0.09	0.00	1
I_MI_all_10_90_n_mn_C2	0.02	0.02	0.03	0.04	**0.23**	0.02	-0.06	1
I_MI_all_10_90_n_mn_C3	0.07	0.05	0.04	0.10	0.13	0.10	0.06	0
I_MI_all_5_95_mn_C1	-0.11	-0.13	0.08	-0.18	-0.11	**-0.30**	0.08	1
I_MI_all_5_95_mn_C2	-0.11	-0.10	0.07	**-0.21**	0.05	**-0.33**	0.11	2
I_MI_all_5_95_mn_C3	-0.09	-0.07	0.05	**-0.27**	0.14	**-0.25**	0.07	2
I_MI_all_5_95_n_mn_C1	0.03	0.03	0.03	0.05	**0.20**	0.08	-0.04	1
I_MI_all_5_95_n_mn_C2	0.02	0.02	0.02	0.03	0.19	0.04	-0.05	0
I_MI_all_5_95_n_mn_C3	0.07	0.05	0.03	0.10	0.13	0.07	0.04	0
I_MI_all_mn_C1	-0.12	-0.14	0.08	-0.19	-0.16	**-0.33**	0.08	1
I_MI_all_mn_C2	-0.12	-0.11	0.07	**-0.22**	0.02	**-0.35**	0.12	2
I_MI_all_mn_C3	-0.10	-0.08	0.05	**-0.29**	0.12	**-0.27**	0.07	2
I_MI_si_10_90_mn_C1	-0.11	-0.11	0.10	-0.19	**-0.53**	**-0.32**	0.06	2
I_MI_si_10_90_mn_C2	-0.14	-0.11	0.05	**-0.27**	**-0.50**	**-0.43**	0.11	3
I_MI_si_10_90_mn_C3	-0.16	-0.16	0.01	**-0.35**	-0.11	**-0.40**	-0.03	2
I_MI_si_5_95_mn_C1	-0.11	-0.11	0.09	-0.18	**-0.53**	**-0.33**	0.06	2
I_MI_si_5_95_mn_C2	-0.14	-0.11	0.05	**-0.27**	**-0.51**	**-0.44**	0.11	3
I_MI_si_5_95_mn_C3	-0.16	-0.16	0.01	**-0.35**	-0.11	**-0.41**	-0.04	2
I_MI_si_mn_C1	-0.11	-0.12	0.09	-0.19	**-0.54**	**-0.35**	0.06	2
I_MI_si_mn_C2	-0.14	-0.12	0.05	**-0.27**	**-0.52**	**-0.46**	0.12	3
I_MI_si_mn_C3	-0.17	-0.17	0.00	**-0.37**	-0.13	**-0.42**	-0.04	2
I_NDG2_1st_mn	0.03	-0.02	0.08	0.04	**-0.21**	0.04	0.02	1
I_NDG2_1st_p50	0.02	-0.03	0.07	0.02	-0.15	0.04	0.01	0

Feature*	All trees	Pinus resinosa	Pinus strobus	Pinus sylvestris	Picea abies	Picea glauca	Larix laricina	Count of correlations ≥ 0.2 or < -0.2
I_NDG2_1st_p75	0.03	-0.02	0.08	0.05	**-0.22**	0.04	0.00	1
I_NDG2_1st_p90	0.04	-0.01	0.08	0.06	**-0.23**	0.03	0.00	1
I_NDG2_1st_p95	0.04	-0.01	0.07	0.06	**-0.21**	0.03	0.02	1
I_NDG2_all_mn	0.00	-0.05	0.07	0.02	-0.20	0.00	0.00	0
I_NDG2_all_p50	-0.01	-0.04	0.05	0.00	-0.09	0.01	-0.03	0
I_NDG2_all_p75	0.01	-0.05	0.07	0.02	-0.20	0.01	-0.02	0
I_NDG2_all_p90	0.02	-0.04	0.08	0.05	**-0.24**	0.02	-0.04	1
I_NDG2_all_p95	0.03	-0.03	0.06	0.05	**-0.22**	0.02	0.01	1
I_NDG2_si_mn	0.09	0.04	0.12	0.12	**-0.22**	0.16	0.09	1
I_NDG2_si_p50	0.09	0.04	0.10	0.11	**-0.21**	0.17	0.08	1
I_NDG2_si_p75	0.07	0.02	0.09	0.09	**-0.21**	0.11	0.02	1
I_NDG2_si_p90	0.06	0.01	0.07	0.09	-0.18	0.08	0.03	0
I_NDG2_si_p95	0.06	0.01	0.07	0.08	-0.16	0.07	0.03	0
I_PE_1st_p05_C1	-0.04	-0.04	0.01	-0.08	0.12	-0.14	0.08	0
I_PE_1st_p05_C2	-0.04	-0.03	-0.01	-0.11	0.09	-0.15	0.05	0
I_PE_1st_p05_C3	-0.05	-0.04	0.01	-0.16	**0.22**	-0.15	0.07	1
I_PE_1st_p10_C1	-0.04	-0.04	0.03	-0.09	0.15	-0.14	0.08	0
I_PE_1st_p10_C2	-0.04	-0.03	0.01	-0.13	0.12	-0.15	0.07	0
I_PE_1st_p10_C3	-0.06	-0.05	0.01	-0.18	**0.23**	-0.16	0.09	1
I_PE_1st_p25_C1	-0.06	-0.06	0.07	-0.13	0.11	-0.19	0.08	0
I_PE_1st_p25_C2	-0.06	-0.05	0.05	-0.17	0.09	-0.19	0.10	0
I_PE_1st_p25_C3	-0.08	-0.06	0.03	**-0.23**	0.18	**-0.21**	0.06	2
I_PE_1st_p50_C1	-0.10	-0.12	0.10	-0.20	-0.14	**-0.27**	0.08	1
I_PE_1st_p50_C2	-0.10	-0.09	0.08	**-0.22**	-0.01	**-0.31**	0.11	2
I_PE_1st_p50_C3	-0.10	-0.08	0.06	**-0.27**	0.10	**-0.25**	0.05	2
I_PE_1st_p75_C1	-0.11	-0.13	0.10	**-0.21**	**-0.39**	**-0.33**	0.08	3
I_PE_1st_p75_C2	-0.13	-0.11	0.08	**-0.26**	**-0.22**	**-0.40**	0.12	3
I_PE_1st_p75_C3	-0.11	-0.10	0.05	**-0.30**	0.01	**-0.29**	0.04	2
I_PE_1st_p90_C1	-0.11	-0.11	0.07	-0.16	**-0.46**	**-0.34**	0.08	2
I_PE_1st_p90_C2	-0.13	-0.11	0.06	**-0.24**	**-0.33**	**-0.41**	0.14	3
I_PE_1st_p90_C3	-0.12	-0.12	0.03	**-0.32**	-0.08	**-0.32**	0.04	2
I_PE_1st_p95_C1	-0.10	-0.10	0.06	-0.13	**-0.45**	**-0.33**	0.07	2

Feature*	All trees	Pinus resinosa	Pinus strobus	Pinus sylvestris	Picea abies	Picea glauca	Larix laricina	Count of correlations ≥ 0.2 or < -0.2
I_PE_1st_p95_C2	-0.13	-0.10	0.06	**-0.21**	**-0.37**	**-0.42**	0.15	3
I_PE_1st_p95_C3	-0.13	-0.12	0.02	**-0.33**	-0.14	**-0.32**	0.02	2
I_PE_all_p05_C1	-0.03	-0.05	0.00	-0.05	0.11	-0.11	0.08	0
I_PE_all_p05_C2	-0.05	-0.05	-0.02	-0.10	0.10	-0.17	0.04	0
I_PE_all_p05_C3	-0.02	-0.01	-0.01	-0.10	**0.22**	-0.10	0.05	1
I_PE_all_p10_C1	-0.03	-0.04	0.02	-0.06	0.17	-0.13	0.11	0
I_PE_all_p10_C2	-0.05	-0.04	0.00	-0.10	0.12	-0.16	0.05	0
I_PE_all_p10_C3	-0.04	-0.02	0.00	-0.13	**0.23**	-0.13	0.07	1
I_PE_all_p25_C1	-0.05	-0.05	0.04	-0.09	**0.21**	-0.16	0.09	1
I_PE_all_p25_C2	-0.06	-0.06	0.02	-0.11	0.19	-0.18	0.08	0
I_PE_all_p25_C3	-0.06	-0.04	0.03	-0.18	**0.23**	-0.17	0.09	1
I_PE_all_p50_C1	-0.09	-0.10	0.07	-0.16	0.05	**-0.24**	0.06	1
I_PE_all_p50_C2	-0.10	-0.09	0.07	-0.17	0.15	**-0.27**	0.08	1
I_PE_all_p50_C3	-0.08	-0.05	0.05	**-0.22**	0.18	**-0.22**	0.08	2
I_PE_all_p75_C1	-0.12	-0.14	0.10	**-0.20**	**-0.26**	**-0.33**	0.06	3
I_PE_all_p75_C2	-0.13	-0.12	0.08	**-0.23**	-0.04	**-0.36**	0.10	2
I_PE_all_p75_C3	-0.10	-0.08	0.06	**-0.27**	0.07	**-0.26**	0.05	2
I_PE_all_p90_C1	-0.12	-0.13	0.08	-0.17	**-0.43**	**-0.35**	0.06	2
I_PE_all_p90_C2	-0.13	-0.12	0.07	**-0.25**	**-0.25**	**-0.41**	0.13	3
I_PE_all_p90_C3	-0.11	-0.11	0.04	**-0.31**	-0.02	**-0.30**	0.05	2
I_PE_all_p95_C1	-0.11	-0.11	0.06	-0.14	**-0.45**	**-0.35**	0.07	2
I_PE_all_p95_C2	-0.13	-0.11	0.06	**-0.23**	**-0.31**	**-0.41**	0.14	3
I_PE_all_p95_C3	-0.12	-0.12	0.04	**-0.32**	-0.09	**-0.31**	0.03	2
I_PE_si_p05_C1	-0.12	-0.14	0.10	**-0.20**	**-0.42**	**-0.32**	0.05	3
I_PE_si_p05_C2	-0.15	-0.13	0.04	**-0.25**	**-0.44**	**-0.43**	0.09	3
I_PE_si_p05_C3	-0.18	-0.16	-0.06	**-0.30**	0.02	**-0.39**	-0.11	2
I_PE_si_p10_C1	-0.11	-0.13	0.11	**-0.21**	**-0.45**	**-0.32**	0.05	3
I_PE_si_p10_C2	-0.15	-0.13	0.05	**-0.26**	**-0.46**	**-0.43**	0.08	3
I_PE_si_p10_C3	-0.18	-0.16	-0.04	**-0.32**	-0.01	**-0.39**	-0.10	2
I_PE_si_p25_C1	-0.11	-0.12	0.11	**-0.22**	**-0.50**	**-0.32**	0.06	3
I_PE_si_p25_C2	-0.14	-0.11	0.05	**-0.27**	**-0.49**	**-0.43**	0.09	3
I_PE_si_p25_C3	-0.17	-0.16	0.00	**-0.33**	-0.05	**-0.39**	-0.08	2

Feature*	All trees	Pinus resinosa	Pinus strobus	Pinus sylvestris	Picea abies	Picea glauca	Larix laricina	Count of correlations ≥ 0.2 or < -0.2
I_PE_si_p50_C1	-0.11	-0.12	0.10	-0.20	**-0.53**	**-0.31**	0.06	2
I_PE_si_p50_C2	-0.14	-0.11	0.05	**-0.26**	**-0.50**	**-0.42**	0.10	3
I_PE_si_p50_C3	-0.15	-0.16	0.02	**-0.34**	-0.10	**-0.40**	-0.04	2
I_PE_si_p75_C1	-0.11	-0.10	0.07	-0.15	**-0.50**	**-0.31**	0.06	2
I_PE_si_p75_C2	-0.13	-0.10	0.04	**-0.26**	**-0.48**	**-0.43**	0.12	3
I_PE_si_p75_C3	-0.14	-0.15	0.01	**-0.34**	-0.15	**-0.36**	0.00	2
I_PE_si_p90_C1	-0.09	-0.08	0.05	-0.11	**-0.46**	**-0.30**	0.06	2
I_PE_si_p90_C2	-0.12	-0.09	0.04	**-0.21**	**-0.46**	**-0.42**	0.14	3
I_PE_si_p90_C3	-0.14	-0.14	0.01	**-0.34**	**-0.21**	**-0.34**	0.00	3
I_PE_si_p95_C1	-0.09	-0.08	0.04	-0.10	**-0.44**	**-0.29**	0.05	2
I_PE_si_p95_C2	-0.11	-0.08	0.04	-0.20	**-0.43**	**-0.40**	0.14	2
I_PE_si_p95_C3	-0.14	-0.13	0.01	**-0.34**	**-0.23**	**-0.34**	0.00	3
I_RCG2_1st_mn	-0.03	0.02	-0.08	-0.04	**0.22**	-0.03	-0.02	1
I_RCG2_1st_p50	-0.02	0.03	-0.07	-0.02	0.17	-0.03	-0.01	0
I_RCG2_1st_p75	-0.03	0.02	-0.08	-0.04	**0.23**	-0.03	0.01	1
I_RCG2_1st_p90	-0.04	0.01	-0.08	-0.05	**0.24**	-0.03	0.01	1
I_RCG2_1st_p95	-0.04	0.01	-0.07	-0.05	**0.22**	-0.03	-0.02	1
I_RCG2_all_mn	0.00	0.05	-0.07	-0.02	**0.21**	0.01	0.01	1
I_RCG2_all_p50	0.01	0.04	-0.04	0.01	0.10	0.00	0.03	0
I_RCG2_all_p75	-0.01	0.05	-0.07	-0.01	**0.21**	0.01	0.02	1
I_RCG2_all_p90	-0.02	0.04	-0.08	-0.04	**0.25**	-0.01	0.04	1
I_RCG2_all_p95	-0.03	0.03	-0.07	-0.05	**0.23**	-0.01	0.00	1
I_RCG2_si_mn	-0.09	-0.04	-0.12	-0.12	**0.23**	-0.16	-0.09	1
I_RCG2_si_p50	-0.09	-0.04	-0.11	-0.11	**0.23**	-0.17	-0.08	1
I_RCG2_si_p75	-0.07	-0.02	-0.10	-0.09	**0.22**	-0.10	-0.01	1
I_RCG2_si_p90	-0.06	-0.01	-0.08	-0.09	0.19	-0.07	-0.03	0
I_RCG2_si_p95	-0.06	-0.01	-0.07	-0.08	0.17	-0.06	-0.03	0
I_RM_1st_mn_all_mn_C1	0.01	0.01	0.06	-0.04	**-0.25**	0.00	0.05	1
I_RM_1st_mn_all_mn_C2	0.03	0.05	0.02	-0.05	**-0.27**	0.04	0.11	1
I_RM_1st_mn_all_mn_C3	-0.11	-0.11	0.01	-0.17	**-0.27**	-0.14	-0.03	1
Count of correlations ≥ 0.2 or < -0.2	0	0	0	56	88	83	0	227

*Individual channel intensity features which did not have a correlation value larger than |±0.2| with the mean scan angle in all the three channels and for all species are not presented in the table. They are listed here : DI_1st_kurt, DI_all_kurt, DI_si_cv, DI_si_kurt, DI_si_skew, IR_all_lm, IR_si_lm, MI_1st_10_90_n_mn, 1st_5_95_n_mn, MI_si_10_90_n_mn, MI_si_5_95_n_mn. The normalized indices NDG1 and NDIR, ainsi que les ratios RCG1 and RCG2 had no correlation value larger than |±0.2| to the mean scan angle for any combinations of return type (all, si, 1st) and statistic (mn, p50, p75, p90, p95).

Table B.3 : Correlations between normalized intensity features and mean scan angle

Feature*	All trees	Pinus resinosa	Pinus strobus	Pinus sylvestris	Picea abies	Picea glauca	Larix laricina	Count of correlations ≥ 0.2 or < -0.2
I_DI_1st_cv_C1	-0.05	-0.04	-0.05	-0.02	**-0.33**	-0.04	-0.01	1
I_DI_1st_cv_C2	-0.01	-0.02	-0.03	0.04	**-0.21**	0.02	0.03	1
I_DI_1st_cv_C3	-0.08	-0.06	-0.04	-0.09	**-0.37**	-0.08	-0.02	1
I_DI_1st_sd_C1	-0.03	-0.01	0.02	0.02	**-0.22**	0.05	-0.03	1
I_DI_1st_sd_C2	-0.01	0.01	0.06	0.03	-0.08	0.04	0.06	0
I_DI_1st_sd_C3	-0.06	-0.01	-0.03	-0.09	-0.05	-0.04	-0.07	0
I_DI_1st_skew_C1	-0.05	-0.05	-0.10	-0.02	**-0.26**	-0.07	-0.02	1
I_DI_1st_skew_C2	-0.02	-0.01	-0.08	0.02	**-0.21**	-0.02	0.01	1
I_DI_1st_skew_C3	-0.07	-0.06	-0.09	-0.05	**-0.24**	-0.04	-0.05	1
I_DI_all_cv_C1	-0.06	-0.05	-0.02	-0.05	**-0.39**	-0.05	-0.02	1
I_DI_all_cv_C2	0.00	0.01	0.00	0.00	**-0.33**	0.04	0.07	1
I_DI_all_cv_C3	-0.09	-0.07	-0.02	-0.12	**-0.38**	-0.09	-0.01	1
I_DI_all_skew_C1	-0.03	-0.03	-0.07	-0.02	**-0.31**	-0.04	0.01	1
I_DI_all_skew_C2	-0.01	0.00	-0.07	0.00	**-0.33**	0.04	0.05	1
I_DI_all_skew_C3	-0.09	-0.07	-0.10	-0.10	**-0.30**	-0.07	-0.07	1
I_MI_1st_10_90_mn_C1	0.02	0.06	0.09	0.06	0.17	0.12	-0.01	0
I_MI_1st_10_90_mn_C2	0.01	0.03	0.11	-0.02	0.19	0.01	0.05	0
I_MI_1st_10_90_mn_C3	0.01	0.10	0.02	-0.02	**0.34**	0.05	-0.06	1
I_MI_1st_10_90_n_mn_C1	0.03	0.03	0.07	0.01	**0.25**	0.06	0.02	1
I_MI_1st_10_90_n_mn_C2	0.01	0.00	0.06	-0.02	0.17	-0.03	0.00	0
I_MI_1st_10_90_n_mn_C3	0.06	0.06	0.07	0.05	**0.23**	0.03	0.04	1
I_MI_1st_5_95_mn_C1	0.02	0.06	0.09	0.06	0.16	0.13	-0.01	0
I_MI_1st_5_95_mn_C2	0.01	0.03	0.11	-0.02	0.19	0.01	0.05	0
I_MI_1st_5_95_mn_C3	0.01	0.10	0.01	-0.02	**0.34**	0.05	-0.05	1
I_MI_1st_5_95_n_mn_C1	0.04	0.04	0.07	0.01	**0.25**	0.07	0.06	1

Feature*	All trees	Pinus resinosa	Pinus strobus	Pinus sylvestris	Picea abies	Picea glauca	Larix laricina	Count of correlations ≥ 0.2 or < -0.2
I_MI_1st_5_95_n_mn_C2	0.01	0.01	0.06	-0.03	0.16	-0.01	0.00	0
I_MI_1st_5_95_n_mn_C3	0.07	0.06	0.08	0.06	**0.25**	0.06	0.08	1
I_MI_1st_mn_C1	0.02	0.06	0.08	0.06	0.13	0.12	-0.01	0
I_MI_1st_mn_C2	0.01	0.03	0.11	-0.02	0.18	0.01	0.05	0
I_MI_1st_mn_C3	0.00	0.09	0.01	-0.03	**0.33**	0.04	-0.07	1
I_MI_all_10_90_mn_C1	0.02	0.05	0.07	0.08	**0.31**	0.10	-0.03	1
I_MI_all_10_90_mn_C2	0.00	0.01	0.10	0.01	**0.30**	-0.01	0.01	1
I_MI_all_10_90_mn_C3	0.03	0.12	0.02	0.03	**0.39**	0.08	-0.05	1
I_MI_all_10_90_n_mn_C1	0.03	0.03	0.06	0.02	**0.35**	0.04	0.01	1
I_MI_all_10_90_n_mn_C2	0.00	0.00	0.05	0.00	**0.33**	-0.02	-0.05	1
I_MI_all_10_90_n_mn_C3	0.08	0.06	0.07	0.09	**0.30**	0.06	0.06	1
I_MI_all_5_95_mn_C1	0.02	0.05	0.07	0.08	**0.29**	0.11	-0.03	1
I_MI_all_5_95_mn_C2	0.00	0.01	0.10	0.01	**0.29**	-0.01	0.01	1
I_MI_all_5_95_mn_C3	0.03	0.12	0.01	0.03	**0.39**	0.08	-0.05	1
I_MI_all_5_95_n_mn_C1	0.04	0.04	0.07	0.03	**0.33**	0.04	0.02	1
I_MI_all_5_95_n_mn_C2	0.01	0.01	0.05	0.00	**0.31**	-0.03	-0.06	1
I_MI_all_5_95_n_mn_C3	0.08	0.06	0.08	0.11	**0.31**	0.07	0.09	1
I_MI_all_mn_C1	0.01	0.05	0.06	0.08	**0.25**	0.11	-0.03	1
I_MI_all_mn_C2	0.00	0.01	0.10	0.01	**0.28**	-0.01	0.02	1
I_MI_all_mn_C3	0.02	0.12	0.01	0.02	**0.38**	0.08	-0.06	1
I_NDG2_1st_mn	0.03	-0.02	0.08	0.05	**-0.22**	0.04	0.01	1
I_NDG2_1st_p50	0.02	-0.02	0.06	0.02	-0.16	0.04	0.01	0
I_NDG2_1st_p75	0.03	-0.02	0.08	0.05	**-0.22**	0.05	-0.01	1
I_NDG2_1st_p90	0.04	-0.01	0.07	0.06	**-0.23**	0.03	-0.01	1
I_NDG2_1st_p95	0.04	-0.01	0.07	0.06	**-0.21**	0.03	0.02	1
I_NDG2_all_mn	0.00	-0.05	0.06	0.03	**-0.20**	0.00	-0.01	1

Feature*	All trees	Pinus resinosa	Pinus strobus	Pinus sylvestris	Picea abies	Picea glauca	Larix laricina	Count of correlations ≥ 0.2 or < -0.2
I_NDG2_all_p50	-0.01	-0.04	0.04	0.00	-0.10	0.01	-0.03	0
I_NDG2_all_p75	0.01	-0.04	0.07	0.02	**-0.21**	0.00	-0.03	1
I_NDG2_all_p90	0.02	-0.03	0.07	0.05	**-0.24**	0.02	-0.04	1
I_NDG2_all_p95	0.03	-0.03	0.06	0.06	**-0.23**	0.02	0.00	1
I_NDG2_si_mn	0.09	0.04	0.11	0.12	**-0.22**	0.16	0.09	1
I_NDG2_si_p50	0.09	0.04	0.10	0.11	**-0.21**	0.17	0.07	1
I_NDG2_si_p75	0.07	0.02	0.09	0.09	**-0.21**	0.11	0.01	1
I_NDG2_si_p90	0.06	0.01	0.07	0.09	-0.18	0.08	0.02	0
I_NDG2_si_p95	0.06	0.01	0.07	0.08	-0.16	0.07	0.02	0
I_PE_1st_p05_C1	0.02	0.02	0.00	0.02	**0.22**	-0.02	0.02	1
I_PE_1st_p05_C2	-0.01	0.00	0.00	-0.04	0.15	-0.06	0.00	0
I_PE_1st_p05_C3	0.03	0.06	-0.01	0.02	**0.35**	0.02	-0.03	1
I_PE_1st_p10_C1	0.03	0.03	0.02	0.03	**0.27**	0.00	0.02	1
I_PE_1st_p10_C2	0.00	0.01	0.02	-0.04	0.19	-0.04	0.02	0
I_PE_1st_p10_C3	0.04	0.07	-0.01	0.02	**0.38**	0.04	-0.02	1
I_PE_1st_p25_C1	0.03	0.05	0.06	0.04	**0.29**	0.04	0.00	1
I_PE_1st_p25_C2	0.01	0.02	0.06	-0.03	**0.20**	-0.01	0.04	1
I_PE_1st_p25_C3	0.03	0.08	0.01	0.00	**0.36**	0.03	-0.05	1
I_PE_1st_p50_C1	0.02	0.05	0.10	0.05	0.17	0.12	0.00	0
I_PE_1st_p50_C2	0.01	0.03	0.12	-0.02	**0.20**	0.02	0.03	1
I_PE_1st_p50_C3	0.01	0.09	0.03	-0.01	**0.32**	0.05	-0.05	1
I_PE_1st_p75_C1	0.01	0.06	0.09	0.05	0.00	0.15	-0.02	0
I_PE_1st_p75_C2	0.01	0.04	0.12	-0.01	0.12	0.04	0.04	0
I_PE_1st_p75_C3	-0.01	0.08	0.02	-0.04	**0.27**	0.05	-0.05	1
I_PE_1st_p90_C1	0.00	0.03	0.06	0.06	-0.10	0.12	-0.02	0
I_PE_1st_p90_C2	0.01	0.05	0.10	0.02	0.06	0.05	0.06	0
I_PE_1st_p90_C3	-0.02	0.06	0.00	-0.05	**0.21**	0.04	-0.05	1
I_PE_1st_p95_C1	0.00	0.02	0.04	0.05	-0.11	0.11	-0.02	0
I_PE_1st_p95_C2	0.01	0.04	0.10	0.04	0.04	0.07	0.07	0
I_PE_1st_p95_C3	-0.03	0.05	-0.01	-0.06	0.16	0.04	-0.08	0
I_PE_all_p05_C1	0.03	0.03	-0.01	0.08	**0.27**	0.04	0.01	1
I_PE_all_p05_C2	-0.01	-0.01	-0.02	-0.02	0.18	-0.07	-0.02	0

Feature*	All trees	Pinus resinosa	Pinus strobus	Pinus sylvestris	Picea abies	Picea glauca	Larix laricina	Count of correlations ≥ 0.2 or < -0.2
I_PE_all_p05_C3	0.06	0.08	-0.03	0.07	**0.35**	0.07	-0.05	1
I_PE_all_p10_C1	0.04	0.04	0.01	0.09	**0.35**	0.03	0.02	1
I_PE_all_p10_C2	0.00	0.00	0.01	0.00	**0.22**	-0.05	-0.02	1
I_PE_all_p10_C3	0.06	0.09	-0.02	0.07	**0.38**	0.07	-0.04	1
I_PE_all_p25_C1	0.04	0.05	0.02	0.08	**0.40**	0.04	0.00	1
I_PE_all_p25_C2	0.00	0.00	0.03	0.01	**0.30**	-0.03	0.00	1
I_PE_all_p25_C3	0.06	0.10	0.00	0.07	**0.40**	0.08	-0.03	1
I_PE_all_p50_C1	0.02	0.05	0.06	0.06	**0.33**	0.09	-0.03	1
I_PE_all_p50_C2	0.00	0.00	0.09	0.00	**0.31**	-0.02	0.00	1
I_PE_all_p50_C3	0.04	0.12	0.02	0.04	**0.39**	0.08	-0.03	1
I_PE_all_p75_C1	0.01	0.05	0.09	0.06	0.12	0.13	-0.03	0
I_PE_all_p75_C2	0.00	0.02	0.11	0.00	**0.24**	0.03	0.02	1
I_PE_all_p75_C3	0.01	0.11	0.03	0.00	**0.32**	0.08	-0.05	1
I_PE_all_p90_C1	0.00	0.03	0.06	0.06	-0.04	0.13	-0.04	0
I_PE_all_p90_C2	0.01	0.04	0.11	0.02	0.12	0.03	0.04	0
I_PE_all_p90_C3	-0.01	0.08	0.00	-0.03	**0.27**	0.07	-0.05	1
I_PE_all_p95_C1	-0.01	0.01	0.04	0.05	-0.09	0.11	-0.03	0
I_PE_all_p95_C2	0.01	0.04	0.10	0.03	0.08	0.06	0.05	0
I_PE_all_p95_C3	-0.02	0.06	0.00	-0.05	**0.21**	0.05	-0.07	1
I_PE_si_p05_C1	0.00	0.00	0.10	0.02	-0.16	0.02	-0.04	0
I_PE_si_p05_C2	-0.04	-0.03	0.06	-0.07	**-0.21**	-0.12	0.00	1
I_PE_si_p05_C3	-0.11	-0.07	-0.08	-0.15	0.15	**-0.22**	-0.17	1
I_PE_si_p10_C1	0.01	0.02	0.11	0.03	-0.16	0.05	-0.04	0
I_PE_si_p10_C2	-0.03	-0.01	0.08	-0.05	**-0.20**	-0.09	-0.01	1
I_PE_si_p10_C3	-0.11	-0.06	-0.07	-0.15	0.15	-0.20	-0.17	0
I_RCG1_si_mn	-0.10	-0.06	-0.13	-0.07	**0.20**	-0.09	-0.14	1
I_RCG2_1st_mn	-0.03	0.02	-0.08	-0.04	**0.22**	-0.03	-0.01	1
I_RCG2_1st_p50	-0.02	0.02	-0.06	-0.02	0.17	-0.03	-0.01	0
I_RCG2_1st_p75	-0.03	0.02	-0.08	-0.05	**0.23**	-0.04	0.01	1
I_RCG2_1st_p90	-0.04	0.01	-0.08	-0.06	**0.24**	-0.03	0.01	1
I_RCG2_1st_p95	-0.04	0.01	-0.07	-0.05	**0.22**	-0.03	-0.02	1
I_RCG2_all_mn	0.00	0.05	-0.06	-0.02	**0.21**	0.01	0.01	1

Feature*	All trees	Pinus resinosa	Pinus strobus	Pinus sylvestris	Picea abies	Picea glauca	Larix laricina	Count of correlations ≥ 0.2 or < -0.2
I_RCG2_all_p50	0.01	0.04	-0.04	0.00	0.11	0.00	0.03	0
I_RCG2_all_p75	-0.01	0.04	-0.07	-0.01	**0.22**	0.01	0.03	1
I_RCG2_all_p90	-0.02	0.03	-0.08	-0.05	**0.25**	-0.01	0.04	1
I_RCG2_all_p95	-0.03	0.03	-0.06	-0.05	**0.24**	-0.01	0.00	1
I_RCG2_si_mn	-0.09	-0.04	-0.12	-0.12	**0.23**	-0.16	-0.08	1
I_RCG2_si_p50	-0.09	-0.04	-0.10	-0.11	**0.23**	-0.17	-0.07	1
I_RCG2_si_p75	-0.07	-0.02	-0.09	-0.09	**0.22**	-0.10	-0.01	1
I_RCG2_si_p90	-0.06	-0.02	-0.07	-0.09	0.20	-0.07	-0.02	0
I_RCG2_si_p95	-0.06	-0.01	-0.07	-0.08	0.18	-0.06	-0.02	0
I_RM_1st_mn_all_mn_C1	0.01	0.01	0.06	-0.04	**-0.24**	0.00	0.05	1
I_RM_1st_mn_all_mn_C2	0.03	0.05	0.02	-0.05	**-0.27**	0.04	0.11	1
I_RM_1st_mn_all_mn_C3	-0.11	-0.10	0.01	-0.17	**-0.27**	-0.14	-0.03	1
Count of correlations ≥ 0.2 or < -0.2	0	0	0	0	89	1	0	90

*Individual channel intensity features which did not have a correlation value larger than |±0.2| with the mean scan angle in all the three channels and for all species are not presented in the table. They are listed here : DI_1st_kurt, DI_all_kurt, DI_all_sd, DI_si_cv, DI_si_kurt, DI_si_sd, DI_si_skew, IR_all_lm, IR_si_lm, IR_all_sd, IR_si_lm , IR_si_sd, MI_si_10_90_mn, MI_si_10_90_n_mn, MI_si_5_95_mn, MI_si_5_95_n_mn, MI_si_mn, PE_si_p25, PE_si_p50, PE_si_p75, PE_si_p90, PE_si_p95. The normalized indices NDG1 and NDIR, and the ratio RCIR had no correlation value larger than |±0.2| to the mean scan angle for any combinations of return type (all, si, 1st) and statistic (mn, p50, p75, p90, p95). The same applies for RCG1, except for the combination si_mn.

Table B.4 : Comparison of the classification accuracy capability of different feature categories as a function of scan angle class .

Features	Normalization	Channel	No of features	Overall accuracy	Accuracy in class angle 1	Accuracy in class angle 2	Accuracy in class angle 3
3D	N.O.	C1	64	0.60	0.61	0.60	0.58
3D	N.O.	C2	64	0.61	0.61	0.63	0.58
3D	N.O.	C3	64	0.59	0.60	0.57	0.64
3D	N.O.	C321	64	0.64	0.63	0.65	0.61
Intensity	raw	C1	53	0.54	0.51	0.58	0.53
Intensity	raw	C2	53	0.43	0.44	0.44	0.40
Intensity	raw	C3	53	0.58	0.56	0.60	0.59
Intensity	raw	C1_C2	30	0.40	0.41	0.40	0.40
Intensity	raw	C1_C3	30	0.37	0.39	0.36	0.36
Intensity	raw	C2_C3	30	0.50	0.49	0.53	0.47
Intensity	normalized	C1	53	0.64	0.64	0.68	0.58
Intensity	normalized	C2	53	0.52	0.52	0.54	0.48
Intensity	normalized	C3	53	0.64	0.64	0.64	0.61
Intensity	normalized	C1_C2	30	0.40	0.42	0.40	0.40
Intensity	normalized	C1_C3	30	0.37	0.38	0.35	0.36
Intensity	normalized	C2_C3	30	0.51	0.50	0.53	0.47
Intensity	raw	all	249	0.75	0.75	0.77	0.72
Intensity	normalized	all	249	0.79	0.78	0.81	0.76
3D + Intensity	raw	all	505	0.83	0.82	0.84	0.82
3D + Intensity	normalized	all	505	**0.85**	**0.84**	**0.86**	**0.83**

BIBLIOGRAPHIE

Ahokas, E., et al. (2016). Towards automatic single-sensor mapping by multispectral airborne laser scanning. Dans L. Halounova, et al. (dir.), 23rd International Archives of the Photogrammetry, Remote Sensing and Spatial Information Sciences Congress, ISPRS 2016, (p. 155-162). International Society for Photogrammetry and Remote Sensing. doi: 10.5194/isprsarchives-XLI-B3-155-2016

Arumäe, T. et M. Lang. (2018). Estimation of canopy cover in dense mixed-species forests using airborne lidar data. *European Journal of Remote Sensing*, 51 (1), 132-141. 10.1080/22797254.2017.1411169

Asner, G. P. (1998). Biophysical and Biochemical Sources of Variability in Canopy Reflectance. *Remote Sensing of Environment*, 64 (3), 234-253. http://dx.doi.org/10.1016/S0034-4257(98)00014-5

Asner, G. P., et al. (2014). Functional and biological diversity of foliar spectra in tree canopies throughout the Andes to Amazon region. *New Phytologist*, 204 (1), 127-139. 10.1111/nph.12895

Avery, T. E. (1978). Forester's guide to aerial photo interpretation. Agriculture Handbook, U.S. Department of Agriculture, Forest Service. 308

Axelsson, A., et al. (2018). Exploring Multispectral ALS Data for Tree Species Classification. *Remote Sensing*, 10 (2), 183-198. doi:10.3390/rs10020183

Bakuła, K., et al. (2016). Testing of land cover classification from multispectral airborne laser scanning data. *Int. Arch. Photogramm. Remote Sens. Spatial Inf. Sci.*, XLI-B7, 161-169. 10.5194/isprs-archives-XLI-B7-161-2016

Baldeck, C. A. et G. P. Asner. (2014). Improving remote species identification through efficient training data collection. *Remote Sensing*, 6 (4), 2682-2698.

Bater, C. W., et al. (2011). Stability of sample-based scanning-LiDAR-derived vegetation metrics for forest monitoring. *IEEE Transactions on Geoscience and Remote Sensing*, 49 (6 PART 2), 2385-2392. 10.1109/TGRS.2010.2099232

Beaudoin, A., et al. (2014). Mapping attributes of Canada's forests at moderate resolution through kNN and MODIS imagery. *Canadian Journal of Forest Research*, 44 (5), 521-532. 10.1139/cjfr-2013-0401

Belgiu, M. et L. Drăguţ. (2016). Random forest in remote sensing: A review of applications and future directions. *ISPRS Journal of Photogrammetry and Remote Sensing*, 114, 24-31.

Berger, J.-P., et al. (2015). Norme de stratification écoforestière. Quatrième inventaire écoforestier du Québec méridional

Beucher, S. et F. Meyer. (1993). The Morphological Approach to Segmentation: The Watershed Transformation [Chapitre de livre]. Dans E. R. Dougherty (dir.), *Mathematical Morphology in Image Processing* (p. 433-482). New York, Basel, Hong Kong: Marcel Dekker

Blair, J. B. et M. A. Hofton. (1999). Modeling laser altimeter return waveforms over complex vegetation using high-resolution elevation data. *Geophysical Research Letters*, 26 (16), 2509-2512.

Blomley, R., et al. (2017). Tree species classification using within crown localization of waveform LiDAR attributes. *ISPRS Journal of Photogrammetry and Remote Sensing*, 133, 142-156. https://doi.org/10.1016/j.isprsjprs.2017.08.013

Bolyn, C., et al. (2018). Forest mapping and species composition using supervised per pixel classification of sentinel-2 imagery. *Biotechnology, Agronomy and Society and Environment*, 22 (3), 172-187.

Bradbury, R. B., et al. (2005). Modelling relationships between birds and vegetation structure using airborne LiDAR data: A review with case studies from agricultural and woodland environments. *Ibis*, 147 (3), 443-452. 10.1111/j.1474-919x.2005.00438.x

Brandtberg, T. (2007). Classifying individual tree species under leaf-off and leaf-on conditions using airborne lidar. *ISPRS Journal of Photogrammetry and Remote Sensing*, 61 (5), 325-340. 10.1016/j.isprsjprs.2006.10.006

Brandtberg, T., et al. (2003). Detection and analysis of individual leaf-off tree crowns in small footprint, high sampling density lidar data from the eastern deciduous forest in North America. *Remote Sensing of Environment*, 85 (3), 290-303. 10.1016/S0034-4257(03)00008-7

Breiman, L. (2001). Random forests. *Machine Learning*, 45 (1), 5-32. 10.1023/A:1010933404324

Brosofske, K. D., et al. (2014). A review of methods for mapping and prediction of inventory attributes for operational forest management. *Forest Science*, 60 (4), 733-756. 10.5849/forsci.12-134

Budei, B. C. et B. St-Onge. (2018). Variability of multispectral lidar 3D and intensity features with individual tree height and its influence on needleleaf tree species identification. *Canadian Journal of Remote Sensing*, 44 (4), 263-286. 10.1080/07038992.2018.1478724

Budei, B. C., et al. (2018). Identifying the genus or species of individual trees using a three-wavelength airborne lidar system. *Remote Sensing of Environment*, 204, 632-647. https://doi.org/10.1016/j.rse.2017.09.037

Cao, L., et al. (2016). Tree species classification in subtropical forests using small-footprint full-waveform LiDAR data. *International Journal of Applied Earth Observation and Geoinformation*, 49, 39-51. https://doi.org/10.1016/j.jag.2016.01.007

Chasmer, L., et al. (2006). Examining the influence of changing laser pulse repetition frequencies on conifer forest canopy returns. *Photogrammetric Engineering and Remote Sensing*, 72 (12), 1359-1367. Récupéré de http://www.scopus.com/inward/record.url?eid=2-s2.0-33845381872&partnerID=40&md5=f6b3a65bc3269a22a702e1757ce1507b

Chen, C., et al. (2004). Using Random Forest to Learn Imbalanced Data. [Document électronique], Récupéré de http://www.stat.berkeley.edu/tech-reports/666.pdf

Chen, J. M. et S. G. Leblanc. (1997). Four-scale bidirectional reflectance model based on canopy architecture. *IEEE Transactions on Geoscience and Remote Sensing*, 35 (5), 1316-1337.

Chen, Y., et al. (2010). Two-channel hyperspectral LiDAR with a supercontinuum laser source. *Sensors*, 10 (7), 7057-7066. 10.3390/s100707057

City of Toronto. (2010). Every Tree Counts. A Portrait of Toronto's Urban Forest. Récupéré de http://www.yumpu.com/en/document/view/30028908/every-tree-counts-a-portrait-of-torontos-urban-forest-i-tree

Coren, F. et P. Sterzai. (2006). Radiometric correction in laser scanning. *International Journal of Remote Sensing*, 27 (15), 3097-3104. 10.1080/01431160500217277

Dalponte, M., et al. (2012). Tree species classification in the Southern Alps based on the fusion of very high geometrical resolution multispectral/hyperspectral images and LiDAR data. *Remote Sensing of Environment*, 123, 258-270. 10.1016/j.rse.2012.03.013

Dalponte, M., et al. (2014). Tree crown delineation and tree species classification in boreal forests using hyperspectral and ALS data. *Remote Sensing of Environment*, 140, 306-317. 10.1016/j.rse.2013.09.006

Deng, S., et al. (2016). Comparison of tree species classifications at the individual tree level by combining ALS data and RGB images using different algorithms. *Remote Sensing*, 8 (12) 10.3390/rs8121034

Dinuls, R., et al. (2012). Tree species identification in mixed baltic forest using LiDAR and multispectral data. *IEEE Journal of Selected Topics in Applied Earth Observations and Remote Sensing*, 5 (2), 594-603. 10.1109/JSTARS.2012.2196978

Disney, M. I., et al. (2010). Simulating the impact of discrete-return lidar system and survey characteristics over young conifer and broadleaf forests. *Remote Sensing of Environment*, 114 (7), 1546-1560. 10.1016/j.rse.2010.02.009

Eid, T., et al. (2004). Comparing stand inventories for large areas based on photo-interpretation and laser scanning by means of cost-plus-loss analyses. *Scandinavian Journal of Forest Research*, 19 (6), 512-523.

Falkowski, M. J., et al. (2010). Landscape-scale parameterization of a tree-level forest growth model: A k-nearest neighbor imputation approach incorporating LiDAR data. *Canadian Journal of Forest Research*, 40 (2), 184-199. 10.1139/X09-183

Fang, F., et al. (2018). Combining high spatial resolution multi-temporal satellite data with leaf-on LiDAR to enhance tree species discrimination at the crown level. *International Journal of Remote Sensing*, 1-19. 10.1080/01431161.2018.1504343

Farrar, J. L. (1995). *Trees in Canada*. Ottawa: Fitzhenry & Whiteside Ltd.

Fassnacht, F. E., et al. (2016). Review of studies on tree species classification from remotely sensed data. *Remote Sensing of Environment*, 186, 64-87. http://dx.doi.org/10.1016/j.rse.2016.08.013

Felbermeier, B., et al. (2010). Study on user requirements for remote sensing applications in forestry. Dans B. Szekely et W. Wagner (dir.), ISPRS Technical Commission VII Symposium on Advancing Remote Sensing Science, (p. 210-212). International Society for Photogrammetry and Remote Sensing

Fernández-Delgado, M., et al. (2014). Do we need hundreds of classifiers to solve real world classification problems? *Journal of Machine Learning Research*, 15, 3133-3181.

Fernandez-Diaz, J. C., et al. (2016). Capability Assessment and Performance Metrics for the Titan Multispectral Mapping Lidar. *Remote Sensing*, 8 (11), 936-969. doi:10.3390/rs8110936

Fricker, G. A., et al. (2019). A convolutional neural network classifier identifies tree species in mixed-conifer forest from hyperspectral imagery. *Remote Sensing*, 11 (19) 10.3390/rs11192326

García, M., et al. (2010). Estimating biomass carbon stocks for a Mediterranean forest in central Spain using LiDAR height and intensity data. *Remote Sensing of Environment*, 114 (4), 816-830.

Gatziolis, D. (2011). Dynamic range-based intensity normalization for airborne, discrete return lidar data of forest canopies. *Photogrammetric Engineering and Remote Sensing*, 77 (3), 251-259.

Gaulton, R., et al. (2013). The potential of dual-wavelength laser scanning for estimating vegetation moisture content. *Remote Sensing of Environment*, 132, 32-39.

Gaveau, D. L. A. et R. A. Hill. (2003). Quantifying canopy height underestimation by laser pulse penetration in small-footprint airborne laser scanning data. *Canadian Journal of Remote Sensing*, 29 (5), 650-657.

Ghosh, A., et al. (2014). A framework for mapping tree species combining hyperspectral and LiDAR data: Role of selected classifiers and sensor across three spatial scales. *International Journal of Applied Earth Observation and Geoinformation*, 26, 49-63. http://dx.doi.org/10.1016/j.jag.2013.05.017

Gobakken, T. et E. Næsset. (2008). Assessing effects of laser point density, ground sampling intensity, and field sample plot size on biophysical stand properties derived from airborne laser scanner data. *Canadian Journal of Forest Research*, 38 (5), 1095-1109.

Goetz, S., et al. (2007). Laser remote sensing of canopy habitat heterogeneity as a predictor of bird species richness in an eastern temperate forest, USA. *Remote Sensing of Environment*, 108 (3), 254-263.

Gong, W., et al. (2015). Investigating the potential of using the spatial and spectral information of multispectral LiDAR for object classification. *Sensors (Switzerland)*, 15 (9), 21989-22002. 10.3390/s150921989

Goodwin, N. R., et al. (2006). Assessment of forest structure with airborne LiDAR and the effects of platform altitude. *Remote Sensing of Environment*, 103 (2), 140-152. 10.1016/j.rse.2006.03.003

Goodwin, N. R., et al. (2007). Development of a simulation model to predict LiDAR interception in forested environments. *Remote Sensing of Environment*, 111 (4), 481-492.

Gorgens, E. B., et al. (2017). A method for optimizing height threshold when computing airborne laser scanning metrics. *Photogrammetric Engineering and Remote Sensing*, 83 (5), 343-350. 10.14358/PERS.83.5.343

Guenther, G. C. (1985). Airborne laser hydrography: System design and performance factors. NOAA Professional Paper Series. Rockville, MD, National Ocean Service 1, National Oceanic and Atmospheric Administration

Hakala, T., et al. (2015). Technical Note: Multispectral lidar time series of pine canopy chlorophyll content. *Biogeosciences*, 12 (5), 1629-1634. 10.5194/bg-12-1629-2015

Hakala, T., et al. (2012). Full waveform hyperspectral LiDAR for terrestrial laser scanning. *Optics Express*, 20 (7), 7119-7127. 10.1364/OE.20.007119

Hallé, F., et al. (1978). *Tropical trees and forests, An architectural analysis*. New-York: Springer-Verlag.

Hamraz, H., et al. (2017). Forest understory trees can be segmented accurately within sufficiently dense airborne laser scanning point clouds. *Scientific Reports*, 7 (1) 10.1038/s41598-017-07200-0

Harikumar, A., et al. (2017). An internal crown geometric model for conifer species classification with high-density LiDAR Data. *IEEE Transactions on Geoscience and Remote Sensing*, 55 (5), 2924-2940. 10.1109/TGRS.2017.2656152

Heikkinen, V., et al. (2011). An SVM classification of tree species radiometric signatures based on the Leica ADS40 sensor. *IEEE Transactions on Geoscience and Remote Sensing*, 49 (11 PART 2), 4539-4551. 10.1109/TGRS.2011.2141143

Heinzel, J. et B. Koch. (2011). Exploring full-waveform LiDAR parameters for tree species classification. *International Journal of Applied Earth Observation and Geoinformation*, 13 (1), 152-160.

Heinzel, J. et B. Koch. (2012). Investigating multiple data sources for tree species classification in temperate forest and use for single tree delineation. *International Journal of Applied Earth Observation and Geoinformation*, 18 (1), 101-110. 10.1016/j.jag.2012.01.025

Heller, R. C., et al. (1964). Identification of tree species on large-scale panchromatic and color aerial photographs. Agriculture Handbook, U.S. Department of Agriculture, Forest Service. 261

Hershey, R. R. et W. A. Befort (1995). Aerial photo guide to New England forest cover types. General Technical Report. Radnor, PA, U. S. Department of Agriculture

Hollaus, M., et al. (2009). Tree species classification based on full-waveform airborne laser scanning data*.* Silvilaser 2009, Texas, USA, October 14-16, 2009.

Holmgren, J., et al. (2003a). Estimation of tree height and stem volume on plots using airborne laser scanning. *Forest Science*, 49 (3), 419-428.

--------. (2003b). Simulating the effects of lidar scanning angle for estimation of mean tree height and canopy closure. *Canadian Journal of Remote Sensing*, 29 (5), 623-632.

Holmgren, J. et Å. Persson. (2004). Identifying species of individual trees using airborne laser scanner. *Remote Sensing of Environment*, 90 (4), 415-423. 10.1016/S0034-4257(03)00140-8

Holmgren, J., et al. (2008). Species identification of individual trees by combining high resolution LiDAR data with multi-spectral images. *International Journal of Remote Sensing*, 29 (5), 1537-1552.

Hopkinson, C. (2007). The influence of flying altitude, beam divergence, and pulse repetition frequency on laser pulse return intensity and canopy frequency distribution. *Canadian Journal of Remote Sensing*, 33 (1-4), 312-324.

Hopkinson, C. et L. Chasmer. (2009). Testing LiDAR models of fractional cover across multiple forest ecozones. *Remote Sensing of Environment*, 113 (1), 275-288.

Hopkinson, C., et al. (2016). Multisensor and Multispectral LiDAR Characterization and Classification of a Forest Environment. *Canadian Journal of Remote Sensing*, 42 (5), 501-520.

Hovi, A., et al. (2016). LiDAR waveform features for tree species classification and their sensitivity to tree- and acquisition related parameters. *Remote Sensing of Environment*, 173, 224-237. http://dx.doi.org/10.1016/j.rse.2015.08.019

Hu, B. (2016). Improving individual tree delineation using mulriple-wavelength lidar data. 2016 IEEE International Geoscience and Remote Sensing Symposium (IGARSS), 10-15 July 2016, (p. 3182-3185). doi: 10.1109/IGARSS.2016.7729823

Hudak, A. T., et al. (2016). Mapping Forest Structure and Composition from Low-Density LiDAR for Informed Forest, Fuel, and Fire Management at Eglin Air Force Base, Florida, USA. *Canadian Journal of Remote Sensing*, 42 (5), 411-427. 10.1080/07038992.2016.1217482

Hudak, A. T., et al. (2006). Regression modeling and mapping of coniferous forest basal area and tree density from discrete-return lidar and multispectral satellite data. *Canadian Journal of Remote Sensing*, 32 (2), 126-138.

Hughes, G. (1968). On the mean accuracy of statistical pattern recognizers. *IEEE Transactions on Information Theory*, 14 (1), 55-63. 10.1109/TIT.1968.1054102

Hyyppä, J. et M. Inkinen. (1999). Detecting and estimating attributes for single trees using laser scanner. *The photogrammetric journal of Finland*, 16 (2), 27-42.

Hyyppä, J., et al. (2001). A segmentation-based method to retrieve stem volume estimates from 3-D tree height models produced by laser scanners. *IEEE Transactions on Geoscience and Remote Sensing*, 39 (5), 969-975.

Immitzer, M., et al. (2012). Tree species classification with Random forest using very high spatial resolution 8-band worldView-2 satellite data. *Remote Sensing*, 4 (9), 2661-2693. 10.3390/rs4092661

Irish, J. L. et W. J. Lillycrop. (1999). Scanning laser mapping of the coastal zone: the SHOALS system. *ISPRS Journal of Photogrammetry and Remote Sensing*, 54 (2), 123-129. https://doi.org/10.1016/S0924-2716(99)00003-9

Isenburg, M. (2014). LAStools - efficient LiDAR processing software (version 141017, unlicensed). [Document électronique].

Jelalian, A. V. (1992). *Laser radar systems*. Boston: Artech House.

Jenkins, J. C., et al. (2003). National-scale biomass estimators for United States tree species. *Forest Science*, 49 (1), 12-35.

Jones, T. G., et al. (2010). Assessing the utility of airborne hyperspectral and LiDAR data for species distribution mapping in the coastal Pacific Northwest, Canada.

Remote Sensing of Environment, 114 (12), 2841-2852. https://doi.org/10.1016/j.rse.2010.07.002

Kaasalainen, S., et al. (2009). Radiometric calibration of LIDAR intensity with commercially available reference targets. *IEEE Transactions on Geoscience and Remote Sensing*, 47 (2), 588-598. 10.1109/tgrs.2008.2003351

Kaasalainen, S., et al. (2011). Absolute radiometric calibration of ALS intensity data: Effects on accuracy and target classification. *Sensors*, 11 (11), 10586-10602. 10.3390/s111110586

Kashani, A. G., et al. (2015). A review of LIDAR radiometric processing: From ad hoc intensity correction to rigorous radiometric calibration. *Sensors (Switzerland)*, 15 (11), 28099-28128. 10.3390/s151128099

Kim, S. (2010). LIDAR-based species classification using multivariate cluster analysis. American Society for Photogrammetry and Remote Sensing Annual Conference 2010: Opportunities for Emerging Geospatial Technologies, San Diego, CA, (p. 405-416).

Kim, S., et al. (2011). Classifying individual tree genera using stepwise cluster analysis based on height and intensity metrics derived from airborne laser scanner data. *Remote Sensing of Environment*, 115 (12), 3329-3342. 10.1016/j.rse.2011.07.016

Kim, S., et al. (2009). Tree species differentiation using intensity data derived from leaf-on and leaf-off airborne laser scanner data. *Remote Sensing of Environment*, 113 (8), 1575-1586.

Ko, C., et al. (2012). Mapping tree genera using discrete LiDAR and geometric tree metrics. *Bosque*, 33 (3), 313-319. 10.4067/S0717-92002012000300015

Ko, C., et al. (2013). Tree genera classification with geometric features from high-density airborne LiDAR. *Canadian Journal of Remote Sensing*, 39 (SUPPL.1), S73-S85.

Koch, B. (2010). Status and future of laser scanning, synthetic aperture radar and hyperspectral remote sensing data for forest biomass assessment. *ISPRS Journal of Photogrammetry and Remote Sensing*, 65 (6), 581-590. http://dx.doi.org/10.1016/j.isprsjprs.2010.09.001

Koch, B., et al. (2006). Detection of individual tree crowns in airborne lidar data. *Photogrammetric Engineering and Remote Sensing*, 72 (4), 357-363.

Koenig, K. et B. Höfle. (2016). Full-waveform airborne laser scanning in vegetation studies-A review of point cloud and waveform features for tree species classification. *Forests*, 7 (9) 10.3390/f7090198

Korhonen, L., et al. (2011). Airborne discrete-return LIDAR data in the estimation of vertical canopy cover, angular canopy closure and leaf area index. *Remote Sensing of Environment*, 115 (4), 1065-1080. 10.1016/j.rse.2010.12.011

Korhonen, L. et F. Morsdorf. (2014). Estimation of canopy cover, gap fraction and leaf area index with airborne laser scanning [Chapitre de livre]. Dans M. Maltamo, et al. (dir.), *Forestry applications of airborne laser scanning: Concepts and case studies* (p. 397–417). Dordrecht: Springer

Korpela, I., et al. (2010a). Range and AGC normalization in airborne discrete-return LiDAR intensity data for forest canopies. *ISPRS Journal of Photogrammetry and Remote Sensing*, 65 (4), 369-379. 10.1016/j.isprsjprs.2010.04.003

Korpela, I., et al. (2010b). Tree species classification using airborne LiDAR - effects of stand and tree parameters, downsizing of training set, intensity normalization, and sensor type. *Silva Fennica*, 44 (2), 319-339.

Korpela, I., et al. (2009). Small-footprint discrete-return lidar in tree species recognition. Dans C. Heipke, Jacobsen,K., Müller,S., Sörgel,U. (dir.), ISPRS Hannover Workshop 2009, High-Resolution Earth Imaging for Geospatial Information, Hannover, Germany, June 2-5, 2009. Récupéré de http://www.isprs.org/proceedings/XXXVIII/1_4_7-W5/paper/Korpela-137.pdf

Koukoulas, S. et G. A. Blackburn. (2005). Mapping individual tree location, height and species in broadleaved deciduous forest using airborne LIDAR and multi-spectral remotely sensed data. *International Journal of Remote Sensing*, 26 (3), 431-455. 10.1080/0143116042000298289

Kukkonen, M., et al. (2019a). Comparison of multispectral airborne laser scanning and stereo matching of aerial images as a single sensor solution to forest inventories by tree species. *Remote Sensing of Environment*, 231, 111208. https://doi.org/10.1016/j.rse.2019.05.027

Kukkonen, M., et al. (2019b). Multispectral Airborne LiDAR Data in the Prediction of Boreal Tree Species Composition. *IEEE Transactions on Geoscience and Remote Sensing*, 57 (6), 3462-3471. 10.1109/TGRS.2018.2885057

Lambert, M. C., et al. (2005). Canadian national tree aboveground biomass equations. *Canadian Journal of Forest Research*, 35 (8), 1996-2018.

Larcher, W. (2003). *Physiological plant ecology*, 4th. Berlin: Springer.

Latifi, H., et al. (2015). Forest inventories by LiDAR data: A comparison of single tree segmentation and metric-based methods for inventories of a heterogeneous temperate forest. *International Journal of Applied Earth Observation and Geoinformation*, 42, 162-174. 10.1016/j.jag.2015.06.008

Leckie, D. G., et al. (1998). Computer-assisted photointerpretation aids to forest inventory mapping: Some possible approaches. Proceedings of the International Forum on Automated Interpretation of High Spatial Resolution Digital Imagery for Forestry, (p. 10-12).

Leckie, D. G., et al. (2017). Production of a Large-Area Individual Tree Species Map for Forest Inventory in a Complex Forest Setting and Lessons Learned. *Canadian Journal of Remote Sensing*, 43 (2), 140-167. 10.1080/07038992.2017.1286974

Lee, H., et al. (2010). Adaptive clustering of airborne LiDAR data to segment individual tree crowns in managed pine forests. *International Journal of Remote Sensing*, 31 (1), 117-139.

Li, J., et al. (2013). Classification of tree species based on structural features derived from high density LiDAR data. *Agricultural and Forest Meteorology*, 171-172, 104-114. 10.1016/j.agrformet.2012.11.012

Li, J., et al. (2010). Individual tree species classification using structure features from high density airborne LiDAR data. International Geoscience and Remote Sensing Symposium (IGARSS), Honolulu, HI, 25-30 July, (p. 2099-2102). doi: 10.1109/IGARSS.2010.5651629

Liaw, A. et M. Wiener. (2002). Classification and regression by randomForest. *R News*, 2 (3), 18-22. Récupéré de http://www.bios.unc.edu/~dzeng/BIOS740/randomforest.pdf

Lim, K., et al. (2008). Examining the effects of sampling point densities on laser canopy height and density metrics. *Forestry Chronicle*, 84 (6), 876-885.

Lin, Y. et J. Hyyppä. (2016). A comprehensive but efficient framework of proposing and validating feature parameters from airborne LiDAR data for tree species classification. *International Journal of Applied Earth Observation and Geoinformation*, 46, 45-55. https://doi.org/10.1016/j.jag.2015.11.010

Lindberg, E., et al. (2014). Delineation of tree crowns and tree species classification from full-waveform airborne laser scanning data using 3-d ellipsoidal clustering. *IEEE Journal of Selected Topics in Applied Earth Observations and Remote Sensing*, 7 (7), 3174-3181. 10.1109/JSTARS.2014.2331276

Lindberg, E. et J. Holmgren. (2017). Individual Tree Crown Methods for 3D Data from Remote Sensing. *Current Forestry Reports*, 3 (1), 19-31. 10.1007/s40725-017-0051-6

Liu, J., et al. (2018a). Large off-nadir scan angle of airborne LiDAR can severely affect the estimates of forest structure metrics. *ISPRS Journal of Photogrammetry and Remote Sensing*, 136, 13-25. 10.1016/j.isprsjprs.2017.12.004

Liu, L., et al. (2017). Mapping urban tree species using integrated airborne hyperspectral and LiDAR remote sensing data. *Remote Sensing of Environment*, 200, 170-182. https://doi.org/10.1016/j.rse.2017.08.010

Liu, Y., et al. (2018b). Forest type identification with random forest using Sentinel-1A, Sentinel-2A, multi-temporal Landsat-8 and DEM data. *Remote Sensing*, 10 (6) 10.3390/rs10060946

Lovell, J. L., et al. (2005). Simulation study for finding optimal lidar acquisition parameters for forest height retrieval. *Forest Ecology and Management*, 214 (1-3), 398-412.

Magnussen, S. et P. Boudewyn. (1998). Derivations of stand heights from airborne laser scanner data with canopy-based quantile estimators. *Canadian Journal of Forest Research*, 28 (7), 1016-1031.

Maltamo, M., et al. (2004). The accuracy of estimating individual tree variables with airborne laser scanning in a boreal nature reserve. *Canadian Journal of Forest Research*, 34 (9), 1791-1801.

Maltamo, M., et al. (2007). Comparison of basal area and stem frequency diameter distribution modelling using airborne laser scanner data and calibration estimation. *Forest Ecology and Management*, 247 (1-3), 26-34.

Marrs, J. et W. Ni-Meister. (2019). Machine Learning Techniques for Tree Species Classification Using Co-Registered LiDAR and Hyperspectral Data. *Remote Sensing*, 11 (7), 819. Récupéré de http://www.mdpi.com/2072-4292/11/7/819

Matikainen, L., et al. (2016). Multispectral airborne laser scanning for automated map updating. Dans L. Halounova, et al. (dir.), 23rd International Archives of the Photogrammetry, Remote Sensing and Spatial Information Sciences Congress, ISPRS 2016, (p. 323-330). International Society for Photogrammetry and Remote Sensing. doi: 10.5194/isprsarchives-XLI-B3-323-2016

McKenney, D. W., et al. (2003). Opportunities for improved risk assessments of exotic species in Canada using bioclimatic modeling. *Environmental Monitoring and Assessment*, 88 (1-3), 445-461. 10.1023/A:1025502030803

Messier, C., et al. (1999). Functional ecology of advance regeneration in relation to light in boreal forests. *Canadian Journal of Forest Research*, 29 (6), 812-823.

Millet, J. (2012). *L'architecture des arbres des régions tempérées : son histoire, ses concepts, ses usages*. Quebec: MultiMondes.

Moffiet, T., et al. (2005). Airborne laser scanning: Exploratory data analysis indicates potential variables for classification of individual trees or forest stands according to species. *ISPRS Journal of Photogrammetry and Remote Sensing*, 59 (5), 289-309.

Montaghi, A. (2013). Effect of scanning angle on vegetation metrics derived from a nationwide Airborne Laser Scanning acquisition. *Canadian Journal of Remote Sensing*, 39 (SUPPL.1), S152-S173. 10.5589/m13-052

Morsdorf, F., et al. (2008). Assessment of the influence of flying altitude and scan angle on biophysical vegetation products derived from airborne laser scanning. *International Journal of Remote Sensing*, 29 (5), 1387-1406.

Morsdorf, F., et al. (2009). Assessing forest structural and physiological information content of multi-spectral LiDAR waveforms by radiative transfer modelling. *Remote Sensing of Environment*, 113 (10), 2152-2163. 10.1016/j.rse.2009.05.019

Morsy, S., et al. (2016). Airborne multispectral LiDAR data for land-cover classification and land/water mapping using different spectral indexes. *ISPRS Ann. Photogramm. Remote Sens. Spatial Inf. Sci.*, III-3, 217-224. 10.5194/isprs-annals-III-3-217-2016

Mutlu, M., et al. (2008). Mapping surface fuel models using lidar and multispectral data fusion for fire behavior. *Remote Sensing of Environment*, 112 (1), 274-285.

Næsset, E. (1997). Determination of mean tree height of forest stands using airborne laser scanner data. *ISPRS Journal of Photogrammetry and Remote Sensing*, 52 (2), 49-56.

--------. (2004). Effects of different flying altitudes on biophysical stand properties estimated from canopy height and density measured with a small-footprint airborne scanning laser. *Remote Sensing of Environment*, 91 (2), 243-255.

--------. (2009). Effects of different sensors, flying altitudes, and pulse repetition frequencies on forest canopy metrics and biophysical stand properties derived from small-footprint airborne laser data. *Remote Sensing of Environment*, 113 (1), 148-159.

--------. (2011). Estimating above-ground biomass in young forests with airborne laser scanning. *International Journal of Remote Sensing*, 32 (2), 473-501. 10.1080/01431160903474970

Næsset, E. et K. O. Bjerknes. (2001). Estimating tree heights and number of stems in young forest stands using airborne laser scanner data. *Remote Sensing of Environment*, 78 (3), 328-340.

Næsset, E., et al. (2004). Laser scanning of forest resources: The nordic experience. *Scandinavian Journal of Forest Research*, 19 (6), 482-499.

Næsset, E. et T. Økland. (2002). Estimating tree height and tree crown properties using airborne scanning laser in a boreal nature reserve. *Remote Sensing of Environment*, 79 (1), 105-115.

Naveed, F. et B. Hu. (2017). Individual tree crown delineation using multi-wavelength titan LiDAR data. Dans E. Honkavaara, et al. (dir.), International Archives of the Photogrammetry, Remote Sensing and Spatial Information Sciences - ISPRS Archives, (p. 143-148). International Society for Photogrammetry and Remote Sensing. doi: 10.5194/isprs-archives-XLII-3-W3-143-2017

Nevalainen, O., et al. (2014). Fast and nondestructive method for leaf level chlorophyll estimation using hyperspectral LiDAR. *Agricultural and Forest Meteorology*, 198, 250-258. 10.1016/j.agrformet.2014.08.018

Nilsson, M. (1996). Estimation of tree heights and stand volume using an airborne lidar system. *Remote Sensing of Environment*, 56 (1), 1-7.

Okhrimenko, M., et al. (2019). Multi-spectral lidar: Radiometric calibration, canopy spectral reflectance, and vegetation vertical SVI profiles. *Remote Sensing*, 11 (13) 10.3390/rs11131556

Okhrimenko, M. et C. Hopkinson. (2019). Investigating the consistency of uncalibrated multispectral lidar vegetation indices at different altitudes. *Remote Sensing*, 11 (13) 10.3390/rs11131531

Ørka, H. O., et al. (2013). Characterizing forest species composition using multiple remote sensing data sources and inventory approaches. *Scandinavian Journal of Forest Research*, 28 (7), 677-688. 10.1080/02827581.2013.793386

Ørka, H. O., et al. (2012). Simultaneously acquired airborne laser scanning and multispectral imagery for individual tree species identification. *Canadian Journal of Remote Sensing*, 38 (2), 125-138. 10.5589/m12-021

Ørka, H. O., et al. (2009). Classifying species of individual trees by intensity and structure features derived from airborne laser scanner data. *Remote Sensing of Environment*, 113 (6), 1163-1174.

Ørka, H. O., et al. (2010). Effects of different sensors and leaf-on and leaf-off canopy conditions on echo distributions and individual tree properties derived from airborne laser scanning. *Remote Sensing of Environment*, 114 (7), 1445-1461. 10.1016/j.rse.2010.01.024

Packalén, P. et M. Maltamo. (2008). Estimation of species-specific diameter distributions using airborne laser scanning and aerial photographs. *Canadian Journal of Forest Research*, 38 (7), 1750-1760.

Pang, Y., et al. (2011). Impact of footprint diameter and off-nadir pointing on the precision of canopy height estimates from spaceborne lidar. *Remote Sensing of Environment*, 115 (11), 2798-2809. 10.1016/j.rse.2010.08.025

Pant, P., et al. (2013). Evaluation of simulated bands in airborne optical sensors for tree species identification. *Remote Sensing of Environment*, 138, 27-37. https://doi.org/10.1016/j.rse.2013.07.016

Parkan, M. J. 2019. « Combined use of airborne laser scanning and hyperspectral imaging for forest inventories ». Trad. de: *eng*. EPFL.

Perron, R. 2018. « Identification automatisée par lidar aérien de l'espèce d'arbres individuels en forêt boréale aménagée ». (Mémoire de maîtrise). Montréal, Département de Géographie, UQAM.

Persson, Å., et al. (2002). Detecting and measuring individual trees using an airborne laser scanner. *Photogrammetric Engineering and Remote Sensing*, 68 (9), 925-932.

Persson, Å., et al. (2004). Tree species classification of individual trees in Sweden by combining high resolution laser data with high resolution near-infrared digital images. *Internatinal Archives of Photogrammetry and Remote Sensing*, 36 (8), 204-207.

Persson, M., et al. (2018). Tree species classification with multi-temporal Sentinel-2 data. *Remote Sensing*, 10 (11) 10.3390/rs10111794

Pilarska, M. et W. Ostrowski. (2019). Evaluating the possibility of tree species classification with dual-wavelength. International Archives of the Photogrammetry, Remote Sensing and Spatial Information Sciences - ISPRS Archives, (p. 1097-1103). doi: 10.5194/isprs-archives-XLII-2-W13-1097-2019

Popescu, S. C., et al. (2002). Estimating plot-level tree heights with lidar: Local filtering with a canopy-height based variable window size. *Computers and Electronics in Agriculture*, 37 (1-3), 71-95.

Pu, R., et al. (2018). Assessing the Potential of Multi-Seasonal High Resolution Pléiades Satellite Imagery for Mapping Urban Tree Species. 2018 Fifth International Workshop on Earth Observation and Remote Sensing Applications (EORSA), 18-20 June 2018, (p. 1-5). doi: 10.1109/EORSA.2018.8598563

Puttonen, E., et al. (2010). Individual tree species classification by illuminated-Shaded area separation. *Remote Sensing*, 2 (1), 19-35. 10.3390/rs2010019

R Core Team. (2015). R: A language and environment for statistical computing [Document électronique]. Vienna, Austria: R Foundation for Statistical Computing.

Rana, P., et al. 2018. «Towards A Generalized Method For Tree Species Classification Using Multispectral Airborne Laser Scanning In Ontario, Canada». In *IGARSS* (Valencia, Spain, 27 july 2018), sous la dir. de. Valencia, Spain.

Rana, P., et al. (2020). Feature standardization across areas of interest to optimize field sampling for individual tree species classification. *Remote Sensing of Environment*, (in press)

Regional Municipality of York (2010). York regional forest management plan 1998-2018, Summary March 2010. En ligne. <www.york.ca>.

Reitberger, J., et al. (2009). 3D segmentation of single trees exploiting full waveform LIDAR data. *ISPRS Journal of Photogrammetry and Remote Sensing*, 64 (6), 561-574.

Richardson, J. J., et al. (2009). Modeling approaches to estimate effective leaf area index from aerial discrete-return LIDAR. *Agricultural and Forest Meteorology*, 149 (6-7), 1152-1160. 10.1016/j.agrformet.2009.02.007

Riegl. (2017). Dual channel waveform processing airborne LiDAR scanning system for high-point density and ultra wide area mapping: Riegl VQ-1560i datasheet Récupéré de http://www.riegl.com/nc/products/airborne-scanning/produktdetail/product/scanner/55/

Roncat, A., et al. (2014). Radiometrically calibrated features of full-waveform lidar point clouds based on statistical moments. *IEEE Geoscience and Remote Sensing Letters*, 11 (2), 549-553. 10.1109/LGRS.2013.2274557

Rosenqvist, Å., et al. (2003). A review of remote sensing technology in support of the Kyoto Protocol. *Environmental Science & Policy*, 6 (5), 441-455.

Roussel, J. R., et al. (2018). A mathematical framework to describe the effect of beam incidence angle on metrics derived from airborne LiDAR: The case of forest canopies approaching turbid medium behaviour. *Remote Sensing of Environment*, 209, 824-834. 10.1016/j.rse.2017.12.006

Roussel, J. R., et al. (2017). Removing bias from LiDAR-based estimates of canopy height: Accounting for the effects of pulse density and footprint size. *Remote Sensing of Environment*, 198, 1-16. 10.1016/j.rse.2017.05.032

Rowe, J. S. (1972). Forest regions of Canada. Ottawa, Canadian Forestry Service

Sasaki, T., et al. (2012). Object-based classification of land cover and tree species by integrating airborne LiDAR and high spatial resolution imagery data. *Landscape and Ecological Engineering*, 8 (2), 157-171. 10.1007/s11355-011-0158-z

Sayn-Wittenstein, L. (1960). Recognition of tree species on airphotographs by crown characteristicxs. Technical note. Ottawa, Forest Research Division

Schaepman-Strub, G., et al. (2006). Reflectance quantities in optical remote sensing—definitions and case studies. *Remote Sensing of Environment*, 103 (1), 27-42. https://doi.org/10.1016/j.rse.2006.03.002

Shaker, A., et al. (2019). Automatic land-water classification using multispectral airborne LiDAR data for near-shore and river environments. *ISPRS Journal of Photogrammetry and Remote Sensing*, 152, 94-108. 10.1016/j.isprsjprs.2019.04.005

Sheeren, D., et al. (2016). Tree species classification in temperate forests using Formosat-2 satellite image time series. *Remote Sensing*, 8 (9) 10.3390/rs8090734

Shi, Y., et al. (2018a). Tree species classification using plant functional traits from LiDAR and hyperspectral data. *International Journal of Applied Earth Observation and Geoinformation*, 73, 207-219. https://doi.org/10.1016/j.jag.2018.06.018

Shi, Y., et al. (2018b). Important LiDAR metrics for discriminating forest tree species in Central Europe. *ISPRS Journal of Photogrammetry and Remote Sensing*, 137, 163-174. 10.1016/j.isprsjprs.2018.02.002

Solberg, S., et al. (2006). Mapping defoliation during a severe insect attack on Scots pine using airborne laser scanning. *Remote Sensing of Environment*, 102 (3-4), 364-376.

St-Onge, B., et al. (2015). Characterizing the height structure and composition of a boreal forest using an individual tree crown approach applied to photogrammetric point clouds. *Forests*, 6 (11), 3899-3922. 10.3390/f6113899

St-Onge, B. et B. C. Budei. (2015). Individual tree species identification using the multispectral return intensities of the Optech Titan LiDAR system. SilviLaser, La Grande Motte, France, 28–30 September 2015, (p. 71–73).

Sugumaran, R. et M. Voss. (2007). Object-oriented classification of LIDAR-fused hyperspectral imagery for tree species identification in an Urban environment. 2007 Urban Remote Sensing Joint Event, URS, Paris.

Suratno, A., et al. (2009). Tree species identification in mixed coniferous forest using airborne laser scanning. *ISPRS Journal of Photogrammetry and Remote Sensing*, 64 (6), 683-693.

Teo, T. A. et H. M. Wu. (2017). Analysis of land cover classification using multi-wavelength LiDAR system. *Applied Sciences (Switzerland)*, 7 (7) 10.3390/app7070663

Thompson, I. D., et al. (2007). Accuracy of forest inventory mapping: Some implications for boreal forest management. *Forest Ecology and Management*, 252 (1-3), 208-221. 10.1016/j.foreco.2007.06.033

Tompalski, P., et al. (2014). Simulating the impacts of error in species and height upon tree volume derived from airborne laser scanning data. *Forest Ecology and Management*, 327, 167-177. http://dx.doi.org/10.1016/j.foreco.2014.05.011

Törmä, M. (2000). Estimation of tree species proportions of forest stands using laser scanning. *Proc. of XIXth ISPRS Conference*, 33, 1524-1531.

Ustin, S. L., et al. (2009). Retrieval of foliar information about plant pigment systems from high resolution spectroscopy. *Remote Sensing of Environment*, 113 (SUPPL. 1), S67-S77. 10.1016/j.rse.2008.10.019

Valladares, F. et Ü. Niinemets. (2007). The Architecture of Plant Crowns [Chapitre de livre]. Dans F. Pugnaire et F. Valladares (dir.), *Functional Plant Ecology*. Boca Raton: CRC Press

van Aardt, J. A. N. et R. H. Wynne. (2007). Examining pine spectral separability using hyperspectral data from an airborne sensor: An extension of field‐based results. *International Journal of Remote Sensing*, 28 (2), 431-436. 10.1080/01431160500444772

Van Ewijk, K. Y., et al. (2014). Predicting fine-scale tree species abundance patterns using biotic variables derived from LiDAR and high spatial resolution imagery. *Remote Sensing of Environment*, 150, 120-131. 10.1016/j.rse.2014.04.026

Vastaranta, M., et al. (2014). Multisource Single-Tree Inventory in the Prediction of Tree Quality Variables and Logging Recoveries. *Remote Sens*, 6, 3475-3491.

Vaughn, N. R., et al. (2012). Tree species detection accuracies using discrete point lidar and airborne waveform lidar. *Remote Sensing*, 4 (2), 377-403. 10.3390/rs4020377

Vauhkonen, J., et al. (2013). Classification of spruce and pine trees using active hyperspectral LiDAR. *IEEE Geoscience and Remote Sensing Letters*, 10 (5), 1138-1141. 10.1109/LGRS.2012.2232278

Vauhkonen, J., et al. (2010). Imputation of single-tree attributes using airborne laser scanning-based height, intensity, and alpha shape metrics. *Remote Sensing of Environment*, 114 (6), 1263-1276. 10.1016/j.rse.2010.01.016

Vauhkonen, J., et al. (2014). Tree species recognition based on airborne laser scanner and complementary data sources [Chapitre de livre]. Dans M. Maltamo, et al. (dir.), *Forestry Applications of Airborne Laser Scanning* (p. 135-156): Springer

Vauhkonen, J., et al. (2008). Effects of pulse density on predicting characteristics of individual trees of Scandinavian commercial species using alpha shape metrics based on airborne laser scanning data. *Canadian Journal of Remote Sensing*, 34 (SUPPL. 2)

Vauhkonen, J., et al. (2009). Identification of scandinavian commercial species of individual trees from airborne laser scanning data using alpha shape metrics. *Forest Science*, 55 (1), 37-47.

Vega, C., et al. (2014). PTrees: A point-based approach to forest tree extraction from lidar data. *International Journal of Applied Earth Observation and Geoinformation*, 33, 98-108. http://dx.doi.org/10.1016/j.jag.2014.05.001

Vesterdal, L., et al. (2013). Do tree species influence soil carbon stocks in temperate and boreal forests? *Forest Ecology and Management*, 309, 4-18. 10.1016/j.foreco.2013.01.017

Wagner, W., et al. (2006). Gaussian decomposition and calibration of a novel small-footprint full-waveform digitising airborne laser scanner. *ISPRS Journal of Photogrammetry and Remote Sensing*, 60 (2), 100-112.

Wang, C. K., et al. (2013). Airborne dual-wavelength LiDAR data for classifying land cover. *Remote Sensing*, 6 (1), 700-715.

Wei, G., et al. (2012). Multi-wavelength canopy LiDAR for remote sensing of vegetation: Design and system performance. *ISPRS Journal of Photogrammetry and Remote Sensing*, 69, 1-9. 10.1016/j.isprsjprs.2012.02.001

White, J. C., et al. (2016). Remote Sensing Technologies for Enhancing Forest Inventories: A Review. *Canadian Journal of Remote Sensing*, 42 (5), 619-641. 10.1080/07038992.2016.1207484

Wichmann, V., et al. (2015). Evaluating the potential of multispectral airborne LiDAR for topographic mapping and land cover classification. *ISPRS Ann. Photogramm. Remote Sens. Spatial Inf. Sci.*, II-3/W5, 113-119. 10.5194/isprsannals-II-3-W5-113-2015

Wing, M. G., et al. (2010). Applying LiDAR technology for tree measurements in burned landscapes. *International Journal of Wildland Fire*, 19 (1), 104-114. 10.1071/WF08170

Woodhouse, I. H., et al. (2011). A multispectral canopy LiDAR demonstrator project. *IEEE Geoscience and Remote Sensing Letters*, 8 (5), 839-843. 10.1109/LGRS.2011.2113312

Wright, I. J., et al. (2004). The worldwide leaf economics spectrum. *Nature*, 428 (6985), 821-827.

Wulder, M. A., et al. (2008). The role of LiDAR in sustainable forest management. *Forestry Chronicle*, 84 (6), 807-826.

Wulder, M. A., et al. (2012). Lidar sampling for large-area forest characterization: A review. *Remote Sensing of Environment*, 121, 196-209. 10.1016/j.rse.2012.02.001

Yan, W. Y. et A. Shaker. (2014). Radiometric correction and normalization of airborne LiDAR intensity data for improving land-cover classification. *IEEE Transactions on Geoscience and Remote Sensing*, 52 (12), 7658-7673. 10.1109/TGRS.2014.2316195

--------. (2017). Correction of overlapping multispectral lidar intensity data: Polynomial approximation of range and angle effects. International Archives of the Photogrammetry, Remote Sensing and Spatial Information Sciences - ISPRS Archives, (p. 177-182). doi: 10.5194/isprs-archives-XLII-3-W1-177-2017

Yao, W., et al. (2012). Tree species classification and estimation of stem volume and DBH based on single tree extraction by exploiting airborne full-waveform LiDAR data. *Remote Sensing of Environment*, 123, 368-380. 10.1016/j.rse.2012.03.027

You, H., et al. (2017). Quantifying the effects of normalisation of airborne LiDAR intensity on coniferous forest leaf area index estimations. *Remote Sensing*, 9 (2) 10.3390/rs9020163

Yu, X., et al. (2017). Single-Sensor Solution to Tree Species Classification Using Multispectral Airborne Laser Scanning. *Remote Sensing*, 9 (2), 108.

Yu, X., et al. (2014). Assessment of low density full-waveform airborne laser scanning for individual tree detection and tree species classification. *Forests*, 5 (5), 1011-1031. 10.3390/f5051011

Zhang, Z., et al. (2016). Object-based tree species classification in urban ecosystems using LiDAR and hyperspectral data. *Forests*, 7 (6) 10.3390/f7060122

Zheng, G., et al. (2017). Retrieving Directional Gap Fraction, Extinction Coefficient, and Effective Leaf Area Index by Incorporating Scan Angle Information From Discrete Aerial Lidar Data. *IEEE Transactions on Geoscience and Remote Sensing*, 55 (1), 577-590. 10.1109/TGRS.2016.2611651

Zhou, T., et al. (2018). Bayesian and classical machine learning methods: A Comparison for tree species classification with LiDAR waveform signatures. *Remote Sensing*, 10 (1) 10.3390/rs10010039

Zou, X., et al. (2016). 3D land cover classification based on multispectral lidar point clouds. 23rd International Archives of the Photogrammetry, Remote Sensing and Spatial Information Sciences Congress, ISPRS 2016, (p. 741-747). International Society for Photogrammetry and Remote Sensing. doi: 10.5194/isprsarchives-XLI-B1-741-2016